# MODELLING AND CONTROL OF COAL PROCESSING PLANTS

by

**Ewald Jonathan Meyer**

Submitted in partial fulfillment of the requirements for the degree
Philosophiae Doctor (Electronic Engineering)

in the

Department of Electrical, Electronic and Computer Engineering
Faculty of Engineering, Built Environment and Information Technology

UNIVERSITY OF PRETORIA

February 2016

# SUMMARY

---

## MODELLING AND CONTROL OF COAL PROCESSING PLANTS

by

**Ewald Jonathan Meyer**

| | |
|---|---|
| Promoter(s): | Prof Ian Craig |
| Department: | Electrical, Electronic and Computer Engineering |
| University: | University of Pretoria |
| Degree: | Philosophiae Doctor (Electronic Engineering) |
| Keywords: | Bin level control, coal beneficiation, control systems, comminution, dense medium cyclone, dense medium drum, dynamic modelling, materials handling, model predictive control, coal, observers, system identification, unscented Kalman filter |

Models are developed and verified with industrial data. These models are then controlled using nonlinear model predictive control (NMPC). It was found that there are very few available dynamic models for coal processes, other than the separation unit models developed by the author and study leader. Additional dynamic models for a coal comminution circuit were also developed.

The mathematical details of the models developed for a coal plant are presented in this thesis. Model system identification was used to solve for unknown model parameters, to fit the dynamic models to actual industrial production data.

The specific coal unit process dynamic models developed and used in this thesis are:

- Vibratory feeders;
- Single- and double-deck screens;

- Bin with three compartments;
- A dense medium drum; and
- A dense medium cyclone.

Applying NMPC to the dynamic models allowed for simulated improvements to be made to the comminution and separation circuits used in this research. It was shown that the throughput on a comminution circuit could be increased by 3.6% resulting in a downstream separator yield improvement of 3.2%. By applying NMPC to the separation circuit, it was shown that separation yield can be improved by 6.9% with a decrease in product ash (improvement in grade) for a drum separator by 1.5% and cyclone separator by 0.4%.

The unscented Kalman filter (UKF) was simulated on the dynamic models developed to illustrate how an actual controller could be implemented such that the dynamic model states could be updated over time. The UKF acts as an observer such that unmeasured states can be fed back to the controller.

In summary, the thesis gives a realistic account for the application of NMPC for coal processing and with the potential yield improvements of 10% (based on the 3.2% yield improvement due to the comminution circuit control and the 6.9% improvement due to the separator circuit control), could increase a South African coal company's annual revenue by approximately R175.5 million per annum.

A proposal regarding the application of NMPC for coal mine-wide optimisation is also given.

# OPSOMMING

---

## MODELLERING EN BEHEER VAN STEENKOOLAANLEGTE

deur

**Ewald Jonathan Meyer**

| | |
|---|---|
| Promotor(s): | Prof Ian Craig |
| Departement: | Elektriese, Elektroniese en Rekenaar-Ingenieurswese |
| Universiteit: | Universiteit van Pretoria |
| Graad: | Philosophiae Doctor (Elektroniese Ingenieurswese) |
| Sleutelwoorde: | Beheerstelsels, opgaarhouer-vlakbeheer, dinamiese modellering, digte medium drom, digte medium sikloon, komminusie, materiaalhantering, model voorspellende kontrole, steenkool, waarnemers, stelselidentifikasie, *unscented Kalman filter* |

Modelle is ontwikkel en geverifieer aan die hand van industriële data. Hierdie modelle is dan beheer met behulp van nie-lineêre model voorspellende kontrole (NMVK). Daar is gevind dat daar baie min dinamiese modelle vir steenkoolprosesse beskikbaar is buiten die skeiding-eenheid-modelle ontwikkel deur die outeur en studieleier. Addisionele dinamiese modelle vir ’n steenkool-komminusie-aanleg is ook ontwikkel.

Die wiskundige besonderhede van die modelle wat ontwikkel is vir ’n steenkool-aanleg word aangebied in hierdie tesis. Modelstelsel-identifikasie is gebruik om oplossings te gee vir onbekende model-parameters en om die dinamiese modelle te pas by die werklike industriële produksiedata.

Die spesifieke eenheidsproses steenkool dinamiese modelle wat geontwikkel en gebruik word in hierdie tesis is:

- Vibrerende voerders;

- Enkel- en dubbel-dek skerms;
- Bin met drie kompartemente;
- 'N digte medium drom; and
- 'N digte medium sikloon.

Die toepassing van NMVK op die dinamiese modelle het toegelaat dat gesimuleerde verbeterings aangebring kon word. Daar is getoon dat die deurset op 'n komminusie-aanleg 3.6% verhoog kan word wat kan lei tot 'n stroomaf skeiding-opbrengs verbetering van 3.2%. Deur die toepassing van NMVK op die skeiding-aanleg, is daar getoon dat skeiding-opbrengs met 6.9% verbeter kan word met 'n afname in die produk-as (verbetering in graad) vir 'n drom skeier met 1.5% en sikloon-skeier met 0.4%.

Die *unscented Kalman filter* (UKF) is nageboots op die dinamiese modelle wat ontwikkel is om te illustreer hoe 'n werklike kontroleerder sodanig geïmplementeer kan word dat die toestand van die dinamiese modelle met verloop van tyd opgedateer kan word. Die UKF dien as 'n waarnemer sodat ongemete toestande teruggevoer kan word na die kontrolleerder.

Om op te som: die tesis gee 'n realistiese scenario vir die toepassing van NMVK op steenkoolverwerking. Met die potensiële groter opbrengs van 10% (gebaseer op die 3.2% groter opbrengs as gevolg van die kontrole van die komminusie-aanleg en die 6.9% groter opbrengs weens die kontrole van die skeiding-eenheid) kan 'n Suid-Afrikaanse steenkoolmaatskappy se jaarlikse inkomste met 175.5 miljoen per jaar styg.

Daar word ook 'n voorstel aan die hand gedoen oor die toepassing van NMVK vir die optimalisering van die steenkoolmyn in sy geheel.

# LIST OF ABBREVIATIONS

| | |
|---|---|
| CFD | Computational fluid dynamics |
| DC | Direct current |
| DMC | Dense medium cyclone |
| DMD | Dense medium drum |
| DMS | Dense medium separation |
| EKF | Extended Kalman filter |
| EPM | Écart probable moyen |
| GRV | Gaussian random variables |
| IEA | International Energy Agency |
| MPC | Model predictive control |
| NMPC | Nonlinear model predictive control |
| NRMSE | Normalised root mean square error |
| ODE | Ordinary differential equations |
| PGNAA | Prompt gamma neutron activation analysis |
| RD | Relative density |
| ROM | Run-of-mine |
| SG | Specific gravity |
| UKF | Unscented Kalman filter |
| USD | United States dollars |
| UT | Unscented transform |

# NOMENCLATURE

$\alpha$ Unscented Kalman filter spread of the sigma points around the random variable mean ($\bar{\mathbf{x}}$)

$\alpha_c$ DMC separator (subscript $c$) volume and volumetric split ratio

$\alpha_d$ Drum separator (subscript $d$) volume and volumetric split ratio

$\alpha_{ds,c}$ Double-deck screen (subscript $ds$) percentage of mass split for mass component $i$ for the bottom deck (subscript $c$)

$\alpha_{ds,o}$ Double-deck screen (subscript $ds$) percentage of mass split for mass component $i$ for the top deck (subscript $o$)

$\alpha_{ss}$ Single-deck screen (subscript $ss$) percentage of mass split for mass component $i$

$\bar{y}_{\mathscr{M}}$ System identification dynamic model (subscript $\mathscr{M}$) measured output statistical mean

$\beta$ Unscented Kalman filter parameter used to incorporate prior knowledge of the distribution of the random variable ($\mathbf{x}$)

$\beta_b$ Bin (subscript $b$) stockpile maximum height ratio

$\chi_i$ Unscented Kalman filter $i$th sigma vector

$\Delta\rho_{c,med}$ DMC separator (subscript $c$) difference between the overflow and underflow medium density (subscript $med$) and the feed medium density

$\Delta\rho_{d,med}$ Drum separator (subscript $d$) proportionality constant relating difference in feed component density (subscript $\rho_{d,med}$) with either density of floats or sinks

$\varepsilon$ System identification model prediction error

$\gamma_i$ Unscented Kalman filter $i$th sigma vector nonlinear function

$\kappa$ Unscented Kalman filter secondary scaling parameter

$\lambda$ Unscented Kalman filter scaling parameter

$\bar{\mathbf{x}}$ Unscented Kalman filter random variable mean

$\chi$ Unscented Kalman filter nonlinear function ($\mathbf{y}$) statistics

$\hat{\mathbf{y}}(t)$ Model predictive control output prediction

$\mathbf{P}_{\mathbf{x}}$ Unscented Kalman filter random variable covariance

$\mathbf{P}$ Model predictive control coefficient that considers sequences in future behaviour of rapid input changes $[\Delta\mathbf{u}(t+j) = \mathbf{u}(t+j) - \mathbf{u}(t+j-1)]$

$\mathbf{P}_0$ Unscented Kalman filter initial original state

$\mathbf{P}_0^a$ Unscented Kalman filter initial covariances

$\mathbf{P}_n$ Unscented Kalman filter initial measurement noise

$\mathbf{P}_v$ Unscented Kalman filter initial process noise

$\mathbf{Q}$ Model predictive control coefficient that considers sequences in future behaviour of input error $[\mathbf{u}(t+j) - \mathbf{u}_s]$

$\mathbf{R}$ Model predictive control coefficient that considers sequences in future behaviour of the error $[\hat{\mathbf{y}}(t+j) - \mathbf{y}_s]$

| | |
|---|---|
| $\mathbf{s}$ | Model predictive control soft constraints in output variables |
| $\mathbf{T}$ | Model predictive control coefficient that considers sequences in future soft constraints ($\mathbf{s}$) |
| $\mathbf{u}(t)$ | Model predictive control field action |
| $\mathbf{u}_s(t)$ | Model predictive control desired steady-state inputs |
| $\mathbf{x}$ | Unscented Kalman filter random variable |
| $\mathbf{y}$ | Unscented Kalman filter nonlinear function $g(\mathbf{x})$ |
| $\mathbf{y}_s(t)$ | Model predictive control output reference trajectory |
| fit | System identification goodness of the fit |
| FPE | System identification Akaike's final prediction error |
| $\mathrm{y}_{\mathscr{M}}$ | System identification dynamic model (subscript $\mathscr{M}$) measured output |
| $\mathrm{y}_{\mathrm{td},\mathscr{M}}$ | System identification dynamic model (subscript $\mathscr{M}$) measured output after time delay (subscript $td$) |
| $\mathscr{M}_*$ | Mathematical representation of a dynamic model (subscript $*$) |
| $\rho_{25}$ | Specific gravity (SG) at 25% |
| $\rho_{50}$ | Separation cutpoint with a partition factor of 50% (subscript 50) |
| $\rho_{75}$ | Specific gravity (SG) at 75% |

$\rho_b$ Bulk density of material in bin (subscript $b$)

$\rho_{c,i,*}$ Density of mass component (subscript $*$) in the DMC separator (subscript $c$) feed (subscript $i$) mix

$\rho_{c,i}$ Density of the DMC separator (subscript $c$) feed (subscript $i$) mix

$\rho_{c,o,*}$ Density of mass component (subscript $*$) in the DMC separator (subscript $c$) overflow (subscript $o$)

$\rho_{c,o}$ Density of the DMC separator (subscript $c$) overflow (subscript $o$)

$\rho_{c,u,*}$ Density of mass component (subscript $*$) in the DMC separator (subscript $c$) underflow (subscript $u$)

$\rho_{c,u}$ Density of the DMC separator (subscript $c$) underflow (subscript $u$)

$\rho_{d,f,*}$ Density of mass component (subscript $*$) in the drum separator (subscript $d$) floats (subscript $f$)

$\rho_{d,f}$ Density of the drum separator (subscript $d$) floats (subscript $f$)

$\rho_{d,i,*}$ Density of mass component (subscript $*$) in the drum separator (subscript $d$) feed (subscript $i$) mix

$\rho_{d,i,ore}$ Drum separator (subscript $d$) ore (subscript $i, ore$) density

$\rho_{d,i}$ Density of the drum separator (subscript $d$) feed (subscript $i$) mix

$\rho_{d,s,*}$ Density of mass component (subscript $*$) in the drum separator (subscript $d$) sinks (subscript $s$)

$\rho_{d,s}$ Density of the drum separator (subscript $d$) sinks (subscript $s$)

$\rho_{i,med}$ Dense medium separation feed medium (subscript $i, med$) density

$\tau_f$ Feeder (subscript $f$) time constant

$\tau_{bf,1}$ Bin feeder no. 1 (subscript $bf, 1$) characteristic time constant

$\tau_{bf,2}$ Bin feeder no. 2 (subscript $bf, 2$) characteristic time constant

$\tau_{cr}$ Crusher (subscript $cr$) time constant

$\tau_{ds,c}$ Time taken for ore to be transported over a bottom deck (subscript $c$) of a double-deck screen (subscript $ds$) component $i$

$\tau_{ds,o}$ Time taken for ore to be transported over a top deck (subscript $o$) of a double-deck screen (subscript $ds$) component $i$

$\tau_{ss,o}$ Time taken for ore to be transported over (subscript $o$) a single-deck screen (subscript $ss$) component $i$

$\tau_{ss,u}$ Time taken for ore to be transported through (subscript $u$) a single-deck screen (subscript $ss$) component $i$

$\tau_{u,ds,c}$ Time taken for ore to be transported through (subscript $u$) a bottom deck (subscript $c$) of a double-deck screen (subscript $ds$) component $i$

$\tau_{u,ds,o}$ Time taken for ore to be transported through (subscript $u$) a top deck (subscript $o$) of a double-deck screen (subscript $ds$) component $i$

$\theta_i$ System identification $i$th model parameter consisting of $d_{\mathscr{M}}$ parameters in total

$\widehat{y}_{\mathscr{M}}$ System identification dynamic model (subscript $\mathscr{M}$) simulated output

$A_c$ DMC separator (subscript $c$) inlet cross-sectional area

$A_b$ Bin (subscript $b$) stockpile maximum geometric base area

$A_{drm}$ Drum separator partition curve parameter

$A_{ore}$ Effective cross-sectional area of an ore particle

$a_{pc}$ Relative density fraction in clean coal in the development of a partition curve (subscript $pc$)

$B_{drm}$ Drum separator partition curve parameter

$b_i$ M-curve $i$th process model parameter containing 5 parameters in total (i.e. $i = 1 \ldots 5$)

$b_{pc}$ Relative density fraction of total clean coal in the development of a partition curve (subscript $pc$)

$C_{ore}$ Drag coefficient of an ore particle

$c_{pc}$ Relative density fraction in discard in the development of a partition curve (subscript $pc$)

$d$ Model predictive control slew rate

$D_c$ DMC separator (subscript $c$) diameter

$d_{ore}$ Average particle size of ore (subscript $ore$)

$d_{pc}$ Relative density fraction of total discard in the development of a partition curve (subscript $pc$)

$E_p$ Écart probable moyen or separation efficiency

$e_{pc}$ Relative density fraction reconstructed feed in the development of a partition curve (subscript $pc$)

$f_f$ Feeder (subscript $f$) motor speed

$F_g$ Downward gravitational force on an ore particle

$f_{bf,1}$ Bin feeder no. 1 (subscript $bf,1$) variable speed drive frequency

$f_{bf,2}$ Bin feeder no. 2 (subscript $bf,2$) variable speed drive frequency

$g$ Acceleration due to gravity

$h_c$ DMC separator (subscript $c$) head height

$H_b$ Bin (subscript $b$) stockpile maximum geometric height

$h_b$ Bin (subscript $b$) stockpile maximum height

$I_{cr,min}$ Motor current when crusher (subscript $cr$) has no load (subscript $min$)

$I_{cr}$ Crusher (subscript $cr$) motor current

$J$ Model predictive control objective function

$K_f$ Feeder (subscript $f$) proportionality constant relating motor speed to mass flow rate

$K_{b,1}$ Bin (subscript $b$) stockpile maximum height ratio proportionality constant for sigmoid relationship

$K_{b,2}$ Bin (subscript $b$) stockpile maximum height ratio proportionality constant for sigmoid relationship

$K_{bf,1,1}$ Bin feeder no. 1 (subscript $bf,1$) proportionality constant for inverse exponential relationship

$K_{bf,1,2}$ Bin feeder no. 1 (subscript $bf,1$) proportionality constant for inverse exponential relationship

$K_{bf,1,3}$ Bin feeder no. 1 (subscript $bf,1$) proportionality constant for sigmoid relationship

$K_{bf,1,4}$ Bin feeder no. 1 (subscript $bf,1$) proportionality constant for sigmoid relationship

$K_{bf,1}(h_b)$ Bin feeder no. 1 (subscript $bf,1$) proportionality function of bin level $h_b$

$K_{bf,2,1}$ Bin feeder no. 2 (subscript $bf,1$) proportionality constant for inverse exponential relationship

$K_{bf,2,2}$ Bin feeder no. 2 (subscript $bf,1$) proportionality constant for inverse exponential relationship

$K_{bf,2,3}$ Bin feeder no. 2 (subscript $bf,1$) proportionality constant for sigmoid relationship

$K_{bf,2,4}$ Bin feeder no. 2 (subscript $bf,1$) proportionality constant for sigmoid relationship

$K_{bf,2}(h_b)$ Bin feeder no. 2 (subscript $bf,2$) proportionality function of bin level $h_b$

$K_{c,o,*}$ DMC separator (subscript $c$) proportionality constant relating densities for mass component (subscript $*$) in overflow (subscript $o$)

$K_{c,o}$ DMC separator (subscript $c$) proportionality constant relating densities in overflow (subscript $o$)

$K_{c,u,*}$ DMC separator (subscript $c$) proportionality constant relating densities for mass component (subscript $*$) in underflow (subscript $u$)

$K_{c,u}$ DMC separator (subscript $c$) proportionality constant relating densities in underflow (subscript $u$)

$K_{cr,k,1}$ Crusher (subscript $cr$) mass hold-up proportionality constant for solids retained above size interval $k$

$K_{cr,k,2}$ Crusher (subscript $cr$) motor current proportionality constant for solids retained above size interval $k$

$K_{cr,k,3}$ Crusher (subscript $cr$) motor current proportionality constant for torque load at solids retained above size interval $k$

$K_{d,f,*}$ Drum separator (subscript $d$) proportionality constant relating densities for mass component (subscript $*$) in floats (subscript $f$)

$K_{d,f}$ Drum separator (subscript $d$) proportionality constant relating densities in floats (subscript $f$)

$K_{d,s,*}$ Drum separator (subscript $d$) proportionality constant relating densities for mass component (subscript $*$) in sinks (subscript $s$)

$K_{d,s}$ Drum separator (subscript $d$) proportionality constant relating densities in sinks (subscript $s$)

$L$ Unscented Kalman filter dimension of random variable ($\mathbf{x}$)

$L_{b,1}$ Bin stockpile maximum geometric base depth (subscript $b,1$)

$l_{b,1}$ Bin stockpile base depth (subscript $b,1$)

$L_{b,2}$ Bin stockpile maximum geometric base length (subscript $b,2$)

$l_{b,2}$ Bin stockpile base depth (subscript $b,2$)

$l_b$ Bin (subscript $b$) stockpile relative level

$m_f$ Mass on a feeder (subscript $f$)

$m_{bf,1}$ Bin feeder no. 1 (subscript $bf,1$) mass state

$m_{bf,2}$ Bin feeder no. 2 (subscript $bf,2$) mass state

$m_b$ Bin (subscript $b$) mass state

$m_{cr}$ Mass in crusher(subscript $cr$)

$M_{ds,c,i}$ Double-deck screen (subscript $ds$) mass of ore for mass component $i$ on the bottom deck (subscript $c$)

$M_{ds,o,i}$ Double-deck screen (subscript $ds$) mass of ore for mass component $i$ on the top deck (subscript $o$)

$M_{ss,i}$ Single-deck screen (subscript $ss$) mass of ore for mass component $i$

$P_{c,i}$ DMC separator (subscript $c$) inlet pressure

$p_i$ Drum separator partition factor $i$th parameter containing 3 parameters in total (i.e. $i = 1 \dots 3$)

$Q_{c,i,*}$ Volumetric flow rate of mass component (subscript $*$) in the DMC separator (subscript $c$) feed (subscript $i$) mix

$Q_{c,o,*}$ Volumetric flow rate of mass component (subscript $*$) in the DMC separator (subscript $c$) overflow (subscript $o$)

$Q_{c,o}$ Volumetric flow rate of the material overflow (subscript $o$) within the DMC separator (subscript $c$)

$Q_{c,s,*}$ Volumetric flow rate of mass component (subscript $*$) in the DMC separator (subscript $c$) underflow (subscript $u$)

$Q_{c,u}$ Volumetric flow rate of the material underflow (subscript $u$) within the DMC separator (subscript $c$)

$Q_{d,f,*}$ Volumetric flow rate of mass component (subscript $*$) in the drum separator (subscript $d$) floats (subscript $f$)

$Q_{d,f}$ Volumetric flow rate of the material of floats (subscript $f$) within the drum separator (subscript $d$)

$Q_{d,i,*}$ Volumetric flow rate of mass component (subscript $*$) in the drum separator (subscript $d$) feed (subscript $i$) mix

$Q_{d,s,*}$ Volumetric flow rate of mass component (subscript $*$) in the drum separator (subscript $d$) sinks (subscript $s$)

$Q_{d,s}$ Volumetric flow rate of the material of sinks (subscript $s$) within the drum separator (subscript $d$)

$R_c$ DMC separator (subscript $c$) effective radius near the spigot

$R_{cr,i,k}$ Crusher (subscript $cr$) feed (subscript $i$) fraction of solids retained above size interval $k$

$R_{cr,o,k}$ Crusher (subscript $cr$) product (subscript $o$) fraction of solids retained above size interval $k$

$t$ Time

$t_{td}$ Time delay

$V_N$ System identification loss function with $N$ values in the estimation data set ($Z^N$)

$V_t$ System identification loss function terminating (subscript $t$) threshold

$v_t$ Drum separator particle terminal velocity

$v_{100}$ Drum separator terminal velocity allowing for sinks to be recovered 100%

$V_b$ Volume of material within the bin (subscript $b$)

$v_{c,i}$ DMC separator (subscript $c$) inlet (subscript $i$) tangential velocity

$V_{c,o}$ Volume split of the overflow (subscript $o$) within the DMC separator (subscript $c$)

$V_{c,u}$ Volume split of the underflow (subscript $u$) within the DMC separator (subscript $c$)

$V_c$ Volume of the material within the DMC separator (subscript $c$)

$V_{d,f}$ Volume of the material of floats (subscript $f$) within the drum separator (subscript $d$)

$V_{d,s}$ Volume of the material of sinks (subscript $s$) within the drum separator (subscript $d$)

$V_d$ Volume of the material within the drum separator (subscript $d$)

$W_i$ Unscented Kalman filter $i$th sigma vector corresponding weight

$W_{b,i}$ Bin (subscript $b$) mass flow rate input (subscript $i$)

$W_{b,o,1}$ Bin (subscript $b$) mass flow rate output no. 1 (subscript $o,1$)

$W_{b,o,2}$ Bin (subscript $b$) mass flow rate output no. 2 (subscript $o,2$)

$W_{b,o,3}$ Bin (subscript $b$) mass flow rate output no. 3 (subscript $o,3$)

$W_{bf,o,1}$ Bin feeder (subscript $bf$) mass flow rate output no. 1 (subscript $o,1$)

$W_{bf,o,2}$ Bin feeder (subscript $bf$) mass flow rate output no. 2 (subscript $o,2$)

$W_{c,i}$ Mass feed rate of the DMC separator (subscript $c$) feed (subscript $i$) mix

$W_{c,o}$ Mass feed rate of the DMC separator (subscript $c$) overflow (subscript $o$)

$W_{c,u}$ Mass feed rate of the DMC separator (subscript $c$) underflow (subscript $u$)

$W_{cr,i}$ Mass flow rate into (subscript $i$) a crusher (subscript $cr$)

$W_{cr,o}$ Mass flow rate from (subscript $o$) a crusher (subscript $cr$)

$W_{d,f}$ Mass feed rate of the drum separator (subscript $d$) floats (subscript $f$)

$W_{d,i}$ Mass feed rate of the drum separator (subscript $d$) feed (subscript $i$) mix

$W_{d,s}$ Mass feed rate of the drum separator (subscript $d$) sinks (subscript $s$)

$W_{ds,c,i}$ Double-deck screen (subscript $ds$) mass feed rate of the ore overflow exiting mass component $i$ on the bottom deck (subscript $c$)

$W_{ds,o,i}$ Double-deck screen (subscript $ds$) mass feed rate of the ore overflow exiting mass component $i$ on the top deck (subscript $o$)

$W_{f,o}$ Mass flow rate from a feeder (subscript $f$)

$W_{ss,i}$ Single-deck screen (subscript $ss$) mass feed rate of the ore overflow exiting mass component $i$

$W_{u,ds,c,i}$ Double-deck screen (subscript $ds$) mass feed rate of the undersized (subscript $u$) ore exiting mass component $i$ from the bottom deck (subscript $c$)

$W_{u,ds,o,i}$ Double-deck screen (subscript $ds$) mass feed rate of the undersized (subscript $u$) ore exiting mass component $i$ from the top deck (subscript $o$)

$W_{u,ss,i}$ Single-deck screen (subscript $ss$) mass feed rate of the ore underflow (subscript $u$) exiting mass component $i$

$x_{c,i,*}$ Percentage of mass component (subscript $*$) in the DMC separator (subscript $c$) feed (subscript $i$) mix

$x_{c,o,*}$ Percentage of mass component (subscript $*$) in the DMC separator (subscript $c$) overflow (subscript $o$)

$x_{c,u,*}$ Percentage of mass component (subscript $*$) in the DMC separator (subscript $c$) underflow (subscript $u$)

$x_{d,f,*}$ Percentage of mass component (subscript $*$) in the drum separator (subscript $d$) floats (subscript $f$)

$x_{d,i,*}$ Percentage of mass component (subscript $*$) in the drum separator (subscript $d$) feed (subscript $i$) mix

$x_{d,s,*}$ Percentage of mass component (subscript $*$) in the drum separator (subscript $d$) sinks (subscript $s$)

$x_{f,ash}$ M-curve process model product or float ash (subscript $f, ash$) percentage

$x_{i,ash}$ M-curve process model feed ash (subscript $i, ash$) content

$y$ M-curve process model yield

$Y(\rho_{i,med})$ Partition factor as a function of feed medium density ($\rho_{i,med}$)

$Y_c$ Cyclone separator (subscript $c$) partition factor

$Y_d$ Drum separator (subscript $d$) partition factor

$Y_d(\rho_{i,med})$ Drum separator (subscript $d$) partition factor as a function of feed medium density ($\rho_{i,med}$)

$y_{pc}$ Yield for clean coal in the development of a partition curve (subscript $pc$)

# TABLE OF CONTENTS

# CHAPTER 1 INTRODUCTION

## 1.1 PROBLEM STATEMENT

### 1.1.1 Context of the problem

The International Energy Agency (IEA) has indicated that the global coal demand growth has slowed down in recent years and is estimated to grow at a rate of 2.1% per year through 2019 (International Energy Agency, 2014b). Coal prices are declining and many coal producers have been operating at a loss in the last two years driven by take-or-pay agreements or financial liabilities. The operational costs have been lowered by some companies, not only through economies of scale, effective management and budget disciplines, but also through external factors such as depreciation of local currencies.

Coal accounts for 41% of the world's electricity generation (Pooe and Mathu, 2011). In the South African context, about 75% of its coal is used locally, primarily for electricity generation and synthetic fuels. South Africa's coal reserves largely consists of bituminous coal (96%), while anthracite (2%), and metallurgical coal (2%) account for the remaining portion (Eberhard, 2011). Figure 1.1 illustrates the coal prices over the past three years for thermal coal and coking coal (Metals Consulting International, 2015). In the South African context, Figure 1.2 shows the historical record of export coal (Barrientos and Soria, 2015). All prices are given in United States dollars (USD) per metric ton.

Given the steady decreasing trend in coal prices over the past three to four years, as illustrated in Figures 1.1 and 1.2, there is a need to optimise coal operations with the objectives of increasing throughput and grade while minimising cost. The South African National Energy Development Institute have developed a roadmap for the South African coal value chain (South African National Energy Development Institute, 2015). Trends and opportunities in the coal preparation value chain

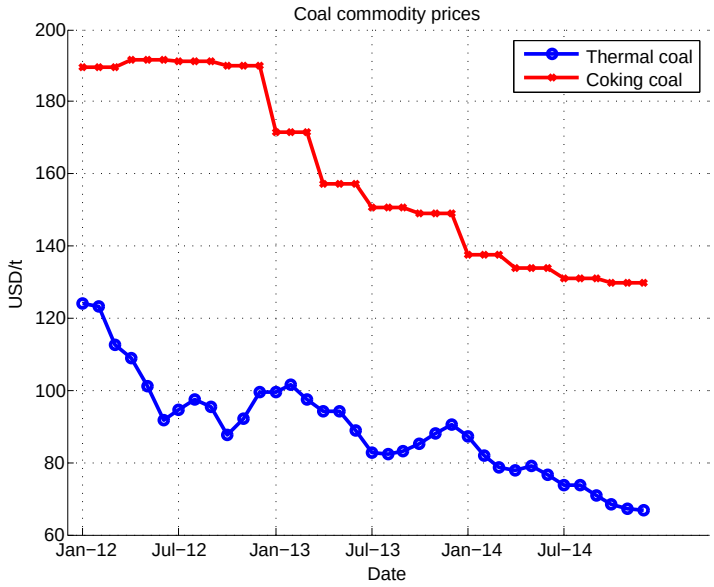


**Figure 1.1:** Commodity coal price history [data taken from Metals Consulting International (2015)].

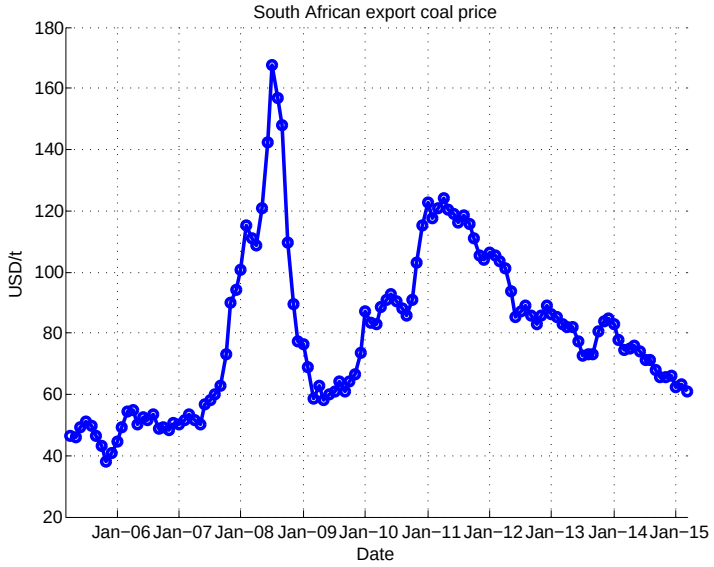


**Figure 1.2:** South African export coal price history [data taken from Barrientos and Soria (2015)].

primarily include metallurgical solutions such as dry coal processing, simultaneous washing of coarse and small coal, agglomeration of ultra-fine coal and thermal drying techniques.

Other contributing technologies in fine coal processing include water-based separation, chemical separation, magnetic and electrical separation, computers and process control, and materials science (Klima *et al.*, 2012; Arnold *et al.*, 2007). Although these coal beneficiation technologies can improve the coal value chain, current coal plants can be managed more effectively through the use of metallurgical accounting, control and simulation (Wills and Napier-Munn, 2006). With recent developments in the field of control systems, opportunities exist to improve current and future coal plants through better control of yield, throughput and grade (Meyer and Craig, 2010).

### 1.1.2 Research gap

The current gap in the field of research applied to coal processing is the development of model-based control systems to improve coal plant performance. Research gaps that this thesis address are as follows:

- The development of dynamic models for coal plants.
- The development of a partition curve from a dynamic model in coal beneficiation.
- Development, design and simulation of a model predictive controller (MPC) for a coal beneficiation process.
- Discussion on the implementation and benefits of MPC in coal processing.

## 1.2 RESEARCH OBJECTIVE AND QUESTIONS

The objectives of this research are as follows:

- Improve current knowledge and understanding of mathematical modelling and process control in coal beneficiation.

- Contribute to the research field of applied process control in minerals processing.
- To synthesise knowledge between the fields of control systems and coal metallurgy.
- Contribute to the coal processing industry by proposing a solution to improve coal plant operations.

The following research questions arise when considering the above research objectives:

- What is the current knowledge of model-based control, such as MPC, in coal beneficiation?
- Does a dynamic model exist for coal beneficiation using dense medium separation (DMS) and has model-based control been applied to the process?
- What are the benefits if model-based control is implemented for a coal DMS process?

## 1.3 HYPOTHESIS AND APPROACH

With the development and identification of a dynamic model describing a coal beneficiation process, it will be possible to design a model-based controller. If MPC is used, it should be shown through simulation that MPC performs better than existing control techniques employed at an actual coal plant. The MPC simulated for an existing coal process should show a theoretical improvement in yield in the order of ten percent over a limited time frame.

The approach to be followed for this research involves a standard control system design procedure where a dynamic model of a coal process will be identified and used to design a MPC. An approach to implement this controller design will be discussed.

## 1.4 RESEARCH GOALS

The proposed research goals are as follows:

1. Study an actual coal beneficiation process and determine the control objectives of the process.

2. Identify dynamic models of the process and validate the models by generating their steady-state partition curve for the DMS areas.

3. Determine the control variables and design a MPC system for the models.

4. Simulate the controller and determine the theoretical improvement made to the process by comparing the simulation results to the actual plant data.

5. Discuss the possible implementation of the controller and possible improvements that can be made in terms of measurement and control.

## 1.5 RESEARCH CONTRIBUTION

The contribution this research will make to the coal processing field is the development of plant verified dynamic models for process control. These dynamic models are used to design model-based controllers that can illustrate potential benefits in throughput, yield and product quality through simulation. The process control research field will benefit by having a simulated application of MPC in coal processing. The following publications have resulted from this work:

- Meyer, E. J., Craig, I. K., Alvarado, V., 2015. Unscented kalman filter for a coal run-of-mine bin, *Proceedings of the 4th Workshop on Mining, Mineral and Metal Processing, Oulu, Finland*, IFAC, IFAC.

- Meyer, E., Craig, I., 2015. Dynamic model for a dense medium drum separator in coal beneficiation, *Minerals Engineering* **77**: 78–85.

- Meyer, E. J., Craig, I. K., 2014. Coal dense medium separation dynamic and steady-state modelling for process control, *Minerals Engineering* **65**(15), 98–108.

- Meyer, E. J., Craig, I. K., 2011. Development of a steady-state partition curve from a dense medium cyclone dynamic model in coal beneficiation, *Proceedings of the 18th IFAC World Congress, Milan, Italy*, Vol. 18, IFAC, IFAC, pp. 10523–10528.

- Meyer, E. J., Craig, I. K., 2010. The development of dynamic models for a dense medium separation circuit in coal beneficiation, *Minerals Engineering* **23**(10): 791–805.

## 1.6 OVERVIEW OF STUDY

Various aspects regarding the available literature on model-based control applied to coal processing is detailed in Chapter 2. The literature study covers primarily the available literature in the development of dynamic modelling for minerals processing unit operations in DMS plants. Chapter 3 details the method used in this thesis to detail the model-based control approach for coal beneficiation plants using DMS. Mathematical models representing the process dynamics of an actual coal process are shown. The MPC algorithm is also explained. In order to implement the model-based controller, an observer is necessary. The unscented Kalman filter (UKF) algorithm is used to illustrate how an observer can be applied to the dynamic models. The UKF algorithm is explained in Chapter 3 as well. Chapter 4 shows the simulation results of the dynamic models, MPC and UKF based on an actual coal plant. Chapter 5 discusses the meaning of the results in Chapter 4. A conclusion of the thesis is given in Chapter 6.

# CHAPTER 2 LITERATURE STUDY

## 2.1 CHAPTER OBJECTIVES

The objectives of this chapter are to determine and show what the current status in literature is regarding the application of control systems to coal plants. In order to define the scope of the literature regarding coal plants, a generic minerals processing flowsheet given in Figure 2.1 shows what unit operations are applicable to this research.

Run-of-mine (ROM) coal ore is either communited or stockpiled for comminution at a later stage. Comminution typically involves the crushing and screening of ore to generate a specific particle size classification for downstream separation (Hayes, 2003). Material that has been sized is usually stored in a silo or bin to act as a buffer between comminution and separation. Coal is primarily separated through gravity or density. Final product is stockpiled and handled for sales.

The scope of the literature study and thesis will include dynamic modelling applied to coal ROM stockpiling right through to coal separation using DMS. Additional literature relating to model-based control in minerals processing and coal are also studied.

## 2.2 DYNAMIC MODELLING FOR ROM STOCKPILING, COMMINUTION AND BIN STORAGE

A minerals processing plant usually receives ROM ore and processes the ore to increase its value. The material is then reduced in size through comminution and separated by sizing before beneficiation. Firth (2009) has identified management approaches that can make a difference to a DMS plant performance.

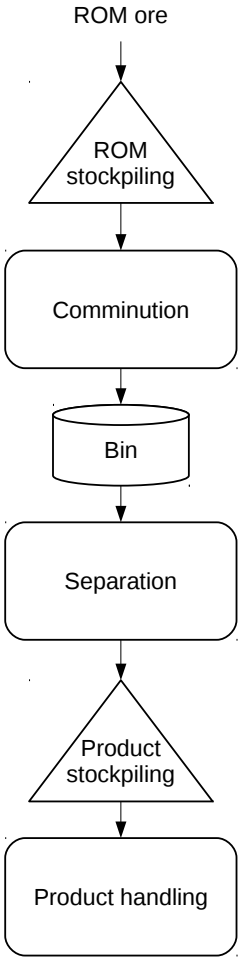


**Figure 2.1:** Generic minerals processing flowsheet [adapted from Wills and Napier-Munn (2006)].

One of the critical factors that can impact a DMS operation is the solids feed rate. The importance of managing the ROM feed to the DMS process cannot be underestimated. In order to ensure continuous flow of material to the minerals processing plant, a storage buffer such as a bin or silo is typically used. If the storage buffer is incorrectly managed, the feed of material to the plant is suboptimal and inefficient.

The available literature regarding the mathematical modelling of these unit processes are detailed below. Typical equipment used within the ROM stockpiling, comminution and bin unit operations include feeders, conveyors, crushers and screens.

A model of a vibratory bowl feeder has been developed using equations of motion (Maul and Thomas, 1997). Stockpile bunker feeders are typically linear vibratory feeders and therefore the bowl feeder

model is not applicable in most cases. Another model developed by Lim (1997) shows another dynamic model of a linear vibratory feeder also based on equations of motion. These dynamic models are more specific to the mechanical behaviour of the feeders and cannot be used for modelling of mass flow.

A similar approach to the mass flow model of a powder feeder system developed by Thayalan and Landers (2006) will be used in this thesis. This principle of dynamic behaviour is based on conservation of mass (Stephanopoulos, 1984). Many of the other equipment models for coal processing are developed using conservation of mass or mass of components.

More detailed mathematical models of crushing equipment are also available in literature such as to improve plant design based on required yield and product shape (Bengtsson *et al.*, 2009), determining the gap setting of an industrial double-roll crusher (Cotabarren *et al.*, 2008) and optimising the design of a differential and grading toothed roll crusher (Zhao *et al.*, 2008). Although these models are useful for the design of crushing plants, they are not necessarily applicable for process control. Similarily, discrete element method simulations (Cleary and Sinnott, 2014) can clearly simulate the breakage of particles. However, these simulations are computationally expensive and usually unsuitable for continuous control and optimisation.

Leite (1990) has developed kinetic models for crushers and screens and also shown how to simulate these systems in closed circuit. The closed circuit used by Leite (1990) similarily represents parts of the coal process in this thesis. As a result, the models derived by Leite (1990) will be used as reference for development of dynamic crushing models. A more recent publication showing models for dynamic crushing plant behaviour is also available in Asbjörnsson *et al.* (2013). Other work on closed crushing circuits include metallurgical models relating process variables using nomographs (Tsakalakis, 2000).

Literature that was found on bin and silo mathematical modelling concentrates on the modelling of flow patterns of material within the vessel. Sielamowicz *et al.* (2014) used linear and nonlinear regression to model the eccentric flow of material within a silo. Dynamic load modelling of cyclic flow of bulk solids during gravity discharge in bins has also been developed in detail (Roberts and Wensrich, 2002; Chen *et al.*, 2005; Tüzün and Nedderman, 1985).

Other mathematical models of bins and silos make use of finite element analysis to describe the three-dimensional flow of material within the vessels. Constitutive models have been developed from material tests and used in finite element calculations for static wall pressures for the prevention of silo damage from coal (Ooi *et al.*, 1996). Similar approaches making use of discrete element methods to describe the mechanical behaviour of material filling and emptying in silos is also available (González-Montellano *et al.*, 2011, 2012).

The use of multiple vibratory bars to control silo stress situations, if silo wall friction and contents can be controlled, has been demonstrated (Hatamura and Takeuchi, 1991). In this case it was shown that only the lateral pressure near the base of a silo was controlled.

Although the modelling methods described above are useful for analysis of material within a bin or silo, they are not suitable for process control (Seborg *et al.*, 1995). The literature describing the control applied to feed processes and silos is limited when compared to the bin and control objectives required for this thesis.

A computer simulation for screens has been developed by Firth *et al.* (1983) and it is indicated that Gottfried (1973) has developed a model for wet screening. This model is a steady-state model and can be used to evaluate the partition coefficients per particle size fraction. The dynamic model of a screen developed by Meyer and Craig (2010) is used in this thesis as it describes the time evolution of material flowing over and through the screen. King (2001) has detailed a considerable number of minerals processing mathematical models. However, these models do not typically include the time evolution of process variables and cannot be used directly for control purposes.

Given the limited availability of dynamic models for bins from the available literature, the process dynamics of a bin are modelled using the principle of mass conservation (Stephanopoulos, 1984). Many of the dynamic models used in this thesis are greybox models and typically include nonlinear process dynamics with associated unknown model parameters. These unknown parameters are determined through system identification techniques described by Ljung (1987). By identifying the unknown parameters with actual plant data the model fit can be determined. Details of this technique has been applied to the dense medium cyclone (DMC) by Meyer (2010).

## 2.3 DYNAMIC MODELLING FOR COAL SEPARATION

Raw coal that is mined contains a number of impurities and is typically processed to improve its overall quality. The mineral processing of this ROM coal involves a complicated and sophisticated operation including comminution, classification and separation. These separation processes normally make use of particle classification on the basis of density (England *et al.*, 2002). Coal, typically being lighter, is separated from the heavier gangue by utilising the difference in specific gravity. These processes can make use of mediums that are made to have specific relative densities to ensure the separation of coal from gangue.

A coal DMS plant makes use of the principle of density separation to upgrade mined coal and produce metallurgical coal or power station coal. The objective of the DMS plant operation is to produce coal product within a minimum quality specification and maximum possible yield (England *et al.*, 2002). Meyer and Craig (2010) have indicated that coal DMS plants do not typically operate at steady state and that setpoint changes should be tracked appropriately in terms of ash content and yield. Almost all DMS plants are only automatically controlled at the regulatory control level in terms of medium density and ore feed rate and there are significant financial implications if the average yield and ash content of product coal can be controlled and optimised.

Coal beneficiation primarily makes use of gravity separation in coal washing (Majumder *et al.*, 2004). It is explained that DMS, specifically the DMC, is the main processing unit used for cleaning coal, beneficiating nearly 55% of coal that is washed worldwide (Honaker and Patwardhan, 2006; De Korte, 2003a). The United States makes use of the DMS process for 65% of its washed coal. It can be determined from the data collected by De Korte (2003b) that 98% of the 53 coal-preparation plants in South Africa are making use of the DMC as their beneficiating unit.

Many static models have been developed for dense medium separation circuits. However, these models are typically not suitable for dynamic controller design for which models that describe the time evolution of variables are required. Napier-Munn (1991) developed a static model for a DMC, which incorporates the partition factor as a function of relative density (RD) and ore feed particle size. This model was derived by substituting equations from Lynch (1977); King and Juckes (1984) and King and Juckes (1988).

Scott and Napier-Munn (1992) developed a similar type of model in which the separation efficiency has been used. Another technique that has been used to model the size-density partition surface of a DMC without the use of the pivot phenomena is stochastic modelling (Rao *et al.*, 2003). A model, which incorporates both size and density partitions, was developed by Rao (2004) who used a Weibull function. This efficiency model makes use of pivot coordinates and density that is size-dependent, as developed by Plitt (1971). A more complicated model developed by Clarkson (1983) makes use of a force balance with turbulence to include more operating variables to simulate the performance of separation. Erasmus (1973) developed an equation which can be fitted to the partition curve by making use of an ideal washer in which no misplacement occurs. This can be evaluated cyclically over time (Napier-Munn, 1991) to obtain an imperfect performance regression model (Erasmus, 1973) that must be fitted to sink and float data.

A computer simulation by Firth *et al.* (1983) was developed to simulate the efficiency of a DMS processes. This technique requires a large number of partition coefficient data sets and feed composition data divided into several relative density fractions with respect to each size fraction. Sufficient information on the separation process and ore feed size distribution with washability data is required in order for the simulation to be accurate. The minerals processing model detailed by King (2001) require similar information regarding population balances of material properties such as particle size or RD fraction.

A number of hydrocyclone models have been developed and are described by Chen *et al.* (2000). These models, however, are primarily developed for particle size classification and not particle separation due to density.

Other DMC models have been developed that make use of more sophisticated techniques such as computational simulations using Eulerian models for the medium and Lagrangian models for the coal particles (Suasnabar and Fletcher, 1999). Brennan (2003) reports on an algebraic slip mixture model which makes use of computational fluid dynamics (CFD) to solve the Reynolds averaged Navier-Stokes equations. Cortés and Gil (2007) indicate that CFD modelling can become very costly owing to the unsteady nature of the flow that requires large eddy simulations or direct numerical simulations.

CFD models that incorporate Navier-Stokes equations (Cortés and Gil, 2007) have also been developed for the DMC; however, these models are computationally very costly and are difficult to incorporate

into an online controller.

A model developed for dense medium baths or drums is referred to by Napier-Munn (1991). This model, developed by Scott and Lyman (1987), uses sedimentation theory to express the separation cutpoint within the drum. Napier-Munn (1991) determined a partition factor equation for the drum separator.

Dynamic process models for the coal DMS process are limited in the available published literature (Meyer and Craig, 2010). Steady-state models developed by Napier-Munn (1991) cannot be used for process control purposes due to the need for time-varying process variables. DMS process models developed by Lyman *et al.* (1982) and Lyman *et al.* (1983) show dynamic process simulations which only focus on the regulatory control aspects such as medium density. A linear relationship between medium density and product coal ash content is assumed. This linear relationship can be viewed as a limitation as the model is only valid within a narrow medium density band.

The dynamic models developed by Meyer and Craig (2010) are detailed in such a way that they can be used to simulate time-varying coal product quality and throughput. These models are based on first principles using conservation of mass and mass of components (Stephanopoulos, 1984) and can be used for simulating and validating process control strategies for DMS circuits. The models developed in Meyer and Craig (2010) were validated by comparing their responses to experimental data obtained from a fine coal DMC circuit. These data were generated from step changes in medium density, and the resulting changes in product ash content were carefully observed (Figure 2.2).

The dynamic process models develop by Meyer and Craig (2010) were for a fine coal DMC. Additional dynamic modelling and verification were conducted for a coarse cyclone in Meyer and Craig (2014). Equipment and operating conditions were different, with the yield being much higher than that of the fine cyclone. Two experiments were performed to verify the models developed in Meyer and Craig (2014). The first experiment used a step change in throughput while medium density was kept constant. The second experiment used a step change in medium density while throughput was kept constant. These steps were found by searching historical production data for large input changes such that the derived models could be validated over a wide range of operating conditions.

Additional validation for the dynamic models of Meyer and Craig (2010) are presented in Meyer and

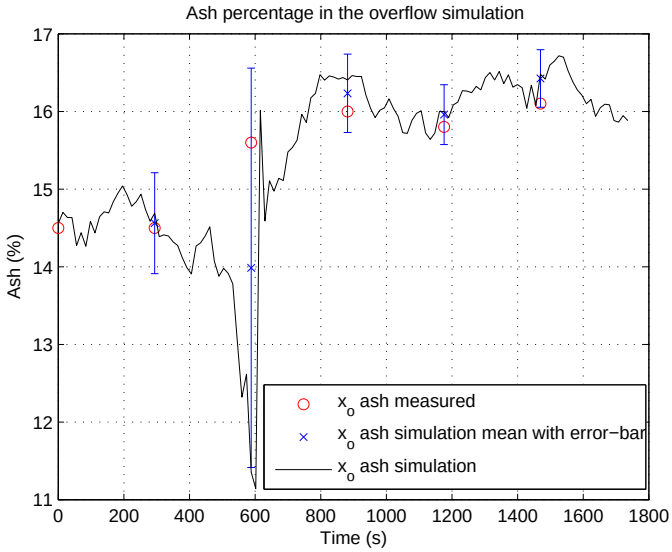


**Figure 2.2:** DMC dynamic model simulated ash content (with error-bar having 95% confidence interval) compared to measured ash content in overflow [taken from Meyer and Craig (2010)].

Craig (2011), where the DMC model was reduced to a steady-state model which represents a DMC partition curve. Meyer and Craig (2014) further validates the DMC model by reducing the dynamic model developed from each experiment into a steady-state partition curve.

Meyer and Craig (2011) shows how a dynamic DMC model can be reduced to a steady-state model. This steady-state model is similar to that of a partition curve used to determine the efficiency of a DMC. The principle used to generate such a curve is float and sink analysis where coal samples are collected and separated using different relative density fractions.

England *et al.* (2002) details the float and sink analysis used in this thesis. Figure 2.3 illustrates how a sample is separated using containers with liquids of decreasing specific gravity (SG). The float of each container is recovered and used as feed for the next container. The analysis is performed at steady-state as each container must allow the sample to settle and separate.

By analysing the sinks at each density fraction, it is possible to generate a partition curve (England *et al.*, 2002). Figure 2.4 shows the actual partition curve of a coarse DMC as determined from plant data (Meyer and Craig, 2014).

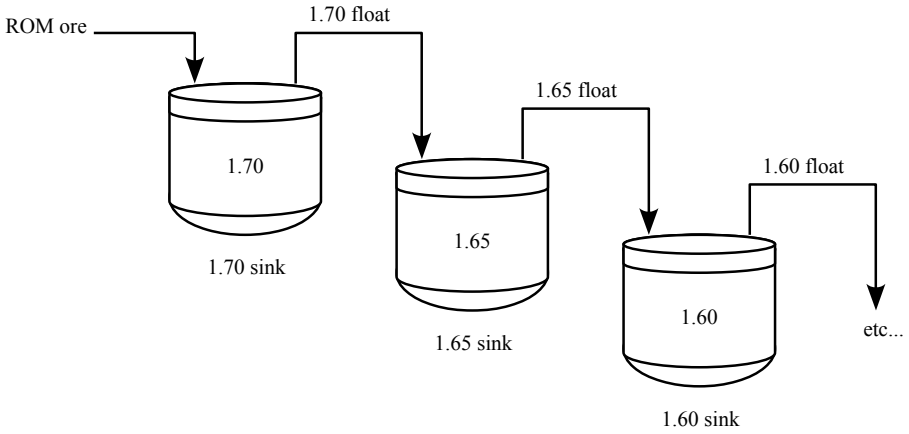


**Figure 2.3:** Sink and float analysis used to determine a partition curve (numerical values represent liquid SG).

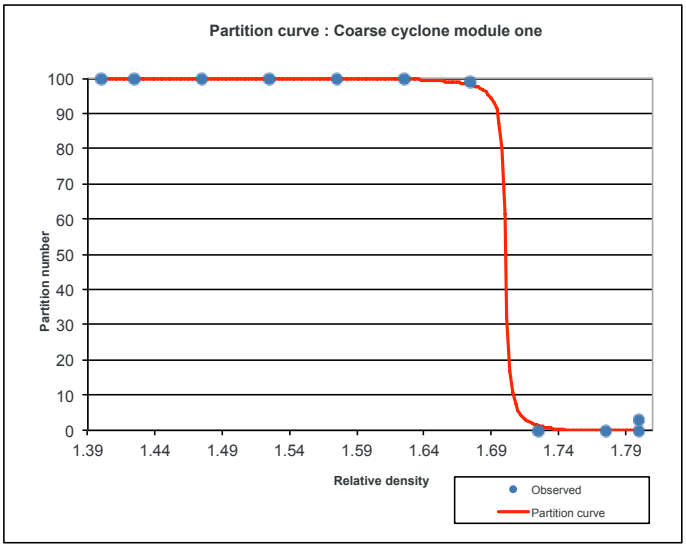


**Figure 2.4:** Actual coarse cyclone (-25+6mm coal) partition curve [taken from Meyer and Craig (2014)].

The separation cutpoint ($\rho_{50}$) can be determined as 1701 kg/m$^3$ - this is the specific density where a particle will have an equal chance of reporting to a float or sink. The écart probable moyen (EPM) is determined as 0.0020 SG based on the partition curve in Figure 2.4. This low EPM is possibly due to the organic efficiency (ratio between actual yield achieved and theoretical yield from washability data) being very high (100%).

The simulated steady-state partition curve was shown to be similar to that in Figure 2.4. The predicted

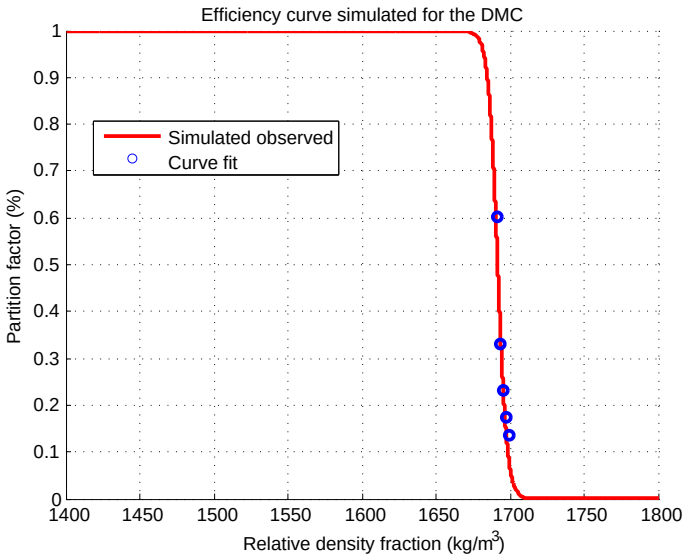


**Figure 2.5:** Simulated efficiency curve for the DMC using the steady-state model reduced from a dynamic DMC model [taken from Meyer and Craig (2014)].

mass distributions to float and sink products at different particle densities in the feed ($\rho_{i,ore}$) are obtained by simulating the partition factor at different medium densities. By starting with a finite amount of mass in the feed and simulating the separation at steady-state at a high density, the resulting mass in the float can be used as the feed for the next steady-state simulation. With decreasing medium density iterations, the resulting partition factors can be obtained. The simulation should start slightly higher than the expected $\rho_{50}$ to generate the efficiency portion of the curve. Figure 2.5 was generated by simulating the dynamic simulations at steady-state and plotting the results.

Table 2.1 shows a summary of the efficiency parameters that Meyer and Craig (2014) obtained for the simulated partition curve and the actual plant operation cyclone efficiency curve. This simulation indicates that a dynamic DMC model can be reduced to a realistic steady-state model from which a partition curve can be generated. The actual partition curve in Figure 2.4 was determined at a different time period to when the simulated partition curve was generated. This could be a possible reason as to why the EPM differs slightly between the actual and simulated partition curve.

An additional aspect incorporated into the DMC model includes the pressure measurement (Figure 2.6) of the feed to the cyclone to relate to the density of the feed mix (Meyer and Craig, 2014).

Another dynamic model developed by Meyer and Craig (2015) is of the dense medium drum (DMD)

**Table 2.1:** Partition curve efficiency results summary.

| Efficiency parameter | Simulated steady-state model results (SG) | Actual plant results (SG) |
|---|---|---|
| $\rho_{50}$ | 1.692 | 1.701 |
| $E_p$ | 0.0035 | 0.0020 |

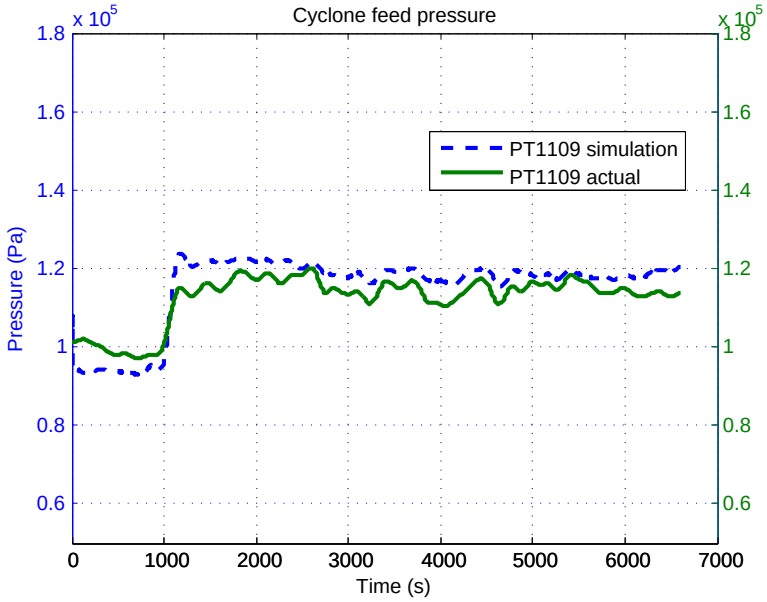


**Figure 2.6:** DMC dynamic model simulated feed pressure (PT1109) versus actual feed pressure [taken from Meyer and Craig (2010)].

separator. This model is based on a Wemco drum. DMDs are unit processes that are typically used to beneficiate coal, iron ore and other minerals by making use of density separation. Some coal dense medium separation plants typically include a DMD separator to process larger sized coal particles. The operational management of this unit process is often limited to localised control of medium density and feed mass flow rate. The DMD model parameters were determined using system identification (Ljung, 1987) and the performance of the model was evaluated using actual plant data from a Wemco drum. Coal washability and drum partitioning behaviour were also used to estimate the grade of the product for model grade simulation and validation.

The dynamic models developed by Meyer and Craig (2010) (author's Master of Engineering degree) for the fine coal DMC, coarse (Meyer and Craig, 2014) DMC and DMD (Meyer and Craig, 2015) are

detailed and used in this thesis.

## 2.4 MODEL-BASED CONTROL IN MINERALS PROCESSING AND COAL PREPARATION

Implementing a control system requires a high level of process understanding (Lipták, 1995) that can lead to improved plant performance in terms of stability and economics (Bauer and Craig, 2008). Process control enables the reduction of plant upsets due to disturbances and ensures a plant keeps to its desired setpoints, i.e. it reduces the difference between the desired specifications and measured controlled variables. Control systems typically make use of a mathematical model that incorporates the plant dynamics, and a well controlled plant will reach its steady state in the fastest time possible after startup, process setpoint changes and process disturbances.

By applying the concepts of process control to coal DMS, there is an opportunity to improve product yield and quality, e.g. reducing ash in the coal products. Process control could allow for an improvement in current coal beneficiation operations and it is for this reason that the dynamic DMS circuit model described here was developed.

Mathematical models are generally used in process controller design to improve process performance and stability and ultimately ensure economic benefits (Bauer and Craig, 2008). It is often necessary to develop a model that is simple enough to be used for control, but sophisticated enough to capture the plant dynamics. Craig and Henning (2000) describe a general control framework, illustrated in Figure 2.7, where a mathematical model of the real plant needs to be developed before a control system can be designed. Once the control system performs satisfactorily in simulation it is then implemented and monitored to ensure its value has been realised.

Bauer and Craig (2008) show that the process control method of choice is MPC (Camacho and Bordons, 2004). The MPC makes use of a dynamic model to predict future outputs based on current and past inputs and outputs. Using a reference setpoint, calculated future errors are used by an optimiser with a cost function and process constraints to determine future process inputs. This thesis will also discuss the possible cost functions and process constraints applicable to coal processing plants.

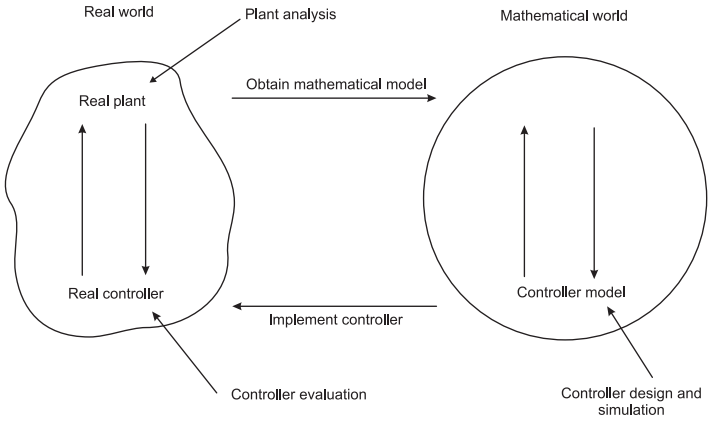


**Figure 2.7:** General control framework [taken from Craig and Henning (2000)].

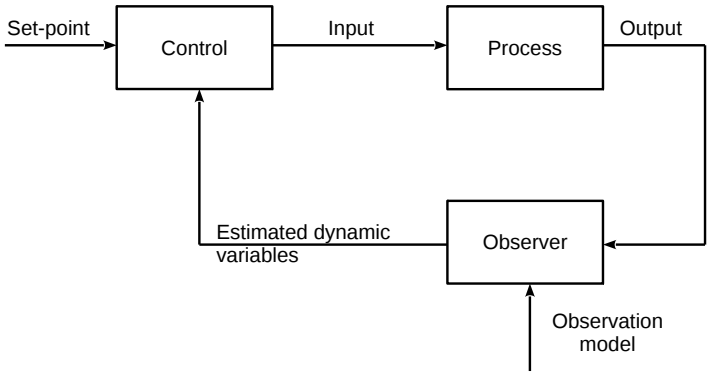


**Figure 2.8:** General control loop [adapted from Hodouin (2011)].

Hodouin (2011) describes methods for automatic control, observation and optimisation in mineral processing plants. Figure 2.8 indicates how a typical control system operates with a given observer. The observer uses measured outputs with an observation model to estimate dynamic variables for control. In this case the dynamic coal models can be used as an observer model. An observer such as the UKF can improve the estimation of the state variables for a control system. The improved state variable estimation is ideal for a practical implementation of a control system of for example a DMS plant as it can improve the accuracy of the state estimates fed to the controller.

In order to the increase the accuracy of the model fit, an observer is typically used. The specific observer used in this thesis is the UKF. Various other nonlinear filters are available (Daum, 2005) such as particle filters, batch filters and exact recursive filters. Daum (2005) indicates that nonlinear filters usually provide vastly superior performance compared to the traditional Kalman filter. Particle filters make use of Monte Carlo integration using importance sampling for the prediction of statistical

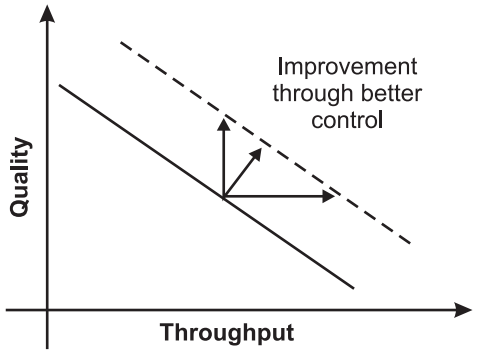


**Figure 2.9:** General throughput versus quality relationship with improvement through better control [taken from Bauer and Craig (2008)].

outputs. The Monte Carlo integration of particle filtering will not be used. However, an example of particle filtering applied to a ROM ore mill has been shown by Olivier *et al.* (2012b). Batch filters use numerical integration to solve for prediction of outputs over a single batch of data. This approach is similar to the system identification approach used in this thesis. However, instead of solving for unknown states, unknown parameters are solved for. Exact recursive filters use numerical integration of ordinary differential equations (ODEs) to solve for sufficient statistics in the exponential family of probability densities. The term "exact" implies that partial differential equations are transformed into ODEs where the Kalman filter is an example of this.

Daum (2005) describes the extended Kalman filter (EKF) and the UKF as different to the Kalman filter in that they do not apply only to linear-Gaussian problems. The EKF (Julier and Uhlmann, 1997) predicts outputs based on linear approximations of the process dynamics by simply using the first-order Taylor series expansion of the system state equations. The UKF does not use simple linear approximations like the EKF. The UKF (Wan and Van der Merwe, 2000) instead uses a more accurate approximation to evaluate the multidimensional integrals required. Since many of the coal models developed already have the form of nonlinear state equations, the UKF is applied to perform the state observations.

The relationship between yield and ash through the washability characteristics of the coal (England *et al.*, 2002) can be used to evaluate the quality of the coal product. Figure 2.9 illustrates the typical inverse relationship between throughput and quality (Bauer and Craig, 2008). Using coal washability, a similar inverse relationship would occur between coal throughput and yield.

Although many of the sources available in literature show the application of observers for estimation and control in minerals processing, no literature was found relating to coal DMS plants. Meyer and Craig (2015) show how the UKF was applied to coal bins for storage or buffer capacity. Herbst *et al.* (1992) have used a Kalman filter to estimate the ball and rock holdup for the model-based control of a semi-autonomous grinding mill. Olivier *et al.* (2012b) have shown how to apply both state and parameter estimation using dual particle filters and applied them to a run-of-mine ore mill. Further work on observers applied to milling include a fractional order disturbance observer and a Bode ideal cut-off observer (Olivier *et al.*, 2012a). Wilson *et al.* (1998) describe experiences in implementing the EKF on an industrial batch reactor which is related to a specific chemical process. In the coal environment, Clarke *et al.* (1989) use a Kalman filter to estimate the load and pressure of coal-fired boilers. Pindyck (1999) show an interesting application where a Kalman filter was used to estimate the forecasting of oil, coal and natural gas prices.

MPC has been applied to a coal feeding process over six belt conveyors for a coal-fired power plant (Luo *et al.*, 2014). Nonlinear coal mill modelling and its application to MPC has also been shown (Cortinovis *et al.*, 2013). The objective of the MPC was to improve energy efficiency through coordinating belt speed and feed rate or coordinating operating status and time. Open loop optimal control has also been applied to belt conveyors (Zhang and Xia, 2010, 2011). Optimal energy management for a jaw crushing process in deep mines has shown that by using a switching control technique, it is possible to reduce energy cost and consumption of a jaw crushing station (Numbi *et al.*, 2014).

Zhang and Xia (2014) have shown how MPC can be applied to the models developed by Meyer and Craig (2010) to simulate the control of carbon content by manipulating the density of medium in real-time according to feedback of DMC outputs. This thesis will apply a similar approach to Zhang and Xia (2014) for the control of a coal plant. Another article by Zhang *et al.* (2015) illustrates how optimal control can be used to control the DMC based on minimizing medium density to reduce energy costs while keeping the percentage of carbon content in the DMC product stable.

An interesting simulation result obtained by Zhang and Xia (2014) is the performance of a MPC in tracking a set value of carbon content with delayed measurements. This is very applicable for the control of product grade in coal plants as the measured product grade is usually measured at very slow intervals due to the time taken for sampling and laboratory analysis. Figure 2.10 illustrates the mean deviation from a set carbon content value as delays in sampling are introduced. The more the delay,

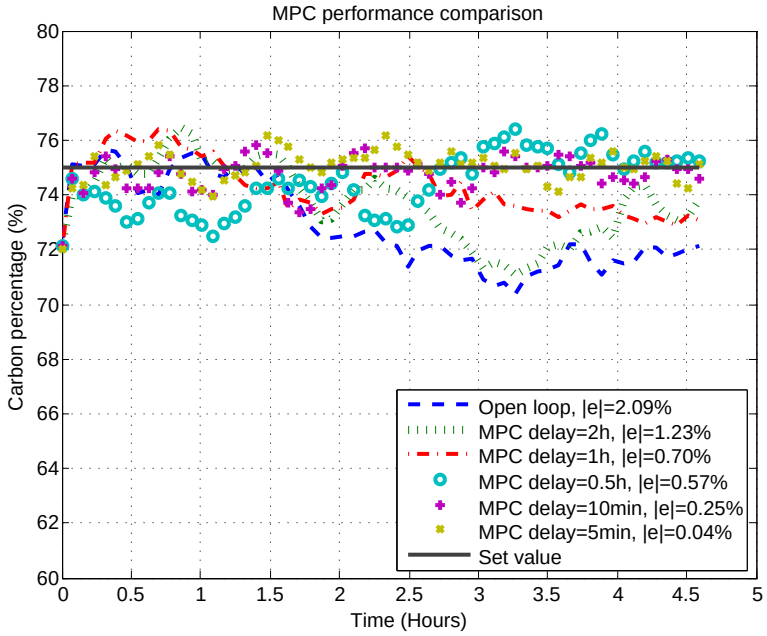


**Figure 2.10:** MPC performance conparison of DMC carbon content with varying time delay [taken from Zhang and Xia (2014)]. $|e|$ is the mean deviation from the set value.

the more the error in achieving better control for an applicable set value in carbon content.

# CHAPTER 3 METHODS

## 3.1 CHAPTER OVERVIEW

This chapter describes the methods used to address the research objectives and questions given in Chapter 1. A specific coal plant process will be used for the evaluation of model-based control. An overview of this process is given, followed by a detailed description of available dynamic models for coal unit processes or equipment. The system identification process is briefly described to explain how dynamic models are fitted to process data by solving for unknown parameters. Steady-state models that are applicable to coal processing are also explained. Finally, a detailed description of MPC is given with a proposed implementation architecture for coal plants.

## 3.2 COAL PROCESS OVERVIEW

This section provides an overview of an actual coal process that was used for this thesis. The comminution and separation unit processes shown in Figure 2.1 are shown in some more detail in Figures 3.1 and 3.2.

The comminution process (Figure 3.1) is typically fed by a ROM stockpile with a number of feeders onto a single conveyor belt. The ROM feed from the stockpile is then screened with the oversize being crushed in closed circuit. The undersize is typically fed into a bin to act as a buffer to ensure consistent feed to the separation unit process further downstream.

The separation unit process (Figure 3.2) is fed by the ROM material from the comminution unit process. The ROM material is further classified to be processed by either a DMD for larger sized

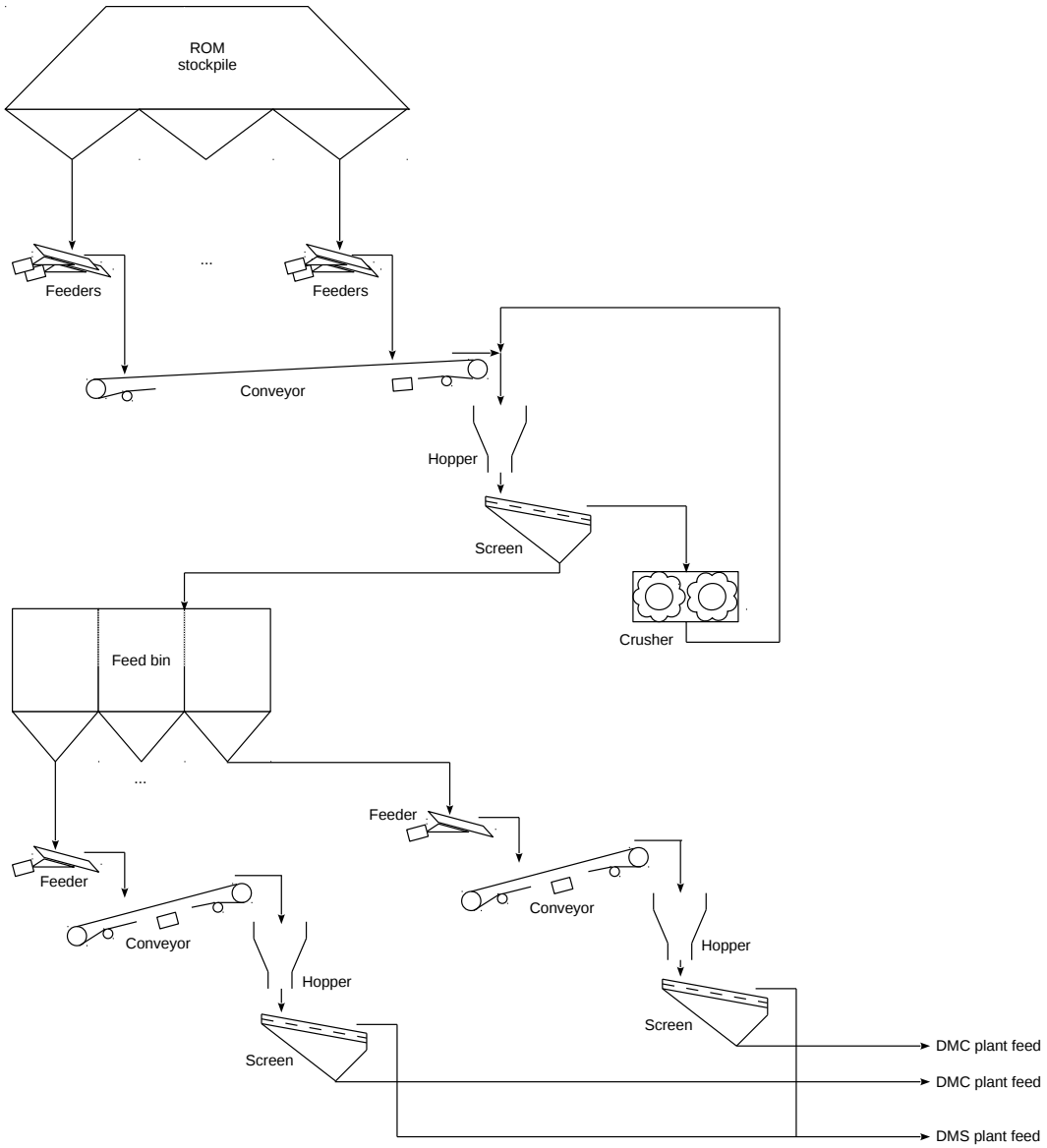


**Figure 3.1:** Simplified comminution unit process flow diagram.

particles (+28mm) or a DMC for smaller sized particles (-28mm). Finer coal material (-1mm) is fed to a thickener where process water is recovered while the fines are made into a cake through a belt filter or filter press.

Details of the DMD and DMC separation processes are shown in Figures 3.3 and 3.4. The DMD separation process (Figure 3.3) mixes the ROM material with magnetite medium in a mixing box and is separated by a DMD. The coal (less dense than the medium) floats while the discard (more dense than the medium) sinks. The sinks are collected by a rotating drum and collected into a launder at the centre of the DMD. Both floats (product) and sinks (discard) are rinsed in separate streams using a

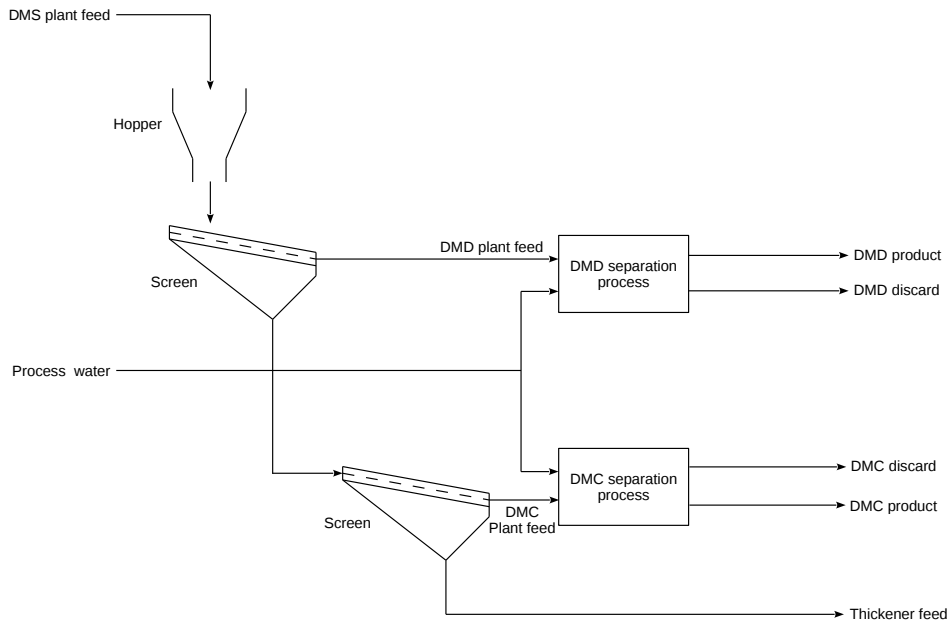


**Figure 3.2:** Simplified separation unit process flow diagram.

drain and rinse screen. Magnetite medium is recovered and recycled back into the circuit.

The DMC separation process (Figure 3.4) also uses magnetite medium to separate product from discard. However, the process is much faster with the DMC. Both product and discard are also rinsed in separate streams through a drain and rinse screen, similar to that of the DMD separation process. Magnetite medium is also recovered and recycled back into the circuit.

## 3.3 DYNAMIC MODELS

Detailed descriptions of the process dynamics for each equipment typically used in the primary coal value chain of coal processing are given below. These equipment have also been labelled in Figures 4.1, 4.33, 3.3 and 3.4. The mathematical models used in this thesis are described below.

### 3.3.1 Feeder model

The stockpile bunker and feed bin draw points in Figure 4.1 are modelled using a vibratory feeder dynamic model. A model of a vibratory bowl feeder has been developed using equations of motion (Maul and Thomas, 1997). The stockpile bunker feeders are linear vibratory feeders and therefore

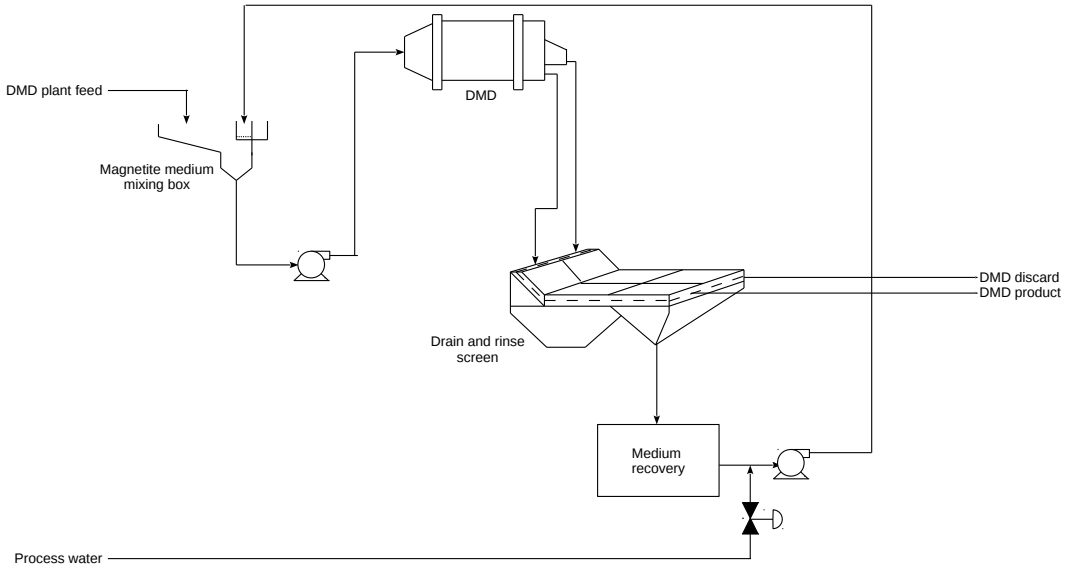


**Figure 3.3:** Simplified DMD separation unit process flow diagram.

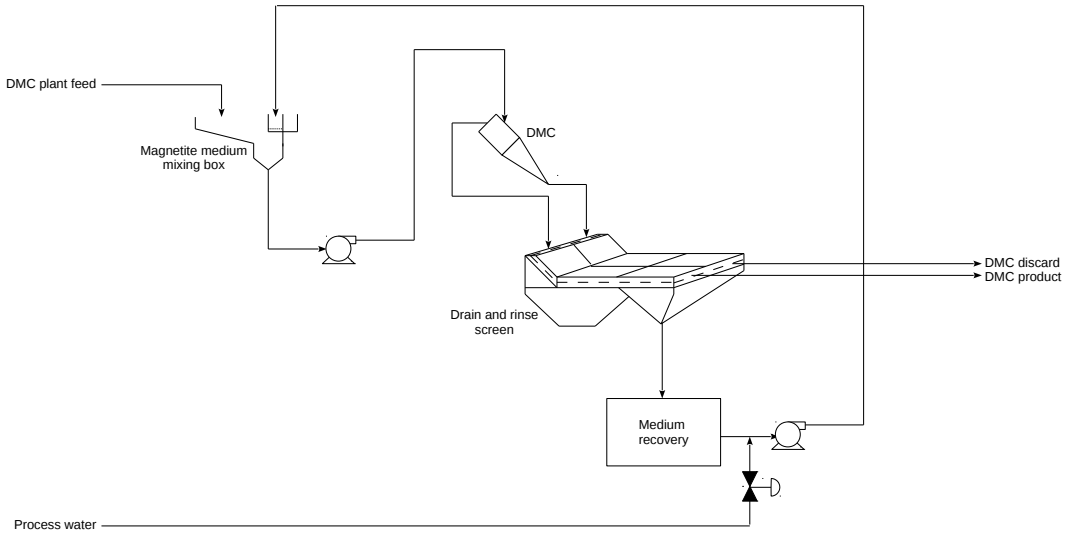


**Figure 3.4:** Simplified DMC separation unit process flow diagram.

the bowl feeder model is not applicable in this case. Another model developed by Lim (1997) shows another dynamic model of a linear vibratory feeder also based on equations of motion. These dynamic models are more specific to the mechanical behaviour of the feeders and cannot be used for modelling of mass flow.

A similar approach to the mass flow model of a powder feeder system developed by Thayalan and Landers (2006) and Meyer *et al.* (2015) will be used in this thesis. Figure 3.5 illustrates an example of

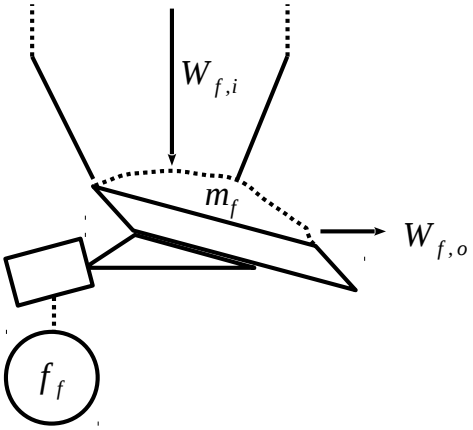


**Figure 3.5:** Feeder model schematic.

**Table 3.1:** Feeder model variables and descriptions

| Variable | Description |
|---|---|
| $m_f$ | Mass on feeder (kg) |
| $\tau_f$ | Feeder time constant (s) |
| $K_f$ | Feeder proportionality constant (kg) |
| $f_f$ | Feeder motor speed (Hz) |
| $W_{f,o}$ | Mass flow rate from a feeder (kg/s) |

a feeder system. From a conservation of mass perspective (Stephanopoulos, 1984), using a first order system, the rate of change in mass on a feeder ($m_f$) can be described as,

$$\frac{dm_f}{dt} = K_f f_f - \frac{m_f}{\tau_f}, \tag{3.1}$$

where $\tau_f$ is the time constant for the system to reach approximately 63.2% of its final value, $K_f$ is the proportionality constant relating motor speed to a mass flow rate and $f_f$ is the motor speed.

The mass flow rate of material fed to the stockpile is not known and as a result, it is assumed that the stockpile volume is always full. The output of the feeder is described as follows,

$$W_{f,o} = \frac{m_f}{\tau_f}, \tag{3.2}$$

where $W_{f,o}$ is the mass flow rate from the feeder. Table 3.1 describes the variables used for the feeder model.

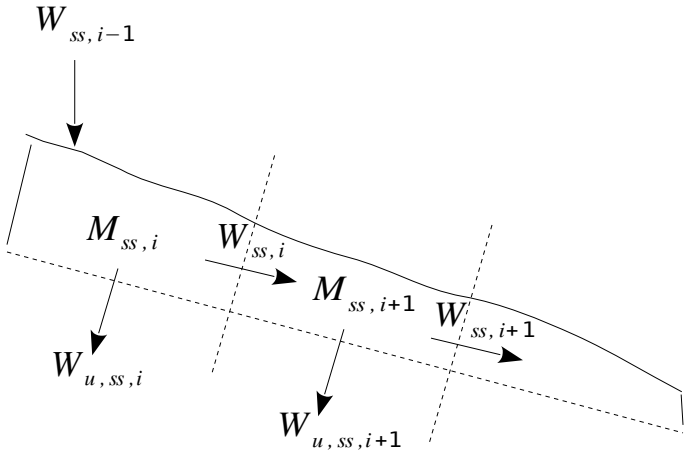


**Figure 3.6:** Simplified representation of the mass distribution for a single-deck screen [adapted from Meyer and Craig (2010)].

In the case of the bin model described below, its feeders' behaviour is more complex. As a result the proportionality constant $K_f$ becomes a function of the bin level. Details of this behaviour are explained in the bin model subsection below.

### 3.3.2 Screen model

In the development of a dynamic model for a single-deck screen by Meyer and Craig (2010), the conservation of overall mass was used. This was applied to each section of the screen to form an approximation of a distributed parameter system. Figure 3.6 illustrates a simplification of this mass distribution. The following is a list of assumptions were made for the modelling of the single deck screen:

- The screen is a distributed parameter system, but can be approximated with $n$ first order lumped parameter systems or components.
- The overflow and underflow mass feed rates ($W_{ss,i}$ and $W_{u,ss,i}$) of each component $i$ are proportional to their mass ($M_{ss,i}$) on top of each component $i$.
- The proportion of mass split ($\alpha_{ss}$) for each component $i$ is dependent on the particle size distribution of the feed ($\sqrt[n]{\frac{W_{ss,n}}{W_{ss,0}}}$).

**Table 3.2:** Single-deck screen model variables and descriptions

| Variable | Description |
|---|---|
| $W_{ss,i-1}$ | Mass feed rate of the ore fed into component $i$ (kg/s) |
| $W_{ss,i}$ | Mass feed rate of the ore overflow exiting mass component $i$ (kg/s) |
| $W_{u,ss,i}$ | Mass feed rate of the ore underflow exiting mass component $i$ (kg/s) |
| $M_{ss,i}$ | Mass of ore for mass component $i$ (kg) |
| $\alpha_{ss}$ | Percentage of mass split for mass component $i$ |
| $\tau_{ss,o}$ | Time taken for ore to be transported over screen component $i$ (s) |
| $\tau_{ss,u}$ | Time taken for ore to be transported through screen component $i$ (s) |

Using these assumptions, the rate of change of mass of component $i$ is given as,

$$\frac{dM_{ss,i}}{dt} = W_{ss,i-1} - \alpha_{ss}\frac{M_{ss,i}}{\tau_{ss,o}} - (1-\alpha_{ss})\frac{M_{ss,i}}{\tau_{ss,u}}. \tag{3.3}$$

Modelling each mass component $i$ of the single-deck screen for a maximum of $n$ components, result in $W_{ss,0}$ being the initial feed into the screen and $W_{ss,n}$ being the final mass feed rate of the oversize material. The undersize material is collected and can be taken as the sum of all underflow mass components (i.e. $\sum_{i=1}^{n} W_{u,ss,i}$). The associated variables for this model are described in table 3.2.

Similar to the development of the single-deck screen dynamic model, the conservation of overall mass is also used here, and is applied to each section of each deck of a double-deck screen to form an approximation of a distributed parameter system (Meyer and Craig, 2010). Figure 3.7 illustrates a simplification of the mass distribution for the double deck screen with associated variables for this model described in Table 3.3. The following is a list of assumptions made:

- Each deck of the screen is a distributed parameter system, but can be approximated with $n$ first order lumped parameter systems or components.

- The overflow and underflow mass feed rates ($W_{ds,o,i}$, $W_{u,ds,o,i}$, $W_{ds,c,i}$, and $W_{u,ds,c,i}$) of each component $i$ are proportional to their mass ($M_{ds,o,i}$ and $M_{ds,c,i}$) on top of each component $i$ for both the top and bottom deck.

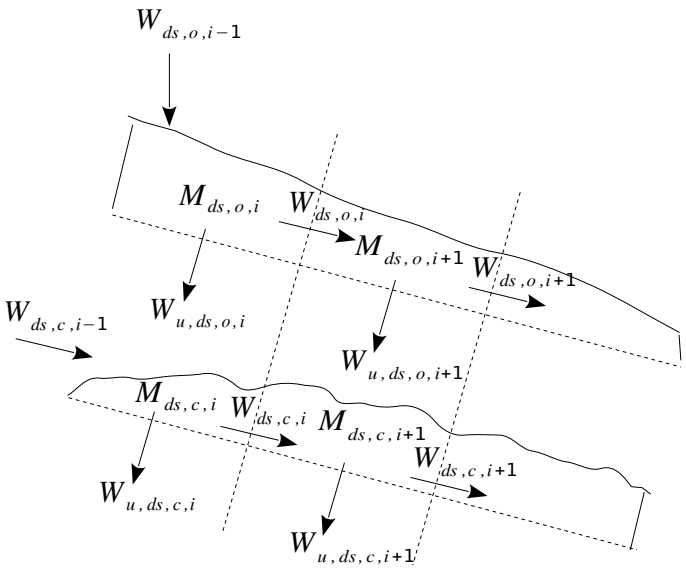


**Figure 3.7:** Simplified representation of the mass distribution for a double-deck screen [adapted from Meyer and Craig (2010)].

- The proportion of mass split ($\alpha_{ds,o}$ and $\alpha_{ds,c}$) for each component $i$ on the top and bottom deck is dependent on the particle size distribution of the feed ($\sqrt[n]{\frac{W_{ds,o,n}}{W_{ds,o,0}}}$ and $\sqrt[n]{\frac{W_{ds,c,n}}{W_{ds,o,0}}}$).

Using these assumptions, the top and bottom rate of change of mass of component $i$ is given as:

$$\frac{dM_{ds,o,i}}{dt} = W_{ds,o,i-1} - \alpha_{ds,o}\frac{M_{ds,o,i}}{\tau_{ds,o}} - (1-\alpha_{ds,o})\frac{M_{ds,o,i}}{\tau_{u,ds,o}}, \tag{3.4}$$

$$\frac{dM_{ds,c,i}}{dt} = W_{ds,c,i-1} + W_{u,ds,o,i} - \alpha_{ds,c}\frac{M_{ds,c,i}}{\tau_{ds,c}} - (1-\alpha_{ds,c})\frac{M_{ds,c,i}}{\tau_{u,ds,c}}. \tag{3.5}$$

Modelling each mass component $i$ of each deck for a maximum of $n$ components, result in $W_{ds,o,0}$ being the initial feed into the double-deck screen, $W_{ds,o,n}$ being the final mass feed rate of the oversize material for the top deck and $W_{ds,c,n}$ being the final mass feed rate of the oversize material for the bottom deck or coarse material. The undersize material of the bottom deck is collected and can be taken as the sum of all underflow mass components (i.e. $\sum_{i=1}^{n} W_{u,ds,c,i}$).

The screen models used in this thesis are simplified to only have one mass state on each deck. This implies that the screen model has been lumped (i.e. $n = 1$).

**Table 3.3:** Double-deck screen model variables and descriptions

| Variable | Description |
|---|---|
| $W_{ds,o,i-1}$ | Mass feed rate of the ore fed into component $i$ on the top deck (kg/s) |
| $W_{ds,o,i}$ | Mass feed rate of the ore overflow exiting mass component $i$ on the top deck (kg/s) |
| $W_{u,ds,o,i}$ | Mass feed rate of the undersized ore exiting mass component $i$ from the top deck (kg/s) |
| $M_{ds,o,i}$ | Mass of ore on the top deck for mass component $i$ (kg) |
| $\alpha_{ds,o}$ | Percentage of mass split on the top deck for mass component $i$ |
| $\tau_{ds,o}$ | Time taken for ore to be transported over the top deck screen component $i$ (s) |
| $\tau_{u,ds,o}$ | Time taken for ore to be transported through the top deck screen component $i$ (s) |
| $W_{ds,c,i-1}$ | Mass feed rate of the ore fed into component $i$ on the bottom deck (kg/s) |
| $W_{ds,c,i}$ | Mass feed rate of the ore overflow exiting mass component $i$ on the bottom deck (kg/s) |
| $W_{u,ds,c,i}$ | Mass feed rate of the undersized ore exiting mass component $i$ from the bottom deck (kg/s) |
| $M_{ds,c,i}$ | Mass of ore on the bottom deck for mass component $i$ (kg) |
| $\alpha_{ds,c}$ | Percentage of mass split on the bottom deck for mass component $i$ |
| $\tau_{ds,c}$ | Time taken for ore to be transported over the bottom deck screen component $i$ (s) |
| $\tau_{u,ds,c}$ | Time taken for ore to be transported through the bottom deck screen component $i$ (s) |

### 3.3.3 Crusher model

Although various crusher mathematical models are available in literature as discussed in Chapter 2, no specific dynamic model for a double roll crusher could be found in the available literature. However, a dynamic model of a ball mill by Rajamani and Herbst (1991) was found. Although the physical operation and mechanism of particle size reduction is different between a double roll crusher and ball mill, the process description of material entering the ball mill and exiting with a different particle size

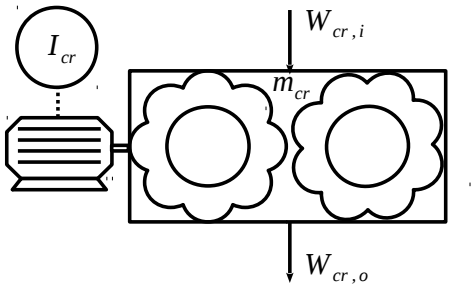


**Figure 3.8:** Crusher model schematic.

distribution is similar to that of a double roll crusher. On the basis that the double roll crusher and ball mill reduce material in particle size, the ball mill dynamic model from Rajamani and Herbst (1991) was modified and simplified to represent a double roll crusher model. Other mill models have also been used in various MPC and model predictive static programming applications (Coetzee *et al.*, 2010; Le Roux *et al.*, 2014). However, these mill models were not considered for the double roll crusher model development.

The dynamic mill model from Rajamani and Herbst (1991) describes a simplified ball mill operating in open circuit with a feed rate of $M_{MF}$ and size reduction occurring in the mill as,

$$\frac{dHR_{MP,k}}{dt} = M_{MF}R_{MF,k} - F_k HR_{MP,k} - M_{MF}R_{MP,k}, \tag{3.6}$$

where $M_{MF}$ is the fresh solids feed rate, $H$ is the mill hold-up mass, $R_{MP,k}$ and $R_{MF,k}$ are the fraction of solids retained above size interval $k$ in product (subscript $MP$) and feed (subscript $MF$). $F_k$ is a product of a selection function [$S_k = S_k^E(P/H)$] and breakage function ($S_k^E$) which is approximately invariant. The power drawn from the mill ($P = VI$) is the product of the voltage ($V$) and current ($I$) required to drive the mill motor system.

In the case of Rajamani and Herbst (1991) the mill hold-up ($H$) is assumed constant allowing for Equation 3.6 to model the dynamics of change in product fraction of solids ($R_{MP,k}$). For the dynamic model of the double roll crusher, the opposite is assumed where the hold-up ($m_{cr}$) in the crusher is dynamic while the product fraction of solids is constant ($R_{cr,o,k}$). A representation of a simplified crusher that is used for this thesis can be found in Figure 3.8.

It is assumed that the crusher has one mass state ($m_{cr}$) representing the material hold-up within it. Using conservation of mass (Stephanopoulos, 1984) and the ball mill dynamic model (Equation 3.6),

the rate of change in mass state within the crusher can be represented as,

$$\frac{dm_{cr}}{dt} = \frac{R_{cr,i,k}}{R_{cr,o,k}} W_{cr,i} - \frac{m_{cr}}{\tau_{cr}} - K_{cr,k,1} I_{cr}, \tag{3.7}$$

where $W_{cr,i}$ is the mass flow rate of the feed into the crusher, $R_{cr,i,k}$ and $R_{cr,o,k}$ are the feed (subscript $i$) and product ($o$) fraction of solids retained above size interval $k$. $\tau_{cr}$ is the time constant of the crushed material discharged from the crusher, $I_{cr}$ is the motor current drawn for the rotation of the crusher rollers and $K_{cr,k,1}$ is the proportionality constant incorporating the constants from the selection function such as voltage ($U_a$) and breakage rate ($S_k^E$).

Assuming that the motor driving the double roll crusher is direct current (DC), it is possible to describe the dynamics of the motor electric armature current ($i_a$) and mechanical system motor speed ($\omega_m$). Yildiz (2012) and Mahfouz *et al.* (2013) represent the system dynamics of a DC motor as follows,

$$E_c + R_a i_a + L_a \frac{di_a}{dt} = U_a, \tag{3.8}$$

$$B_1 \omega_m + J \frac{d\omega_m}{dt} = T_e - T_L, \tag{3.9}$$

where $E_c = K_b \omega_m$ is the back electromotive force, $T_e = K_b i_a$ is the produced torque, $U_a$ is the terminal voltage of the DC motor, $R_a$ is the armeture resistance, $T_L$ is the load torque (assumed to be related to the crusher mass state $m_{cr}$ with proportionality constant $K_L$), $J$ is the torque of inertia and $B_1$ is the viscous friction coefficient. $K_b$ is a proportionality constant for both torque and back electromotive force.

By assuming the mechanical system motor speed acceleration ($\frac{d\omega_m}{dt}$) is zero, it is possible to rearrange Equations 3.8 and 3.9 with simplified proportionality constants as follows,

$$\frac{dI_{cr}}{dt} = K_{cr,k,2} - \frac{K_{cr,k,2}}{I_{cr,min}} I_{cr} + K_{cr,k,3} m_{cr}, \tag{3.10}$$

where $I_{cr_m in}$ is the crusher motor current at no load, $K_{cr,k,2} = \frac{U_a}{L_a}$ and $K_{cr,k,3} = \frac{K_b K_L}{B_1 L_a}$ are a proportionality constants relating the rate of change in crusher motor current to motor current and load torque.

It is assumed that the load torque is proportional to the crusher hold-up mass ($m_{cr}$). Equation 3.10 is simplified to only two parameters ($K_{cr,k,2}$ and $K_{cr,k,3}$) by deriving the relationship for $\omega_m = \frac{K_b I_{cr,min}}{B_1}$ from Equation 3.9 by assuming $m_{cr} = 0$ at no load and a minimum motor current ($I_{cr,min}$). Substituting the resultant $\omega_m$ into Equation 3.8 yields the relationship $\frac{U_a}{I_{cr,min}} = \frac{K_b^2}{B_1} + R_a$ which allows for the proportionality constant $K_{cr,k,2}$ to be used twice in Equation 3.10.

**Table 3.4:** Crusher model variables and descriptions

| Variable | Description |
|---|---|
| $m_{cr}$ | Mass in crusher (kg) |
| $R_{cr,i,k}$ | Feed fraction of solids retained above size interval $k$ |
| $R_{cr,o,k}$ | Product fraction of solids retained above size interval $k$ |
| $\tau_{cr}$ | Crusher time constant (s) |
| $K_{cr,k,1}$ | Crusher mass hold-up proportionality constant for size interval $k$ incorporating the crusher selection function [kg/(sA)] |
| $I_{cr,min}$ | Motor current when crusher has no load (A) |
| $I_{cr}$ | Crusher motor current (A) |
| $K_{cr,k,2}$ | Crusher motor current proportionality constant for size interval $k$ (A/s) |
| $K_{cr,k,3}$ | Crusher motor current proportionality constant for torque load at size interval $k$ [A/(kg.s)] |
| $W_{cr,o}$ | Mass flow rate from a crusher (kg/s) |
| $W_{cr,i}$ | Mass flow rate into a crusher (kg/s) |

The output equations of the crusher are described as follows,

$$\mathbf{y_{cr}} = \begin{pmatrix} y_{cr,1} \\ y_{cr,2} \end{pmatrix} = \begin{pmatrix} W_{cr,o} \\ I_{cr} \end{pmatrix} = \begin{pmatrix} \frac{m_{cr}}{\tau_{cr}} \\ I_{cr} \end{pmatrix}. \tag{3.11}$$

Table 3.4 describes the variables used for the crusher model.

### 3.3.4 Bin model

The bin model developed by Meyer *et al.* (2015) is very relevant to this thesis and the model details are used as input below. The bin model has been modified for this thesis from Meyer *et al.* (2015) to obtain a more accurate representation of the bin dynamics over a larger operating range. The bin process is in general relatively simple, in that ROM coal ore is fed into the bin while three product flow lines remove material from the bin. An illustration of the bin and process flow is shown in Figure 3.9.

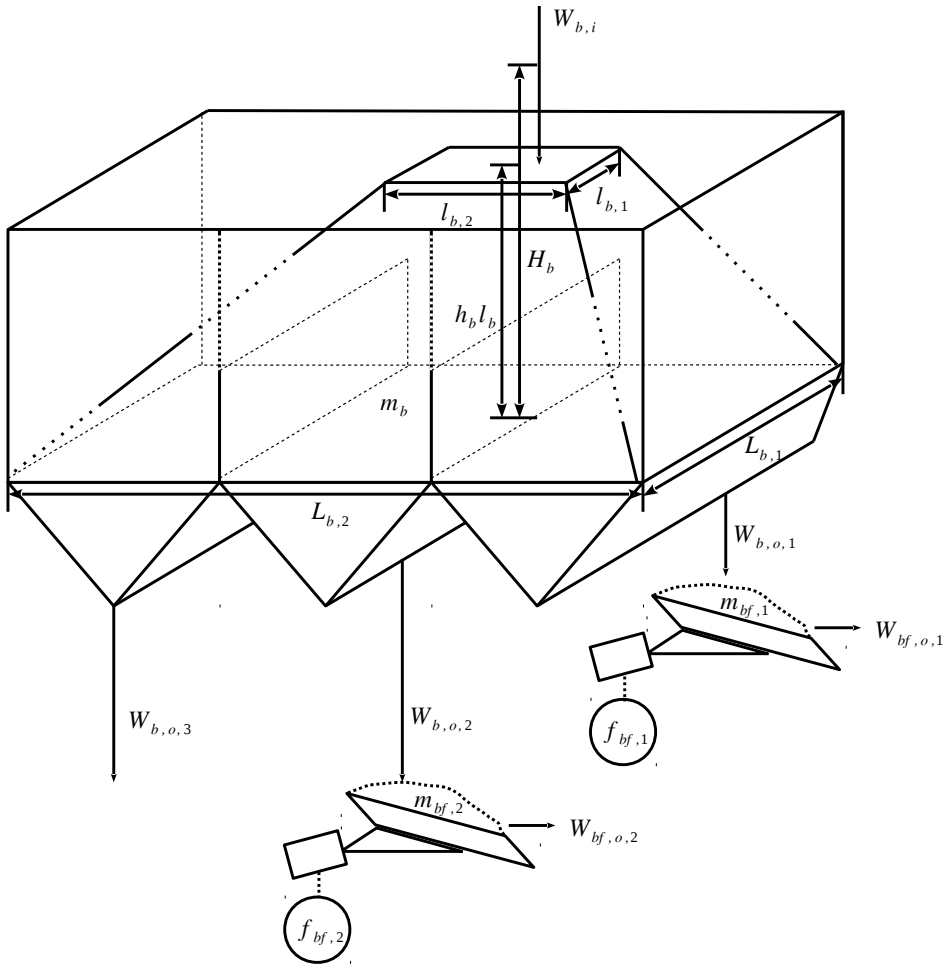


**Figure 3.9:** Bin process flow schematic [taken from Meyer *et al.* (2015)].

It was found that the geometry of the material within the bin can be simplified to a pyramid polyhedron shape. However, when the material reaches the apex of the pyramid, its shape is modified. This means that when the bin level is low, there is always a flat surface area representing the top of the stockpile (i.e. it approximates a constant volume). As the bin level reaches full capacity, the stockpile within the bin behaves more like a pyramid stockpile.

The conical bottom sections are catered for by assuming the mass within them forms part of the two feeder systems ($f_{bf,1}$ and $f_{bf,2}$) and the manually actuated bin mass flow rate ($W_{b,o,3}$).

Table 3.5 gives a description of the variables that have been used for the bin model. The third product mass flow rate ($W_{b,o,3}$) is manually actuated through a chute flap gate. This flap gate is rarely opened and only used if material flow to a different plant area becomes too low. The remaining two product

**Table 3.5:** Variables describing the bin process

| Name | Description |
|---|---|
| $W_{b,i}$ | Bin mass flow rate input (kg/s) |
| $m_b$ | Bin mass state (kg) |
| $W_{b,o,1}$ | Bin mass flow rate output no. 1 (kg/s) |
| $W_{b,o,2}$ | Bin mass flow rate output no. 2 (kg/s) |
| $W_{b,o,3}$ | Bin mass flow rate output no. 3 (kg/s) |
| $m_{bf,1}$ | Bin feeder no. 1 mass state (kg) |
| $m_{bf,2}$ | Bin feeder no. 2 mass state (kg) |
| $f_{bf,1}$ | Bin feeder no. 1 variable speed drive frequency (Hz) |
| $f_{bf,2}$ | Bin feeder no. 2 variable speed drive frequency (Hz) |
| $W_{bf,o,1}$ | Bin feeder no. 1 mass flow rate output (kg/s) |
| $W_{bf,o,2}$ | Bin feeder no. 2 mass flow rate output (kg/s) |
| $H_b$ | Bin stockpile maximum geometric height (m) |
| $L_{b,1}$ | Bin stockpile maximum geometric base depth (m) |
| $L_{b,2}$ | Bin stockpile maximum geometric base length (m) |
| $h_b$ | Bin stockpile maximum height (m) |
| $l_b$ | Bin stockpile relative level (%) |
| $l_{b,1}$ | Bin stockpile base depth (m) |
| $l_{b,2}$ | Bin stockpile base length (m) |
| $A_b = L_{b,1}L_{b,2}$ | Bin stockpile maximum geometric base area ($m^2$) |
| $\beta_b$ | Bin stockpile height ratio |

mass flow rates ($W_{bf,o,1}$ and $W_{bf,o,2}$) are actuated through vibratory feeders where the feeder motor speeds ($f_{bf,1}$ and $f_{bf,2}$) are varied by using variable speed drives.

The current problems and challenges relating to this piece of equipment are the accurate measurement and control of the bin level. It is possible for the bin to easily overflow and run empty during operation. The material flow further downstream is therefore affected and as a result the manually actuated chute flap ($W_{b,o,3}$) is opened to try and correct the material imbalance.

The dynamic model for the bin can be derived by using the principle of mass conservation as detailed in Stephanopoulos (1984). In order to derive these equations, the following assumptions were made:

- The bin feeders' feed mass flows ($W_{b,o,1}$ and $W_{b,o,2}$) are proportional to their variable speed drive frequencies $f_{bf,1}$ and $f_{bf,2}$ through proportionality functions $K_{bf,1}$ and $K_{bf,2}$ respectively.
- The bin feeders' proportionality functions ($K_{bf,1}$ and $K_{bf,2}$) vary with the bin level $l_b$ in a particular fashion.
- The bin feeders' mass ($m_{bf,1}$ and $m_{bf,2}$) have a characteristic time constant $\tau_{bf,1}$ and $\tau_{bf,2}$ respectively for their mass transport of material.
- The bulk density ($\rho_b$) of the material within the bin is constant.
- The volume ($V_b$) of material within the bin approximates a pyramid polyhedron stockpile shape which varies over time as material is fed and removed from the bin.
- The volume ($V_b$) of material can be expressed as a function of relative level $l_b$ [$V_b = \frac{1}{3}L_{b,1}L_{b,2}H_b - \frac{1}{3}l_{b,1}l_{b,2}H_b(1-\beta_b l_b)$].
- The bin base length ($l_{b,1}$) and depth ($l_{b,2}$) can be expressed as functions of relative level $l_b$ [$l_{b,1}(l) = L_{b,1}(1-\beta_b l_b)$ and $l_{b,2} = L_{b,2}(1-\beta_b l_b)$].
- The bin stockpile height ratio ($\beta_b$) varies with the bin stockpile relative level ($l_b$) through a sigmoid relationship.

State equations for the mass of material flow are represented as follows,

$$\frac{dm_b}{dt} = W_{b,i} - W_{b,o,1} - W_{b,o,2} - W_{b,o,3}, \tag{3.12}$$

$$\frac{dm_{bf,1}}{dt} = W_{b,o,1} - \frac{m_{bf,1}}{\tau_{bf,1}}, \tag{3.13}$$

$$\frac{dm_{bf,2}}{dt} = W_{b,o,2} - \frac{m_{bf,2}}{\tau_{bf,2}}, \tag{3.14}$$

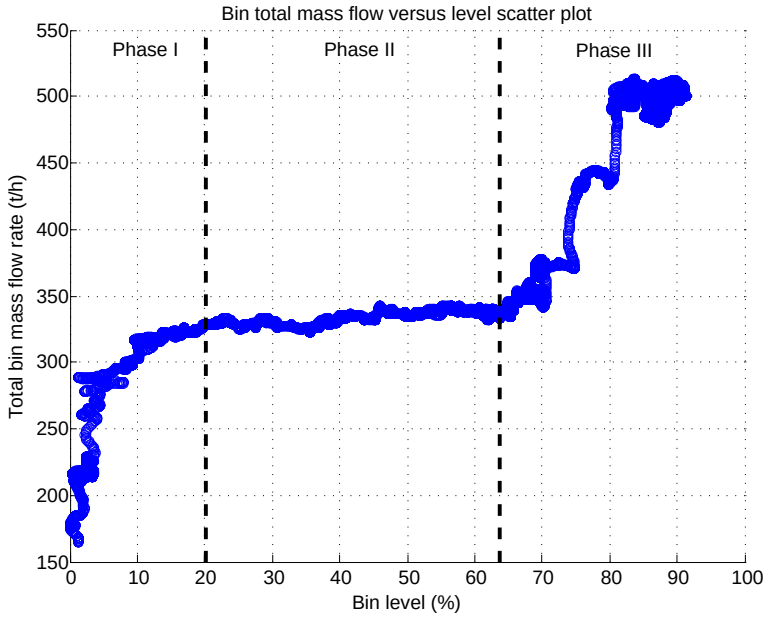


**Figure 3.10:** Bin throughput versus level using actual production data from a coal plant.

where $W_{b,o,1} = K_{bf,1} f_{bf,1}$ and $W_{b,o,2} = K_{bf,2} f_{bf,2}$ describe the mass flow of material leaving the bin feeders no. 1 and 2. These state equations are nonlinear due to the intermediate mass flow rates $W_{b,o,1}$ and $W_{b,o,2}$ being functions of the product of both their respective feeder frequency inputs ($f_{bf,1}$ or $f_{bf,2}$) and bin level ($l_b$).

In order to determine how the proportionality functions ($K_{bf,1}$ and $K_{bf,2}$) vary with bin level $l_b$, the total mass flow (i.e. $W_{bf,o,1} + W_{bf,o,2}$) from the bin feeders is plotted as a scatter plot with reference to the bin level $l_b$. Figure 3.10 shows the total feed versus bin level scatter plot using actual production data from a coal plant.

Based on Figure 3.10 it can be assumed that the proportionality functions comprise of an inverse exponential function at lower bin levels and a sigmoid function at higher bin levels. The reason for the inverse exponential function at a lower bin level could be due to the feeders not receiving sufficient material. This results in the feeders taking less material at very low levels (indicated as phase I in Figure 3.10). When the bin level reaches an optimum region, the feeders operate in a linear fashion (phase II in Figure 3.10). At very high bin levels the feeders operate at slightly higher rates (phase III in Figure 3.10). This could be due to a significant amount of mass being forced into the feeders resulting in them operating at very high rates. Additionally, material can fall from the top of the stockpile to lower levels resulting in a sudden increase in mass flow rate. Phase III is represented

using a sigmoid function. Based on the above analysis of the bin feeder behaviour, the bin model proportionality function ($K_{bf,1}$ and $K_{bf,2}$) can be described as,

$$K_{bf,1} = K_{bf,1,1}\left(1 - e^{-K_{bf,1,2}l_b}\right) + \frac{K_{bf,1,3}}{1 + e^{K_{bf,1,4}(K_{bf,1,5} - l_b)}}, \tag{3.15}$$

$$K_{bf,2} = K_{bf,2,1}\left(1 - e^{-K_{bf,2,2}l_b}\right) + \frac{K_{bf,2,3}}{1 + e^{K_{bf,2,4}(K_{bf,2,5} - l_b)}}, \tag{3.16}$$

where $K_{bf,1,1}$, $K_{bf,1,2}$, $K_{bf,1,3}$, $K_{bf,1,4}$, $K_{bf,1,5}$, $K_{bf,2,1}$, $K_{bf,2,2}$, $K_{bf,2,3}$, $K_{bf,2,4}$ and $K_{bf,2,5}$ are the associated parameters for the feeders.

By assuming a constant bulk density $\rho_b$ Equation 3.12 can be expressed as a rate of change in volume ($\frac{dm_b}{dt} = \rho_b \frac{dV_b}{dt}$). Given the equation describing the volume as a function of relative level in the above assumptions, the first time derivative of volume is $\frac{dV_b}{dt} = L_{b,1}L_{b,2}H_b\beta_b(1 - \beta_b l_b)^2 \frac{dl_b}{dt}$. By assigning $M_b = \rho_b L_{b,1}L_{b,2}H_b$ the fourth state equation describing the rate of change in stockpile relative height is simplified to,

$$\frac{dl_b}{dt} = \frac{W_{b,i} - W_{b,o,1} - W_{b,o,2} - W_{b,o,3}}{M_b\beta_b(1 - \beta_b l_b)^2}. \tag{3.17}$$

State Equation 3.17 is nonlinear due to the pyramid polyhedron geometry of the stockpile volume within the bin. As described above, the geometry of the bin volume varies with bin level $l_b$. At low bin levels, the material within the bin represents a constant volume. As the bin level increases, the volume starts to resemble a pyramid stockpile. To model the bin volume behaviour the bin stockpile height ratio $\beta_b$ can be made to represent a sigmoid function,

$$\beta_b = \frac{1}{1 + e^{K_{b,1}(K_{b,2} - l_b)}}, \tag{3.18}$$

where $K_{b,1}$ and $K_{b,2}$ are the required parameters.

The output equations defining the bin system include the bin feeder no. 1 and 2 mass flow ($W_{bf,o,1}$ and $W_{bf,o,2}$) and bin stockpile relative level ($l_b$),

$$\mathbf{y_b} = \begin{pmatrix} y_{b,1} \\ y_{b,2} \\ y_{b,3} \end{pmatrix} = \begin{pmatrix} W_{bf,o,1} \\ W_{bf,o,2} \\ l_b \end{pmatrix} = \begin{pmatrix} \frac{m_{bf,1}}{\tau_{bf,1}} \\ \frac{m_{bf,2}}{\tau_{bf,2}} \\ l_b \end{pmatrix}. \tag{3.19}$$

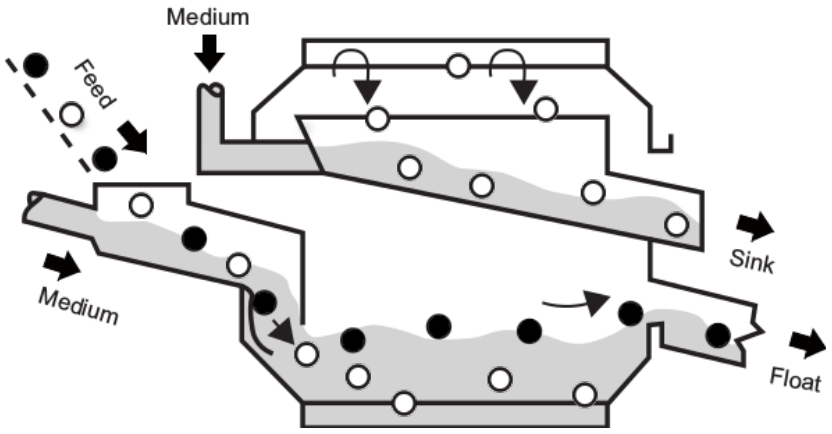


**Figure 3.11:** The Wemco drum [adapted from Wilkes (2006)]. Black particles represent coal while white particles represent discard.

### 3.3.5 Dense medium drum model

Drum separators operate on the principle of float and sink separation where particles of different densities to the medium can either float or sink in the medium due to gravity. Coal feed is mixed with the medium and processed through a relatively static container. England *et al.* (2002) describe two main horizontal drum separators used in industry being the Wemco or Teska drum. Although the principle of operation is similar for each type of drum separator, this thesis will apply the dynamic model to a Wemco drum as this is the industrial unit that was available for the research.

The Wemco drum (Figure 3.11) consists of a steel shell with a tyre and collar construction (Wilkes, 2006) where the drum operates in a longitudinal position. The drum shell rotates using a drive chain. During rotation, medium is added to the feed chute and sinks launder. Sinks are collected by sink lifters and discharged into the sinks launder. Floats exit through the lower exit of the drum.

The dynamic model of the drum separator focusses on throughput equations by making use of the conservation of overall mass. The DMD model developed by Meyer and Craig (2015) is used in this thesis. Conservation of mass of components can be used to model the grade (i.e. ash percentage) of the drum coal product. A model representation of the drum separator can be found in Figure 3.12 while associated variables describing the model are given in Tables 3.6 and 3.7.

**Table 3.6:** Drum input variables

| Variable | Description |
|---|---|
| $W_{d,i}$ | Mass feed rate of the feed mix (kg/s) |
| $\rho_{d,i}$ | Density of the feed mix (kg/m$^3$) |
| $V_d = V_{d,f} + V_{d,s}$ | Volume of the material within the drum (m$^3$) |
| $x_{d,i,ash}$, $x_{d,i,C}$ | Percentage ash and fixed carbon in the feed mix |
| $Q_{d,i,ash}$ | Volumetric flow rate of the ash content in the feed mix (m$^3$/s) |
| $x_{d,i,med}$ | Percentage magnetite medium in the feed mix |
| $\rho_{d,i,med}$ | Density of the magnetite medium in the feed mix (kg/m$^3$) |
| $Q_{d,i,med}$ | Volumetric flow rate of the magnetite medium in the feed mix (m$^3$/s) |

**Table 3.7:** Drum output variables

| Variable | Description |
|---|---|
| $W_{d,f}$ | Mass flow rate of the floats (kg/s) |
| $\rho_{d,f}$ | Density of the floats (kg/m$^3$) |
| $Q_{d,f}$ | Volumetric flow rate of the floats (m$^3$/s) |
| $V_{d,f}$ | Volume split of the floats within the drum (m$^3$) |
| $x_{d,f,ash}$ | Percentage ash content in the floats |
| $x_{d,f,med}$ | Percentage magnetite medium in the floats |
| $\rho_{d,f,med}$ | Density of the magnetite medium in the floats (kg/m$^3$) |
| $Q_{d,f,med}$ | Volumetric flow rate of the magnetite medium in the floats (m$^3$/s) |
| $W_{d,s}$ | Mass flow rate of the sinks (kg/s) |
| $\rho_{d,s}$ | Density of the sinks (kg/m$^3$) |
| $Q_{d,s}$ | Volumetric flow rate of the sinks (m$^3$/s) |
| $V_{d,s}$ | Volume split of the sinks within the drum (m$^3$) |
| $x_{d,s,ash}$ | Percentage ash content in the sinks |
| $x_{d,s,med}$ | Percentage magnetite medium in the sinks |
| $\rho_{d,s,med}$ | Density of the magnetite medium in the sinks (kg/m$^3$) |
| $Q_{d,s,med}$ | Volumetric flow rate of the magnetite medium in the sinks (m$^3$/s) |

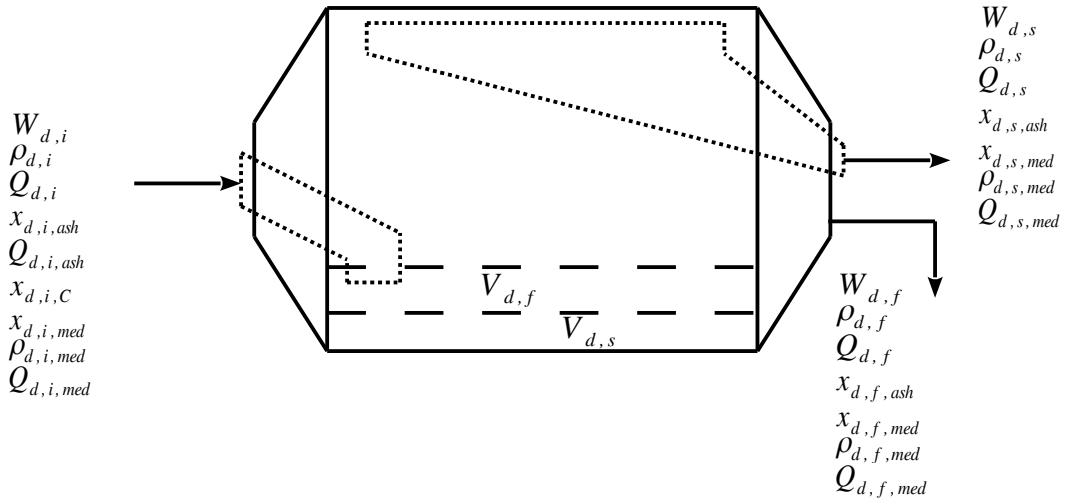


**Figure 3.12:** Model representation of a DMD [taken from Meyer and Craig (2015)].

The following is a list of assumptions that were made:

- The volume of the mix in the drum ($V_d$) is constant.
- The volume of the floats ($V_{d,f}$) and sinks ($V_{d,s}$) mix in the drum is split at a constant ratio $\alpha_d$.
- The volumetric flow rates of the feed ($Q_{d,i}$), floats ($Q_{d,f}$) and sinks ($Q_{d,s}$) are constant before and after a step is introduced in the medium density ($\rho_{d,i,med}$) or feed rate of the ore ($W_{d,i}$).
- The volumetric flow rates of the floats ($Q_{d,f}$) and sinks ($Q_{d,s}$) are split at a constant ratio $\alpha_d$.
- Only ash ($x_{d,i,ash}$), medium ($x_{d,i,med}$) and fixed carbon ($x_{d,i,C}$) components will be considered for the conservation of mass of components in the feed (i.e. $x_{d,i,ash} + x_{d,i,med} + x_{d,i,C} = 1$).
- Medium and ash components are considered for the conservation of mass of components in the floats ($x_{d,f,med}$, $x_{d,f,ash}$) and sinks ($x_{d,s,med}$, $x_{d,s,ash}$).
- The rates of change in mass for the floats ($\frac{dW_{d,f}}{dt}$) and sinks ($\frac{dW_{d,s}}{dt}$) are proportional to the difference in their densities ($\rho_{d,f}$ and $\rho_{d,s}$) to the magnetite medium density ($\rho_{d,i,med}$), the acceleration due to gravity ($g = 9.81$ kg/s$^2$) and the percentage of either ash or carbon in the feed ($x_{d,i,ash}$ or $x_{d,i,C}$).

In order to simplify the model, it is assumed that the volumetric flow is at steady state (i.e. $Q_{d,i} = Q_{d,f} + Q_{d,s}$) and that the floats and sinks are volumetrically split by a proportion $\alpha_d$. This means that $Q_{d,f} = \alpha_d Q_{d,s}$ (i.e. $Q_{d,f} = \frac{\alpha_d Q_{d,i}}{1+\alpha_d}$ and $Q_{d,s} = \frac{Q_{d,i}}{1+\alpha_d}$). Similarly, it is assumed that the drum material volume $V_d$ is separated according to the same split proportion $\alpha_d$ as in the volumetric feed flow (i.e. $V_{d,f} = \frac{\alpha_d V_d}{1+\alpha_d}$ and $V_{d,s} = \frac{V_d}{1+\alpha_d}$). By using the overall conservation of mass the following relationship describing the drum can be developed:

$$V_{d,f}\frac{d\rho_{d,f}}{dt} + V_{d,s}\frac{d\rho_{d,s}}{dt} = W_{d,i} - Q_{d,f}\rho_{d,f} - Q_{d,s}\rho_{d,s}. \tag{3.20}$$

Gravity separation within the drum can be used to model the effects of the dynamics of the density response for the drum. The gravitational force ($g$) indicates that the rates of change in mass for the floats and sinks are proportional to their differences in densities to the medium density. An additional factor was incorporated into the dynamic relationship allowing for the difference in ore density [$\rho_{d,i,ore} = W_{d,i}(1 - x_{d,i,med})/(Q_{d,i} - Q_{d,i,med})$] to medium density ($\rho_{d,i,med}$) to facilitate further separation. The percentage of ash or carbon in the feed will also influence the dynamics of the drum. Proportionality constants for floats ($K_{d,f}$) and sinks ($K_{d,s}$) are used to relate the rates of change of density in floats ($\frac{d\rho_{d,f}}{dt}$) and sinks ($\frac{d\rho_{d,s}}{dt}$) to these factors and yields the following relationships:

$$V_{d,f}\frac{d\rho_{d,f}}{dt} = K_{d,f}(\rho_{d,i,ore} - \rho_{d,i,med})(\rho_{d,i,med} - \rho_{d,f})x_{d,i,C}, \tag{3.21}$$

$$V_{d,s}\frac{d\rho_{d,s}}{dt} = K_{d,s}(\rho_{d,i,med} - \rho_{d,i,ore})(\rho_{d,i,med} - \rho_{d,s})x_{d,i,ash}. \tag{3.22}$$

By combining Equation 3.20 with Equations 3.21 and 3.22, the floats and sinks density state-space equations for the drum separator can be developed.

Similarly, the conservation of mass of the medium component of the feed material can be determined. This results in the following dynamic mass balance for the medium component,

$$\begin{aligned} &V_{d,f}\rho_{d,f}\frac{dx_{d,f,med}}{dt} + V_{d,f}x_{d,f,med}\frac{d\rho_{d,f}}{dt} + V_{d,s}\rho_{d,s}\frac{dx_{d,s,med}}{dt} + V_{d,s}x_{d,s,med}\frac{d\rho_{d,s}}{dt} \\ &\quad = W_{d,i}x_{d,i,med} - Q_{d,f}\rho_{d,f}x_{d,f,med} - Q_{d,s}\rho_{d,s}x_{d,s,med}. \end{aligned} \tag{3.23}$$

To develop solutions for the rates of change in the medium component percentages, some assumptions have to be made. The rates of change in the medium component percentages for the floats and sinks are assumed to be proportional to the difference ($\Delta_{\rho_{d,med}}$) in their feed component density ($\rho_{d,i,med}$) with either the float ($\rho_{d,f,med}$) or sink ($\rho_{d,s,med}$) medium density. It is also assumed that the rates of

change in component percentages are proportional to their acceleration due to gravity ($g$) and inversely proportional to the average particle size of the ore ($d_{ore}$). These factors are taken into consideration by the proportionality constants in the medium floats ($K_{d,f,med}$) and sinks ($K_{d,s,med}$). The following relationships for rates of change in medium components can therefore be determined as:

$$\frac{dx_{d,f,med}}{dt} = K_{d,f,med}(-\Delta_{\rho_{d,med}})(x_{d,i,med} - x_{d,f,med}), \tag{3.24}$$

$$\frac{dx_{d,s,med}}{dt} = K_{d,s,med}(\Delta_{\rho_{d,med}})(x_{d,i,med} - x_{d,s,med}). \tag{3.25}$$

The dynamic mass balance for the ash component can be determined similarly to the medium component by replacing subscript *med* with *ash*. The proportionality constant ($\Delta_{\rho_{d,med}}$) must be replaced by the difference in ash density ($\rho_{d,i,ash}$) to medium density ($\rho_{d,i,med}$). By using the equations in this section, a non-linear model of the drum separator can be derived. The output equations can be determined by applying conservation of mass of components to remove the medium component from the floats ($W_{d,f}$) and sinks ($W_{d,s}$) mass flow rates. The mass feed rate of the feed mix ($W_{d,i}$) is determine by making use of the mixing box model developed in Meyer and Craig (2010).

### 3.3.6 Dense medium cyclone model

The DMC model developed by Meyer and Craig (2010) is used in this thesis. In order to model the throughput of the DMC dynamically, it is necessary to make use of the conservation of overall mass, while the conservation of mass of components is used to model the quality (i.e. ash percentage) of the coal product. A representation of the DMC can be found in Figure 3.13, associated variables describing the model being given in Table 3.8, 3.9 and 3.10.

The following is a list of assumptions that were made:

- The volume of the mix in the cyclone ($V_c$) is constant.
- The volumes of the overflow ($V_{c,o}$) and underflow ($V_{c,u}$) mix in the cyclone and are split at a constant ratio $\alpha_c$.
- The volumetric flow rates of the feed ($Q_{c,i}$), overflow ($Q_{c,o}$) and underflow ($Q_{c,u}$) are constant before and after a step is introduced in the medium density ($\rho_{c,i}$) or feed rate of the ore ($W_{c,i}$).

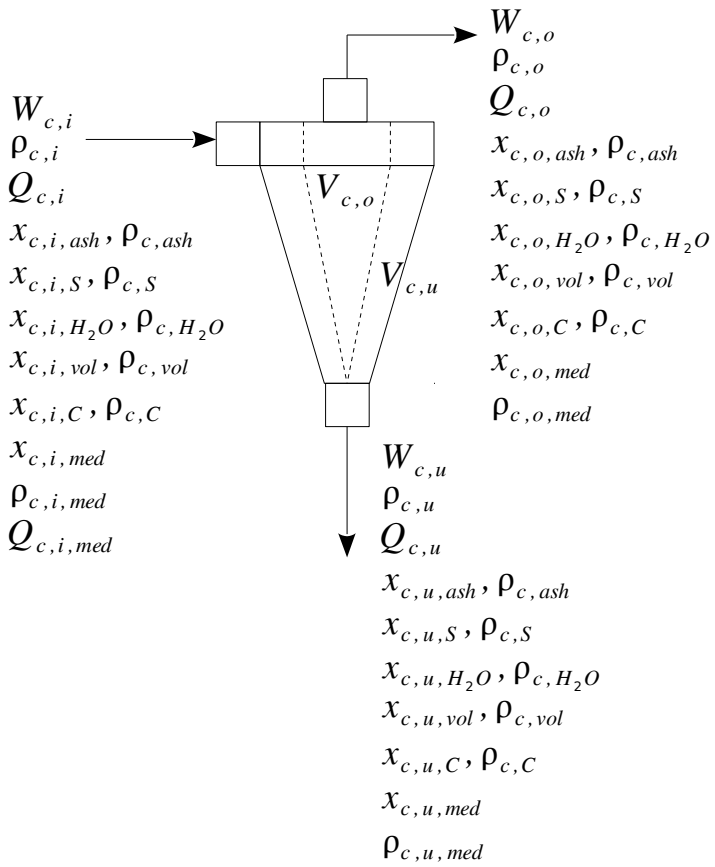


**Figure 3.13:** Simplified representation of a DMC [taken from Meyer and Craig (2010)].

**Table 3.8:** DMC input variables and descriptions

| Variable | Description |
|---|---|
| $W_{c,i}$ | Mass feed rate of the feed mix (kg/s) |
| $\rho_{c,i}$ | Density of the feed mix (kg/m$^3$) |
| $Q_{c,i}$ | Volumetric flow rate of the feed mix (m$^3$/s) |
| $x_{c,i,ash}$, $x_{c,i,S}$, $x_{c,i,H_2O}$, $x_{c,i,vol}$, $x_{c,i,C}$ | Percentage ash, sulphur, water, volatiles and fixed carbon in the feed mix |
| $x_{c,i,med}$ | Percentage magnetite in the feed mix |
| $\rho_{c,i,med}$ | Density of the magnetite medium in the feed mix (kg/m$^3$) |
| $Q_{c,i,med}$ | Volumetric flow rate of the magnetite medium in the feed mix (m$^3$/s) |

**Table 3.9:** DMC output variables and descriptions

| Variable | Description |
|---|---|
| $W_{c,o}$ | Mass feed rate of the overflow (kg/s) |
| $\rho_{c,o}$ | Density of the overflow (kg/m$^3$) |
| $Q_{c,o}$ | Volumetric flow rate of the overflow (m$^3$/s) |
| $x_{c,o,ash}$, $x_{c,o,S}$, $x_{c,o,H_2O}$, $x_{c,o,vol}$, $x_{c,o,C}$ | Percentage ash, sulphur, water, volatiles and fixed carbon in the overflow |
| $x_{c,o,med}$ | Percentage magnetite medium in the overflow |
| $\rho_{c,o,med}$ | Density of the magnetite medium in the overflow (kg/m$^3$) |
| $W_{c,u}$ | Mass feed rate of the underflow (kg/s) |
| $\rho_{c,u}$ | Density of the underflow (kg/m$^3$) |
| $Q_{c,u}$ | Volumetric flow rate of the underflow (m$^3$/s) |
| $x_{c,u,ash}$, $x_{c,u,S}$, $x_{c,u,H_2O}$, $x_{c,u,vol}$, $x_{c,u,C}$ | Percentage ash, sulphur, water, volatiles and fixed carbon in the underflow |
| $x_{c,u,med}$ | Percentage magnetite medium in the underflow |
| $\rho_{c,u,med}$ | Density of the magnetite medium in the underflow (kg/m$^3$) |

- The volumetric flow rates of the overflow ($Q_{c,o}$) and underflow ($Q_{c,u}$) are split at a constant ratio $\alpha_c$.

- Only ash, sulphur, moisture, volatile, medium and fixed carbon components will be considered for the conservation of mass of components in the feed (i.e. $x_{c,i,ash}+x_{c,i,S}+x_{c,i,H_2O}+x_{c,i,vol}+x_{c,i,med}+x_{c,i,C}=1$), overflow (i.e. $x_{c,o,ash}+x_{c,o,S}+x_{c,o,H_2O}+x_{c,o,vol}+x_{c,o,med}+x_{c,o,C}=1$) and underflow (i.e. $x_{c,u,ash}+x_{c,u,S}+x_{c,u,H_2O}+x_{c,u,vol}+x_{c,u,med}+x_{c,u,C}=1$).

- The rates of change in mass for the overflow ($\frac{dW_{c,o}}{dt}$) and underflow ($\frac{dW_{c,u}}{dt}$) are proportional to the difference in their densities ($\rho_{c,o}$ and $\rho_{c,u}$) to the magnetite medium density ($\rho_{c,i,med}$), the acceleration due to a centrifugal force ($\frac{v_{c,i}^2}{R_c}$) and the percentage of either ash or carbon in the feed ($x_{c,i,ash}$ or $x_{c,i,C}$).

- The rates of change in percentages of components to the overflow ($\frac{dx_{c,o,ash}}{dt}$, $\frac{dx_{c,o,S}}{dt}$, $\frac{dx_{c,o,H_2O}}{dt}$, $\frac{dx_{c,o,vol}}{dt}$

**Table 3.10:** DMC parameters and descriptions

| Variable | Description |
|---|---|
| $v_{c,i}$ | Linear velocity of the feed mix (m/s) |
| $V_c = V_{c,o} + V_{c,u}$ | Volume of the material within the cyclone ($m^3$) |
| $\alpha_c$ | Overflow and underflow proportionality constant |
| $A_c$ | Area of the inlet ($m^3$) |
| $R_c$ | Effective radius at which separation takes place near the spigot (m) |
| $d_{ore}$ | Average particle size of the ore (m) |
| $\rho_{c,i,ash}$, $\rho_{c,i,S}$, $\rho_{c,i,H_2O}$, $\rho_{c,i,vol}$, $\rho_{c,i,C}$ | Ash, sulphur, water, volatiles and fixed carbon densities ($kg/m^3$) |
| $V_{c,o}$ | Volume split of the overflow within the DMC ($m^3$) |
| $V_{c,u}$ | Volume split of the underflow within the DMC ($m^3$) |
| $K_{c,o}$ | Proportionality constant for the overflow ($m^3/s$) |
| $K_{c,u}$ | Proportionality constant for the underflow ($m^3/s$) |
| $K_{c,o,ash}$ | Proportionality constant for the ash overflow [$m^3$/(kg.s)] |
| $K_{c,u,ash}$ | Proportionality constant for the ash underflow [$m^3$/(kg.s)] |
| $K_{c,o,S}$ | Proportionality constant for the sulphur overflow [$m^3$/(kg.s)] |
| $K_{c,u,S}$ | Proportionality constant for the sulphur underflow [$m^3$/(kg.s)] |
| $K_{c,o,H_2O}$ | Proportionality constant for the moisture overflow [$m^3$/(kg.s)] |
| $K_{c,u,H_2O}$ | Proportionality constant for the moisture underflow [$m^3$/(kg.s)] |
| $K_{c,o,vol}$ | Proportionality constant for the volatile overflow [$m^3$/(kg.s)] |
| $K_{c,u,vol}$ | Proportionality constant for the volatile underflow [$m^3$/(kg.s)] |
| $K_{c,o,med}$ | Proportionality constant for the magnetite medium overflow [$m^3$/(kg.s)] |
| $K_{c,u,med}$ | Proportionality constant for the magnetite medium underflow [$m^3$/(kg.s)] |
| $K_{c,o,C}$ | Proportionality constant for the fixed carbon overflow [$m^3$/(kg.s)] |
| $K_{c,u,C}$ | Proportionality constant for the fixed carbon underflow [$m^3$/(kg.s)] |

and $\frac{dx_{c,o,C}}{dt}$) and underflow ($\frac{dx_{c,u,ash}}{dt}$, $\frac{dx_{c,u,S}}{dt}$, $\frac{dx_{c,u,H_2O}}{dt}$, $\frac{dx_{c,u,vol}}{dt}$ and $\frac{dx_{c,u,C}}{dt}$) are proportional to the difference in their component densities ($\rho_{c,i,ash}$, $\rho_{c,i,S}$, $\rho_{c,i,H_2O}$, $\rho_{c,i,vol}$ and $\rho_{c,i,C}$) to the magnetite medium density ($\rho_{c,i,med}$), the difference in their component percentages ($x_{c,o,ash}$, $x_{c,o,S}$, $x_{c,o,H_2O}$, $x_{c,o,vol}$, $x_{c,o,C}$, $x_{c,u,ash}$, $x_{c,u,S}$, $x_{c,u,H_2O}$, $x_{c,u,vol}$ and $x_{c,u,C}$) to their corresponding feed percentages ($x_{c,i,ash}$, $x_{c,i,S}$, $x_{c,i,H_2O}$, $x_{c,i,vol}$ and $x_{c,i,C}$), the acceleration due to a centrifugal force ($\frac{v_{c,i}^2}{R_c}$) and inversely proportional to the average particle size of the ore ($d_{ore}$).

In order to simplify the model, it is assumed that the volumetric flow is at steady state (i.e. $Q_{c,i} = Q_{c,o} + Q_{c,u}$) and that the overflow and underflow are volumetrically split by a proportion $\alpha_c$. This means that $Q_{c,o} = \alpha_c Q_{c,u}$ (i.e. $Q_{c,o} = \frac{\alpha_c Q_{c,i}}{1+\alpha_c}$ and $Q_{c,u} = \frac{Q_{c,i}}{1+\alpha_c}$). Similarly, it is assumed that the cyclone volume $V_c$ is separated according to the same split proportion $\alpha_c$ as in the volumetric feed flow (i.e. $V_{c,o} = \frac{\alpha_c V_c}{1+\alpha_c}$ and $V_{c,u} = \frac{V_c}{1+\alpha_c}$). By using the overall conservation of mass the following relationship describing the DMC can be developed:

$$V_{c,o}\frac{d\rho_{c,o}}{dt} + V_{c,u}\frac{d\rho_{c,u}}{dt} = W_{c,i} - Q_{c,o}\rho_{c,o} - Q_{c,u}\rho_{c,u}. \tag{3.26}$$

The concept of the acceleration due to the centrifugal force within the cyclone can be used to model the effects of the dynamics of the density response for the cyclone. The centrifugal force indicates that the rates of change in mass for the overflow and underflow are proportional to their differences in densities to the medium density. The percentage of ash or carbon will also influence the dynamics of the cyclone and can yield the following relationship:

$$V_{c,o}\frac{d\rho_{c,o}}{dt} = K_{c,o}(\rho_{c,i,med} - \rho_{c,o})x_{c,i,C}, \tag{3.27}$$

$$V_{c,u}\frac{d\rho_{c,u}}{dt} = K_{c,u}(\rho_{c,i,med} - \rho_{c,u})x_{c,i,ash}, \tag{3.28}$$

where $\frac{v_{c,i}^2}{R_c} = \frac{Q_{c,i}^2}{A_c^2 R_c}$ is the centrifugal acceleration (where $A_c$ is the cross-sectional area of the inlet and $R_c$ is the effective radius of the cyclone near the spigot where most of the separation takes place). By combining Equation 3.26 with Equations 3.27 and 3.28, the overflow and underflow density transfer functions for the DMC can be developed.

Similarly, the conservation of mass of each component within the ore that is being beneficiated can be determined. The components that were used in this model include ash and medium. This results in the

following dynamic mass balances,

$$V_{c,o}\rho_{c,o}\frac{dx_{c,o,ash}}{dt}+V_{c,o}x_{c,o,ash}\frac{d\rho_{c,o}}{dt}+V_{c,u}\rho_{c,u}\frac{dx_{c,u,ash}}{dt}+V_{c,u}x_{c,u,ash}\frac{d\rho_{c,u}}{dt}$$
$$=W_{c,i}x_{c,i,ash}-Q_{c,o}\rho_{c,o}x_{c,o,ash}-Q_{c,u}\rho_{c,u}x_{c,u,ash}, \quad (3.29)$$

$$V_{c,o}\rho_{c,o}\frac{dx_{c,o,med}}{dt}+V_{c,o}x_{c,o,med}\frac{d\rho_{c,o}}{dt}+V_{c,u}\rho_{c,u}\frac{dx_{c,u,med}}{dt}+V_{c,u}x_{c,u,med}\frac{d\rho_{c,u}}{dt}$$
$$=W_{c,i}x_{c,i,med}-Q_{c,o}\rho_{c,o}x_{c,o,med}-Q_{c,u}\rho_{c,u}x_{c,u,med}, \quad (3.30)$$

To develop solutions for the rates of change in component percentages, some assumptions have to be made. The rates of change in component percentages for the overflow and underflow are assumed to be proportional to the difference in their component densities to the medium density. It is also assumed that the rates of change in component percentages are proportional to the difference in their component percentages to their corresponding feed percentages and their acceleration due to gravity. The rates of change in component percentages are also assumed to be inversely proportional to the average particle size of the ore. This will yield the following relationships:

$$\frac{dx_{c,o,ash}}{dt} = K_{c,o,ash}(\rho_{c,i,med}-\rho_{ash})(x_{c,i,ash}-x_{c,o,ash}), \quad (3.31)$$

$$\frac{dx_{c,u,ash}}{dt} = K_{c,u,ash}(\rho_{ash}-\rho_{c,i,med})(x_{c,i,ash}-x_{c,u,ash}), \quad (3.32)$$

$$\frac{dx_{c,o,med}}{dt} = K_{c,o,med}(\rho_{c,i,med}-\rho_{c,o,med})(x_{c,i,med}-x_{c,o,med}), \quad (3.33)$$

$$\frac{dx_{c,u,med}}{dt} = K_{c,u,med}(\rho_{c,u,med}-\rho_{c,i,med})(x_{c,i,med}-x_{c,u,med}), \quad (3.34)$$

In the case of the percentage of magnetite in Equations 3.33 and 3.34, the difference between the overflow and underflow medium density and the feed medium density is used ($\Delta_{\rho_{c,med}}$=$\rho_{c,i,med}-\rho_{c,o,med}$=$\rho_{c,u,med}-\rho_{c,i,med}$).

By using the equations in this section, a non-linear model of the DMC can be derived. The output equations can be determined by applying conservation of mass of components to remove the medium component from the overflow ($W_{c,o}$) and underflow ($W_{c,u}$) mass flow rates. The mass feed rate of the feed mix ($W_{c,i}$) is determine by making use of the mixing box model developed in Meyer and Craig (2010).

Mukherjee *et al.* (2003) have indicated that a gravity fed DMC can typically have a head height of between 9 and 11 times the cyclone diameter $D_c$. The relationship between RD, pressure and head height is,

$$P_{c,i} = \rho_{c,i} g h_c, \tag{3.35}$$

where $P_{c,i}$ is the cyclone inlet pressure (Pa), $\rho_{c,i}$ is the inlet RD ($\mathrm{kg/m^3}$), $g$ is the gravitational constant ($9.81\mathrm{m/s^2}$) and $h_c$ is the head height of the feed (m) which can be used to determine the DMC inlet density. Meyer and Craig (2014) showed how to make use of Equation 3.35 as a new calculation introduced to the DMC dynamic model developed in Meyer and Craig (2010) to provide an additional calculated measurement point for the process. Unfortunately the coal plant used for this research did not have a pressure transmitter at the cyclone inlet.

### 3.3.7 Time delay model

Many of the models described above are typically combined to form a more complex system for a particular production area. Some of the model outputs need to be delayed to allow for material to be transported from the particular piece of equipment to their final actual physical process measurement point. In many of the models identified with an actual coal plant, it is necessary to include these time delays. The time delays are usually as a result of material being conveyed from one point to another with the output being delayed over a time $t_{td}$ as follows (Seborg *et al.*, 1995),

$$\mathrm{y}_{\mathrm{td},\mathscr{M}}(t) = \mathrm{y}_{\mathscr{M}}(t - t_{td}), \tag{3.36}$$

where $\mathrm{y}_{\mathrm{td},\mathscr{M}}$ is the delayed model output and $\mathrm{y}_{\mathscr{M}}$ is the original model output prior to the delay.

Seborg *et al.* (1995) show that the simplest way to represent a time delay is to use a Taylor series expansion in the Laplace domain. When applying the system output $\mathrm{y}_{\mathscr{M}}$ to a Laplace transfer function $e^{-t_{td}s}$ and approximating to the first order Taylor series expansion,

$$\mathrm{y}_{\mathrm{td},\mathscr{M}}(t) = \mathrm{y}_{\mathscr{M}}(t) - t_{td}\frac{d\mathrm{y}_{\mathscr{M}}}{dt}. \tag{3.37}$$

## 3.4 SYSTEM IDENTIFICATION

Ljung (1987) describes the system identification process where a dynamic model of a system can be fitted to a given set of data describing that system. Figure 3.14 illustrates this process of parameter

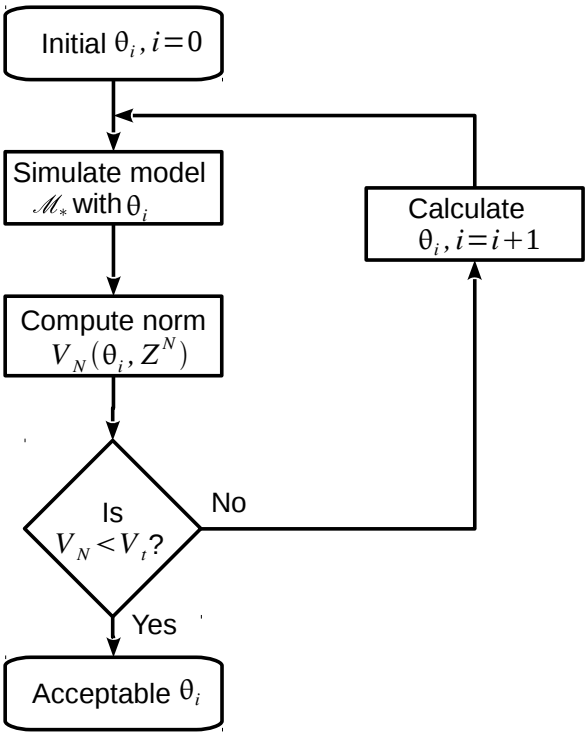


**Figure 3.14:** Parameter estimation process [adapted from Rathaba (2004)]. $\mathscr{M}_*$ refers to the different equipment models.

estimation used by Meyer (2010).

Meyer (2010) shows how the system identification process was used to determine the parameters for coal processing dynamic models ($\mathscr{M}_*$). In this process the prediction error ($\varepsilon$) represents the difference between the measured and the model output for a given set of model parameters. The process of selecting the model parameters that minimise the prediction error is called parameter estimation (Ljung, 1987). The scalar-valued norm approach is used in this paper where the norm of the normalised sum of the square of the prediction errors (loss function) is minimised. The loss function is given as,

$$V_N = \det\left(\frac{1}{N}\sum_{1}^{N}\varepsilon(t,\theta_i)(\varepsilon(t,\theta_i))^T\right), \tag{3.38}$$

where $\theta_i$ represents the $i$th estimated parameter and $N$ is the number of values of each plant measurement in the estimation data set ($Z^N$). When the loss function is below a threshold ($V_t$), the algorithm stops and returns the parameter set ($\theta_i$) which best fit the model to the data set within the required threshold.

The prediction-error identification algorithm that was used is the Trust-Region Reflective Newton numerical optimisation algorithm (Ljung, 2005) for estimating non-linear grey-box models. The

quality of each model ($\mathscr{M}_*$) estimate is measured using Akaike's final prediction error (FPE) (Ljung, 2010),

$$\text{FPE} = V_N(1+2d_{\mathscr{M}}/N), \tag{3.39}$$

where $V_N$ is the loss function and $d_{\mathscr{M}}$ is the number of estimated parameters.

Model parameters are fitted by minimising the loss function over 66% of the data set, while the model goodness of the fit is determined for the full data set for each experiment. Model goodness of the fit (Ljung, 2005) is determined using the normalised root mean square error (NRMSE),

$$\text{fit} = 100\left(1-\frac{|y_{\mathscr{M}}-\hat{y}_{\mathscr{M}}|}{|y_{\mathscr{M}}-\bar{y}_{\mathscr{M}}|}\right), \tag{3.40}$$

where $y_{\mathscr{M}}$ is the measured output, $\hat{y}_{\mathscr{M}}$ is the simulated output and $\bar{y}_{\mathscr{M}}$ is the mean of $y_{\mathscr{M}}$ ($\sum_{i=1}^{N} y_{\mathscr{M},i}/N$). The NRMSE ($|y_{\mathscr{M}}-\hat{y}_{\mathscr{M}}|$) is determined as $\sqrt{\sum_{i=1}^{N}(y_{\mathscr{M},i}-\hat{y}_{\mathscr{M},i})^2}/N$. Similarly, $|y_{\mathscr{M}}-\bar{y_{\mathscr{M}}}|$ is evaluated as $\sqrt{\sum_{i=1}^{N}(y_{\mathscr{M},i}-\bar{y}_{\mathscr{M}})^2}/N$. The NRMSE cost can vary between minus infinity ($-\infty$) and one (1). If the NRMSE cost function is equal to zero, then $\hat{y}_{\mathscr{M}}$ is no better than a straight line at matching $y_{\mathscr{M}}$.

## 3.5 STEADY-STATE MODELS

In coal preparation, there are process models that are normally used to describe the separation characteristics of coal (England *et al.*, 2002). Other process models are typically used to describe the efficiency of the unit (DMC or DMD) separator. These are defined as washability curves and partition curves which are detailed below. The coal washability can be used to provide an estimate of ash content over time based on yield. The dynamic model of the DMC and DMD described earlier can be reduced to a partition curve which validates the developed dynamic models from a metallurgical perspective.

### 3.5.1 Washability curves

Another name for a coal preparation plant is called a wash plant. The washability curve gives an indication of how coal is separated from product and gangue which is the ultimate objective of a coal wash plant. A process model (Wills and Napier-Munn, 2006) used to determine the required density for

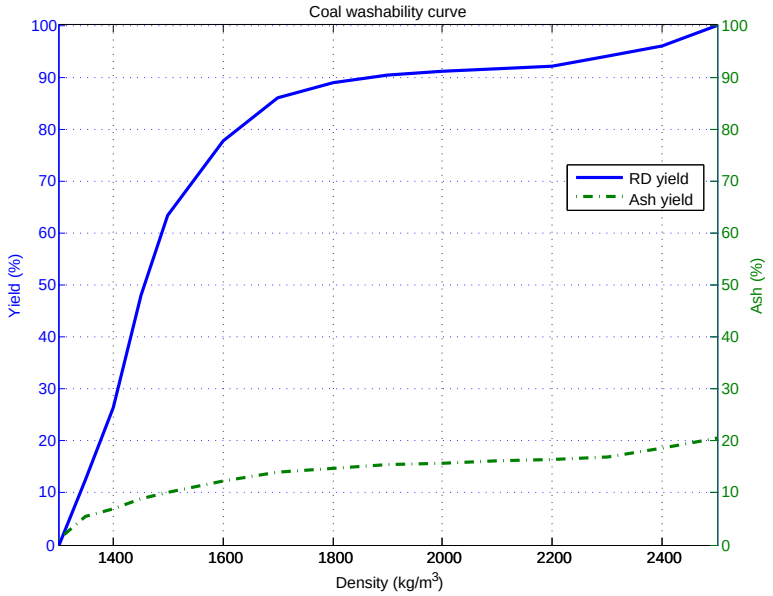


**Figure 3.15:** Coal plant actual washability curve [taken from Meyer and Craig (2015)]. Washability curve data is based on bench 11 from the Grootegeluk formation (Faure *et al.*, 1996).

coal separation and the expected yield of coal of the required grade is a washability curve (Reinhardt, 1911).

The quality of coal is usually measured as ash content which is the amount of incombustible material in the coal. Using float-sink analysis, it is possible to generate a washability curve describing the characteristics of the coal at different RD fractions (England *et al.*, 2002). An example of the coal washability curve describing the coal beneficiated by the industrial coal preparation process used for this thesis is given in Figure 3.15.

Bowen and Jowett (1986) describe various mathematical models for a coal cleaning system to be used for computational calculations for coal washability. The M-curve is a simple curve that can generally fit a conic section equation which typically represents a washability curve. Bowen and Jowett (1986) show a general conic equation that will fit almost any M-curve plot as,

$$b_0 + b_1 x_{f,ash} + b_2 y + b_3 x_{f,ash}^2 + b_4 y^2 + b_5 x_{f,ash} y = 0, \tag{3.41}$$

where $x_{f,ash}$ represents the ash product or float percentage, $y$ represents the yield and the model parameters are given as $b_0$, $b_1$, $b_2$, $b_3$, $b_4$ and $b_5$.

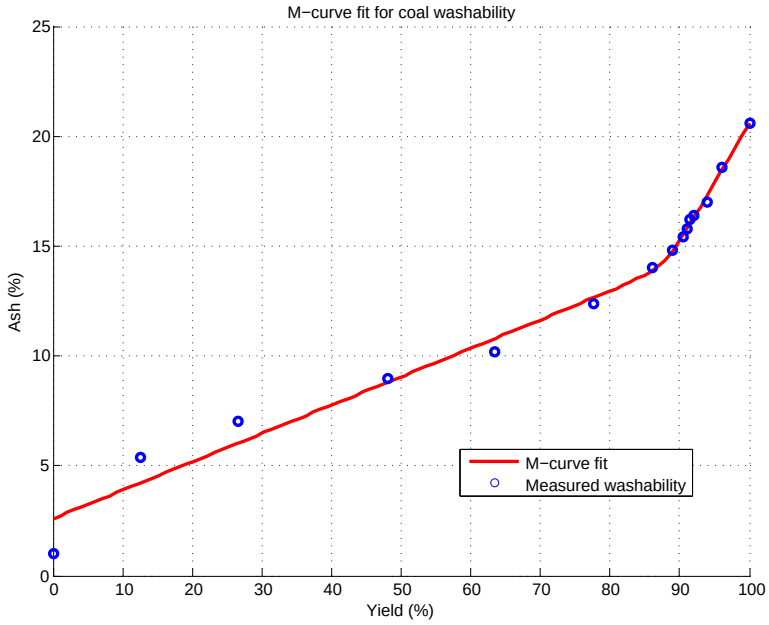


**Figure 3.16:** M-curve of the coal washability [taken from Meyer and Craig (2015)].

**Table 3.11:** M-curve model parameters.

| M-curve parameter | Curve fit parameter results |
|---|---|
| $b_0$ | -0.19 |
| $b_1$ | 6.91 |
| $b_2$ | -0.65 |
| $b_3$ | 21.83 |
| $b_4$ | 1.54 |
| $b_5$ | -14.78 |

Figure 3.16 was generated by fitting Equation 3.41 to the measured washability data from Figure 3.15.

Table 3.11 shows a summary of the parameters for M-curve fit. This result shows that the coal plant product ash content ($x_{f,ash}$) can be expressed as a function of yield ($y$).

The M-curve [developed by Mayer (1950)] parametric equation will be used in this paper to estimate the product ash contents in order to verify the grade as estimated by the dynamic model. The feed ash

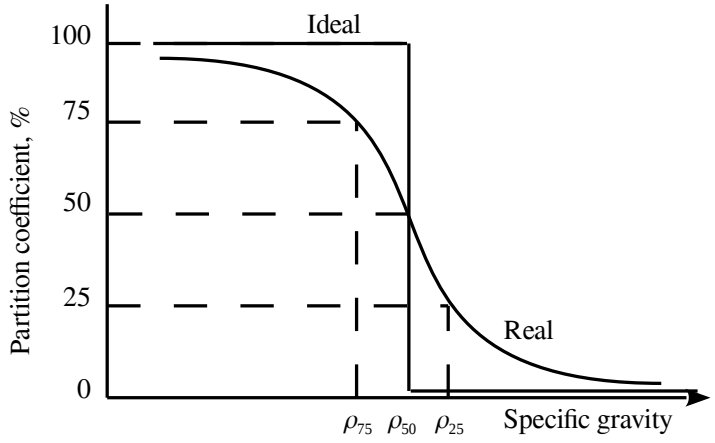


**Figure 3.17:** Example of a partition curve [adapted from England *et al.* (2002)].

content ($x_{i,ash}$) is calculated by reconstituting the feed as follows,

$$x_{i,ash} = \frac{W_f x_{f,ash}}{W_i Y(\rho_{i,med})}, \tag{3.42}$$

where $W_f$ is the product mass rate, $W_i$ is the feed mass rate, $x_{f,ash}$ is the float or product ash contents and $Y(\rho_{i,med})$ is the partition factor described by Equation 3.45 and 3.46 below. In order to reconstitute the feed ash content ($x_{i,ash}$) it is assumed that the partition factor is normalised and shifted to the initial medium density $\rho_{i,med}$ of the separator. It is also assumed that the partition factor represents the average density of material in the overflow or float. The population distribution at each RD fraction is typically not known and therefore cannot be used in this reconstitution.

### 3.5.2 Partition curves

Partition curves describe the efficiency of separation for a DMS unit process. In general, the DMD has a slightly lower efficiency than a DMC. As a result, different process models are used to describe the partition curves for the different separation units. The DMD partition curve is initially explained and is then followed by the DMC partition curve process model.

Figure 3.17 shows an example of a typical partition curve or efficiency curve taken from England *et al.* (2002). The ideal partition curve is a step function allowing for perfect separation. However, since unit processes such as the DMC or DMD do not separate perfectly, the real efficiency curve is typically an S-shaped curve of a cumulative probability distribution. In this example the probability of particles reporting as floats is shown.

The location of the curve is described by the separation cutpoint (the specific RD where a particle can have an equal chance of reporting to a float or sink) and is represented as $\rho_{50}$. The EPM or $E_p$ is an empirical measure of inefficiency. This separation efficiency is typically calculated as follows:

$$\mathrm{E_p} = \frac{\rho_{25} - \rho_{75}}{2}, \tag{3.43}$$

where $\rho_{25}$ is the specific gravity (SG) at 25% and $\rho_{75}$ is the SG at 75% (Terra, 1938).

Float and sink analysis is a technique used to determine properties of coal and assist with the generation of a partition curve. This curve is used to determine the efficiency of a DMS process. Coal samples are separated into two or more RD fractions by using gravity separation. The liquids are made up of different relative densities between that of the discarded material and pure coal.

England *et al.* (2002) describe the process of float and sink analysis (Figure 2.3) which is used in this paper primarily for the steady-state simulation. A sample is separated in a container using a liquid with a high RD. The float is recovered and immersed in a series of containers with consecutively lower liquid densities (Figure 2.3). Typical specific gravities range from 1.30 to 1.70, with typical step intervals of 0.05. It is important to note that this analysis is performed when each container mix is at steady state due to there being a considerable amount of time required for settling to take place.

After each fraction has settled, the sinks are dried and weighed. From these data, a partition curve can be generated.

A partition curve allows the degree of separation and efficiency for a cyclone to be illustrated. Using the yield of clean coal from a plant and the float and sink analysis of the product and discard, the partition factor (ratio of the total clean coal to the feed) per RD fraction can be computed. Table 3.12 shows an example [taken from England *et al.* (2002)] of the data and necessary calculations required to obtain a partition curve.

A yield of 41.6% for clean coal is used as given in the example by England *et al.* (2002).

Figure 3.18 illustrates an example of a partition curve where the partition factor of a plant is shown with respect to RD of the liquid. This figure also shows the RD that will allow for the plant to have a partition factor of 50%.

**Table 3.12:** Example of details and calculations required for a partition curve [data taken from England *et al.* (2002)].

| **RD Fraction** | **Clean Coal** ($y_{pc} = 0.416$) | | **Discard** ($1 - y_{pc} = 0.584$) | | **Reconst. Feed** $b_{pc} + d_{pc} = e_{pc}$ | **Partition Factor** $b_{pc}/e_{pc} \times 100$ |
|---|---|---|---|---|---|---|
| | **Fract. Yield %** ($a_{pc}$) | **Fract. of Total** $a_{pc} \times y_{pc} = b_{pc}$ | **Fract. Yield %** ($c_{pc}$) | **Fract. of Total Coal** $c_{pc}(1 - y_{pc}) = d_{pc}$ | | |
| F1.3 | 43.69 | 18.18 | 0.79 | 0.46 | 18.64 | 97.5 |
| 1.3 - 1.32 | 25.82 | 10.74 | 0.71 | 0.41 | 11.15 | 96.3 |
| 1.32 - 1.34 | 14.23 | 5.92 | 1.29 | 0.75 | 6.67 | 88.8 |
| 1.34 - 1.36 | 11.59 | 4.82 | 3.93 | 2.30 | 7.12 | 67.7 |
| 1.35 - 1.38 | 3.97 | 1.65 | 8.93 | 5.22 | 6.87 | 24.0 |
| 1.38 - 1.40 | 0.40 | 0.17 | 10.36 | 6.05 | 6.22 | 2.7 |
| 1.40 - 1.42 | 0.10 | 0.04 | 9.29 | 5.43 | 5.47 | 0.7 |
| 1.42 - 1.44 | 0.07 | 0.03 | 8.58 | 5.01 | 5.04 | 0.6 |
| 1.44 - 1.46 | 0.03 | 0.01 | 8.58 | 5.01 | 5.02 | 0.2 |
| 1.46 - 1.48 | 0.03 | 0.01 | 7.86 | 4.59 | 4.60 | 0.2 |
| 1.48 - 1.50 | 0.03 | 0.01 | 6.43 | 3.76 | 3.77 | 0.3 |
| S1.50 | 0.03 | 0.01 | 33.24 | 19.41 | 19.42 | 0.05 |
| Whole Coal | 99.99 | 41.59 | 99.99 | 58.40 | 99.99 | – |

A DMC or DMD having a low EPM value means that it will achieve a very good separation through density separation.

Variables that can influence the shape of the partition curve are feed rate, maintenance of equipment and operating variables such as pressure, particle size, amount of magnetite used and contaminants in the medium (De Korte, 2008).

Napier-Munn (1991) referenced a process model for a DMD separator. Sedimentation theory (Scott and Lyman, 1987) was used to detail the separation cutpoint (RD where a particle has an equal chance

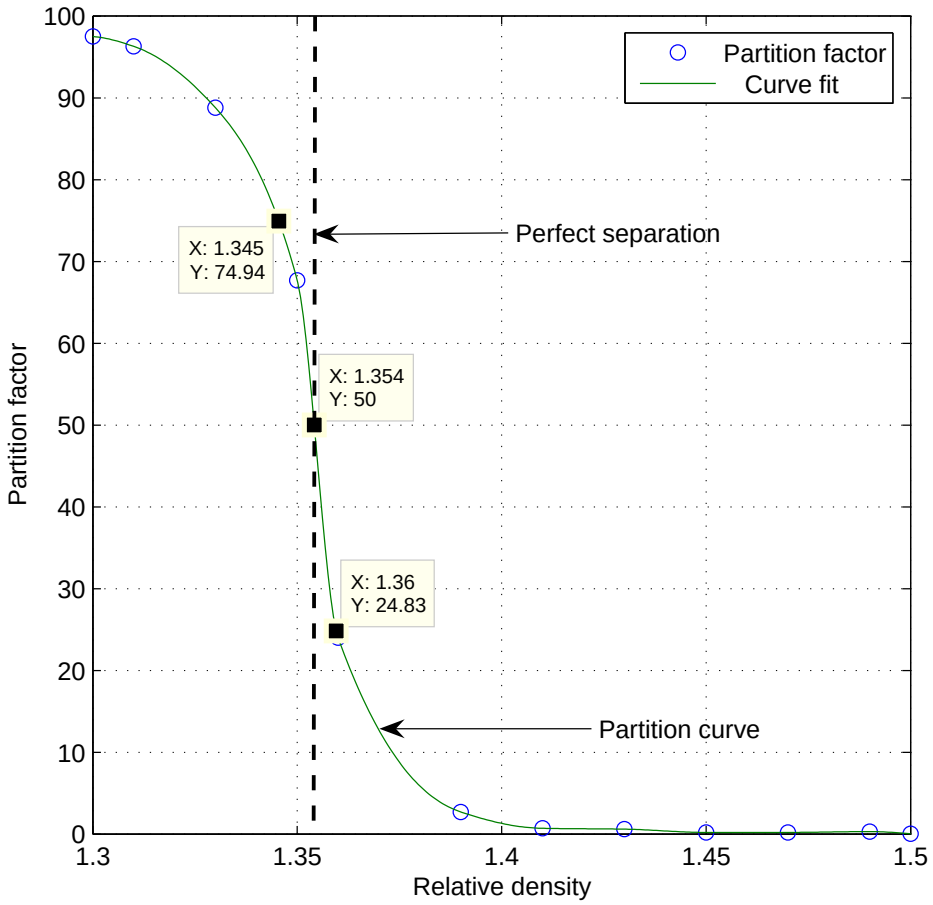


**Figure 3.18:** Partition curve example plotted from Table 3.12.

of reporting to the float or sink). The partition factor (Baguley and Napier-Munn, 1996) for the drum separator is described as,

$$Y_d = \left[1 - (v_{100} - v_t)^2\right]^{\left(\frac{A_{drm}}{d_{ore}^2 + B_{drm}}\right)}, \tag{3.44}$$

where $v_{100}$ is the terminal velocity, which allows for 100% recovery of the sinks, $v_t$ is the terminal velocity of the particle and $A_{drm}$ and $B_{drm}$ are constants that need to be estimated. The particle size is represented by $d_{ore}$.

Using the terminal speed $v_t = \sqrt{\frac{2F_g}{C_{ore}\rho_{i,med}A_{ore}}}$ from Halliday *et al.* (2001) the steady-state partition factor (Equation 3.44) can be made a function of medium density ($\rho_{i,med}$). $F_g$ is the downward gravitational force on the ore particle, $C_{ore}$ is the drag coefficient for the ore particle, $\rho_{i,med}$ is the medium density displacing the ore particle mass per volume and $A_{ore}$ is the effective cross-sectional area of the ore

particle. By assigning parameters $p_1 = v_{100}$, $p_2 = \frac{2F_g}{C_{ore}A_{ore}}$ and $p_3 = \frac{A_{drm}}{d_{ore}^2+B_{drm}}$, a parametric equation for the partition factor can be derived as follows,

$$Y_d(\rho_{i,med}) = \left[1 - \left(p_1 - \sqrt{\frac{p_2}{\rho_{i,med}}}\right)^2\right]^{p_3}. \tag{3.45}$$

Similar results could possibly be obtained by using the terminal velocity correlation published by Concha and Almendra (1979), with an adjustment for shape factor.

The DMD dynamic model can be reduced to a steady-state model and made to represent the partition curve described by 3.45. A partition curve reduced from a dynamic DMD model is given in the next chapter.

A mathematical model for the partition factor ($Y_c$) of a DMC has been developed by Napier-Munn (1991) and looks as follows,

$$Y_c = \frac{1}{1 + e^{\frac{1.099(\rho_{50} - \rho_{i,med})}{E_p}}}, \tag{3.46}$$

where $\rho_{i.med}$ is the RD of the feed medium fraction and $E_p$ is the EPM. This equation expresses the partition curve and is derived by substituting equations from Lynch (1977), King and Juckes (1984) and King and Juckes (1988). This model is a regression model based on steady-state conditions of the ore separated by a DMC. This steady-state model is well known in literature. A dynamic model will be discussed in more detail in this paper. This dynamic model will be reduced to a steady-state model in the next chapter with similar properties to that of Equation 3.46.

## 3.6 MODEL PREDICTIVE CONTROL

This subsection highlights the principle of MPC and indicates the typical requirements for an objective function and constraints applicable for the dynamic models shown in this thesis. Since some of the dynamic models shown in this thesis are nonlinear, nonlinear MPC (NMPC) is described. The NMPC algorithm provided by Grüne and Pannek (2011) was used to perform the simulations in MATLAB®[1].

[1] MATLAB® is a mathematical computing software developed by MathWorks®.

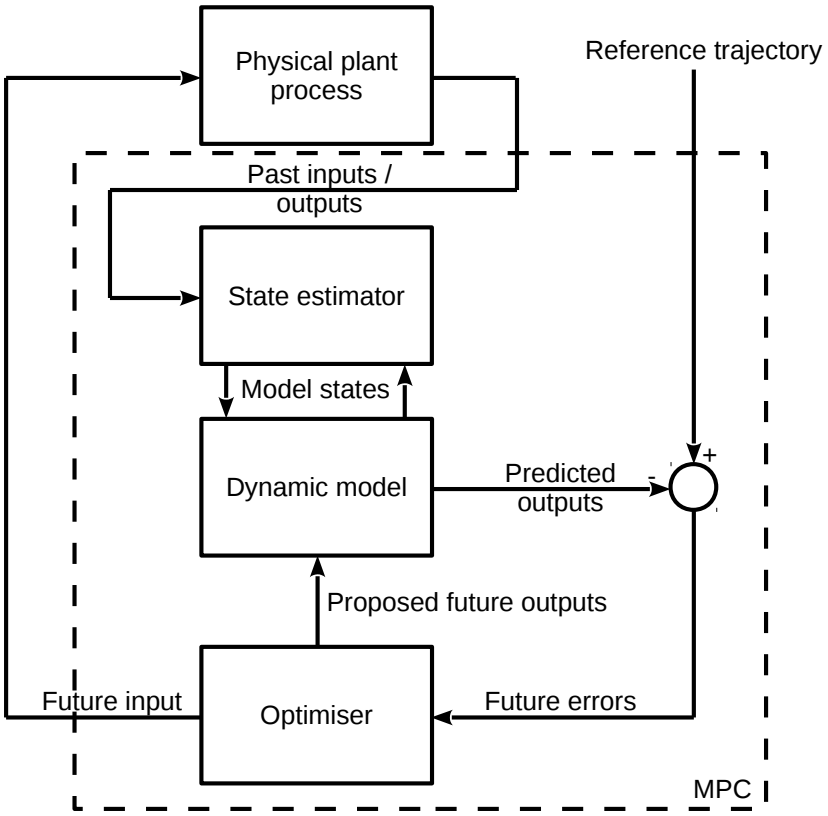


**Figure 3.19:** Proposed MPC implementation architecture [adapted from Hodouin (2011)].

An implementation architecture of MPC is proposed below which gives an indication of the typical components of an MPC and how it should be implemented. A description of NMPC with the various applicable components are given. The UKF algorithm is explained in more detail as the UKF is simulated with some of the dynamic models in the next chapter.

### 3.6.1 Implementation architecture

When implementing MPC, model-plant mismatch can occur due to changes in plant dynamics and nonlinearities in the process (Badwe *et al.*, 2009). Hodouin (2011) proposes a generalised control loop for automatic control, observation and optimisation in mineral processing plants. Figure 3.19 shows a similar control loop adapted for the implementation of MPC on the coal plant dynamic models given earlier in this chapter.

The MPC consists of a state estimator, dynamic model and optimiser. Past inputs and outputs are obtained from the physical plant process measurements. These inputs and outputs are used by a

state estimator to estimate the model states over time to reduce model-plant mismatch. Ideally, the dynamic model parameters should be identified with changes to process conditions. However, in order to implement a practical solution, a state estimator can update the model states based on process and measurement noise disturbances. The dynamic model is used by the optimiser to predict future outputs based on proposed future control moves. The objective of the optimiser is to minimise future errors where the predicted model future outputs are compared to a reference trajectory. Once the optimiser has solved the minimisation problem, the first set of proposed future control moves is sent to the physical plant process actuators for implementation.

### 3.6.2 Nonlinear model predictive control

MPC consists of a model that uses past and current plant values to predict future outputs. Grüne and Pannek (2011) indicate that the difference between NMPC and MPC is that NMPC makes use of a nonlinear model when applying past and current plant values to predict future outputs. The nonlinear plant is usually described by the general state space model,

$$x(t+1) = f(x(t), u(t)), \tag{3.47}$$

$$y(t) = g(x(t)). \tag{3.48}$$

An algorithm is used to propose future control actions based on a required reference trajectory. Using future output errors, an objective function ($J$) and process constraints, an optimiser algorithm is used to determine future inputs for the process and model (Camacho and Bordons, 2004). Various MPC algorithms propose different objective functions for obtaining the control law. However, the objective function to be minimized may take the general form,

$$J = \sum_{j=1}^{N} \|\hat{\mathbf{y}}(t+j) - \mathbf{y}_s\|^2_{\mathbf{R}} + \sum_{j=0}^{M-1} \|\Delta\mathbf{u}(t+j)\|^2_{\mathbf{P}} + \sum_{j=0}^{M-1} \|\mathbf{u}(t+j) - \mathbf{u}_s\|^2_{\mathbf{Q}} + \|\mathbf{s}^2_{\mathbf{T}}\|, \tag{3.49}$$

where $\mathbf{P}$, $\mathbf{Q}$, $\mathbf{R}$ and $\mathbf{T}$ are weighting matrices that consider rapid input changes [$\Delta\mathbf{u}(t+j) = \mathbf{u}(t+j) - \mathbf{u}(t+j-1)$], future behaviour of the input error [$\mathbf{u}(t+j) - \mathbf{u}_s$], future behaviour of the output error [$\hat{\mathbf{y}}(t+j) - \mathbf{y}_s$] and soft constraints ($\mathbf{s}$). The control law [minimizing $J$ to solve for future inputs $\mathbf{u}(t+j)$] is determined over a prediction horizon ($N$) where $\hat{\mathbf{y}}$ is the output prediction and $\mathbf{y}_s$ is the reference trajectory. The control law is also solved for over a control horizon ($M$). Future input [$\mathbf{u}(t+j)$] deviations from the desired steady-state inputs $\mathbf{u}_s$ are also controlled.

The fourth term in Equation 3.49 considers soft constraints in the output variables. The constraints for the process variables are usually used to restrict actuator movement [$u(t)$] and slew rate ($d$). Typical constraints include bounds on the amplitude and slew rate of the control signals and limits on the output [$y(t)$] such as:

$$u_{min} \leq u(t+j) \leq u_{max} \quad \forall j = 0, M-1 \tag{3.50}$$

$$du_{min} \leq u(t+j) - u(t+j-1) \leq du_{max} \quad \forall j = 0, M-1, \tag{3.51}$$

$$y_{min} - s \leq y(t+j) \leq y_{max} + s \quad \forall j = 1, N. \tag{3.52}$$

The soft constraints are indicated by $s$ in constraint Equation 3.52. The application of the objective function $J$ for the coal processes used in this thesis only considers the first two terms in Equation 3.49. This means that future behaviour in output error and and rapid input changes are controlled while future input errors and soft constraints are not applied. Only the prediction horizon $N$, control horizon $M$, weighting matrices $\mathbf{P}$ and $\mathbf{R}$, and output reference trajectory $\mathbf{y}_s$ will be configured for the NMPC simulations in Chapter 4.

The weighting matrices $\mathbf{P}$ and $\mathbf{R}$ are usually represented as diagonal matrices. Lower case letters and subscripts [i.e. $\mathbf{P}_* = \text{diag}([\ p_{*,1} \quad \cdots \quad p_{*,m}\ ])$ and $\mathbf{R}_* = \text{diag}([\ r_{*,1} \quad \cdots \quad r_{*,n}\ ])$] will be used to refer to the different diagonal components for objective function $*$ to simplify the representation of the matrices. The number of inputs is $m$ and outputs is $n$. Similarly, the output reference trajectory ($\mathbf{y}_s$) will have a subscript to represent the relevant vector components [i.e. $\mathbf{y}_s = [\ y_{s,*,1} \quad \cdots \quad y_{s,*,n}\ ]^T$].

The NMPC problem can be solved using the general nonlinear programming problem with $\mathbf{w}^T = [\mathbf{u}^T \mathbf{x}^T \mathbf{y}^T]$, that is,

$$\min_{\mathbf{w}} \quad J(\mathbf{w}), \tag{3.53}$$

$$\text{subject to :} \quad \mathbf{c}(\mathbf{w}) = 0, \mathbf{h}(\mathbf{w}) \leq 0, \tag{3.54}$$

where the equality constraint vector $\mathbf{c}$ corresponds to the model constraints and the inequality constraint vector $\mathbf{h}$ corresponds to Equation 3.52.

Given a set of initial conditions $[x(0)]$, an optimal control sequence $[u(t)^*,\ldots,u(t+M)^*]$ requires a solution via numerical optimisation on the above mentioned nonlinear programming problem with finite horizon $M$. The numerical optimisation problem must remain feasible for all $t$. Closed loop stability is also required for the state-space model (Equation 3.47) when applying the optimal control sequence $[u(t+M)^*]$.

The NMPC general state space model in Equation 3.47 is a discrete-time model. Since the models developed and used in this thesis are continuous-time models, they are firstly discretized before applied to the general nonlinear programming optimisation problem.

### 3.6.3 Unscented Kalman filter

The UKF algorithm is similar to the EKF algorithm as the state distribution is represented by Gaussian random variables (GRV), but specified under a minimal set of carefully chosen sample points (Wan and Van der Merwe, 2000). The sample points capture the true mean and covariance of the GRV when propagated through the true nonlinear system and capture the posterior mean and covariance accurately up to the third order Taylor series expansion term for any nonlinearity. This is primarily achieved by using an unscented transform (UT) detailed by Wan and Van der Merwe (2000).

The UT calculates the statistics of a random variable undergoing nonlinear transformation. Consider a random variable $\mathbf{x}$ propagating through a nonlinear function $\mathbf{y}=g(\mathbf{x})$ where $\mathbf{x}$ has mean $\bar{\mathbf{x}}$ and covariance $\mathbf{P}_{\mathbf{x}}$. The statistics of $\mathbf{y}$ are calculated by forming the matrix $\chi$ of $2L+1$ sigma vectors $\chi_i$ (with corresponding weights $W_i$) where $L$ is the dimension of $\mathbf{x}$. The following equations describe the calculation of the statistics of $\mathbf{y}$,

$$\chi_0 = \bar{\mathbf{x}}, \tag{3.55}$$

$$\chi_i = \bar{\mathbf{x}}+\left(\sqrt{(L+\lambda)\mathbf{P}_{\mathbf{x}}}\right)_i, i=1,..,L, \tag{3.56}$$

$$\chi_i = \bar{\mathbf{x}}-\left(\sqrt{(L+\lambda)\mathbf{P}_{\mathbf{x}}}\right)_{i-L}, i=L+1,..,2L, \tag{3.57}$$

$$W_0^{(m)} = \lambda/(L+\lambda), \tag{3.58}$$

$$W_0^{(c)} = \lambda/(L+\lambda)+(1-\alpha^2+\beta), \tag{3.59}$$

$$W_i^{(m)} = W_i^{(c)} = 1/\{2(L+\lambda)\}, i=1,..,2L, \tag{3.60}$$

where $\lambda = \alpha^2(L+\kappa) - L$ is a scaling parameter. $\alpha$ determines the spread of the sigma points around $\bar{\mathbf{x}}$. $\kappa$ is a secondary scaling parameter and $\beta$ is used to incorporate prior knowledge of the distribution of $\mathbf{x}$. The values for the UT parameters used in this thesis correspond to the values recommended from Wan and Van der Merwe (2000) where $\alpha$ =1E-3, $\kappa = 0$ and $\beta = 2$. The sigma vectors $\chi_i$ are propagated through the nonlinear function,

$$\gamma_i = g(\chi_i), i = 0, .., 2L, \tag{3.61}$$

and the mean and covariance for $\mathbf{y}$ are approximated with weighted sample mean and covariance of the posterior sigma points,

$$\bar{\mathbf{y}} = \sum_{i=0}^{2L} W_i^{(m)} \gamma_i, \tag{3.62}$$

$$\mathbf{P}_{\mathbf{y}} = \sum_{i=0}^{2L} W_i^{(c)} \{\gamma_i - \bar{\mathbf{y}}\}\{\gamma_i - \bar{\mathbf{y}}\}^T. \tag{3.63}$$

The UKF is an extension of the UT to the recursive estimation of $\hat{\mathbf{x}}_k$ given by,

$$\hat{\mathbf{x}}_k = (\text{prediction of } \mathbf{x}_k) + \kappa_k[\mathbf{y}_k - (\text{prediction of } \mathbf{y}_k)], \tag{3.64}$$

with noisy observation $\mathbf{y}_k$. The optimal gain term $\kappa_k$ is expressed as a function of posterior covariance matrices. A detailed derivation and description of the UKF algorithm can be found in the paper from Wan and Van der Merwe (2000). The initialisation of the algorithm requires initial covariances ($\mathbf{P}_0^a$) of the original state ($\mathbf{P}_0$), process noise ($\mathbf{P}_v$) and measurement noise ($\mathbf{P}_n$),

$$\mathbf{P}_0^a = \begin{pmatrix} \mathbf{P}_0 & 0 & 0 \\ 0 & \mathbf{P}_v & 0 \\ 0 & 0 & \mathbf{P}_n \end{pmatrix}. \tag{3.65}$$

The UKF makes use of a discrete-time state space model (Equation 3.64). Similar to the NMPC described above in Subsection 3.6.2, the UKF also requires the conversion of the continuous-time models used in this thesis to discrete time models.

# CHAPTER 4 RESULTS

## 4.1 CHAPTER OVERVIEW

In this chapter the dynamic models developed in Chapter 3 are identified and fitted to specific production data in order to represent a real industrial coal plant. The comminution and separation areas in the general minerals processing flowsheet in Figure 2.1 are used to break down the unit operations. The bin buffer for storage forms part of the comminution area in this study.

Details of each unit operation and process are described with a process flow diagram. The dynamic models are identified and fitted to specific production data taken from an industrial coal plant production historian. Once the dynamic models have been identified, model predictive control design and simulations are performed to show how the controller reacts to certain process disturbances. Simulations of the dynamic models are also performed with a UKF to illustrate how the state estimator would be able to accommodate for model-plant mismatch if the MPC were to be implemented on a real plant. Discussions of the results obtained for each production area are also given.

## 4.2 COAL COMMINUTION AREA

The actual coal comminution area that is used in this thesis is detailed in Figure 4.1. This plant consists of three areas. The first area is a material handling stockpile bunker with associated vibratory feeders. The second area is a closed comminution and sizing circuit. The final area is a material handling bin with three bin sections. Two of the bin sections have a vibratory feeder while the third bin section is manually actuated through a flap gate.

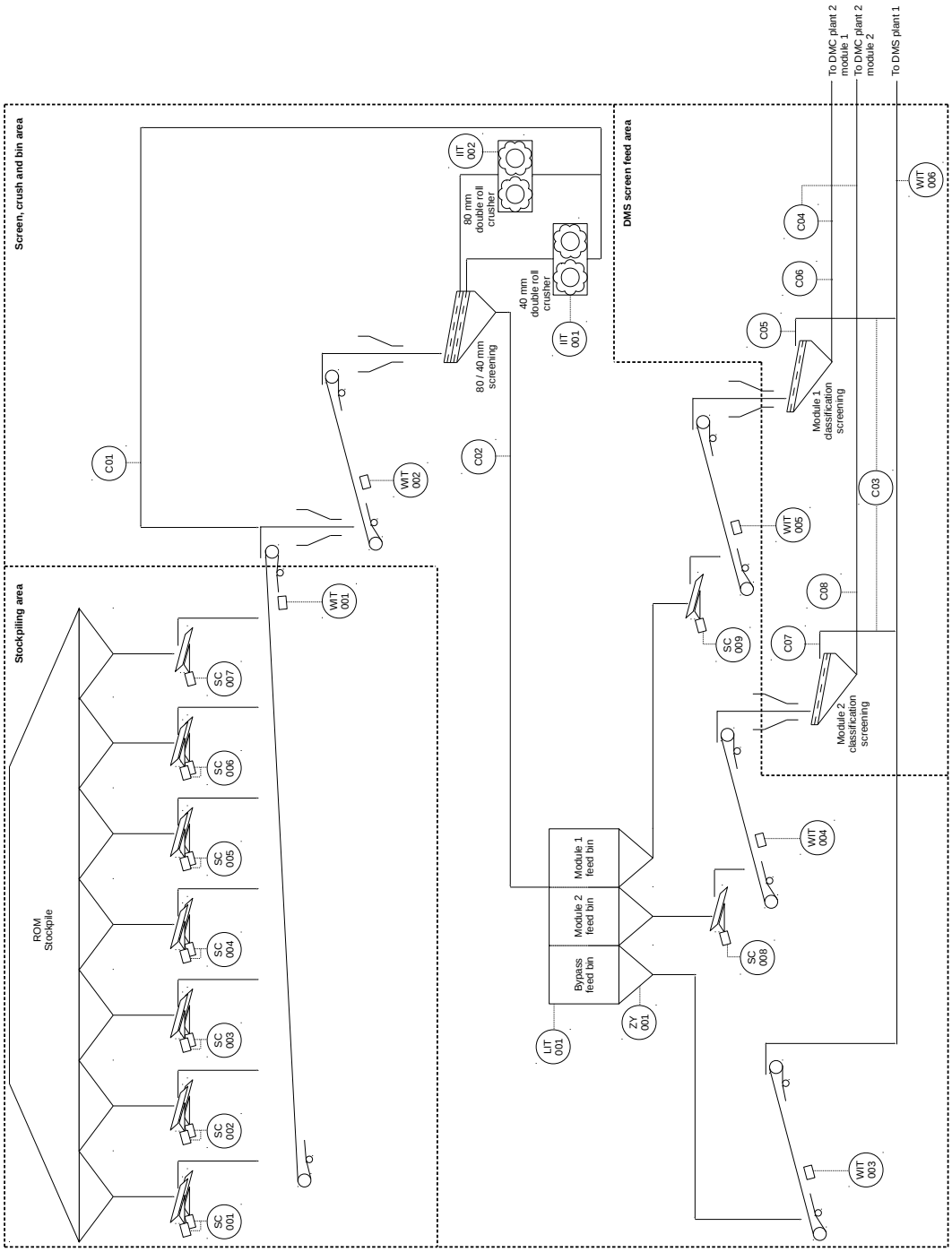


**Figure 4.1:** Coal comminution process flow schematic.

The stockpile bunker is fed by a primary crushing plant which sizes coal run-of-mine to +40mm. Material is drawn from the bunker from seven different points through vibratory feeders (SC001, SC002, SC003, SC004, SC005, SC006 and SC007). The first six points consist of two feeders each, while the last point only consists of one feeder. The draw points that have a pair of feeders only have one variable to actuate both feeders. The total mass flow rate of material drawn from the stockpile bunker is measured with a belt scale (WIT001).

The closed comminution and sizing circuit measures the combined stockpile bunker mass flow and recycle mass flow (C01) that feeds a 40/80mm double deck screen (WIT002). The oversize stream is crushed with an 80mm sized double roll crusher (measured motor current IIT002) while the undersize is crushed with a 40mm double roll crusher (measured motor current IIT001). The -40mm undersize mass flow (C02) is fed to a bin.

The bin area consists of three sections and is fed near the centre of module 1 and 2 bin compartments. Material is emptied from the bypass section manually through the use of a flap gate (ZY001). Module 1 and 2 bin sections are emptied using vibratory feeders (SC008 and SC009). All material mass flow from the bin is measured using belt scales (WIT003, WIT004 and WIT005). The level of the bin (LIT001) is also measured.

The details of all actuator and measurement tags are given in Tables 4.1, 4.2 and 4.3. These tags relate to the tags given in Figure 4.1. The associated variables and equations detailed in Chapter 3 are also given as reference to highlight how the dynamic models associate to the physical process and measurements. The type of measurement or actuation available for each tag are also given.

### 4.2.1 Dynamic model system identification

Based on the coal comminution area in Figure 4.1 and analysing the inputs and outputs, it is possible to break the system down into three dynamic model areas. The first dynamic model area is the stockpiling area while the second dynamic model area is the screening, crushing and bin area. The third dynamic model area consists of the screens responsible for sizing the material from the bin for the relevant DMS plants. The nonlinear dynamic models from Chapter 3 are used to describe the three areas and will consist of parameters relating to the models.

**Table 4.1:** Measurements used in Figure 4.1 for the stockpiling area in the comminution process.

| Name | Description | Type | Variable | Equation |
|---|---|---|---|---|
| SC001 | Stockpile tunnel feeder 1 and 2 motor speed (%) | Variable speed drive | $f_f$ | 3.1 |
| SC002 | Stockpile tunnel feeder 3 and 4 motor speed (%) | Variable speed drive | $f_f$ | 3.1 |
| SC003 | Stockpile tunnel feeder 5 and 6 motor speed (%) | Variable speed drive | $f_f$ | 3.1 |
| SC004 | Stockpile tunnel feeder 7 and 8 motor speed (%) | Variable speed drive | $f_f$ | 3.1 |
| SC005 | Stockpile tunnel feeder 9 and 10 motor speed (%) | Variable speed drive | $f_f$ | 3.1 |
| SC006 | Stockpile tunnel feeder 11 and 12 motor speed (%) | Variable speed drive | $f_f$ | 3.1 |
| SC007 | Stockpile tunnel feeder 13 motor speed (%) | Variable speed drive | $f_f$ | 3.1 |
| WIT001 | Stockpile discharge mass flow rate (t/h) | Belt scale | $W_{f,o}$ | 3.2 |

The system identification approach from Ljung (1987) is used for each model fit. Input-output data taken from an actual coal beneficiation plant production historian were used to fit the models. All data are sampled per second and filtered with a low-pass filter with time period of twenty seconds (i.e. cutoff frequency of 50mHz) to remove measurement noise. The double roll crusher motor currents were filtered using a one hundred second time period (i.e. cutoff frequency of 10mHz) to remove additional frequency components to create a smoother signal for identification. Two thirds of the production data were used to identify the models to allow for an additional one third of production data to be used for model validation. All simulation outputs and model validation results include both the two thirds model identification data and one third model validation data. This means that two thirds of the data within the time-series data was used to identify the model parameters. The model simulation was then allowed to run for another one third of the remaining time-series data. The reason for this is to illustrate that the model is able to use data both with and without prior identification for validation purposes.

**Table 4.2:** Measurements used in Figure 4.1 for the screen, crush and bin area in the comminution process (N/A stands for "not applicable").

| Name | Description | Type | Variable(s) | Equation |
|---|---|---|---|---|
| WIT002 | 40mm screen mass flow rate (t/h) | Belt scale | $W_{ds,o,i-1}$ | 3.4 |
| IIT001 | 40mm crusher motor current (A) | Current transformer | $I_{cr}$ | 3.11 |
| IIT002 | 80mm crusher motor current (A) | Current transformer | $I_{cr}$ | 3.11 |
| C01 | Crushing circuit recycle mass flow rate (t/h) | Calculation | $W_{cr,o}$ | 3.11 |
| C02 | Bin feed mass flow rate (t/h) | Calculation | WIT001+C01 | N/A |
| LIT001 | Bin level (%) | Level meter | $l_b$ | 3.19 |
| WIT003 | Bin bypass mass flow rate (t/h) | Belt scale | $W_{b,o,3}$ | 3.12 |
| ZY001 | Flap gate position | Manual | N/A | N/A |
| WIT004 | Bin module 2 mass flow rate (t/h) | Belt scale | $W_{bf,o,1}$ | 3.19 |
| SC008 | Bin module 2 feeder motor speed (%) | Variable speed drive | $f_{bf,1}$ | 3.13 |
| WIT005 | Bin module 1 mass flow rate (t/h) | Belt scale | $W_{bf,o,2}$ | 3.19 |
| SC009 | Bin module 1 feeder motor speed (%) | Variable speed drive | $f_{bf,2}$ | 3.14 |

#### 4.2.1.1 Stockpiling area

The stockpiling area consists of thirteen feeders with seven bunker draw points. The first six bunker draw points consists of two feeders per draw point while the last draw point only consists of one feeder. Each bunker draw point is actuated with a single motor frequency setpoint for each draw point area. The feeder model from Chapter 3 is used to model each draw point. It is assumed that the stockpile draw points with duel feeders can be represented as one system described by Equations 3.1 and 3.2. The seven stockpile draw point feeder models can be added together to obtain the total mass flow from the stockpile (WIT001). Each draw point is represented by a subscript number (1-7) in the process variables and parameters.

**Table 4.3:** Measurements used in Figure 4.1 for the DMS screen feed area in the comminution process (N/A stands for "not applicable").

| Name | Description | Type | Variable(s) | Equation |
|---|---|---|---|---|
| C03 | Bin module total product oversize (t/h) | Calculation | C05+C07 | N/A |
| C04 | Bin module total product undersize (t/h) | Calculation | C06+C08 | N/A |
| C05 | Bin module 1 classification screen oversize (t/h) | Calculation | $W_{ss,i}$ | 3.3 |
| C06 | Bin module 1 classification screen undersize (t/h) | Calculation | $W_{u,ss,i}$ | 3.3 |
| C07 | Bin module 2 classification screen oversize (t/h) | Calculation | $W_{ss,i}$ | 3.3 |
| C08 | Bin module 2 classification screen undersize (t/h) | Calculation | $W_{u,ss,i}$ | 3.3 |
| WIT006 | Bin total oversize to DMS plant 1 (t/h) | Belt scale | C03+WIT003 | N/A |

Material from each draw point falls onto a conveyor and is combined with the next upstream draw point's mass flow. As a result, each draw point is modelled with a time delay as described by Equation 3.37 in Chapter 3. This results in each feeder's mass flow output (Equation 3.2) being delayed with a time delay $t_{f,td,n}$ where $n$ represents the seven draw points subscript numbers (1-7).

The stockpiling area was fitted to production data from an actual coal plant. In order to obtain independent output responses for the total stockpile mass flow (WIT001) for changes made to each bunker draw point (SC001 - SC007), four sets of experiments were used. These experiments have enough uncorrelated perturbations such that the entire stockpiling area can be identified. The experimental data was taken from a coal plant production historian.

Figures 4.2, 4.3, 4.4 and 4.5 show the system identification input/output results for each experiment for the stockpiling area. The first experiment has production data with uncorrelated perturbations in the first three bunker draw points (SC001 - SC003). The second experiment has uncorrelated perturbations in the third and seventh bunker draw points (SC003 and SC007). Experiment three has uncorrelated perturbations for the fifth, sixth and seventh bunker draw points (SC005 - SC007). Experiment four uses uncorrelated perturbations in the fourth and fifth bunker draw points (SC004 and SC005).

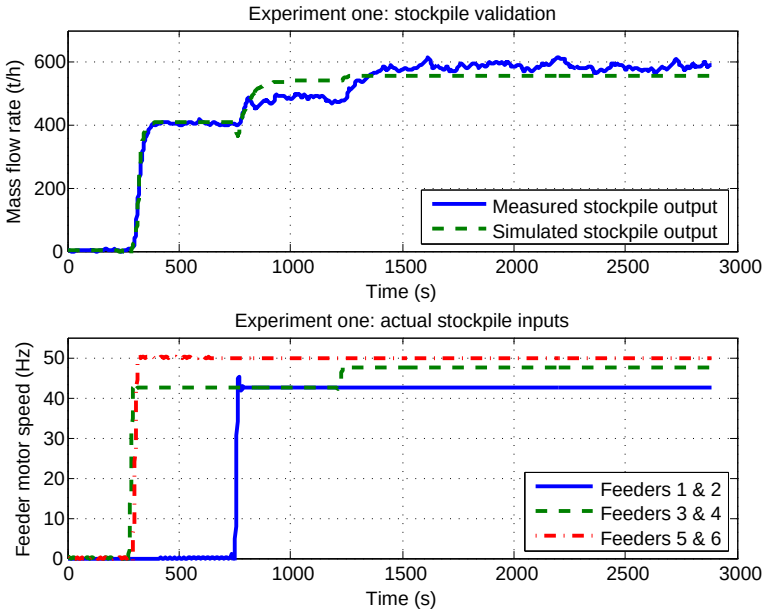


**Figure 4.2:** Stockpiling area, experiment one model validation (Stockpile output = WIT001; Feeders 1 & 2 = SC001; Feeders 3 & 4 = SC002; Feeders 5 & 6 = SC003).

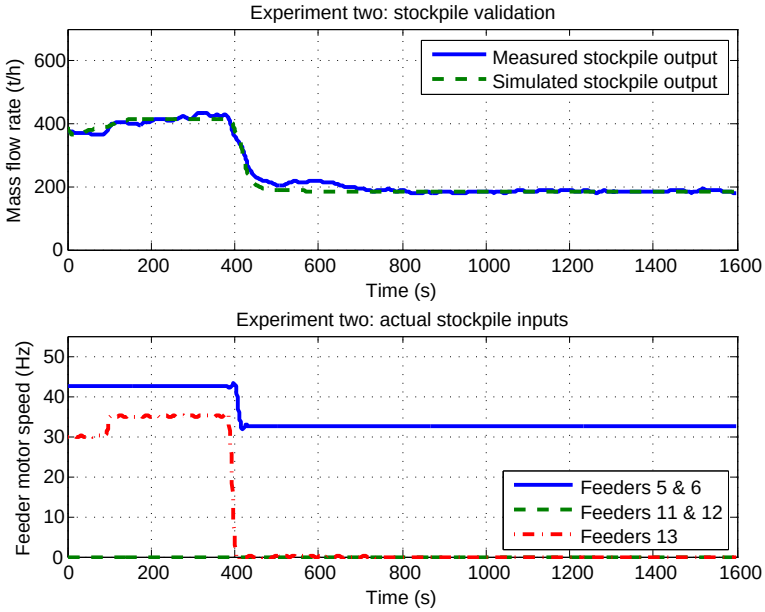


**Figure 4.3:** Stockpiling area, experiment two model validation (Stockpile output = WIT001; Feeders 5 & 6 = SC003; Feeders 11 & 12 = SC006; Feeders 13 = SC007).

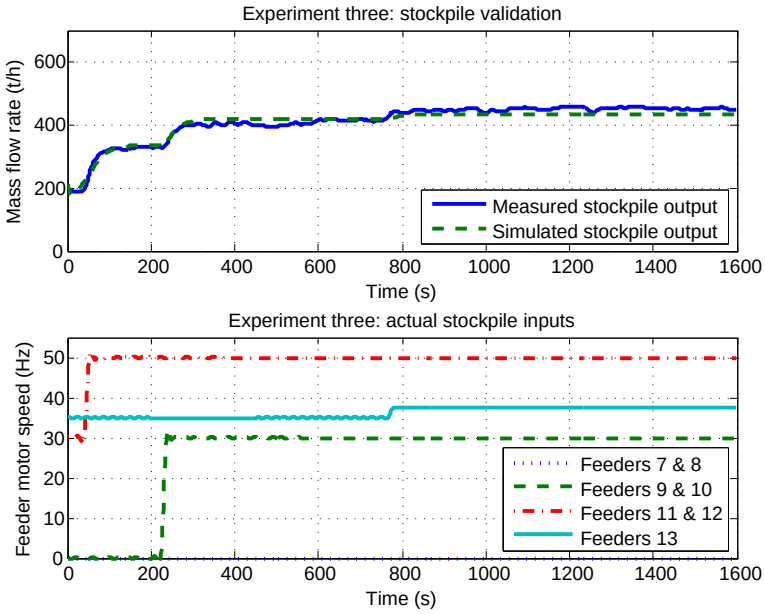


**Figure 4.4:** Stockpiling area, experiment three model validation (Stockpile output = WIT001; Feeders 7 & 8 = SC004; Feeders 9 & 10 = SC005; Feeders 11 & 12 = SC006; Feeders 13 = SC007).

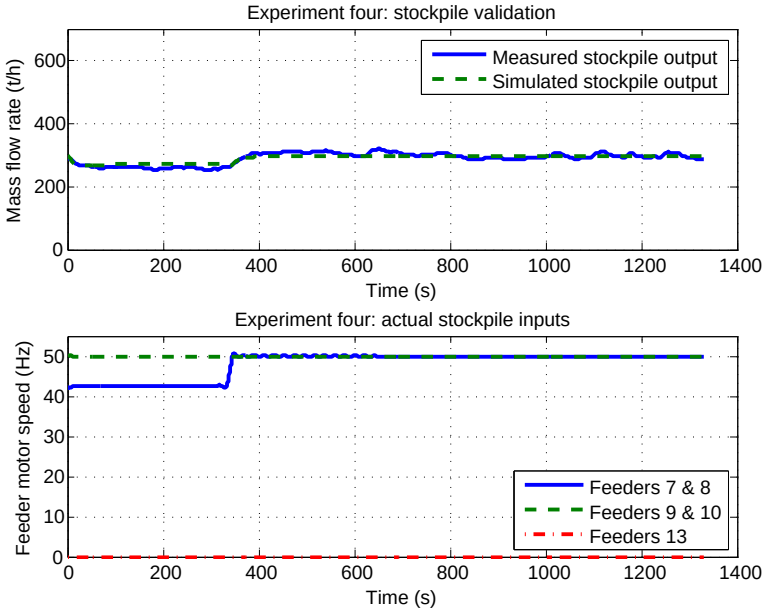


**Figure 4.5:** Stockpiling area, experiment four model validation (Stockpile output = WIT001; Feeders 7 & 8 = SC004; Feeders 9 & 10 = SC005; Feeders 13 = SC007).

**Table 4.4:** Stockpile model parameters.

| Parameter | Value | Description | Equation(s) |
|---|---|---|---|
| $K_{f,1}$ | 0.87 | Stockpile bunker draw point one proportionality constant (kg) | 3.1 |
| $K_{f,2}$ | 0.80 | Stockpile bunker draw point two proportionality constant (kg) | 3.1 |
| $K_{f,3}$ | 1.59 | Stockpile bunker draw point three proportionality constant (kg) | 3.1 |
| $K_{f,4}$ | 0.87 | Stockpile bunker draw point four proportionality constant (kg) | 3.1 |
| $K_{f,5}$ | 0.77 | Stockpile bunker draw point five proportionality constant (kg) | 3.1 |
| $K_{f,6}$ | 0.92 | Stockpile bunker draw point six proportionality constant (kg) | 3.1 |
| $K_{f,7}$ | 1.36 | Stockpile bunker draw point seven proportionality constant (kg) | 3.1 |
| $\tau_{f,1}$ | 48.34 | Stockpile bunker draw point one time constants (s) | 3.1 and 3.2 |
| $\tau_{f,2}$ | 11.60 | Stockpile bunker draw point two time constants (s) | 3.1 and 3.2 |
| $\tau_{f,3}$ | 13.81 | Stockpile bunker draw point three time constants (s) | 3.1 and 3.2 |
| $\tau_{f,4}$ | 16.40 | Stockpile bunker draw point four time constants (s) | 3.1 and 3.2 |
| $\tau_{f,5}$ | 27.14 | Stockpile bunker draw point five time constants (s) | 3.1 and 3.2 |
| $\tau_{f,6}$ | 32.46 | Stockpile bunker draw point six time constants (s) | 3.1 and 3.2 |
| $\tau_{f,7}$ | 23.21 | Stockpile bunker draw point seven time constants (s) | 3.1 and 3.2 |

The parameters that were identified for the stockpile area are given in Table 4.4 with associated time delays given in Table 4.5. The parameters associated with the relevant equations from Chapter 3 are also given.

The model fit and correlation results for the stockpile discharge (WIT001) for each experiment is shown in Table 4.6.

**Table 4.5:** Stockpile model time delays.

| Parameter | Value | Description | Equation |
|---|---|---|---|
| $t_{f,td,1}$ | 24.48 | Stockpile bunker draw point one time delay (s) | 3.37 |
| $t_{f,td,2}$ | 6.62 | Stockpile bunker draw point two time delay (s) | 3.37 |
| $t_{f,td,3}$ | 12.63 | Stockpile bunker draw point three time delay (s) | 3.37 |
| $t_{f,td,4}$ | 9.03 | Stockpile bunker draw point four time delay (s) | 3.37 |
| $t_{f,td,5}$ | 7.19 | Stockpile bunker draw point five time delay (s) | 3.37 |
| $t_{f,td,6}$ | 5.63 | Stockpile bunker draw point six time delay (s) | 3.37 |
| $t_{f,td,7}$ | 0.22 | Stockpile bunker draw point seven time delay (s) | 3.37 |

**Table 4.6:** Stockpile model output (WIT001) validation.

| Experiment | Fit (%) | Correlation |
|---|---|---|
| One | 82.1 | 0.98 |
| Two | 87.4 | 0.99 |
| Three | 72.2 | 0.97 |
| Four | 46.7 | 0.90 |

#### 4.2.1.2 Screen, crush and bin area

The screen, crush and bin area in Figure 4.1 sizes the material from the ROM stockpile (WIT001) and stores the -40mm material in a bin to act as a buffer to feed the downstream DMS plants. Screening and crushing is performed in closed circuit for the oversize material (+40mm). Larger sized material (+80mm) is crushed with an 80mm double roll crusher while the -80mm +40mm material is crushed with a 40mm double roll crusher.

The 40/80mm double deck screen and double roll crushers are modelled using the dynamic systems described in Chapter 3. Crusher motor current (IIT001 and IIT002) and stockpile feed (WIT001) are used as inputs to the closed circuit comminution. Since the undersize feeding the bin (C02) is not measured, the screen and crusher models are combined with the bin model detailed in Chapter 3 and identified using actual plant measurements. The crusher recycle mass flow rate (WIT002), bin level (LIT001) and bin feeder mass flow rates (WIT004 and WIT005) are used as outputs for model

identification.

The only actuators available in the screen, crush and bin area are the two bin feeder motor speeds (SC008 and SC009) while the third bin bypass mass flow rate (WIT003) is a measured disturbance.

A time delay $t_{cr,td}$ was included in the screening and crushing sections after the crushers using the approximation given in Equation 3.37 from Chapter 3. Another time delay approximation $t_{u,ds,c,td}$ was used to represent the transport delay of material from the double-deck screen undersize to the bin feed. Two time delays ($t_{bf,1,td}$ and $t_{bf,1,td}$) are used to represent the time taken by the material to travel from the two bin feeders to the measured outputs (WIT005 and WIT004)

When identifying the screen, crush and bin area dynamic models the different operating conditions (phases I, II and III in Figure 3.10 from Chapter 3) need to be included in the model identification. As a result, three experimental sets of production data were used for the model identification. This allows for sufficient perturbations in the inputs to fit the model over the various operating conditions and bin level behaviour.

Figures 4.6, 4.7, 4.8, 4.9, 4.10, 4.11, 4.12, 4.13 and 4.14 show the system identification input/output results for each experiment for the screen, crush and bin area. The first experiment incorporates phase I and II operating condition (from Figure 3.10). At low bin levels (LIT001), the bin feeder mass flow rates (WIT004 and WIT005) have an inverse exponential rise in mass flow rate.

Experiments two and three contain sufficient changes in the bin level (LIT001) such that the feeder mass flow rates (WIT004 and WIT005) are in phase II and III operating conditions (shown in Figure 3.10). At high bin level readings the feeder mass flow rates have a sigmoid characteristic giving a sudden rise in feeder effectiveness. Experiment three also has a scenario where material from the bin bypass (WIT003) has been opened manually.

Experiments one, two and three have sufficient perturbation in the measured stockpile feed (WIT001) to ensure the 40mm and 80mm crusher measured motor currents (IIT001 and IIT002) and screen and crush recycle measured mass flow (WIT002) contain sufficient process dynamics for the dynamic models developed. All experiments also have conditions for phase II where the bin level is within normal conditions such that the bin feeder mass flow rates behave in a linear fashion.

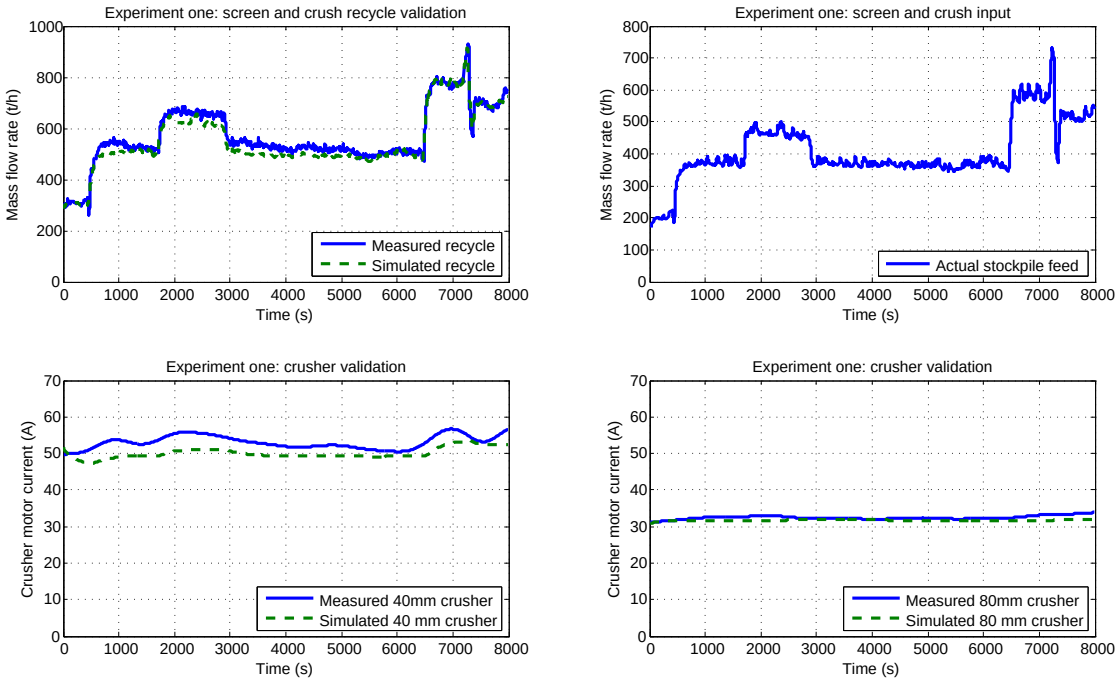


**Figure 4.6:** Screen and crush model validation for experiment one (Recycle = C01; Stockpile feed = WIT001; 40mm crusher = IIT001; 80mm crusher = IIT002).

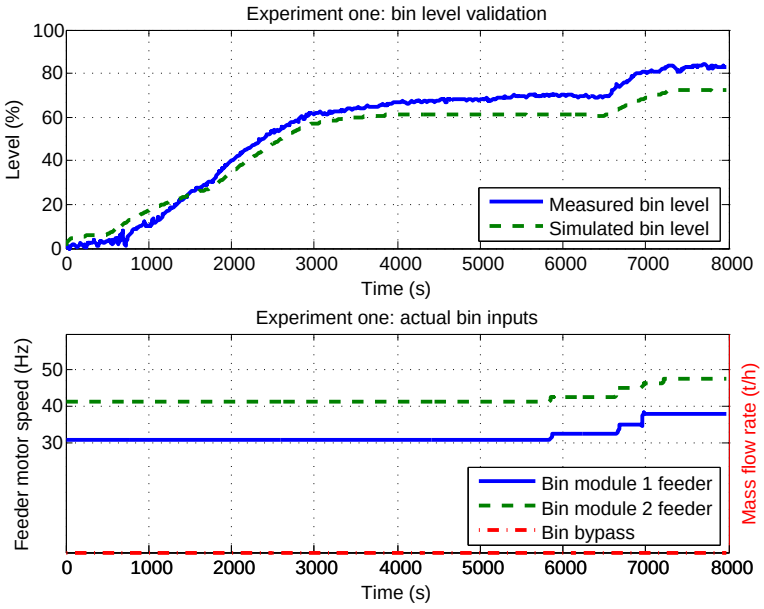


**Figure 4.7:** Bin level model validation for experiment one (Bin level = LIT001; Bin module 1 feeder = SC009; Bin module 2 feeder = SC008; Bin bypass = WIT003).

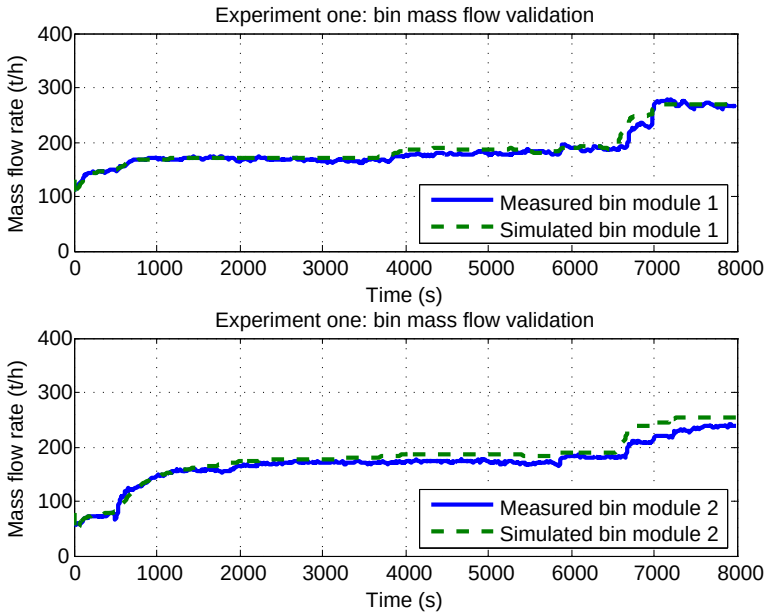


**Figure 4.8:** Bin mass flow model validation for experiment one (Bin module 1 = WIT005; Bin module 2 = WIT004).

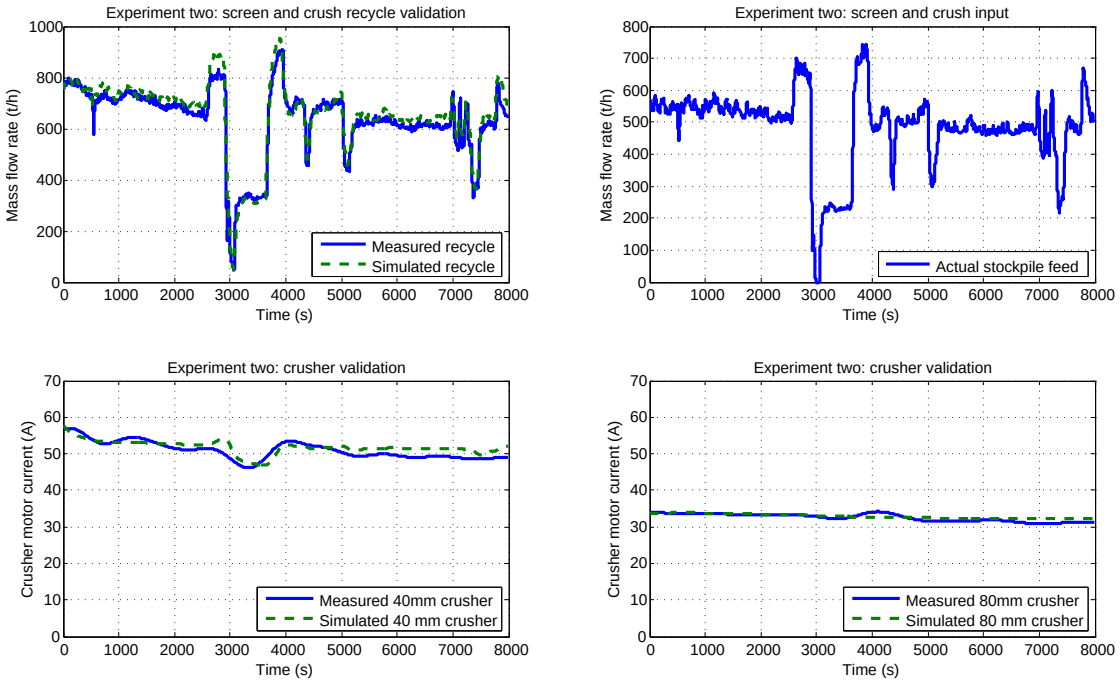


**Figure 4.9:** Screen and crush model validation for experiment two (Recycle = C01; Stockpile feed = WIT001; 40mm crusher = IIT001; 80mm crusher = IIT002).

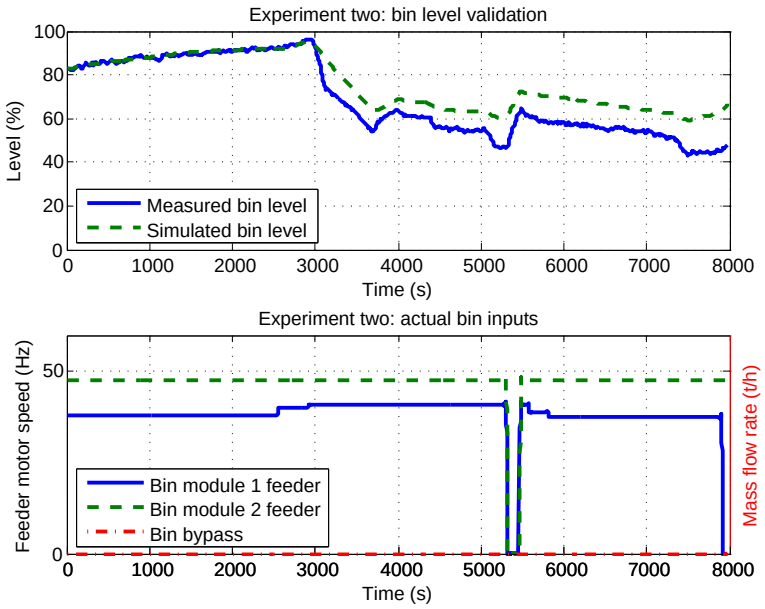


**Figure 4.10:** Bin level model validation for experiment two (Bin level = LIT001; Bin module 1 feeder = SC009; Bin module 2 feeder = SC008; Bin bypass = WIT003).

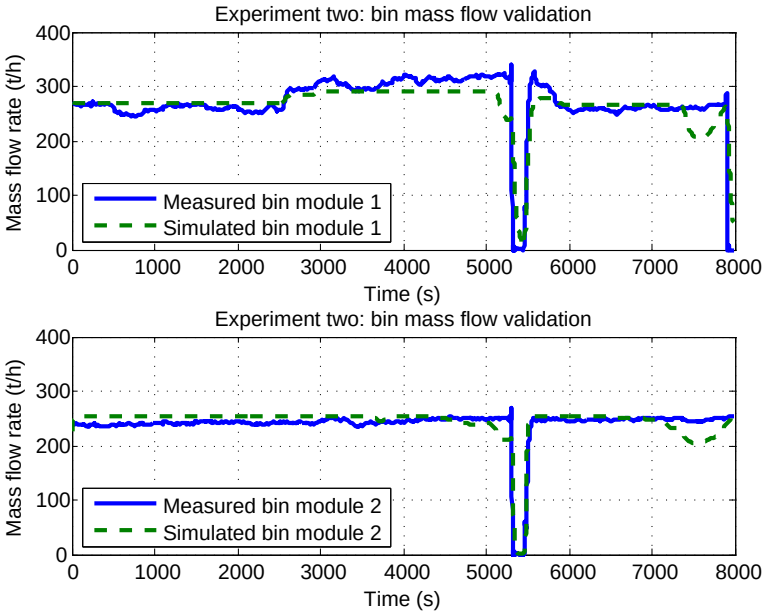


**Figure 4.11:** Bin mass flow model validation for experiment two (Bin module 1 = WIT005; Bin module 2 = WIT004).

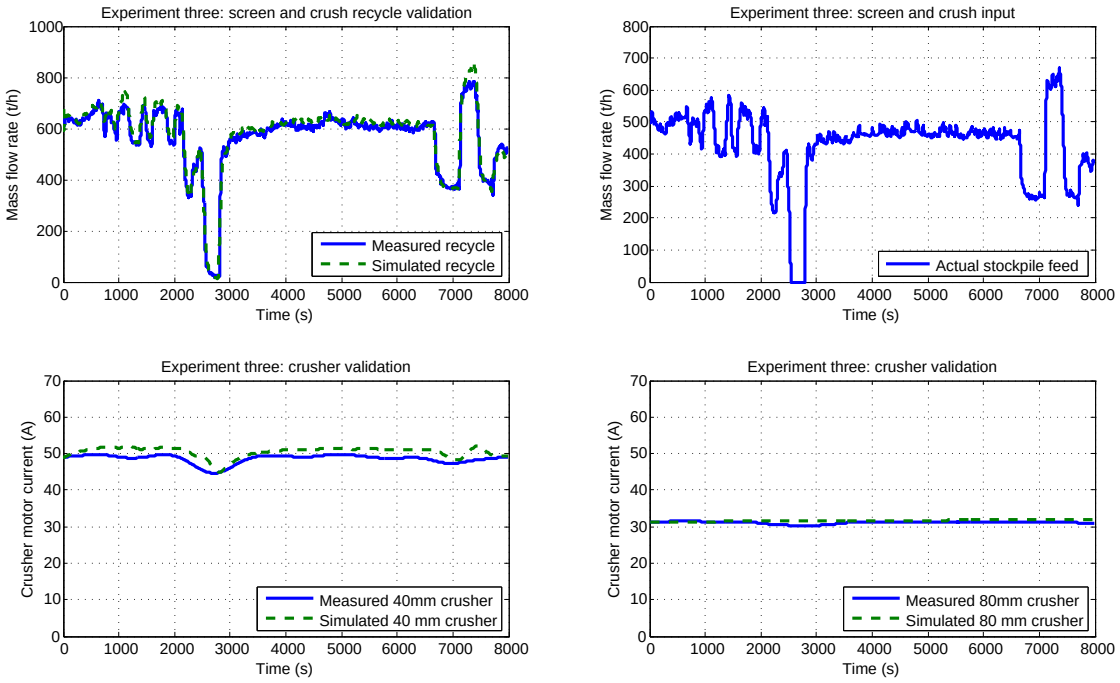


**Figure 4.12:** Screen and crush model validation for experiment three (Recycle = C01; Stockpile feed = WIT001; 40mm crusher = IIT001; 80mm crusher = IIT002).

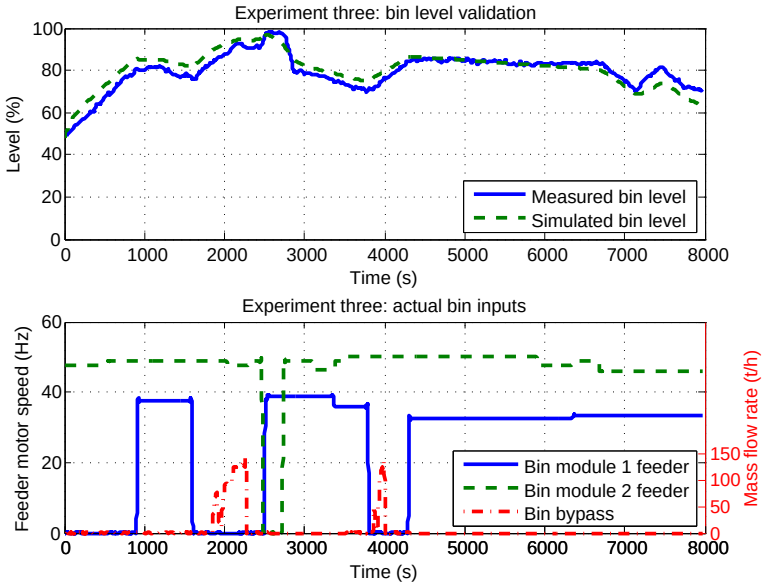


**Figure 4.13:** Bin level model validation for experiment three (Bin level = LIT001; Bin module 1 feeder = SC009; Bin module 2 feeder = SC008; Bin bypass = WIT003).

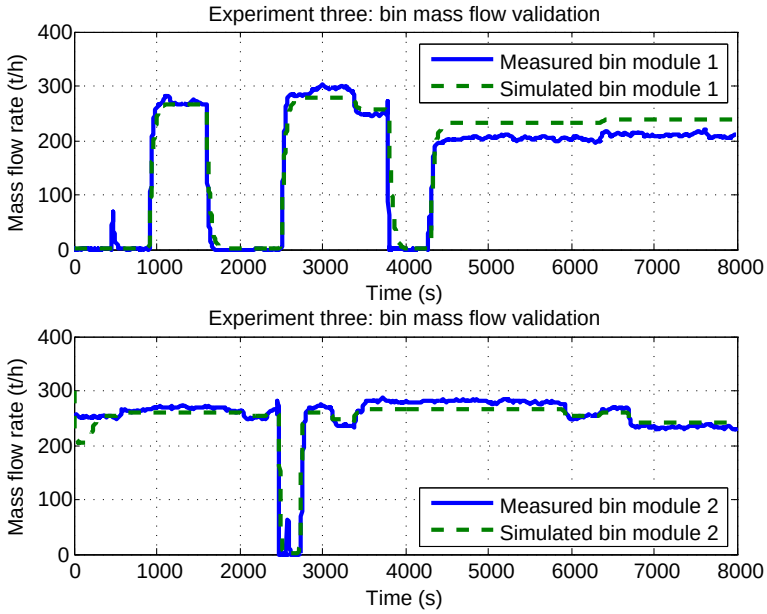


**Figure 4.14:** Bin mass flow model validation for experiment three (Bin module 1 = WIT005; Bin module 2 = WIT004).

**Table 4.7:** Screen and crush model parameters for double-deck screen.

| Parameter | Value | Description | Equation |
|---|---|---|---|
| $\tau_{ds,o}$ | 4.26 | Double-deck screen top deck oversize time constant (s) | 3.4 |
| $\tau_{u,ds,o}$ | 3.82 | Double-deck screen top deck undersize time constant (s) | 3.4 |
| $\tau_{ds,c}$ | 657.24 | Double-deck screen bottom deck oversize time constant (s) | 3.5 |
| $\tau_{u,ds,c}$ | 27.93 | Double-deck screen bottom deck undersize time constant (s) | 3.5 |
| $\alpha_{ds,o}$ | 0.25 | Double-deck screen top deck mass split | 3.4 |
| $\alpha_{ds,c}$ | 0.27 | Double-deck screen bottom deck mass split | 3.5 |

Tables 4.7, 4.8 and 4.9 shows the parameter values that were estimated during the model fit using system identification (Ljung, 1987). The parameters are based on the double-deck screen (Equations 3.4 and 3.5), crusher (Equations 3.7 and 3.10) and bin (Equations 3.15, 3.16, 3.17, 3.18 and 3.19) models derived in Chapter 3. Table 4.10 shows the time delays estimated for the screen, crush and bin system. The parameters associated with the relevant equations from Chapter 3 are also given.

**Table 4.8:** Screen and crush model parameters for double roll crushers.

| Parameter | Value | Description | Equation |
|---|---|---|---|
| $R_{cr,i,80}$ | 0.17 | 80mm double roll crusher feed fraction of solids above 80mm | 3.7 |
| $K_{cr,80,1}$ | 9E-04 | 80mm double roll crusher hold-up proportionality constant [kg/(sA)] | 3.7 |
| $\tau_{cr,80}$ | 29.79 | 80mm double roll crusher time constant (s) | 3.7 |
| $R_{cr,o,80}$ | 0.65 | 80mm double roll crusher product fraction of solids above 80mm | 3.7 |
| $I_{cr,min,80}$ | 42.00 | 80mm double roll crusher motor current at no load (A) | 3.10 |
| $K_{cr,80,2}$ | 0.65 | 80mm double roll crusher motor current proportionality constant for size interval 80mm (A/s) | 3.10 |
| $K_{cr,80,3}$ | 3.03E-05 | 80mm double roll crusher motor current proportionality constant for torque load at size interval 80mm [A/(kg.s)] | 3.10 |
| $R_{cr,i,40}$ | 0.01 | 40mm double roll crusher feed fraction of solids above 40mm | 3.7 |
| $K_{cr,40,1}$ | 2E-04 | 40mm double roll crusher hold-up proportionality constant [kg/(sA)] | 3.7 |
| $\tau_{cr,40}$ | 452.53 | 40mm double roll crusher time constant (s) | 3.7 |
| $R_{cr,o,40}$ | 0.44 | 40mm double roll crusher product fraction of solids above 40mm | 3.7 |
| $I_{cr,min,40}$ | 29.75 | 40mm double roll crusher motor current at no load (A) | 3.10 |
| $K_{cr,40,2}$ | 0.91 | 40mm double roll crusher motor current proportionality constant for size interval 40mm (A/s) | 3.10 |
| $K_{cr,40,3}$ | 4.64E-07 | 40mm double roll crusher motor current proportionality constant for torque load at size interval 40mm [A/(kg.s)] | 3.10 |

**Table 4.9:** Bin model parameters.

| Parameter | Value | Description | Equation |
|---|---|---|---|
| $K_{bf,1,1}$ | 1.52 | Bin function proportionality constant for module one feeder (kg) | 3.15 |
| $K_{bf,1,2}$ | 34.77 | Bin function proportionality constant for module one feeder | 3.15 |
| $K_{bf,1,3}$ | 0.46 | Bin function proportionality constant for module one feeder (kg) | 3.15 |
| $K_{bf,1,4}$ | 280.35 | Bin function proportionality constant for module one feeder | 3.15 |
| $K_{bf,1,5}$ | 0.61 | Bin function proportionality constant for module one feeder | 3.15 |
| $K_{bf,2,1}$ | 1.20 | Bin function proportionality constant for module two feeder (kg) | 3.16 |
| $K_{bf,2,2}$ | 9.77 | Bin function proportionality constant for module two feeder | 3.16 |
| $K_{bf,2,3}$ | 0.28 | Bin function proportionality constant for module two feeder (kg) | 3.16 |
| $K_{bf,2,4}$ | 122.99 | Bin function proportionality constant for module two feeder | 3.16 |
| $K_{bf,2,5}$ | 0.62 | Bin function proportionality constant for module two feeder | 3.16 |
| $\tau_{bf,1}$ | 40.49 | Bin module one feeder time constant (s) | 3.19 |
| $\tau_{bf,2}$ | 13.65 | Bin module two feeder time constant (s) | 3.19 |
| $M_b$ | 9.72E+06 | Proportionality constant for bin stockpile relative level (kg) | 3.17 |
| $K_{b,1}$ | 3.86 | Bin stockpile height ratio parameter | 3.18 |
| $K_{b,2}$ | 1.22 | Bin stockpile height ratio parameter | 3.18 |

**Table 4.10:** Screen, crush and bin model time delays.

| Parameter | Value | Description | Equation |
|---|---|---|---|
| $t_{cr,td}$ | 87.57 | Time delay for crusher recycle (s) | 3.37 |
| $t_{u,ds,c,td}$ | 2.12 | Time delay for bin feed (s) | 3.37 |
| $t_{bf,1,td}$ | 0.55 | Bin module one time delay (s) | 3.37 |
| $t_{bf,2,td}$ | 0.17 | Bin module two time delay (s) | 3.37 |

**Table 4.11:** Screen, crush and bin model output validation (negative fit implies that a portion of the dynamic model does not predict future values well).

| Experiment | Output | Fit (%) | Correlation |
|---|---|---|---|
| One | Screen and crush recycle (WIT002) | 75.3 | 0.99 |
| | 40mm crusher motor current (IIT001) | -82.4 | 0.73 |
| | 80mm crusher motor current (IIT002) | -71.1 | 0.59 |
| | Bin module one feeder (WIT005) | 79.7 | 0.99 |
| | Bin module two feeder (WIT004) | 64.3 | 0.99 |
| | Bin level (LIT001) | 71.8 | 1.00 |
| Two | Screen and crush recycle (WIT002) | 73.2 | 0.98 |
| | 40mm crusher motor current (IIT001) | 30.5 | 0.80 |
| | 80mm crusher motor current (IIT002) | 27.1 | 0.80 |
| | Bin module one feeder (WIT005) | 45.4 | 0.85 |
| | Bin module two feeder (WIT004) | 53.8 | 0.90 |
| | Bin level (LIT001) | 49.0 | 0.98 |
| Three | Screen and crush recycle (WIT002) | 79.3 | 0.99 |
| | 40mm crusher motor current (IIT001) | -71.5 | 0.82 |
| | 80mm crusher motor current (IIT002) | -93.2 | -0.03 |
| | Bin module one feeder (WIT005) | 76.2 | 0.98 |
| | Bin module two feeder (WIT004) | 66.9 | 0.95 |
| | Bin level (LIT001) | 54.3 | 0.90 |

The model fit for the screen, crush and bin system is relatively good and is sufficient for control purposes. Table 4.11 shows a summary of the model fit and correlation for the three experiments.

#### 4.2.1.3 DMS screen feed area

The final production area for the coal comminution circuit is where the ROM material is sized and fed to various DMS plants. In Figure 4.1 the DMS screen feed area consists of many calculation points. In order to identify the two classifying screen modules, the calculation points are necessary for the generation of production data. Given the two bin feed mass flow rates (WIT005 and WIT004), the

measured mass flow rate to DMS plant one (WIT006) and measured bin bypass (WIT003), the total classified overflow (C03) from the classification screens is as follows,

$$\text{C03} = \text{WIT006} - \text{WIT003}. \tag{4.1}$$

As a result, the total classified underflow (C04) is calculated using a mass balance where,

$$\text{C04} = \text{WIT005} + \text{WIT004} - \text{C03}. \tag{4.2}$$

Assuming that the material for the classification screens' products (C05, C06, C07 and C08) are proportional to the bin feed mass flow rates (WIT005 and WIT004), the overflow and underflow of each classification screen can be calculated as follows,

$$\begin{aligned}
\text{C05} &= \text{WIT005}\frac{\text{C03}}{\text{WIT004} + \text{WIT005}}, && (4.3)\\
\text{C06} &= \text{WIT005} - \text{C05}, && (4.4)\\
\text{C07} &= \text{WIT004}\frac{\text{C03}}{\text{WIT004} + \text{WIT005}}, && (4.5)\\
\text{C08} &= \text{WIT004} - \text{C07}. && (4.6)\\
& && (4.7)
\end{aligned}$$

Using the above assumptions, calculations and the single-deck screen model from Chapter 3, the DMS screen feed system (Equation 3.3) can be fitted to production data.

Figures 4.15, 4.16 and 4.17 show the system identification input/output results for the module classification screen system.

Table 4.12 shows the parameter values that were estimated during the model fit using system identification (Ljung, 1987). The parameters are based on the single-deck screen model derived in Chapter 3. Table 4.13 shows the time delays estimated for the bypass stream (WIT003). The parameters associated with the relevant equations from Chapter 3 are also given.

The model fit and correlation results for the DMS classification screens are shown in Table 4.14.

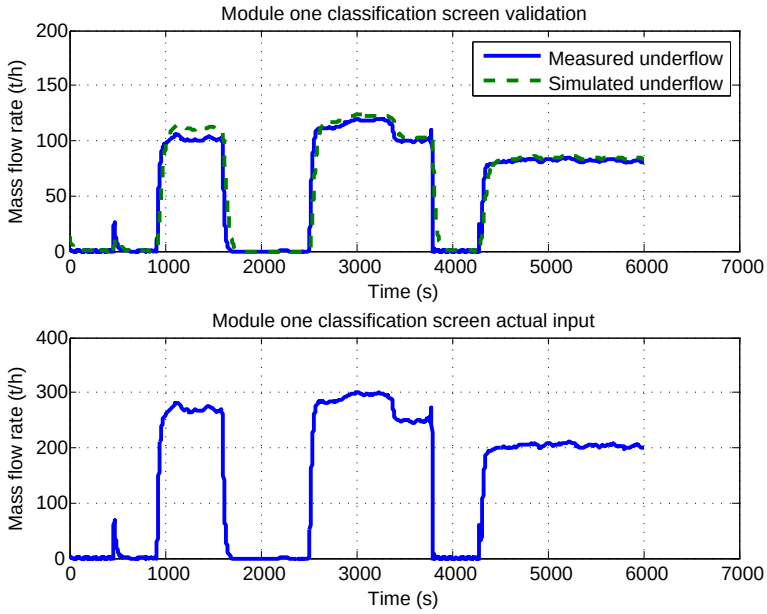


**Figure 4.15:** Module one classification screen undersize validation (Module one classification screen underflow = C06; Module one classification screen actual input = WIT005).

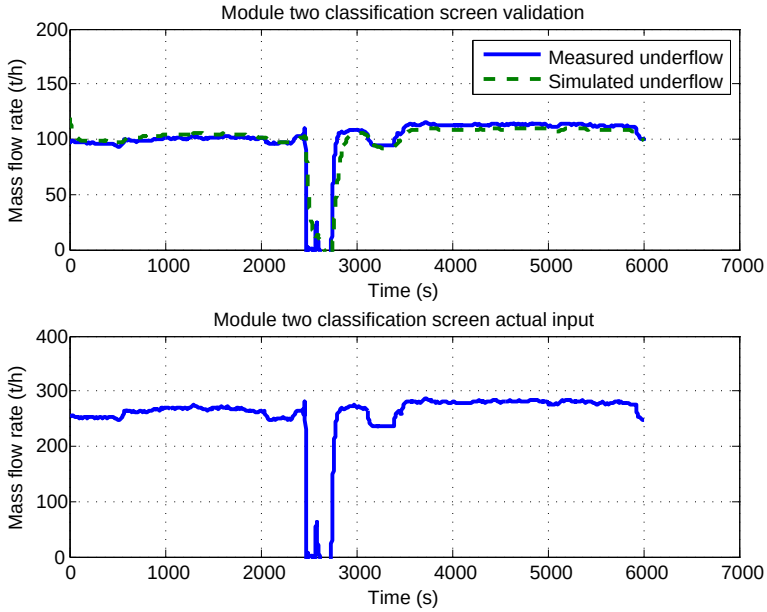


**Figure 4.16:** Module two classification screen undersize validation (Module two classification screen underflow = C08; Module two classification screen actual input = WIT004).

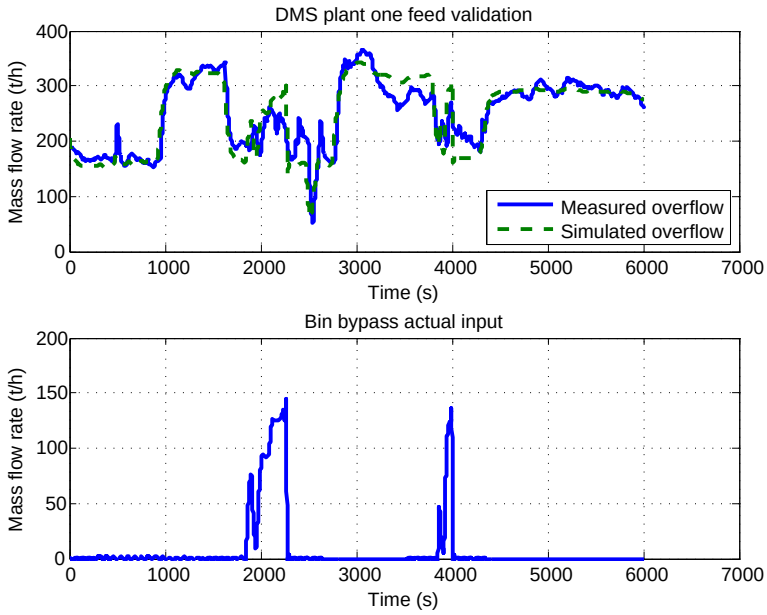


**Figure 4.17:** Module one and two classification screen oversize validation (DMS plant one overflow = WIT006; Bin bypass actual input = WIT003).

**Table 4.12:** Bin classification screen model parameters.

| Parameter | Value | Description | Equation |
|---|---|---|---|
| $\tau_{m1,ss,o}$ | 33.00 | Module 1 single-deck classification screen oversize time constant (s) | 3.3 |
| $\tau_{m1,ss,u}$ | 26.45 | Module 1 single-deck classification screen undersize time constant (s) | 3.3 |
| $\alpha_{m1,ss}$ | 0.64 | Module 1 single-deck classification screen mass split | 3.3 |
| $\tau_{m2,ss,o}$ | 43.55 | Module 2 single-deck classification screen oversize time constant (s) | 3.3 |
| $\tau_{m2,ss,o}$ | 41.89 | Module 2 single-deck classification screen undersize time constant (s) | 3.3 |
| $\alpha_{m2,ss}$ | 0.62 | Module 2 single-deck classification screen mass split | 3.3 |

**Table 4.13:** Bin classification screen model time delay.

| Parameter | Value | Description | Equation |
|---|---|---|---|
| $t_{bp,td}$ | 1.15 | Time delay for bin bypass (s) | 3.37 |

**Table 4.14:** DMS screen feed validation.

| Output | Fit (%) | Correlation |
|---|---|---|
| Module one undersize (C06) | 78.9 | 0.98 |
| Module two undersize (C08) | 61.1 | 0.92 |
| DMS plant one feed (WIT006) | 57.7 | 0.93 |

### 4.2.2 Model predictive control design and simulation

This subsection details the application of model-based process control for the coal comminution circuit detailed above. The objectives of the model-based control (Steyn, 2014a) are as follows:

- Primarily ensure that the bin never runs empty or overflows;
- Maximise plant throughput; and
- Ensure product bin mass flow rate is maintained in proportion with each other.

In order to control the comminution circuit given, it is necessary to test a number of control scenarios for the various areas within the process. Three scenarios are used to test the control simulation of the plant, namely:

- Scenario one: Stockpile area control
- Scenario two: Feed bin control
- Scenario three: Comminution circuit control

The control of the stockpile area tests how the stockpile dynamic model can be controlled through NMPC by adjusting the seven feeder motor frequencies such that the mass flow rate from the stockpile is maintained at a certain reference trajectory. The feed bin control tests how the bin level can be used to change the NMPC objective function to focus on either throughput or maintaining the bin level. The

**Table 4.15:** Stockpile area control conditions.

| Condition | Time period | Description |
|---|---|---|
| One | 0 - 10min | Control WIT001 at 500t/h |
| Two | 10min - 20min | Control WIT001 at 50t/h |
| Three | 20min - 30min | Control WIT001 at 500t/h |
| Four | 30min - 40min | Deactivate three feeder bunkers |

comminution circuit control shows how to automatically start up the plant using the stockpile control while applying the level control of the bin. A disturbance is also introduced to the stockpile product to determine how the controller reacts if additional material is fed into the plant either by front end loaders or manual manipulation of the stockpile feeder system.

#### 4.2.2.1 Stockpile area control

In order to control the stockpile area the seven feeders need to be automatically adjusted by the NMPC to ensure the stockpile output (WIT001) is maintained at a certain reference trajectory ($\text{WIT001}_{\text{SP}}$). To test the control of the stockpile area, four conditions are used (Table 4.15). The first condition is to start the feeders and operate the stockpile output at 500t/h. After ten minutes, the second condition is to lower the stockpile output to 50t/h. The third condition is to bring the stockpile output to 500t/h again after twenty minutes. The stockpile output reference trajectory is illustrated more clearly in Figure 4.18. The fourth condition tests how the NMPC reacts to a situation if the first three feeder bunkers are manually deactivated.

An additional criteria is used for the stockpile area objective so as to ensure that all of the feeders are utilised over time. With the objectives of the stockpile control test conditions described above and the definition of the MPC objective function (Equation 3.49) with typical constraints (Equations 3.50, 3.51 and 3.52), the stockpile output (WIT001) and feeder utilisation ($f_{\text{Util},T}$) are controlled. The feeder utilisation ($f_{\text{Util},T}$) is calculated by averaging the total utilisation of each feeder motor speed over time ($f_{\text{Util},T} = \sum_{i=1}^{7} f_{\text{Util},i}/7$).

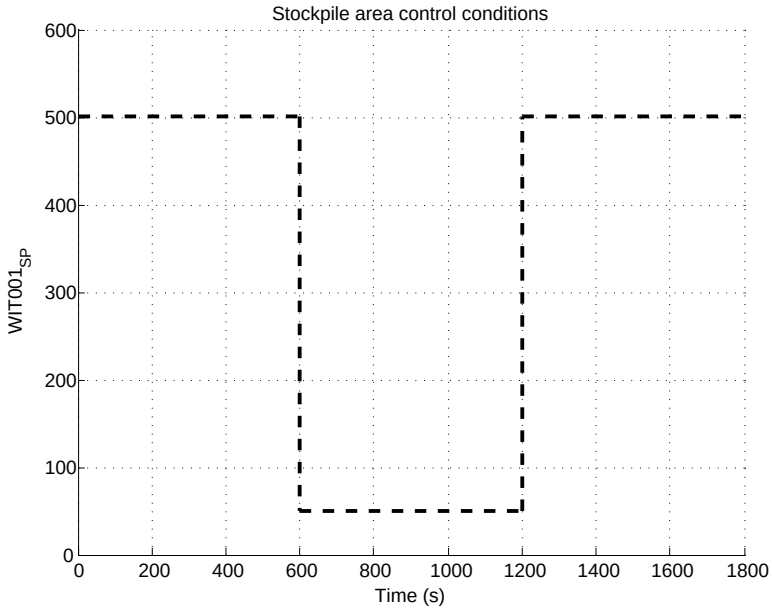


**Figure 4.18:** Stockpile area control conditions ($WIT001_{SP}$=WIT001 setpoint)

This means that the stockpile objective function for the MPC is,

$$\begin{aligned} J_{\text{stockpile}} = & \sum_{j=1}^{N} r_{\text{stockpile},1} |y_{\text{stockpile},1}(t+j) - y_{s,\text{stockpile},1}(t+j)|^2 + \\ & r_{\text{stockpile},2} |y_{\text{stockpile},2}(t+j) - y_{s,\text{stockpile},2}(t+j)|^2 + \\ & \sum_{j=0}^{M-1} \|\Delta \mathbf{u}_{\text{stockpile}}(t+j)\|^2_{\mathbf{P}_{\text{stockpile}}}, \end{aligned} \tag{4.8}$$

where $M = 2$ and $N = 5$. This implies that the prediction horizon is five seconds and control horizon is two seconds. The objective is to ensure the stockpile output WIT001 tracks a reference trajectory $WIT001_{SP}$ and that the feeders are all utilised over time.

Table 4.16 describes the variables and associated values that are used for the MPC objective function $J_{\text{stockpile}}$.

The constraints of the stockpile area are,

$$0 \leq \mathbf{u}_{\text{stockpile}} \leq 50 \quad \forall t, \tag{4.9}$$

$$0 \leq y_{\text{stockpile},1}(t) \leq 600 \quad \forall t, \tag{4.10}$$

such that the inputs for all feeders' variable speed drive frequencies fall within operating ranges of 0Hz and 50Hz. The stockpile product (WIT001) must not exceed 600t/h to ensure that equipment and the process downstream does not overload.

**Table 4.16:** Stockpile area MPC objective function setup.

| Variable | Value or tagname |
|---|---|
| $r_{\text{stockpile},1}$ | 100 |
| $y_{\text{stockpile},1}$ | WIT001 |
| $y_{s,\text{stockpile},1}$ | $\text{WIT001}_{\text{SP}}$ |
| $r_{\text{stockpile},2}$ | 100 |
| $y_{\text{stockpile},2}$ | $f_{\text{Util},T}$ |
| $y_{s,\text{stockpile},2}$ | 0.95 |
| $\mathbf{P}_{\text{stockpile}}$ | $200\mathbf{I}_7$ |
| $\mathbf{u}_{\text{stockpile}}$ | SC001-SC007 |

With the objective function and constraints defined (Equations 4.8, 4.9 and 4.10), the process can be simulated using MPC. The stockpile dynamic model (state Equation 3.1) is used for the MPC future prediction and the control simulation. The NMPC problem can be solved by using the nonlinear programming problem described in Subsection 3.6.2. The objective function (Equation 4.8) is minimised over control moves subject to plant dynamics and input/output constraints detailed above.

Figure 4.19 illustrates the MPC control moves based on the above stockpile objectives and varying conditions. Figure 4.20 illustrates the stockpile output (WIT001) response from the MPC control moves.

During the simulation, the total utilisation for each feeder ($f_{\text{Util},T}$) was calculated and is shown in Table 4.17. The reason for incorporating the feeder utilisation in the objective function is to ensure that the MPC optimisation solver does not select a particular solution and maintain that solution for the feeder motor frequencies throughout the entire operation. In this simulation, the objective for the total feeder utilisation $f_{\text{Util},T}$ is to ensure that all feeders have a utilisation of 95%. This objective is activated every minute. However, during normal operation, it is recommended that this objective is activated every hour. In this simulation, the total utilisation was 78%.

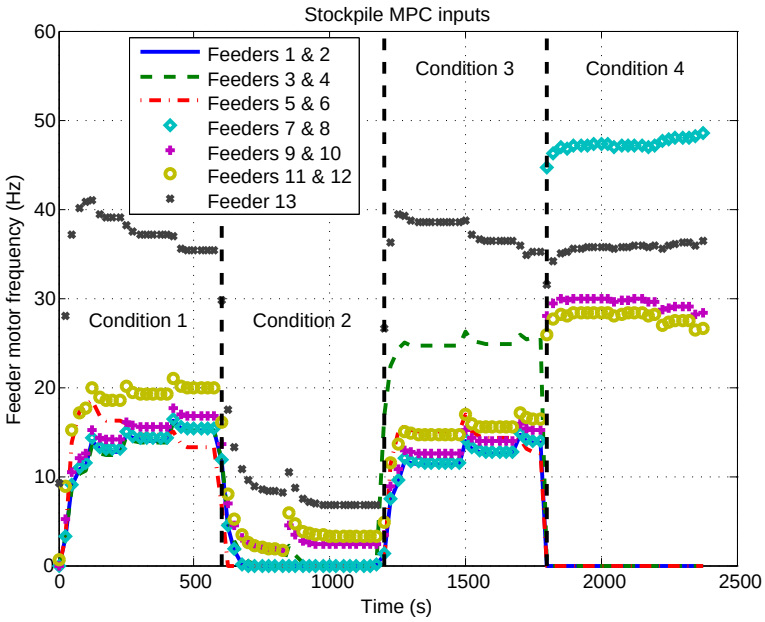


**Figure 4.19:** Stockpile MPC inputs (Feeders 1 & 2 = SC001; Feeders 3 & 4 = SC002; Feeders 5 & 6 = SC003; Feeders 7 & 8 = SC004; Feeders 9 & 10 = SC005; Feeders 11 & 12 = SC006; Feeders 13 = SC007).

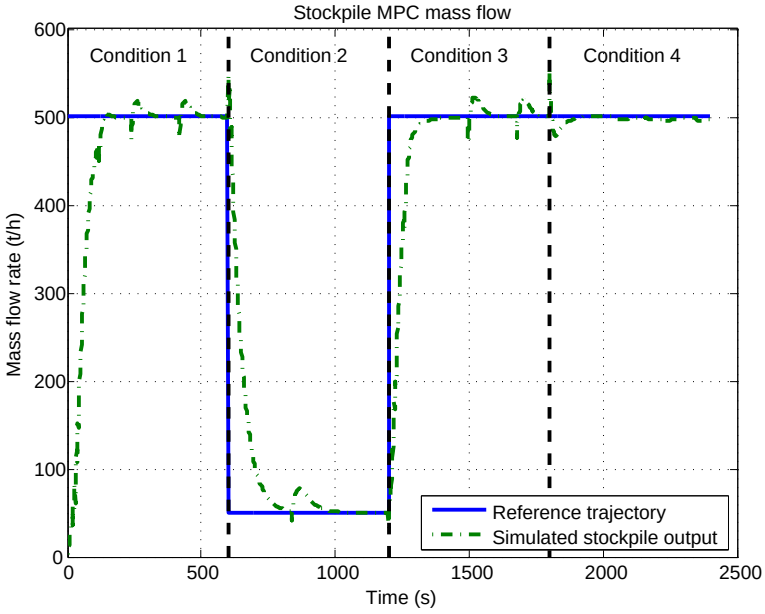


**Figure 4.20:** Stockpile MPC output (Stockpile output = WIT001).

**Table 4.17:** Stockpile feeder utilisation.

| Feeder | Utilisation (%) |
|---|---|
| SC001 ($f_{\text{Util},1}$) | 53 |
| SC002 ($f_{\text{Util},2}$) | 61 |
| SC003 ($f_{\text{Util},3}$) | 50 |
| SC004 ($f_{\text{Util},4}$) | 79 |
| SC005 ($f_{\text{Util},5}$) | 100 |
| SC006 ($f_{\text{Util},6}$) | 100 |
| SC007 ($f_{\text{Util},7}$) | 100 |
| Total ($f_{\text{Util},T}$) | 78 |

#### 4.2.2.2 Feed bin control

For the feed bin area control simulation, it is assumed that the stockpile area is operated manually while the feed bin and DMS screen feed are controlled automatically. This allows for the comparison of the NMPC performance to the manually controlled situation. The production data of experiment three (Sub-subsection 4.2.1.2) that was used for the identification of the screen, crush and bin area models, are used to illustrate the feed bin controller. The simulated manually operated plant response is compared to that of the simulated automatic control.

This implies that the mass flow from the stockpile area (WIT001) is a measured disturbance (since it is the result of manually operating the seven stockpile feeder bunker areas). The screen and crushing process therefore simulates the resulting crusher recycle mass flow (C01) and screen undersize mass flow (C02) being fed to the bin.

The feed bin area has competing objectives. The first objective is to maximise throughput to the DMS plants downstream while ensuring consistent control of the mass flows. The second objective is to ensure that the bin level does not run empty or overflow. By trying to maximise throughput, the bin will naturally run empty. If the feed to the bin becomes too high, the bin could overflow. This balancing act is represented in Figure 4.21.

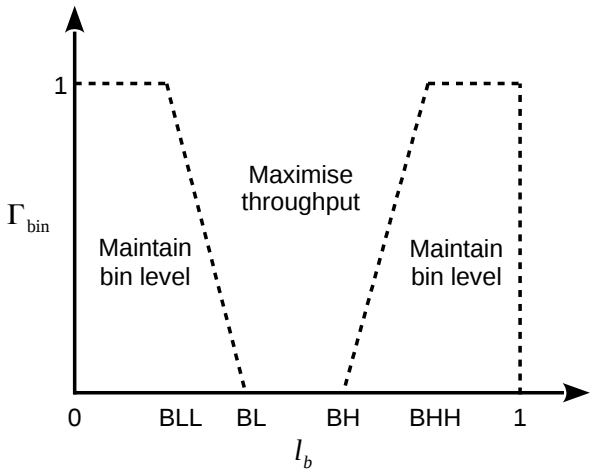


**Figure 4.21:** Feed bin control objective ($\Gamma_{\text{bin}}$ = Objective function factor used in Equation 4.11; $l_b$ = LIT001).

Figure 4.21 illustrates the varying objective of the bin system. At low and high bin levels ($l_b <$ BL or $l_b >$ BH) the objective of the controller should be to ensure the bin level reaches a point within safe limits (i.e. between BL and BH). This is to ensure the bin doesn't overflow or run empty. While the bin level is within safe limits (BL $\leq l_b \leq$ BH) the objective of the controller should be to maximise throughput. Maximising throughput is achieved by controlling module one and two undersize mass flow rates and DMS plant one feed mass flow rates at desired reference trajectories.

The bin level (LIT001) and DMS plant feed mass flow rates (C06, C08 and WIT006) are controlled according to the objectives of the feed bin operation described above and the definition of the MPC objective function (Equation 3.49) with typical constraints (Equations 3.50, 3.51 and 3.52).

This means that the bin objective function for the MPC is,

$$\begin{aligned} J_{\text{bin}} \quad = \quad & \sum_{j=1}^{N} r_{\text{bin},1} |\Gamma_{\text{bin}}(y_{\text{bin},1}(t+j) - y_{s,\text{bin},1}(t+j))|^2 + \\ & r_{\text{bin},2} |(1-\Gamma_{\text{bin}})(y_{\text{bin},2}(t+j) - y_{s,\text{bin},2}(t+j))|^2 + \\ & r_{\text{bin},3} |(1-\Gamma_{\text{bin}})(y_{\text{bin},3}(t+j) - y_{s,\text{bin},3}(t+j))|^2 + \\ & r_{\text{bin},4} |y_{\text{bin},4}(t+j) - y_{s,\text{bin},4}(t+j)|^2 + \\ & \sum_{j=0}^{M-1} \|\Delta \mathbf{u}_{\text{bin}}(t+j)\|^2_{\mathbf{P}_{\text{bin}}}, \end{aligned} \tag{4.11}$$

where the control horizon is two seconds ($M = 2$) and the prediction horizon is five seconds ($N = 5$). The bin objective is to ensure the bin level tracks a reference trajectory of 50% during high and low bin

**Table 4.18:** Bin MPC objective function setup.

| Variable | Value or tagname |
|---|---|
| BLL | 15% |
| BL | 25% |
| BH | 75% |
| BHH | 85% |
| $r_{\text{bin},1}$ | 1000 |
| $y_{\text{bin},1}$ | LIT001 |
| $y_{s,\text{bin},1}$ | 50% |
| $r_{\text{bin},2}$ | 1000 |
| $y_{\text{bin},2}$ | C06+C08 |
| $y_{s,\text{bin},2}$ | 200t/h |
| $r_{\text{bin},3}$ | 1000 |
| $y_{\text{bin},3}$ | WIT006 |
| $y_{s,\text{bin},3}$ | 300t/h |
| $r_{\text{bin},4}$ | 1000 |
| $y_{\text{bin},4}$ | C06 |
| $y_{s,\text{bin},4}$ | C08 |
| $\mathbf{P}_{\text{bin}}$ | $1000\mathbf{I}_2$ |
| $\mathbf{u}_{\text{bin}}$ | SC008-SC009 |

level limits (while $\Gamma_{\text{bin}} = 1$). During safe level limits (while $\Gamma_{\text{bin}} = 0$) objective function $J_{\text{bin}}$ focusses on maintaining the throughput reference trajectories.

Table 4.18 describes the variables and associated values that are used for the MPC objective function $J_{bin}$.

The constraints of the bin are,

$$0 \leq \mathbf{u}_{\text{bin}} \leq 50 \quad \forall t, \tag{4.12}$$

$$0 \leq y_{\text{bin},1}(t) \leq 1 \quad \forall t, \tag{4.13}$$

$$0 \leq \text{C06} \leq 200 \quad \forall t, \tag{4.14}$$

$$0 \leq \text{C08} \leq 200 \quad \forall t, \tag{4.15}$$

$$0 \leq \text{WIT006} \leq 350 \quad \forall t, \tag{4.16}$$

such that the inputs for all feeders' variable speed drive frequencies fall within operating ranges of 0Hz and 50Hz and the bin level remains within 0% and 100%. The DMS plant feed mass flow rates (C06, C08 and WIT006) are also constrained within acceptable limits (Module one and two mass flow rates fall within 0 and 200t/h while DMS plant one's mass flow rate is within 0 and 350t/h).

With the objective function and constraints defined (Equations 4.11, 4.12, 4.13, 4.14, 4.15 and 4.16), the process can be simulated using NMPC. The nonlinear dynamic bin model (state Equations 3.4, 3.5, 3.7, 3.10 and 3.17) is used for the NMPC future prediction and the control simulation of the bin and DMS plant feeds. The NMPC problem can be solved by using the nonlinear programming problem described in Subsection 3.6.2. The objective function (Equation 4.11) is minimised over control moves subject to plant dynamics and input/output constraints detailed above.

Each NMPC simulation input and output are shown in comparison to the manually operated plant simulation response. Figure 4.22 shows the measured disturbances used to simulate the stockpile feed to the process. Figure 4.22 also shows the bin level response with associated objective limits (BLL, BL, BH BHH) as described in Figure 4.21.

Figure 4.22 illustrates the NMPC control moves compared to the actual plant inputs. Figure 4.23 illustrates the plant response for the feeder mass flow rates from the NMPC control moves. These outputs are compared to that of the actual plant output where manual control was applied. Figures 4.24 and 4.25 show the final control objectives where the feeds to the DMS plants (C06, C08 and WIT006) are maximised by controlling them at desired reference trajectories.

In order to measure the performance of the NMPC when compared to that of the actual plant output, a comparison between the manually operated bin throughput and NMPC throughput per DMS plant feed and total throughput are determined. The percentages of gains or losses in throughput are also

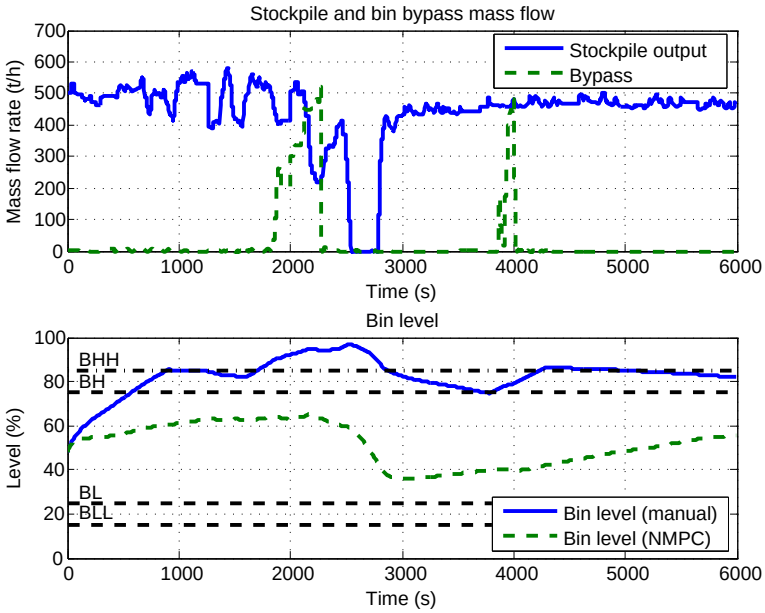


**Figure 4.22:** Bin NMPC measured disturbances and level comparison (Stockpile output = WIT001; Bypass = WIT003; Bin level = LIT001).

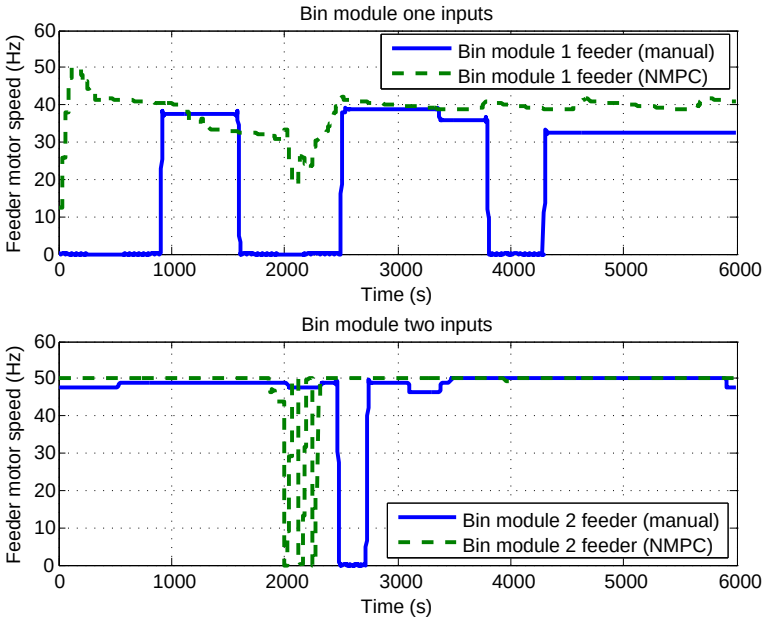


**Figure 4.23:** Bin NMPC motor feeder manipulated variable comparison (Bin module 1 feeder = SC009; Bin module 2 feeder = SC008).

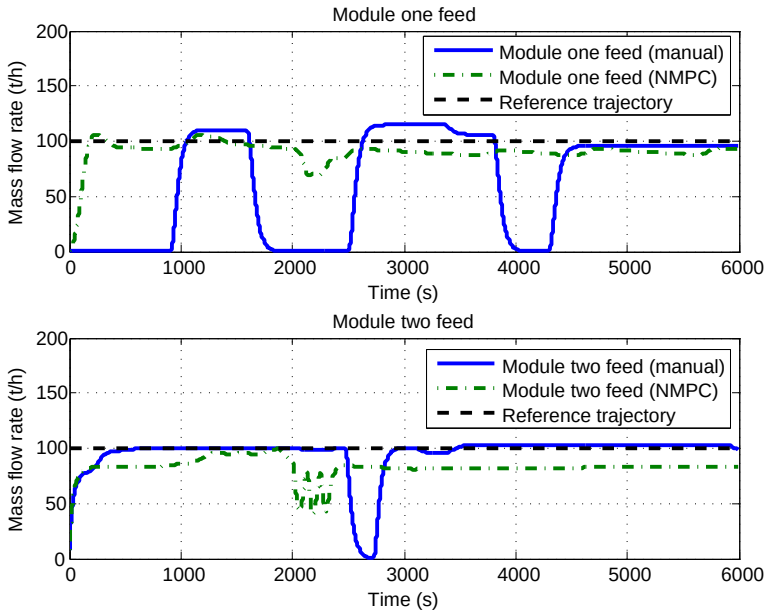


**Figure 4.24:** Bin NMPC module one and two feed comparison (Module one feed = C06; Module two feed = C08).

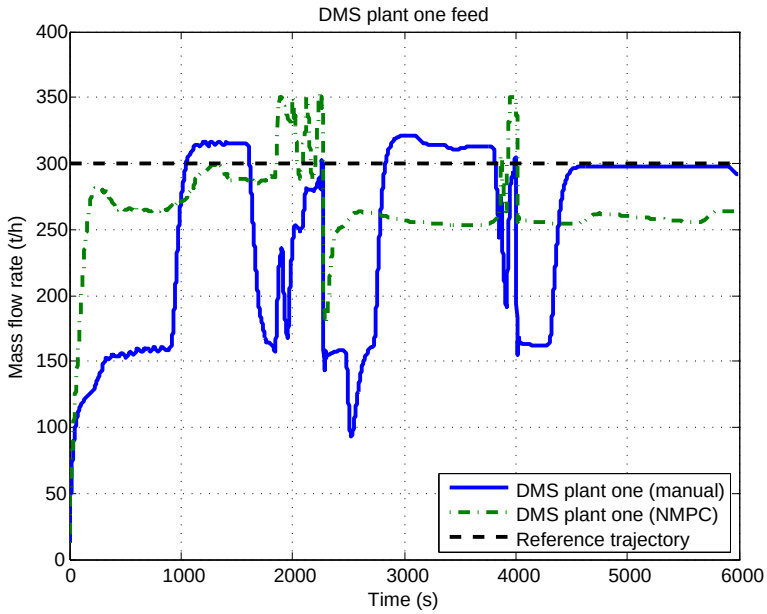


**Figure 4.25:** Bin NMPC DMS plant one feed comparison (DMS plant one feed = WIT006).

**Table 4.19:** Bin manual control versus NMPC performance evaluation (Gains are represented as positive numbers while losses are represented as negative numbers).

| Performance measure | Manual control (t) | NMPC (t) | Gain/loss (%) |
|---|---|---|---|
| C06 | 105 | 150 | 43.5 |
| C08 | 159 | 138 | -13.5 |
| WIT006 | 412 | 443 | 7.5 |
| Total | 676 | 700 | 3.6 |

determined. Gains are represented as positive numbers while losses are represented as negative numbers. Table 4.19 shows a summary of the NMPC performance versus the actual feed bin operation with manual control.

#### 4.2.2.3 Comminution circuit control

The control of the entire comminution circuit simulates the complete startup to shutdown of the plant. The simulation shows how the plant would behave during normal conditions and abnormal conditions.

The same control objective used for the bin system is used in this simulation (Figure 4.21) where at low and high bin levels ($l_b < BL$ or $l_b > BH$) the objective of the controller should be to ensure the bin level stays within safe limits. While the bin level is within safe limits ($BL \leq l_b \leq BH$) the objective of the controller should be to maximise throughput.

The stockpile feeders are controlled to allow for the startup of the plant at 600t/h. The bin level will increase from an initial condition of zero, and once the first low level limit is reached (i.e. $l_b = BLL$), the stockpile mass flow rate is decreased to 500t/h. After the second low level limit the stockpile mass flow is controlled to that of the total bin throughput (i.e. WIT001=C06+C08+WIT006).

A simulated disturbance is entered into the system at $t = 2500$s and stops at $t = 3000$s by introducing material into the stockpile feeder system at 100t/h such that the stockpile conveyor measures the additional tonnages. This could occur in cases where coal is loaded from a front end loader into

the stockpile conveyor without using the dedicated feeder bunker system. Another scenario where additional coal could be added is if a feeder system were to malfunction and coal was manually moved into the bunker.

After $t = 3500$s the plant it shutdown by setting the stockpile mass flow reference trajectory to zero.

The bin level (LIT001) and DMS plant feed mass flow rates (C06, C08 and WIT006) will now be controlled given the objectives of the feed bin operation described above and the definition of the MPC objective function (Equation 3.49) with typical constraints (Equations 3.50, 3.51 and 3.52) and stockpile mass flow rate (WIT001).

This means that the objective function for the MPC is,

$$\begin{aligned} J_{\text{comminution}} = & \sum_{j=1}^{N} r_{\text{comminution},1}|\Gamma_{\text{bin}}(y_{\text{comminution},1}(t+j) - y_{s,\text{comminution},1}(t+j))|^2 + \\ & r_{\text{comminution},2}|(1-\Gamma_{\text{bin}})(y_{\text{comminution},2}(t+j) - y_{s,\text{comminution},2}(t+j))|^2 + \\ & r_{\text{comminution},3}|(1-\Gamma_{\text{bin}})(y_{\text{comminution},3}(t+j) - y_{s,\text{comminution},3}(t+j))|^2 + \\ & r_{\text{comminution},4}|(1-\Gamma_{\text{bin}})(y_{\text{comminution},4}(t+j) - y_{s,\text{comminution},4}(t+j))|^2 + \\ & r_{\text{comminution},5}|y_{\text{comminution},5}(t+j) - y_{s,\text{comminution},5}(t+j)|^2 + \\ & \sum_{j=0}^{M-1} \|\Delta \mathbf{u}_{\text{comminution}}(t+j)\|^2_{\mathbf{P}_{\text{comminution}}}, \end{aligned} \tag{4.17}$$

where the control horizon is two seconds ($M = 2$) and the prediction horizon is five seconds ($N = 5$).

Table 4.20 describes the variables and associated values that are used for the MPC objective function $J_{\text{comminution}}$.

**Table 4.20:** Coal comminution MPC objective function setup.

| Variable | Value or tagname |
|---|---|
| BLL | 60% |
| BL | 75% |
| BH | 85% |
| BHH | 90% |
| $r_{\text{comminution},1}$ | 1000 |
| $y_{\text{comminution},1}$ | LIT001 |
| $y_{s,\text{comminution},1}$ | 80% |
| $r_{\text{comminution},2}$ | 1000 |
| $y_{\text{comminution},2}$ | C06 |
| $y_{s,\text{comminution},2}$ | 100t/h |
| $r_{\text{comminution},3}$ | 1000 |
| $y_{\text{comminution},3}$ | C08 |
| $y_{s,\text{comminution},3}$ | 100t/h |
| $r_{\text{comminution},4}$ | 1000 |
| $y_{\text{comminution},4}$ | WIT006 |
| $y_{s,\text{comminution},4}$ | 300t/h |
| $r_{\text{comminution},5}$ | 1000 |
| $y_{\text{comminution},5}$ | WIT001 |
| $y_{s,\text{comminution},5}$ | C06+C08+WIT006 |
| $\mathbf{P}_{\text{comminution}}$ | $10\mathbf{I}_9$ |
| $\mathbf{u}_{\text{comminution}}$ | SC001-SC009 |

The constraints of the bin are,

$$0 \leq \mathbf{u}_{\text{comminution}} \leq 50 \quad \forall t, \tag{4.18}$$

$$0 \leq y_{\text{comminution},1}(t) \leq 1 \quad \forall t, \tag{4.19}$$

$$0 \leq \text{C06} \leq 200 \quad \forall t, \tag{4.20}$$

$$0 \leq \text{C08} \leq 200 \quad \forall t, \tag{4.21}$$

$$0 \leq \text{WIT006} \leq 350 \quad \forall t, \tag{4.22}$$

such that the inputs for all feeders' variable speed drive frequencies fall within the operating ranges of

0Hz and 50Hz and the bin level remains within 0% and 100%. The DMS plant feed mass flow rates (C06, C08 and WIT006) are also constrained within acceptable limits (Module one and two mass flow rates fall within 0 and 200t/h while DMS plant one's mass flow rate is within 0 and 350t/h).

With the objective function and constraints defined (Equations 4.17, 4.18, 4.19, 4.20, 4.21 and 4.22), the process can be simulated using NMPC. The stockpile, screen and crush, bin and DMS plant feed models (state Equations 3.1, 3.4, 3.5, 3.7, 3.10 and 3.17) are used for the NMPC future prediction and the control simulation. The NMPC problem can be solved by using the nonlinear programming problem described in Subsection 3.6.2. The objective function (Equation 4.17) is minimised over control moves subject to plant dynamics and input/output constraints detailed above.

Figure 4.26 shows the controller outputs for the stockpile feeders. Figure 4.27 shows the simulated output of the stockpile mass flow based on the NMPC objective. The additional stockpile disturbance is also shown in Figure 4.27 with associated crusher motor current outputs.

Figure 4.28 illustrates the bin level response based on the NMPC objectives. Figure 4.28 also shows the NMPC output to the bin feeders to ensure the DMS plant feed objectives are met. Figure 4.29 shows the DMS plant feed response with associated reference trajectory requirements.

### 4.2.3 Unscented Kalman filter simulation

The UKF algorithm was applied to the nonlinear screen, crush and bin model from the comminution circuit derived in this thesis. Given ten states (two double deck screen state Equations 3.4 and 3.5; two crusher state Equations per crusher (80mm and 40mm) 3.7 and 3.10; and four bin model state Equations 3.12, 3.13, 3.14 and 3.17) and six outputs (WIT002, IIT001, IIT002, WIT005, WIT004, LIT001) of the screen, crush and bin system, the initial covariance of the original state ($\mathbf{P}_{s,0}$) was chosen as the identity matrix $\mathbf{I}_{10}$. The standard deviation $\mathbf{Q_s}$ of the process was chosen to be fairly large based on the measurement data,

$$\mathbf{Q_s} = \text{diag}([\ 0.1 \quad 0.1 \quad 0.1 \quad 0.1 \quad 0.1 \quad 0.1 \quad 60 \quad 1 \quad 0.1 \quad 0.05\ ]), \tag{4.23}$$

where the initial covariance for the process noise is determined as $\mathbf{P}_{s,v} = \mathbf{Q_s}^2$.

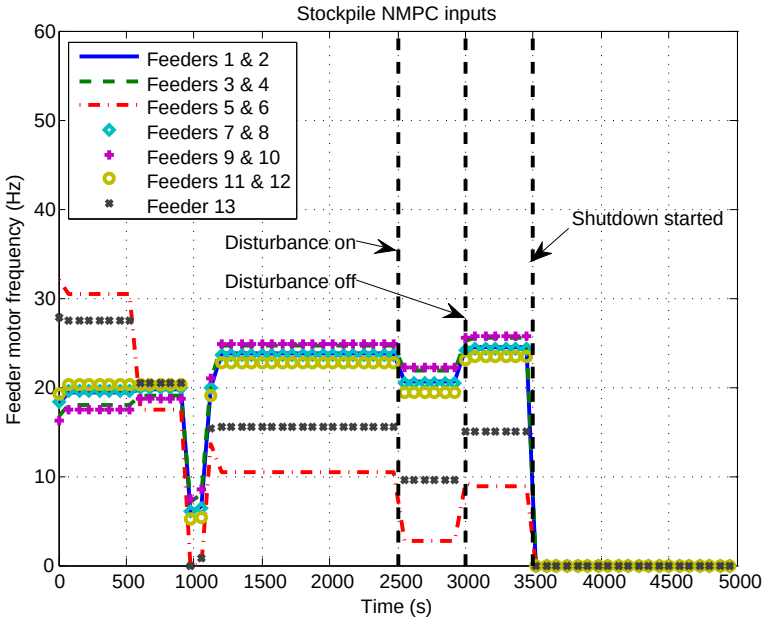


**Figure 4.26:** Bin NMPC input comparison (Feeders 1 & 2 = SC001; Feeders 3 & 4 = SC002; Feeders 5 & 6 = SC003; Feeders 7 & 8 = SC004; Feeders 9 & 10 = SC005; Feeders 11 & 12 = SC006; Feeders 13 = SC007).

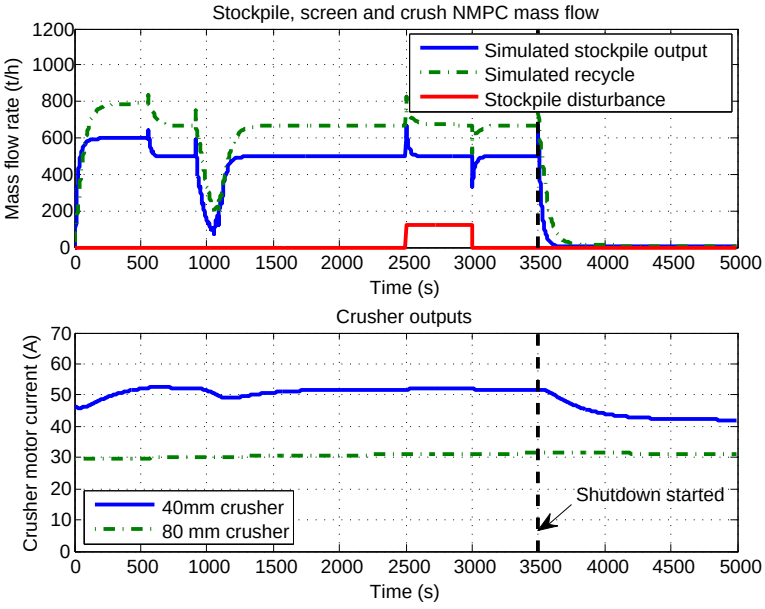


**Figure 4.27:** Bin NMPC input comparison (Stockpile output = WIT001; Recycle = C01; Disturbance = Addition to WIT001; 40mm crusher = IIT001; 80mm crusher = IIT002).

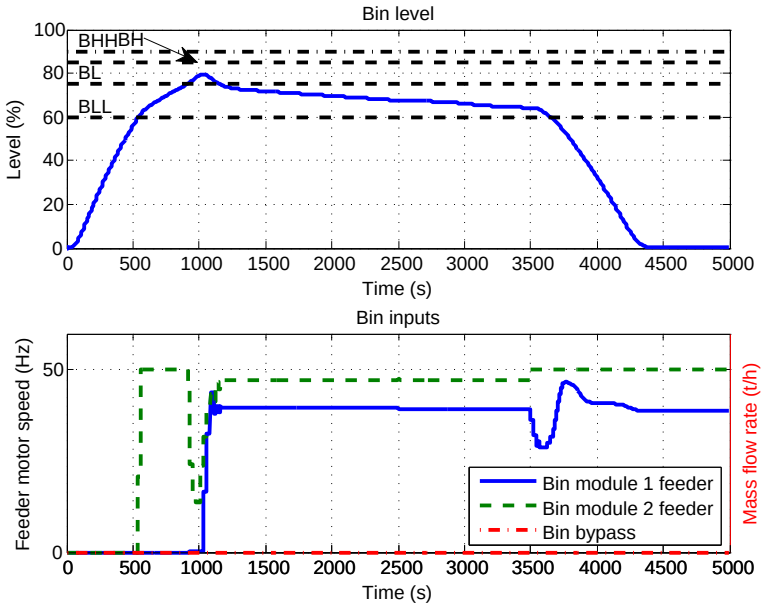


**Figure 4.28:** Bin NMPC input comparison (Bin level = LIT001; Bin module 1 feeder = SC009; Bin module 2 feeder = SC008; Bin bypass = WIT003).

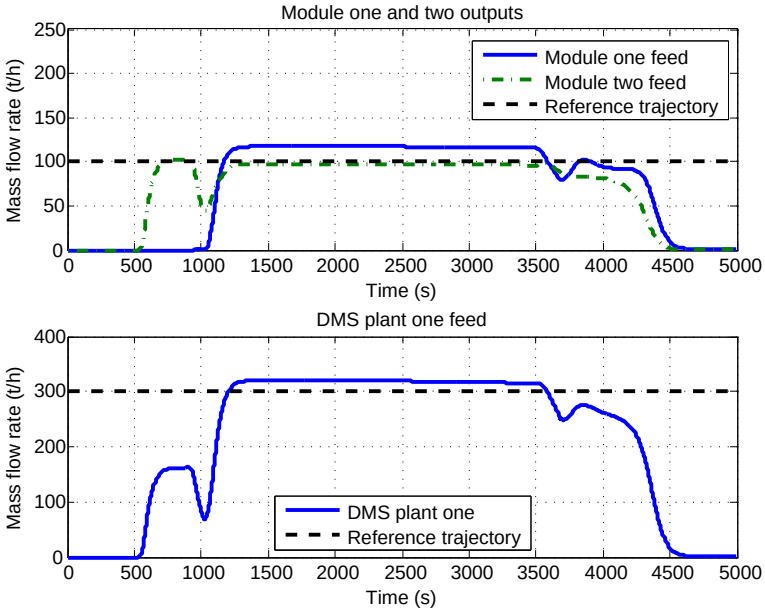


**Figure 4.29:** Bin NMPC input comparison (Module one feed = C06; Module two feed = C08; DMS plant one feed = WIT006).

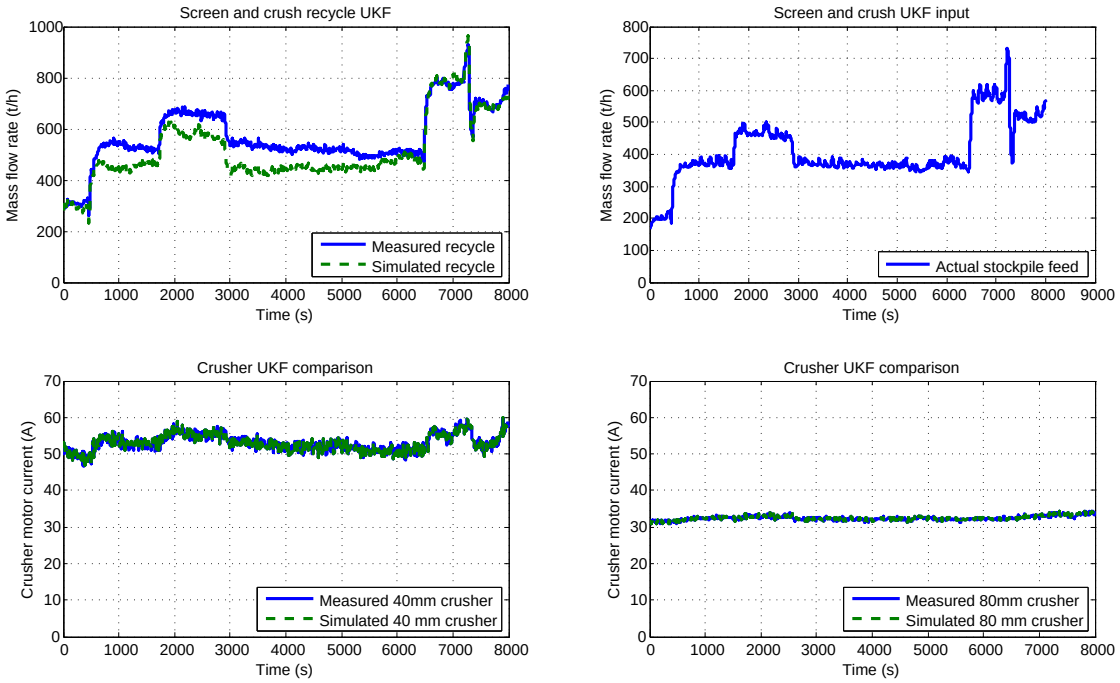


**Figure 4.30:** Screen and crush UKF comparison for experiment one (Recycle = C01; Stockpile feed = WIT001; 40mm crusher = IIT001; 80mm crusher = IIT002).

The standard deviation of all measurement noise was chosen to be a very small value of 1% ($r_s = 0.01$). This implies that the initial covariance for the measurement noise can be determined as $\mathbf{P}_{s,n} = r_s^2 \mathbf{I}_6$.

Figures 4.30, 4.31 and 4.32 illustrate the UKF simulation versus the measured process outputs. The production data of experiment one (Sub-subsection 4.2.1.2) that was used for the identification of the screen, crush and bin area models, are used to illustrate the functioning of the UKF.

Table 4.21 shows a summary of the model fit and correlation for the UKF simulation.

### 4.2.4 Results overview

The coal comminution area was broken down into three unit processes, namely, the stockpiling area; screen, crush and bin area; and the DMS screen feed area. Each unit process area was modelled dynamically using the various equipment models from Chapter 3. These models were identified using multiple experiment data sets to ensure sufficient perturbations are available in the inputs to stimulate

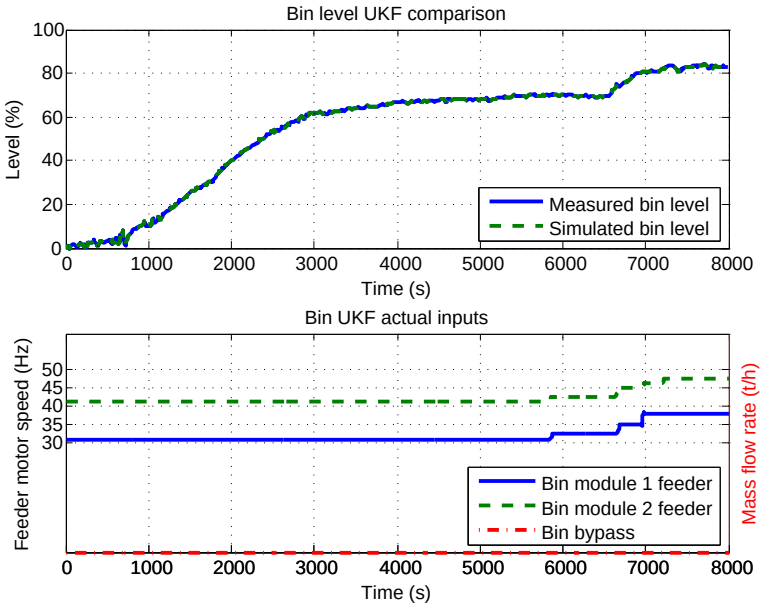


**Figure 4.31:** Bin level UKF comparison for experiment one (Bin level = LIT001; Bin module 1 feeder = SC009; Bin module 2 feeder = SC008; Bin bypass = WIT003).

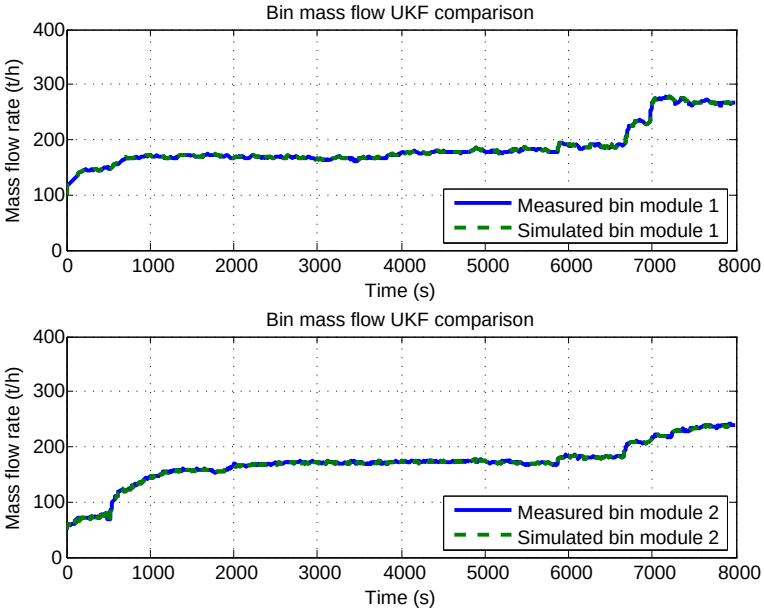


**Figure 4.32:** Bin mass flow UKF comparison for experiment one (Bin module 1 = WIT005; Bin module 2 = WIT004).

**Table 4.21:** Screen, crush and bin model output UKF comparison results.

| Output | Fit (%) | Correlation |
|---|---|---|
| Screen and crush recycle (WIT002) | 43.4 | 0.96 |
| 40mm crusher motor current (IIT001) | 92.9 | 1.00 |
| 80mm crusher motor current (IIT002) | 92.3 | 1.00 |
| Bin module one feeder (WIT005) | 98.9 | 1.00 |
| Bin module two feeder (WIT004) | 98.4 | 1.00 |
| Bin level (LIT001) | 99.8 | 1.00 |

a response in the outputs. The model fits and correlations are sufficient for control purposes as detailed in the various NMPC simulations.

In order to show the control of the communition area, initially only the stockpile area is simulated using NMPC. Thereafter, the control objectives of the feed bin are applied to the NMPC of the feed bin area only. Finally, a total communition area NMPC simulation is given to show startup, shutdown and disturbance rejection.

The UKF algorithm was applied to the feed bin area to illustrate that it is possible to estimate the model states and that the dynamic equipment models can be used for pure simulations.

A detailed discussion of all the coal communition simulation results are given in Chapter 5.

## 4.3 COAL SEPARATION AREA

The actual coal separation area that is used in this thesis is detailed in Figure 4.33. This plant consists of two areas. The first area is a DMD separator with associated medium recovery. The second area is a DMC separator.

The feed to the coal separation area (WIT011) is based on material from the bin total oversize (WIT006) in Figure 4.1. The feed material to the DMS plant (WIT011) is separated using a 28mm screen where the oversize (+28mm) material (C11) is processed by a DMD while the undersize (-28mm+1mm, i.e.

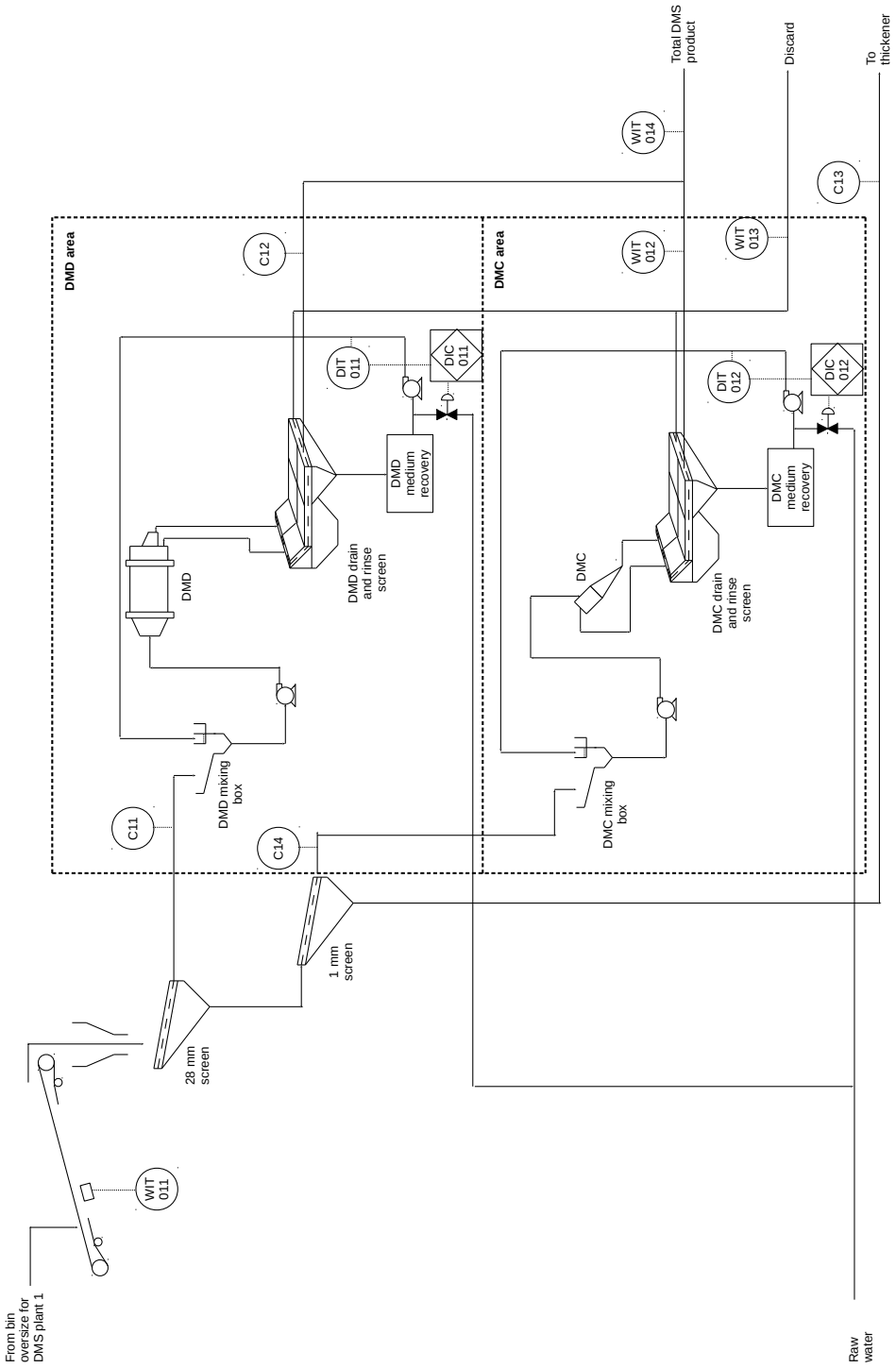


**Figure 4.33:** Coal separation process flow schematic.

smaller than 28mm and larger than 1mm) material (C14) is processed by a DMC. The -1mm material (C13) is removed using a secondary screen (1mm screen) and processed further by a thickener (details of the thickener process are not included as part of the scope in this thesis).

The oversize material (C11) is mixed with medium which is measured at a specific RD (DIT011). The DMD medium RD is controlled (DIC011) using a regulatory controller with the addition of water. The undersize material (C14) is mixed with medium and measured at a specific RD (DIT012). The DMC medium RD is controlled (DIC012) using a regulatory controller similar to that of the DMD.

DMD coal product (C12) and DMC coal product (WIT012) are combined to form the final DMS coal plant product (WIT014) which is separated into saleable products at a wet screening house. A wet screening house is used to produce a small nut product and a pulverised coal injection product which is stacked for specific customers.

All discard from both the DMD and DMC is combined (WIT013) and stored for mine rehabilitation.

The details of all actuator and measurement tags are given in Tables 4.22 and 4.23. These tags relate to the tags given in Figure 4.33. The type of measurement or actuation available for each tag are also given. The associated variables and equations detailed in Chapter 3 are also given as reference to highlight how the dynamic models associate to the physical process and measurements.

### 4.3.1 Dynamic model system identification

Based on the coal separation area in Figure 4.33 and analysing the inputs and outputs, it is possible to break the system into two dynamic model areas. The first dynamic model area is the DMD area while the second dynamic model area is the DMC area. The nonlinear dynamic models from Chapter 3 are used to describe the two areas and will consist of parameters relating to the models. The 28mm and 1mm screen is not modelled as there are no actuators to control the feed mass flow rate to the DMD and DMC specifically. The MPC detailed in the previous section on the coal communition area will ensure that the feeds to the various separation plants are controlled.

**Table 4.22:** Measurements used in Figure 4.33 for the DMD area in the separation process (N/A stands for "not applicable").

| Name | Description | Type | Variable | Equation(s) |
|---|---|---|---|---|
| WIT011 | DMS coal plant total feed material (t/h) | Belt scale | N/A | N/A |
| C11 | DMD separator feed material (t/h) | Calculation | $W_{d,i}$[a] | 3.20 |
| C12 | DMD separator coal product (t/h) | Calculation | $W_{d,f}$[b] | 3.21 |
| DIT011 | DMD separator medium RD (kg/m$^3$) | Density scale | $\rho_{d,i,med}$ | 3.21, 3.22, 3.24 and 3.25 |
| DIC011 | DMD separator medium RD controller | Density controller | N/A | N/A |
| C13 | Thickener feed material (t/h) | Calculation | N/A | N/A |

[a]The mass feed rate of the feed mix ($W_{d,i}$) is determine by making use of the mixing box model developed in Meyer and Craig (2010).

[b]The mass flow rate of the floats ($W_{d,f}$) is calculated by using conservation of mass of components to remove the medium component.

The system identification approach from Ljung (1987) is used for each model fit. Input-output data taken from an actual coal beneficiation plant production historian were used to fit the models. All data are sampled per second and filtered with a low-pass filter with time period of twenty seconds to remove measurement noise. Two thirds of the production data were used to identify the models to allow for an additional one third of production data to be used for model validation. All simulation outputs and model validation results include both the two thirds model identification data and one third model validation data. This means that two thirds of the data within the time-series data was used to identify the model parameters. The model simulation was then allowed to run for another one third of the remaining time-series data. The reason for this is to illustrate that the model is able to use data both with and without prior identification for validation purposes.

Since each separation unit process is going to be modelled for control purposes, it is necessary to have input-output data for the feed, product, discard and associated ash content. Given that some of the tags in the separation process flow diagram in Figure 4.33 are not measured, these input-output data need to be calculated.

**Table 4.23:** Measurements used in Figure 4.33 for the DMC area in the separation process (N/A stands for "not applicable").

| Name | Description | Type | Variable | Equation(s) |
|---|---|---|---|---|
| C14 | DMC separator feed material (t/h) | Calculation | $W_{c,i}{}^{a}$ | 3.26 |
| WIT012 | DMC separator coal product (t/h) | Belt scale | $W_{c,o}{}^{b}$ | 3.27 |
| DIT012 | DMC separator medium RD (kg/m$^3$) | Density scale | $\rho_{c,i,med}$ | 3.27, 3.28, 3.31, 3.32, 3.33 and 3.34 |
| DIC012 | DMC separator medium RD controller | Density controller | N/A | N/A |
| WIT013 | DMS coal plant total discard (t/h) | Belt scale | $W_{d,s} + W_{c,u}{}^{c}$ | 3.22 and 3.28 |
| WIT014 | DMS coal plant total coal product (t/h) | Belt scale | C12 + WIT012 | N/A |

[a]The mass feed rate of the feed mix ($W_{c,i}$) is determine by making use of the mixing box model developed in Meyer and Craig (2010).

[b]The mass flow rate of the overflow ($W_{c,o}$) is calculated by using conservation of mass of components to remove the medium component.

[c]The mass flow rate of the total plant discard ($W_{d,s} + W_{c,u}$) is calculated by using conservation of mass of components to remove their medium components.

Assuming that the 28mm and 1mm screens classify the material received from the bin oversize is based on ratio of both the DMD (WIT014 - WIT012) and DMC (WIT012) (1mm screen) product to total throughput (WIT014), the material feed to each separation process can be calculated as follows,

$$\text{C11} = (\text{WIT011} - \text{C13})\frac{\text{C12}}{\text{WIT014}}, \tag{4.24}$$

$$\text{C14} = (\text{WIT011} - \text{C13})\frac{\text{WIT012}}{\text{WIT014}}, \tag{4.25}$$

where $\text{C12} = \text{WIT014} - \text{WIT012}$ and $\text{C13} = \text{WIT011} - \text{WIT014} - \text{WIT013}$.

In order to fit the DMD and DMC dynamic models for product grade, it is necessary to calculate the ash content using the method from Meyer and Craig (2015). In order to calculate ash content, the coal washability and equipment partitioning behaviour is required. The method used to determine the ash

content in product and feed for both the DMD and DMC is as follows.

Initially the throughput of the coal separation process must be simulated and verified. Based on the verified throughput model, the partition curve can be generated by reducing the dynamic model to a steady-state model. The partition curve result is then used in association with the Equations 3.45 (for DMD), 3.46 (for DMC) and 3.42 to estimate the input-output data for the grade simulation.

The following steps are used to calculate the ash content of the coal separation product grade for system identification:

- Step 1: Fit the DMD or DMC dynamic model to the measured mass flow rate input-output data.
- Step 2: Fit the relevant partition factor function (Equation 3.45 or 3.46) to a steady-state model derived from the dynamic model in step 1.
- Step 3: Calculate the product or float ash content using Equation 3.41.
- Step 4: Calculate the feed ash content using Equation 3.42 with the results from steps 2 and 3.
- Step 5: Calculate the discard or sink ash content using the conservation of mass of components.

#### 4.3.1.1 DMD area

The DMD area consists of a Wemco drum separator as described in Chapter 3. ROM material (+28mm, C11) is mixed with magnetite medium in a DMD mixing box. The feed mix is modelled using the dynamic model of a mixing box developed by Meyer and Craig (2010). The DMD medium RD (DIT011) in the mix is controlled through the addition of water with a regulatory controller (DIC011). DMD floats (C12) and sinks (combined with the DMC sinks, WIT013, and calculated as C11 - C12) are rinsed with a drain and rinse screen such that the medium is collected and recovered for recirculation.

**Table 4.24:** DMD model parameters estimated from input-output data.

| Parameter | Value | Description | Equation(s) |
|---|---|---|---|
| $\alpha_d$ | 0.868 | Float and sink proportionality constant | 3.21, 3.22 and 3.23[a] |
| $K_{d,f}$ | 3.558E-08 | Proportionality constant for the floats [$m^6/(kg.s)$] | 3.21 |
| $K_{d,s}$ | 3.076E-12 | Proportionality constant for the sinks [$m^6/(kg.s)$] | 3.22 |
| $K_{d,f,med}$ | 6.533E-08 | Proportionality constant for the magnetite medium floats [$m^3$/(kg.s)] | 3.24 |
| $K_{d,s,med}$ | 3.955E-14 | Proportionality constant for the magnetite medium sinks [$m^3$/(kg.s)] | 3.25 |
| $K_{d,f,ash}$ | -1.057E-07 | Proportionality constant for the floats ash [$m^3$/(kg.s)] | 3.24[b] |
| $K_{d,s,ash}$ | 1.215E-08 | Proportionality constant for the sinks ash [$m^3$/(kg.s)] | 3.25[c] |
| $\Delta\rho_{d,med}$ | 1.00 | Difference between feed medium density with float or sink medium density (kg/$m^3$) | 3.24 and 3.25 |

[a] $\alpha_d$ is used to determine the volume and volumetric flow rate split for floats and sinks (i.e. $Q_{d,f} = \frac{\alpha_d Q_{d,i}}{1+\alpha_d}$, $Q_{d,s} = \frac{Q_{d,i}}{1+\alpha_d}$, $V_{d,f} = \frac{\alpha_d V_d}{1+\alpha_d}$ and $V_{d,s} = \frac{V_d}{1+\alpha_d}$).
[b] Ash component parameter can be determined similarly to the medium component by replacing subscript *med* with *ash*.
[c] Ash component parameter can be determined similarly to the medium component by replacing subscript *med* with *ash*.

The Wemco drum model derived in Chapter 3 was identified using input-output data from an actual coal plant. Tables 4.24 and 4.25 indicates the parameters that were estimated using actual DMD input-output data. The parameters associated with the relevant equations from Chapter 3 are also given.

Residence time is typically the time it takes for material to be processed through a unit operation while operating at steady-state conditions. The residence time in this model is therefore associated with the volume ($V_d$) and flow rate ($Q_{d,i}$) which are model parameters that require estimation. The five steps used to calculate the ash content of the DMD product for system identification described in Subsection 4.3.1 were used before the associated ash proportionality constants ($K_{d,f,ash}$ and $K_{d,s,ash}$) were solved for.

The input data for the drum separator simulation are shown in Figure 4.34. The feed rate of the drum feed material is not controlled as it is dependant on an upstream comminution plant (Figure 4.1). The

**Table 4.25:** DMD volumetric model parameters estimated from input-output data.

| Parameter | Value | Description | Equation(s) |
|---|---|---|---|
| $Q_{d,i}$ | 0.294 | Volumetric flow rate of the feed mix ($m^3/s$) | 3.21, 3.22 and 3.23[a] |
| $V_d$ | 1.320 | Drum material mix volume ($m^3$) | 3.21, 3.22 and 3.23[b] |
| $\frac{Q_{d,i,med}}{Q_{d,i}}$ | 0.788 | Ratio of the volumetric flow rate of the magnetite medium in the feed mix to overall volumetric flow rate of the feed mix | 3.21 and 3.22[c] |
| $\frac{Q_{d,i,ash}}{(Q_{d,i}-Q_{d,i,med})}$ | 0.111 | Ratio of the volumetric flow rate in the feed ash to the feed ore | 3.24 and 3.25[d] |

[a] $Q_{d,i}$ is used to determine the volumetric flow rates (i.e. $Q_{d,f} = \frac{\alpha_d Q_{d,i}}{1+\alpha_d}$ and $Q_{d,s} = \frac{Q_{d,i}}{1+\alpha_d}$).

[b] $V_d$ is used to determine the volume for floats and sinks (i.e. $V_{d,f} = \frac{\alpha_d V_d}{1+\alpha_d}$ and $V_{d,s} = \frac{V_d}{1+\alpha_d}$).

[c] The ratio of volumetric flow rate to medium is used in the mixing box model developed by Meyer and Craig (2010) and to calculate the product mass flow in floats and discard mass flow in sinks using conservation of mass of components by removing the mass flow rate of medium.

[d] The ratio of the volumetric flow rate in feed ash to feed ore is is used to calculate the float and sink ash contents. Ash component parameter can be determined similarly to the medium component by replacing subscript *med* with *ash*.

density of the drum medium is controlled and is stepped from about 1600 kg/m$^3$ to 1640 kg/m$^3$ as shown in Figure 4.34.

Figure 4.35 illustrates the comparison between the measured drum separator floats product mass rate and the dynamic model predicted output.

Figure 4.36 illustrates the comparison between the measured drum separator sinks discard mass rate and the dynamic model predicted output.

The model estimates for the floats product and sinks discard as shown in Figures 4.35 and 4.36 respectively, are considered to be adequate for process control studies as they are qualitatively accurate.

A process steady-state model derived from the dynamic model is required for the coal ash content system identification. The derivation is based on Meyer and Craig (2011) and Meyer and Craig

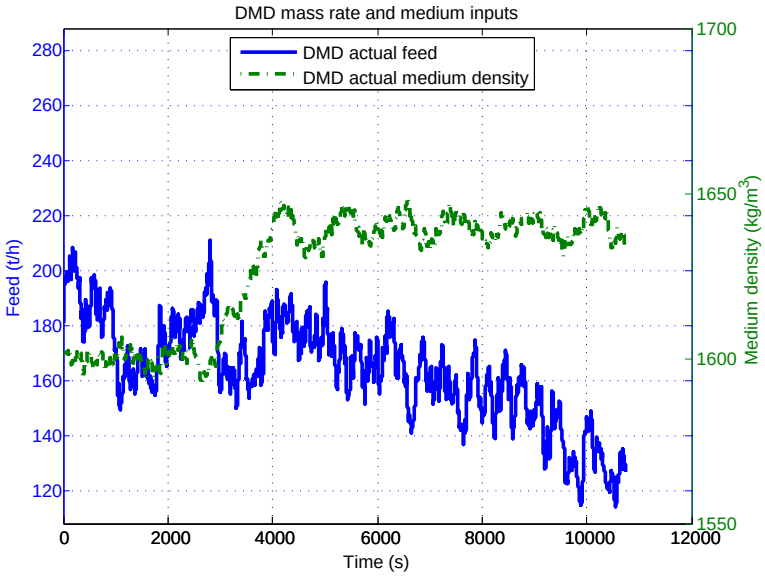


**Figure 4.34:** Input data for DMD throughput simulation (DMD feed = C11; DMD medium density = DIT011). Taken from Meyer and Craig (2015).

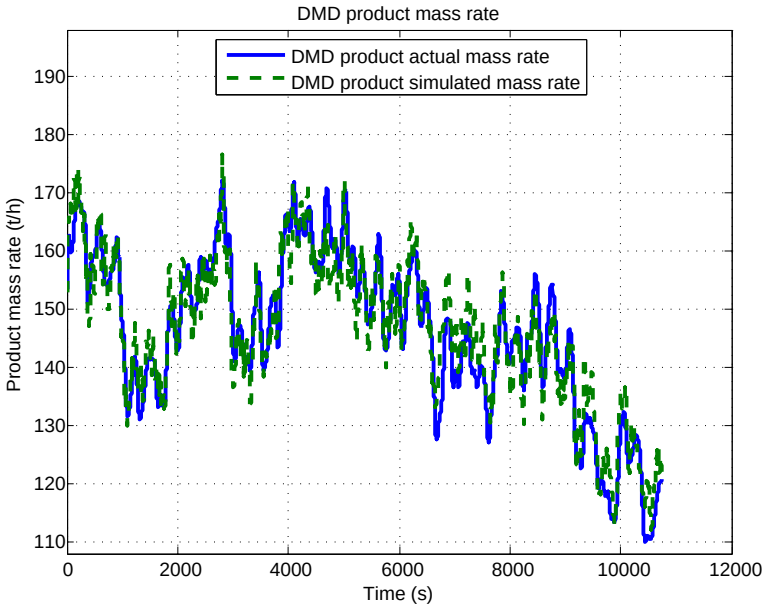


**Figure 4.35:** Drum separator floats product (DMD product = C12). Taken from Meyer and Craig (2015).

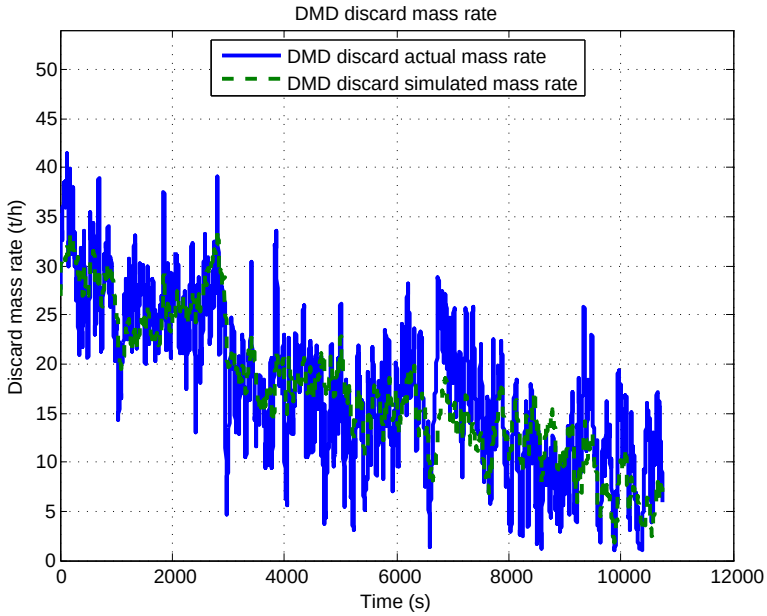


**Figure 4.36:** Drum separator sinks discard (DMD discard = C11 - C12). Taken from Meyer and Craig (2015).

(2014). A model fit was performed using the partition curve from Equation 3.45. The predicted mass distributions to float and sink products at different particle densities in the feed are obtained by simulating the partition factor at different medium densities. By starting with a finite amount of mass in the feed and simulating the separation at steady-state at a high density, the resulting mass in the float can be used as the feed for the next steady-state simulation. With decreasing medium density iterations, the resulting partition factors can be obtained. By fitting Equation 3.45 to the simulated observations the partition curve in Figure 4.37 was generated.

Table 4.26 shows a summary of the parameters for the efficiency curve fit. This simulation indicates that a dynamic drum separator model can be reduced to a realistic steady-state model from which a partition curve can be generated.

Using Equation 3.43 the EPM is determined as 0.021 SG based on the partition curve in Figure 4.37. It was indicated by the process development engineer responsible for the production facility where the Wemco drum separator model has been applied that the separation efficiency results align very well with the actual Wemco drum separator efficiency (Steyn, 2014b). An actual efficiency curve of the Wemco drum separator was not available.

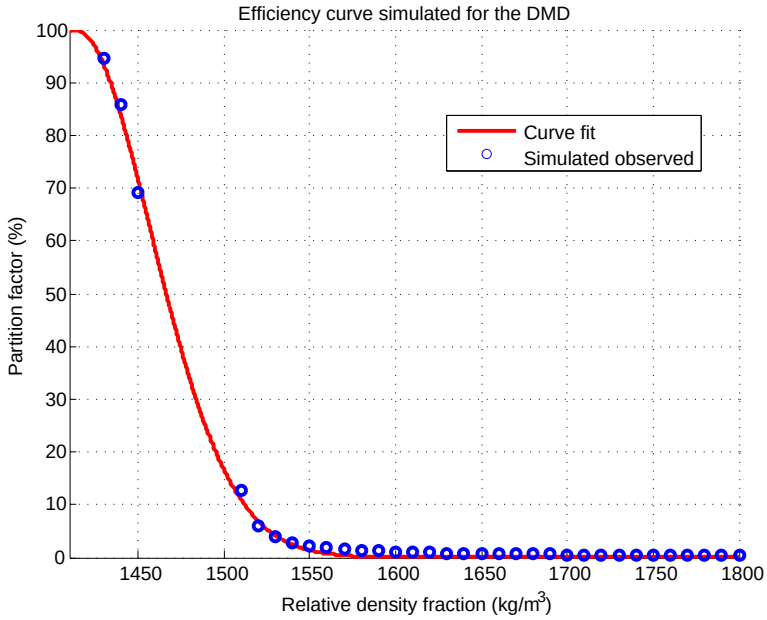


**Figure 4.37:** Simulated efficiency curve for the drum separator using the steady-state model derived from the dynamic drum model [taken from Meyer and Craig (2015)].

**Table 4.26:** Partition curve efficiency model parameters (Equation 3.45).

| Efficiency parameter | Efficiency curve fit parameter results |
|---|---|
| $p_1$ | 0.594 |
| $p_2$ | 498.60 |
| $p_3$ | 5.968E+03 |

Since no online measurement was available to measure the product and discard grade, the method of reconstituting the feed ash component percentage and estimation of the product ash component percentage explained in Chapter 3 is used. The previous efficiency curve results combined with Equations 3.45 and 3.42 are used to estimate the input-output data for the grade simulation. This method assumes that the average float and sink ore density are used instead of density fractions. It is also assumed that a normalised partition curve developed from Figure 4.37 can be applied at the initial medium density of about 1600 kg/m$^3$. When the medium density is increased to about 1640 kg/m$^3$, the partition curve will be applied to the increased medium density setpoint.

The input data for the drum separator grade simulation are shown in Figure 4.38. The feed ash

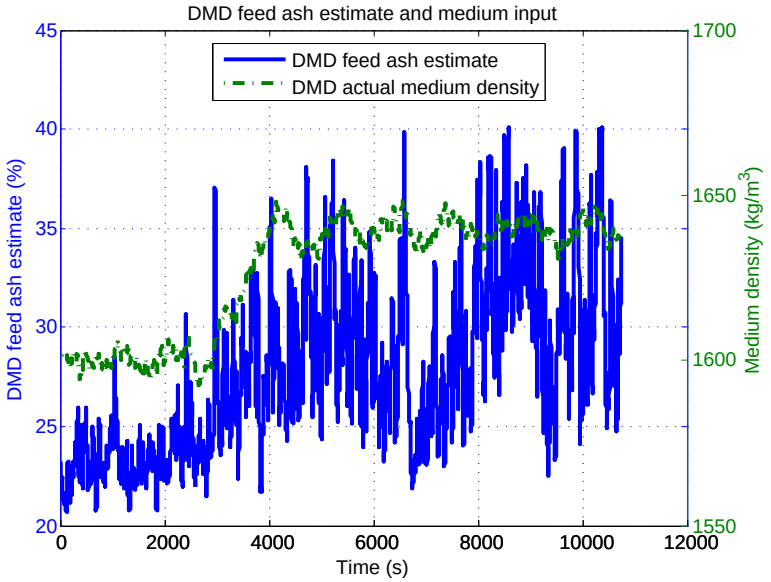


**Figure 4.38:** Input data for grade simulation (DMD feed ash = $x_{d,i,ash}$; DMD medium density = DIT011). Taken from Meyer and Craig (2015).

percentage ($x_{d,i,ash}$ described in Table 3.6) of the drum feed material is not controlled as it is dependant on an upstream mining and blending process. The density of the drum medium is also shown as an input similar to that shown in Figure 4.34.

Figure 4.39 illustrates the comparison between the measured drum separator floats product ash percentage ($x_{d,f,ash}$ described in Table 3.7) and the dynamic model predicted output. A detailed view of the floats product ash percentage comparison is given in Figure 4.40 from time 6000 seconds to 8000 seconds.

Figure 4.41 illustrates the comparison between the measured drum separator sinks discard ash percentage ($x_{d,s,ash}$ described in Table 3.7) and the dynamic model predicted output. A detailed view of the sinks discard ash percentage comparison is given in Figure 4.42 from time 2000 seconds to 4000 seconds.

The model estimates for the floats product ash percentage and sinks discard ash percentage as shown in Figures 4.39 and 4.41 respectively, are considered to be adequate for process control studies as they are qualitatively accurate.

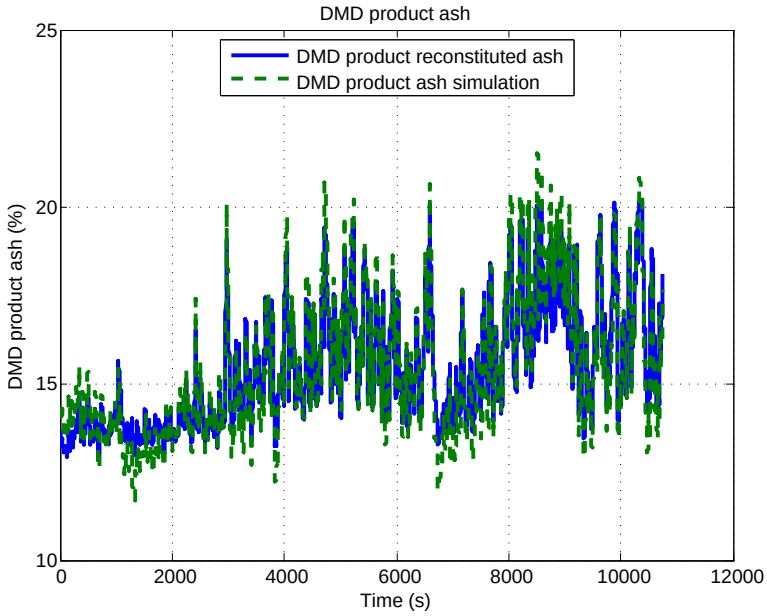


**Figure 4.39:** Drum separator floats product ash percentage simulation (DMD product ash = $x_{d,f,ash}$). Taken from Meyer and Craig (2015).

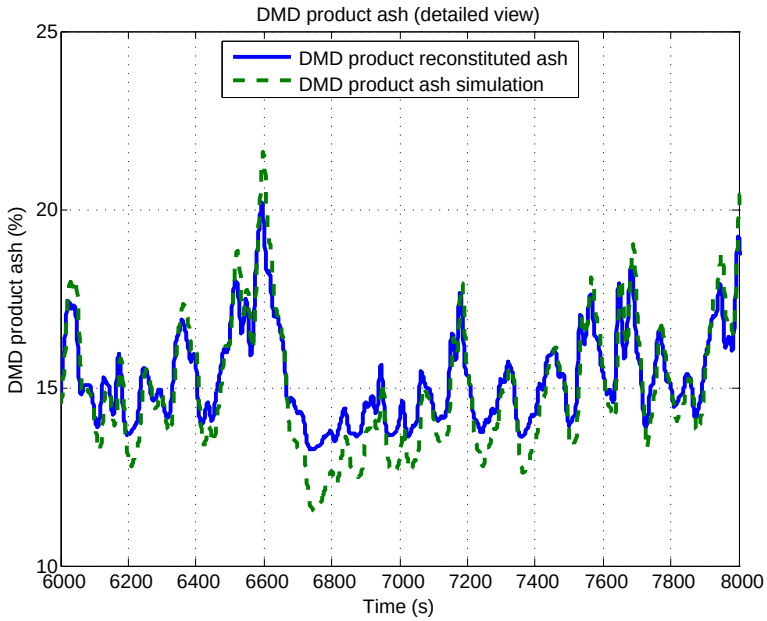


**Figure 4.40:** Drum separator floats product ash percentage simulation (detailed view, DMD product ash = $x_{d,f,ash}$). Taken from Meyer and Craig (2015).

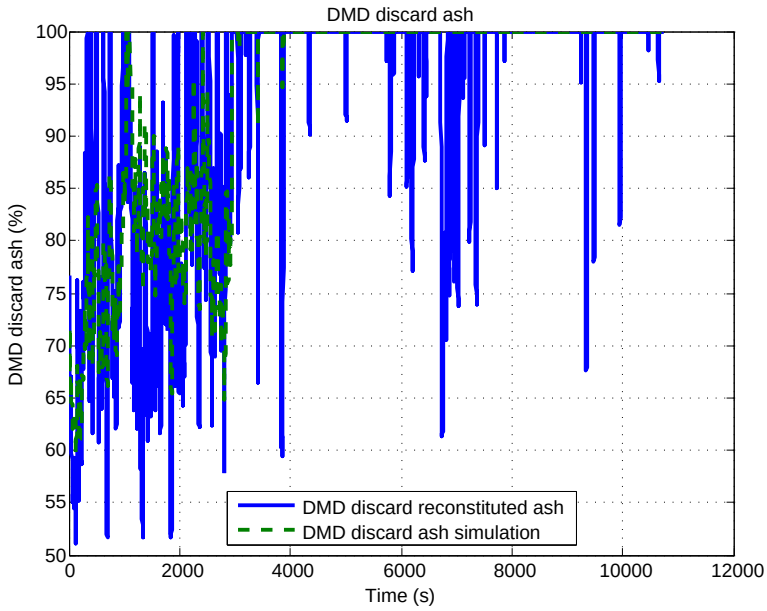


**Figure 4.41:** Drum separator sinks discard ash percentage simulation (DMD discard ash = $x_{d,s,ash}$). Taken from Meyer and Craig (2015).

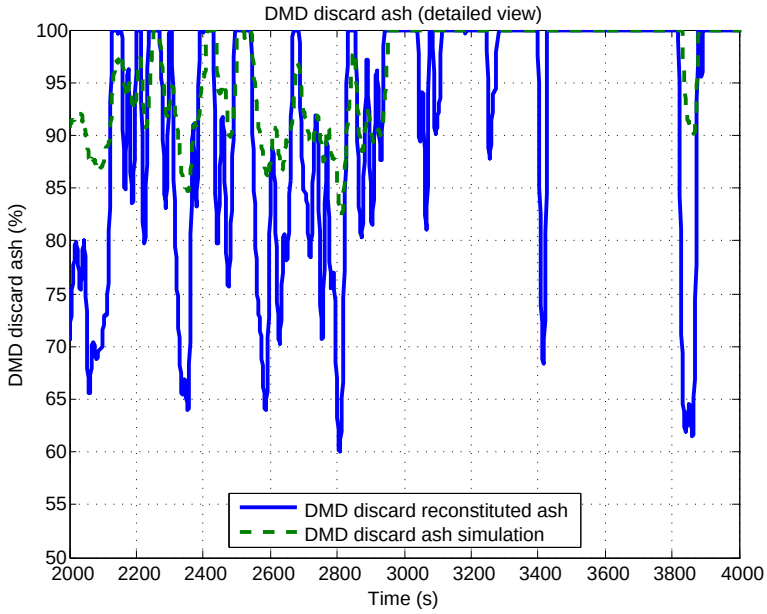


**Figure 4.42:** Drum separator sinks discard ash percentage simulation (detailed view, DMD discard ash = $x_{d,s,ash}$). Taken from Meyer and Craig (2015).

**Table 4.27:** Partition curve efficiency results summary.

| Efficiency parameter | Simulated steady-state model results (SG) |
|---|---|
| $\rho_{50}$ | 1.470 |
| EPM | 0.021 |

**Table 4.28:** Dynamic DMD model performance results summary.

| Output | Fit (%) | Correlation |
|---|---|---|
| Product throughput (C12) | 69.0 | 0.95 |
| Discard throughput (C11 - C12) | 43.5 | 0.83 |
| Product grade (ash) ($x_{d,f,ash}$) | 66.4 | 0.96 |
| Discard grade (ash) ($x_{d,s,ash}$) | 56.3 | 0.57 |

The validation of the dynamic model is further confirmed by the metallurgical steady-state efficiency measures (Table 4.27).

The dynamic model goodness of fit (Ljung, 2005) and correlation between the measured outputs and simulated outputs are given in Table 4.28.

#### 4.3.1.2 DMC area

The DMC area consists of a DMC separator as described in Chapter 3. DMC ROM (C14) material (-28mm+1mm, i.e. smaller than 28mm and larger than 1mm) is mixed with magnetite medium in a DMC mixing box. The feed mix is modelled using the dynamic model of a mixing box developed by Meyer and Craig (2010). The DMC medium RD (DIT012) in the mix is controlled through the addition of water with a regulatory controller (DIC012). DMC overflow (WIT012) and undeflow (combined with the DMC sinks, WIT013, and calculated as C14 - WIT012) are rinsed with a drain and rinse screen such that the medium is collected and recovered for recirculation.

Similar to the DMD model, the DMC model is identified using the throughput and medium input-output

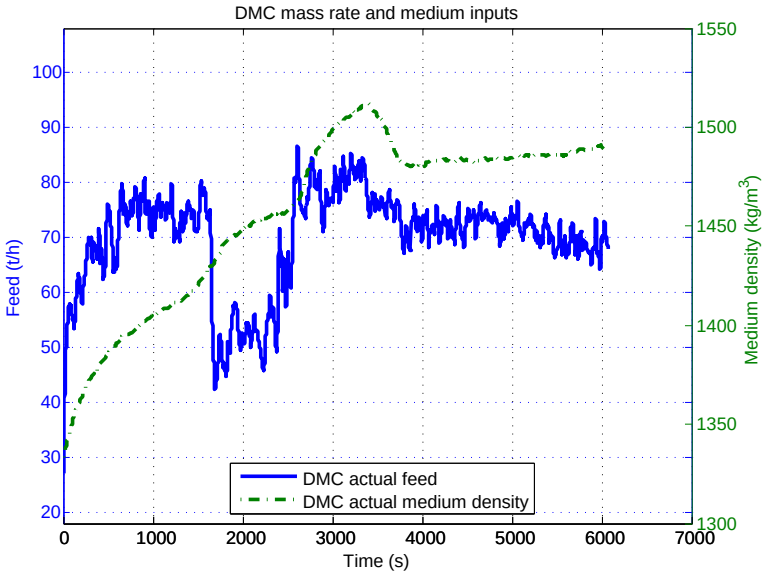


**Figure 4.43:** Input data for DMC throughput simulation (DMC feed = C14; DMC medium density = DIT012).

data. Thereafter, the grade in terms of ash mass of components input-output data were used to fit the remaining dynamic model parameters associated to ash. A cyclone volume ($V_c$) of 0.15m$^3$ and medium density overflow and underflow to feed difference ($\Delta_{\rho_{c,med}}$) of 50kg/m$^3$ were used. The cyclone volumetric throughput assumption is based on the physical cyclone geometry while the medium density differences are typical values taken from literature (Gupta and Yan, 2006; He and Laskowski, 1994).

Tables 4.29 and 4.30 indicates the values that were estimated using production data obtained from a plant production historian. The parameters associated with the relevant equations from Chapter 3 are also given. The five steps used to calculate the ash content of the DMC product for system identification described in Subsection 4.3.1 were used before the associated ash proportionality constants ($K_{c,o,ash}$ and $K_{c,u,ash}$) were solved for.

The input data for the cyclone separator simulation are shown in Figure 4.43. The feed rate of the cyclone feed material is not controlled as it is dependant on an upstream separation plant (Figure 4.33). The density of the cyclone medium is controlled and is increased from about 1350 kg/m$^3$ to 1500 kg/m$^3$ as shown in Figure 4.43.

**Table 4.29:** DMC model parameters estimated from input-output data.

| Parameter | Value | Description | Equation(s) |
|---|---|---|---|
| $\alpha_c$ | 1.184 | Overflow and underflow proportionality constant | 3.27, 3.28, 3.29 and 3.30[a] |
| $K_{c,o}$ | -3.441E-08 | Proportionality constant for the overflow [$m^2$/s] | 3.27 |
| $K_{c,u}$ | 1.807E-07 | Proportionality constant for the underflow [$m^2$/s] | 3.28 |
| $K_{c,o,med}$ | 4.821E-09 | Proportionality constant for the magnetite medium overflow [$m^3$/(kg.s)] | 3.33 |
| $K_{c,u,med}$ | -6.641E-09 | Proportionality constant for the magnetite medium underflow [$m^3$/(kg.s)] | 3.34 |
| $K_{c,o,ash}$ | 2.248E-09 | Proportionality constant for the overflow ash [$m^3$/(kg.s)] | 3.31 |
| $K_{c,u,ash}$ | -2.742E-10 | Proportionality constant for the underflow ash [$m^3$/(kg.s)] | 3.32 |
| $\Delta_{\rho_{c,med}}$ | 50.00 | Difference between feed medium density with the overflow or underflow medium density (kg/$m^3$) | 3.33 and 3.34[b] |

[a] $\alpha_c$ is used to determine the volume and volumetric flow rate split for overflow and underflow (i.e. $Q_{c,o} = \frac{\alpha_c Q_{c,i}}{1+\alpha_c}$, $Q_{c,u} = \frac{Q_{c,i}}{1+\alpha_c}$, $V_{c,o} = \frac{\alpha_c V_c}{1+\alpha_c}$ and $V_{c,u} = \frac{V_c}{1+\alpha_c}$).

[b] $\Delta_{\rho_{c,med}} = \rho_{c,i,med} - \rho_{c,o,med} = \rho_{c,u,med} - \rho_{c,i,med}$.

Figure 4.44 illustrates the comparison between the measured cyclone separator overflow product mass rate and the output predicted by the dynamic model.

Figure 4.45 illustrates the comparison between the measured cyclone separator discard mass rate and the output predicted by the dynamic model.

The model estimates for the DMC product and discard as shown in Figures 4.44 and 4.45 respectively, are considered to be adequate for process control studies as they are qualitatively accurate.

A process steady-state model derived from the dynamic model is required for the coal ash content system identification. The derivation is based on Meyer and Craig (2011) and Meyer and Craig

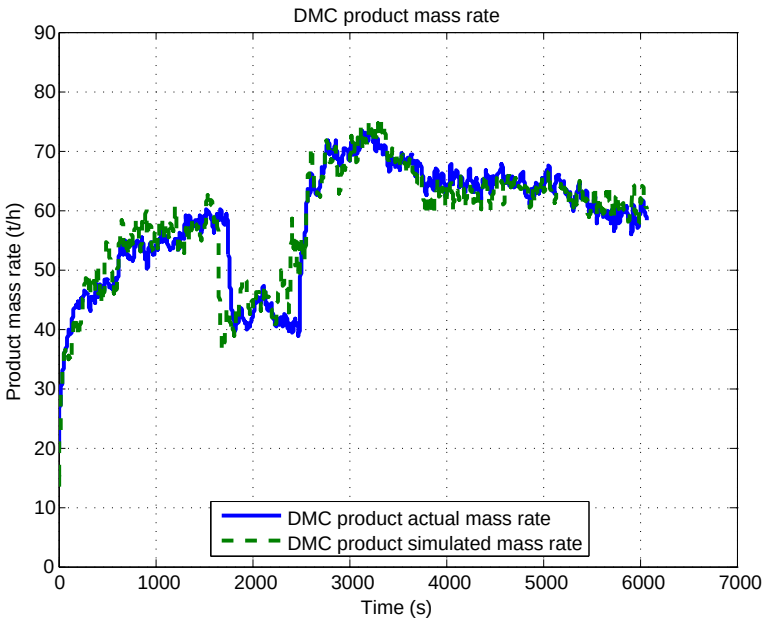


**Figure 4.44:** DMC product (DMC product = WIT012).

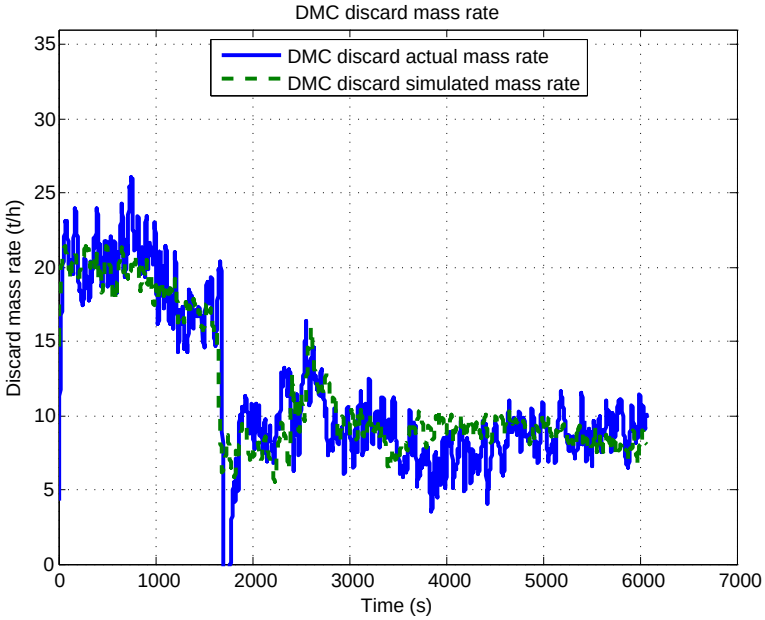


**Figure 4.45:** DMC discard (DMC discard = C14 - WIT012).

**Table 4.30:** DMC volumetric model parameters estimated from input-output data.

| Parameter | Value | Description | Equation(s) |
|---|---|---|---|
| $Q_{c,i}$ | 0.161 | Volumetric flow rate of the feed mix ($m^3/s$) | 3.27, 3.28, 3.29 and 3.30[a] |
| $V_c$ | 0.151 | Cyclone material mix volume ($m^3$) | 3.27, 3.28, 3.29 and 3.30[b] |
| $\frac{Q_{c,i,med}}{Q_{c,i}}$ | 0.887 | Ratio of the volumetric flow rate of the magnetite medium in the feed mix to overall volumetric flow rate of the feed mix | 3.27 and 3.28[c] |
| $\frac{Q_{c,i,ash}}{(Q_{c,i}-Q_{c,i,med})}$ | 0.352 | Ratio of the volumetric flow rate in the feed ash to the feed ore | 3.31 and 3.32[d] |

[a] $Q_{c,i}$ is used to determine the volumetric flow rates (i.e. $Q_{c,o} = \frac{\alpha_c Q_{c,i}}{1+\alpha_c}$ and $Q_{c,u} = \frac{Q_{c,i}}{1+\alpha_c}$).

[b] $V_c$ is used to determine the volumes (i.e. $V_{c,o} = \frac{\alpha_c V_c}{1+\alpha_c}$ and $V_{c,u} = \frac{V_c}{1+\alpha_c}$).

[c] The ratio of volumetric flow rate to medium is used in the mixing box model developed by Meyer and Craig (2010) and to calculate the product mass flow in overflow and discard mass flow in underflow using conservation of mass of components by removing the mass flow rate of medium.

[d] The ratio of the volumetric flow rate in feed ash to feed ore is is used to calculate the overflow and underflow ash contents.

(2014). A model fit was performed using the partition curve from Equation 3.46. The predicted mass distributions to overflow and underflow at different particle densities in the feed are obtained by simulating the partition factor at different medium densities. By starting with a finite amount of mass in the feed and simulating the separation at steady-state at a high density, the resulting mass in the overflow can be used as the feed for the next steady-state simulation. With decreasing medium density iterations, the resulting partition factors can be obtained. By fitting Equation 3.46 to the simulated observations the partition curve in Figure 4.46 was generated.

Table 4.31 shows a summary of the parameters for the efficiency curve fit. This simulation indicates that a dynamic drum separator model can be reduced to a realistic steady-state model from which a partition curve can be generated.

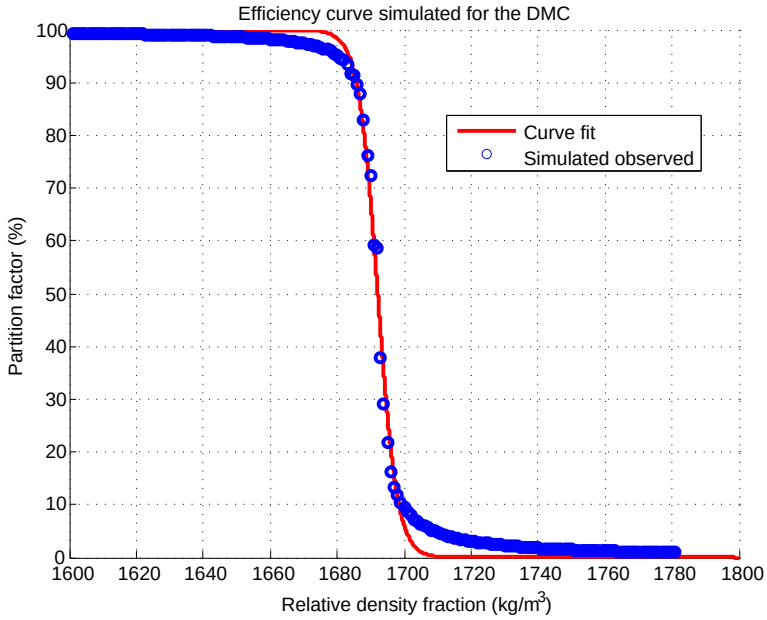


**Figure 4.46:** Simulated efficiency curve for the DMC using the steady-state model derived from the dynamic DMC model.

**Table 4.31:** Partition curve efficiency model parameters (Equation 3.46).

| Efficiency parameter | Simulated steady-state model results (SG) |
|---|---|
| $\rho_{50}$ | 1.692 |
| EPM | 0.003 |

Using Equation 3.43 the EPM is determined as 0.003 SG based on the partition curve in Figure 4.46. It was indicated by the process development engineer responsible for the production facility where the DMC model has been applied that the separation efficiency results align very well with the actual DMC efficiency (Steyn, 2014b). An actual efficiency curve of the DMC was not available.

Since no online measurement was available to measure the product and discard grade, the method of reconstituting the feed ash component percentage and estimation of the product ash component percentage explained in Chapter 3 is used. The previous efficiency curve results combined with Equations 3.46 and 3.42 are used to estimate the input-output data for the grade simulation. This method assumes that the average overflow and underflow ore density are used instead of density fractions. It is also assumed that a normalised partition curve developed from Figure 4.46 can be

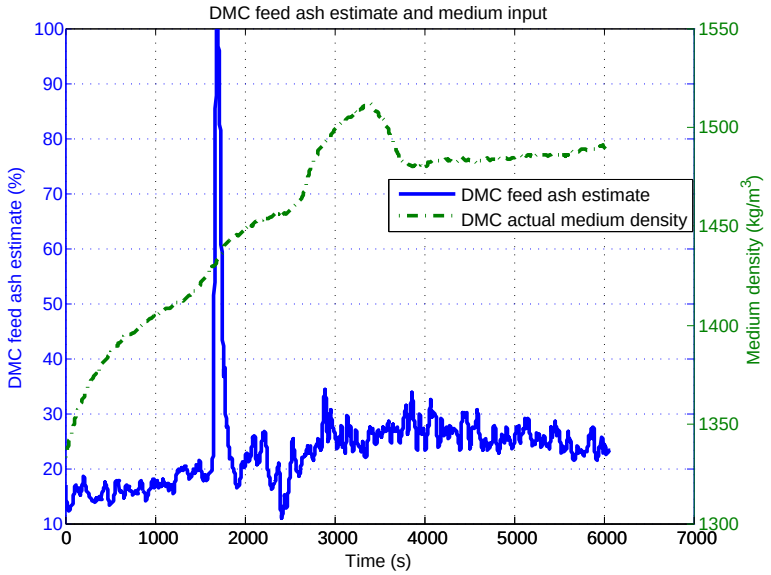


**Figure 4.47:** Input data for grade simulation (DMC feed ash = $x_{c,i,ash}$; DMC medium density = DIT012). The large spike near 1700 seconds is due to the yield becoming 100% as the discard mass flow rate near 1700 seconds becomes zero as shown in Figure 4.45.

applied at the initial medium density of about 1350 kg/m$^3$. When the medium density is increased to about 1500 kg/m$^3$, the partition curve will be applied to the increased medium density setpoint.

The input data for the DMC grade simulation are shown in Figure 4.47. The large spike in ash content near 1700 seconds is due to the plant yield increasing to 100% (the yield increase is clearly shown in Figure 4.45 by the discard mass flow rate becoming zero near 1700 seconds). The feed ash percentage ($x_{c,i,ash}$ as described in Table 3.8) of the DMC feed material is not controlled as it is dependant on an upstream mining and blending process. The density of the DMC medium is also shown as an input similar to that shown in Figure 4.43.

Figure 4.48 illustrates the comparison between the measured DMC product ash percentage ($x_{c,o,ash}$ as described in Table 3.9) and the dynamic model predicted output. A detailed view of the product ash percentage comparison is given in Figure 4.49 from time 1000 seconds to 2000 seconds.

Figure 4.50 illustrates the comparison between the measured DMC discard ash percentage ($x_{c,u,ash}$ as described in Table 3.9) and the dynamic model predicted output. A detailed view of the discard ash percentage comparison is given in Figure 4.51 from time 1000 seconds to 2000 seconds.

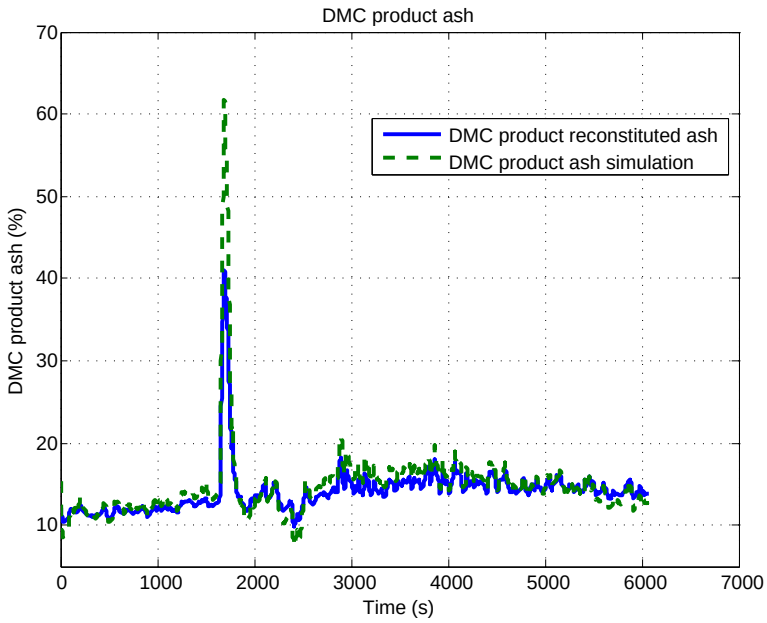


**Figure 4.48:** DMC product ash percentage simulation (DMC product ash = $x_{c,o,ash}$).

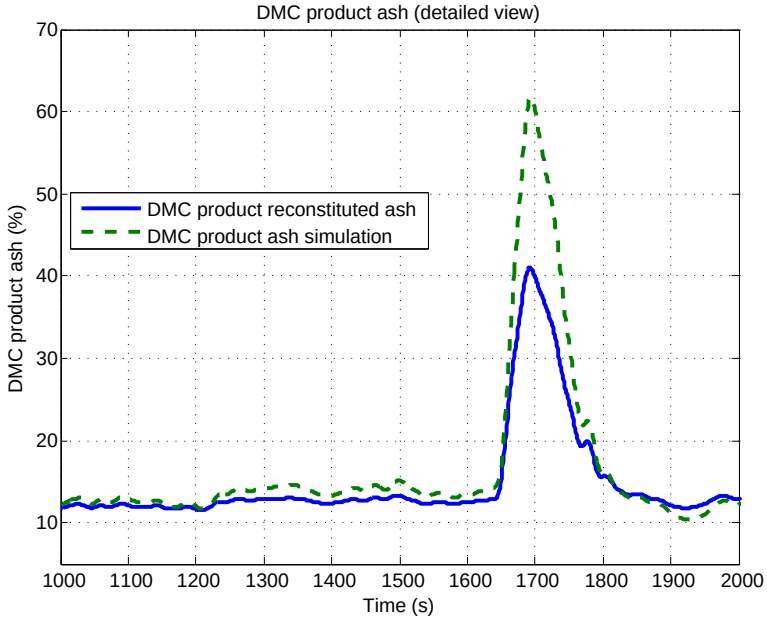


**Figure 4.49:** DMC product ash percentage simulation (detailed view, DMC product ash = $x_{c,o,ash}$).

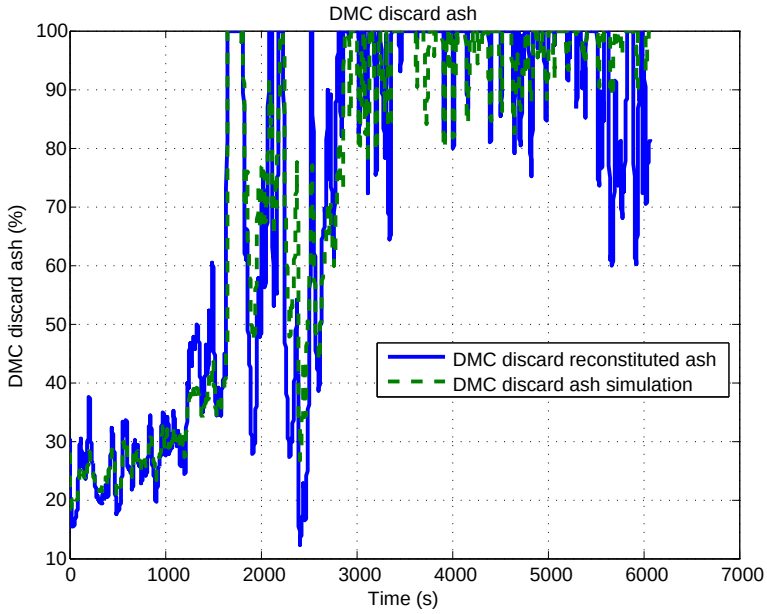


**Figure 4.50:** DMC discard ash percentage simulation (DMC discard ash = $x_{c,u,ash}$).

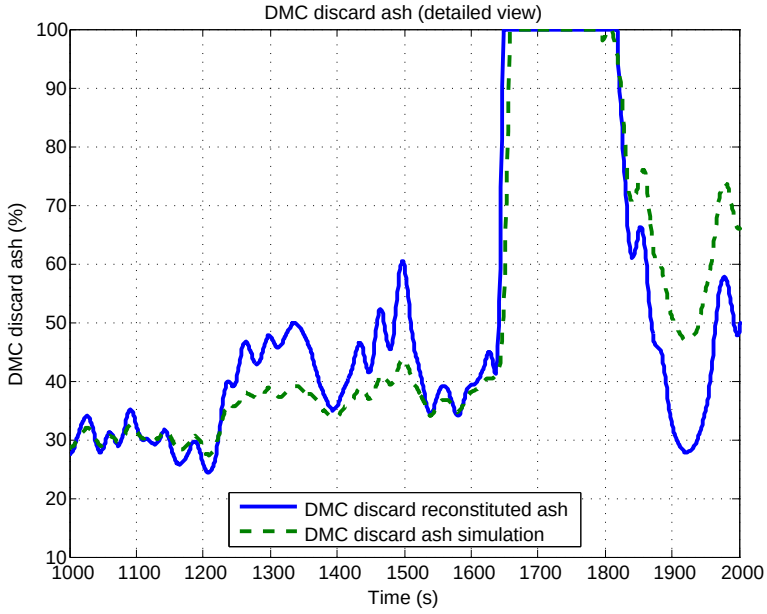


**Figure 4.51:** DMC discard ash percentage simulation (detailed view, DMC discard ash = $x_{c,u,ash}$).

**Table 4.32:** Dynamic DMC model performance results summary.

| Output | Fit (%) | Correlation |
|---|---|---|
| Product throughput (WIT012) | 61.2 | 0.92 |
| Discard throughput (C14 - WIT012) | 56.2 | 0.90 |
| Product grade (ash) ($x_{c,o,ash}$) | 29.3 | 0.98 |
| Discard grade (ash) ($x_{c,u,ash}$) | 46.6 | 0.90 |

The model estimates for the product ash percentage and discard ash percentage as shown in Figures 4.48 and 4.50 respectively, are considered to be adequate for process control studies as they are qualitatively accurate.

The dynamic model goodness of fit (Ljung, 2005) and correlation between the measured outputs and simulated outputs are given in Table 4.32.

### 4.3.2 Model predictive control design and simulation

This subsection details the application of model-based process control for the DMD and DMC circuits detailed above. The objectives of the model-based control (Steyn, 2014a) are as follows:

- Primarily ensure that the product ash content never exceeds contract requirements;
- Maximise plant yield; and
- Ensure product ash content tracks a defined setpoint based on the coal washability and desired product specification.

The DMS process has competing objectives where the first objective is to maximise yield, while the second objective is to ensure that the product ash content does not exceed the desired product specification. By trying to maximise yield, the grade will decrease (i.e. ash increases) as illustrated in Figure 2.9. A proposed objective for the DMS plant is represented in Figure 4.52.

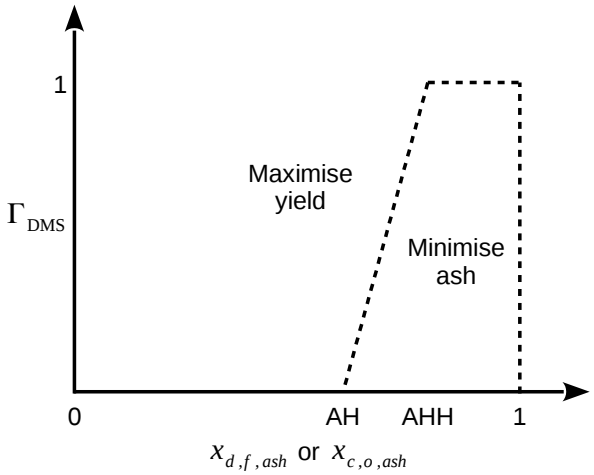


**Figure 4.52:** DMS control objective ($\Gamma_{DMS}$ = Objective function factor used in Equation 4.26; $x_{d,f,ash}$ = DMD product ash; $x_{c,o,ash}$ = DMC product ash).

Figure 4.52 depicts how the controller objective (vertical axis) should change at different product ash contents (horizontal axis) for either the DMD ($x_{d,f,ash}$) or DMC ($x_{c,o,ash}$). While product ash content is within specification (i.e. below AHH), the controller objective should focus on maximising plant yield. If product ash content exceeds the required specification (i.e. larger than AHH), the controller objective should change and focus on bringing the ash content back to the saleable specification.

With the objectives of the DMS process described above and the definition of the MPC objective function (Equation 3.49) with typical constraints (Equations 3.50, 3.51 and 3.52), the DMS plant yield and ash contents can be controlled.

This means that the objective function for the MPC is,

$$\begin{aligned} J_{\text{DMS}} \quad = \quad & \sum_{j=1}^{N} r_{\text{DMS},1} |(1-\Gamma_{\text{DMS}})(y_{\text{DMS},1}(t+j) - y_{s,\text{DMS},1}(t+j))|^2 + \\ & r_{\text{DMS},2} |(\Gamma_{\text{DMS}})(y_{\text{DMS},2}(t+j) - y_{s,\text{DMS},2}(t+j))|^2 + \\ & \sum_{j=0}^{M-1} \mathbf{P}_{\text{DMS}} |\Delta u_{\text{DMS}}(t+j)|^2, \end{aligned} \tag{4.26}$$

where $\Gamma_{\text{DMS}}$ is the variable which changes the objective as indicated in Figure 4.52. $y_{\text{DMS},1}(t+j)$ and $y_{s,\text{DMS},1}$ are the yield output and desired reference trajectory and $y_{\text{DMS},2}(t+j)$ and $y_{s,\text{DMS},2}$ are the product ash and desired reference trajectory. $u_{\text{DMS}}(t+j)$ is the manipulated medium density setpoint.

**Table 4.33:** DMD MPC objective function setup.

| Variable | Value or tagname |
|---|---|
| AH | 14.5% |
| AHH | 15% |
| $r_{\text{DMS},1}$ | 100 |
| $y_{\text{DMS},1}$ | $\frac{C12}{C11}$ |
| $y_{s,\text{DMS},1}$ | 100% |
| $r_{\text{DMS},2}$ | 100 |
| $y_{\text{DMS},2}$ | $x_{d,f,ash}$ |
| $y_{s,\text{DMS},2}$ | 0% |
| $\mathbf{P}_{\text{DMS}}$ | 1 |
| $u_{\text{DMS}}$ | DIT011 |

#### 4.3.2.1 DMD area

The DMD area dynamic model is controlled by manipulating the medium density (DIT011). The input mass flow rate (C11) and ash content ($x_{d,f,ash}$) are assumed to be measured disturbances.

Figure 4.52 illustrates the varying objectives of a DMS which can be applied to the DMD. At high product ash content ($x_{d,f,ash} >$ AH) the objective of the controller should be to reduce the product ash. While the product ash content is below required specifications ($x_{d,f,ash} \leq$ AH), the objective of the controller should be to maximise yield.

Table 4.33 describes the variables and associated values that are used for the MPC objective function $J_{\text{DMS}}$ (Equation 4.26). The control horizon is two seconds while the prediction horizon is one minute ($M = 2$ and $N = 60$).

The constraints of the DMD are,

$$1200 \leq u_{\text{DMS}} \leq 2000 \quad \forall t, \tag{4.27}$$

$$-50 \leq \Delta u_{\text{DMS}} \leq 50 \quad \forall t, \tag{4.28}$$

$$0 \leq y_{\text{DMS},2}(t) \leq 1 \quad \forall t, \tag{4.29}$$

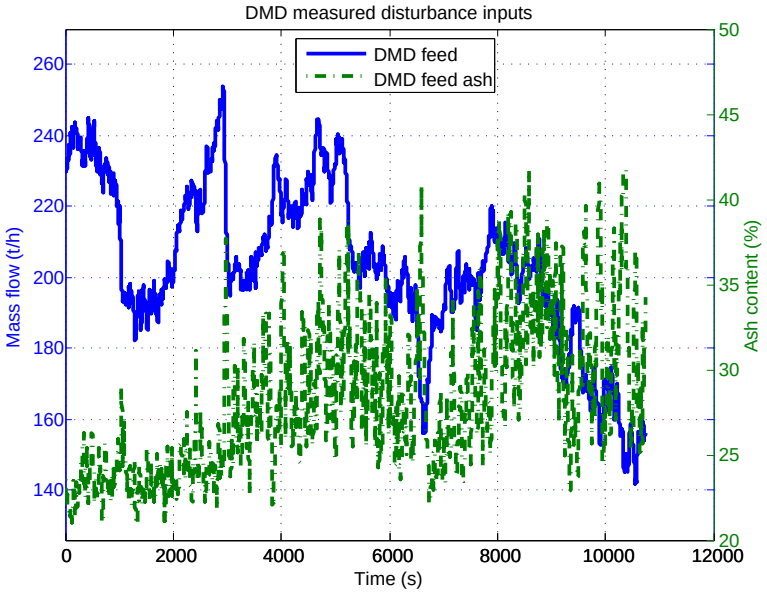


**Figure 4.53:** DMD measured disturbances (DMD feed = C11; DMD feed ash = $x_{d,i,ash}$).

such that the medium density falls within operating ranges of 1200 kg/m$^3$ and 2000 kg/m$^3$ and a slew rate of -50 kg/m$^3$ and 50 kg/m$^3$. The DMD product ash content ($x_{d,f,ash}$) must not exceed 100% and must always remain positive.

With the objective function and constraints defined (Equations 4.26, 4.27, 4.28 and 4.29, the process can be simulated using NMPC. The nonlinear dynamic model described in the previous section is used for the NMPC future prediction and the control simulation of the coal separation process. The NMPC problem can be solved by using the nonlinear programming problem described in Subsection 3.6.2. The objective function (Equation 4.26) is minimised over control moves subject to plant dynamics and input/output constraints detailed above.

Each NMPC simulation input and output are shown in comparison to the DMD plant simulation response where manual control was applied. Figure 4.53 illustrates the DMD feed mass flow rate (C11) and ash content ($x_{d,i,ash}$) measured disturbances used for the NMPC simulation. Figure 4.54 shows a comparison between the manually set medium density (DIT011) versus the NMPC medium density (DIT011) actuation for the DMD. Figures 4.55 and 4.56 illustrates the manual versus NMPC output responses for the float (C12) and sink mass flow rates and associated ash content ($x_{d,f,ash}$ and $x_{d,s,ash}$).

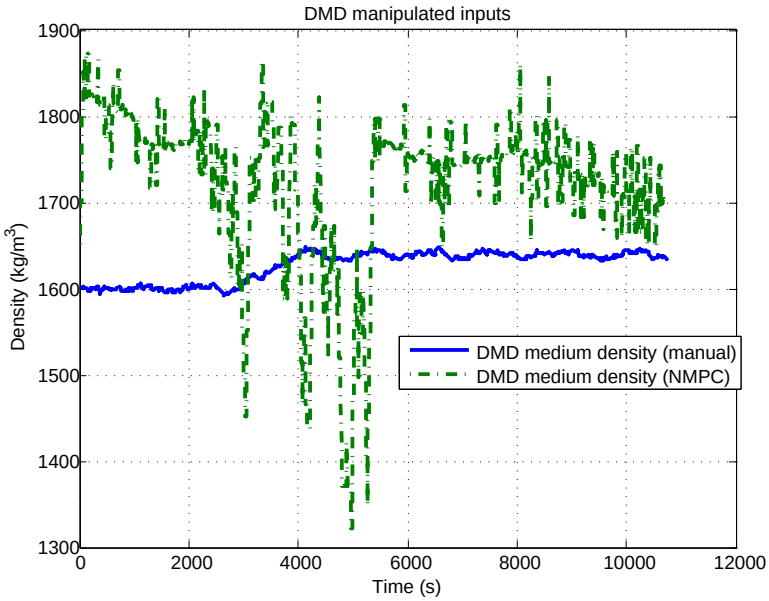


**Figure 4.54:** DMD NMPC manipulated variable comparison (DMD medium density = DIT011).

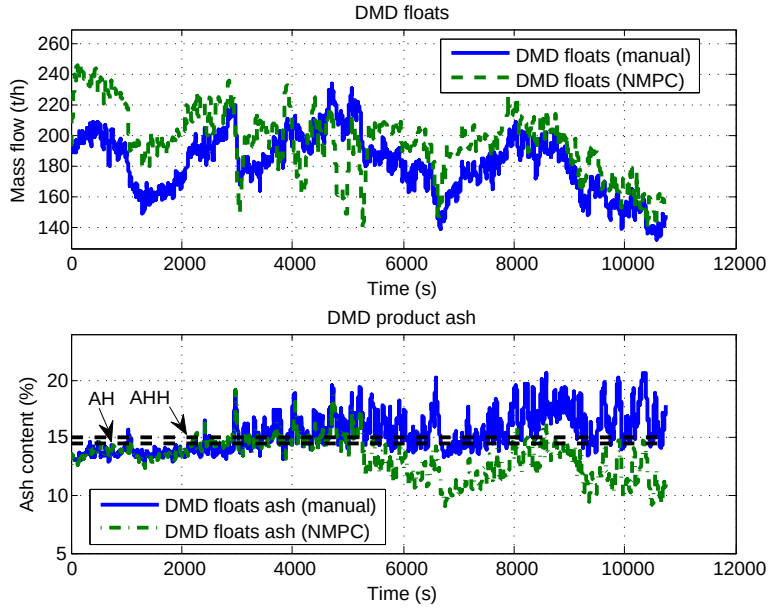


**Figure 4.55:** DMD NMPC floats comparison (DMD floats = C12; DMD floats ash = $x_{d,f,ash}$).

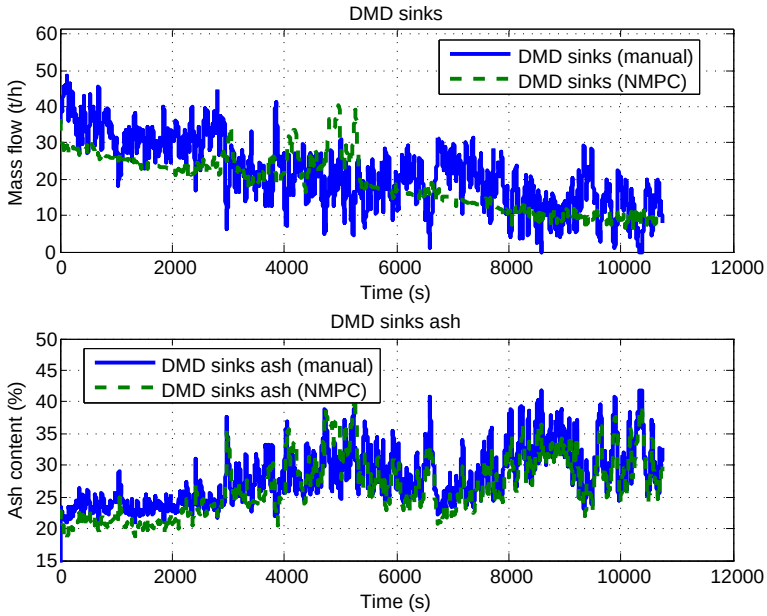


**Figure 4.56:** DMD NMPC sinks comparison (DMD sinks = C11 - C12; DMD sinks ash = $x_{d,s,ash}$).

**Table 4.34:** DMD manual control versus NMPC performance evaluation (Gains are represented as positive numbers while losses are represented as negative numbers).

| Measure | Manual control | NMPC | Gain/loss |
|---|---|---|---|
| Yield (%) | 89.3 | 96.8 | 7.5 |
| Ash content (%) | 14.9 | 13.4 | 1.5 |

Table 4.34 shows the DMD yield and floats weighted ash content while the plant was in manual control versus NMPC. The gains or losses in process yield and ash content from the NMPC are also given. Gains are represented as positive numbers while losses are represented as negative numbers.

#### 4.3.2.2 DMC area

The DMC area dynamic model is controlled by manipulating the medium density (DIT012). The input mass flow rate (C14) and ash content ($x_{c,o,ash}$) are assumed to be measured disturbances.

Similar to the DMD, Figure 4.52 illustrates the varying objectives of a DMS which can be applied to the DMC. At high product ash content ($x_{d,f,ash} >$ AH) the objective of the controller should be to

**Table 4.35:** DMC MPC objective function setup.

| Variable | Value or tagname |
|---|---|
| AH | 14.5% |
| AHH | 15% |
| $r_{\text{DMS},1}$ | 10 |
| $y_{\text{DMS},1}$ | $\frac{WIT012}{C14}$ |
| $y_{s,\text{DMS},1}$ | 88% |
| $r_{\text{DMS},2}$ | 10 |
| $y_{\text{DMS},2}$ | $x_{c,o,ash}$ |
| $y_{s,\text{DMS},2}$ | 14.5% |
| $\mathbf{P}_{\text{DMS}}$ | 1 |
| $u_{\text{DMS}}$ | DIT012 |

reduce the product ash. While the product ash content is below required specifications ($x_{d,f,ash} \leq$ AH), the objective of the controller should be to maximise yield.

Table 4.35 describes the variables and associated values that are used for the MPC objective function $J_{\text{DMS}}$ (Equation 4.26). The control horizon is two seconds while the prediction horizon is sixty seconds ($M = 2$ and $N = 60$).

The constraints of the DMD are,

$$1200 \leq u_{\text{DMS}} \leq 2000 \quad \forall t, \tag{4.30}$$

$$-50 \leq \Delta u_{\text{DMS}} \leq 50 \quad \forall t, \tag{4.31}$$

$$0 \leq y_{\text{DMS},2}(t) \leq 1 \quad \forall t, \tag{4.32}$$

such that the medium density falls within operating ranges of 1200 kg/m$^3$ and 2000 kg/m$^3$ and a slew rate of -50 kg/m$^3$ and 50 kg/m$^3$. The DMC product ash content ($x_{c,o,ash}$) must not exceed 100% and must always remain positive.

With the objective function and constraints defined (Equations 4.26, 4.30, 4.31 and 4.32, the process can be simulated using NMPC. The nonlinear dynamic model described in the previous section is used for the NMPC future prediction and the control simulation of the coal separation process. The NMPC

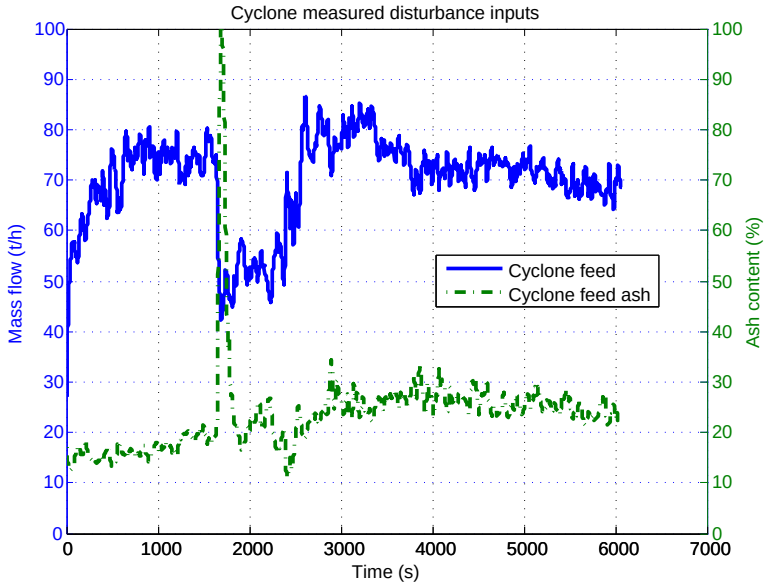


**Figure 4.57:** DMC measured disturbances (Cyclone feed = C14; Cyclone feed ash = $x_{c,i,ash}$). The large spike in cyclone feed ash content near 1700 seconds is due to the yield becoming 100% as the discard mass flow rate near 1700 seconds becomes zero as shown in Figure 4.45.

problem can be solved by using the nonlinear programming problem described in Subsection 3.6.2. The objective function (Equation 4.26) is minimised over control moves subject to plant dynamics and input/output constraints detailed above.

Each NMPC simulation input and output are shown in comparison to the DMC plant simulation response where manual control was applied. Figure 4.57 illustrates the DMC feed mass flow rate (C14) and ash content ($x_{c,i,ash}$) measured disturbances used for the NMPC simulation. The large spike in ash content near 1700 seconds is due to the plant yield increasing to 100% (the yield increase is clearly shown in Figure 4.45 by the discard mass flow rate becoming zero near 1700 seconds). Figure 4.58 shows a comparison between the manually set medium density (DIT012) versus the NMPC medium density (DIT012) actuation for the DMC. Figures 4.59 and 4.60 illustrates the manual versus NMPC output responses for the overflow (WIT012) and underflow mass flow rates and associated ash contents ($x_{c,o,ash}$ and $x_{c,u,ash}$).

Table 4.36 shows the DMC yield and overflow weighted ash content while the plant was in manual control versus NMPC. The gains or losses in process yield and ash content from the NMPC are also given. Gains are represented as positive numbers while losses are represented as negative

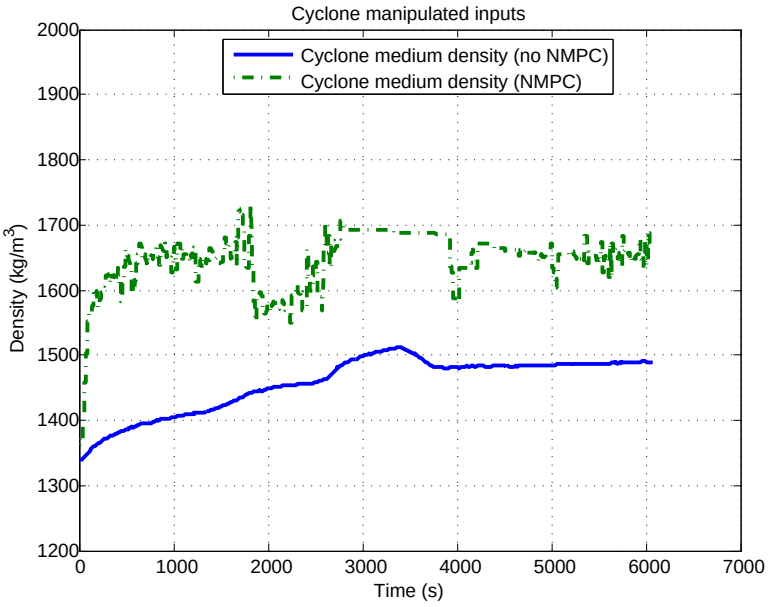


**Figure 4.58:** DMC NMPC manipulated variable comparison (Cyclone medium density = DIT012).

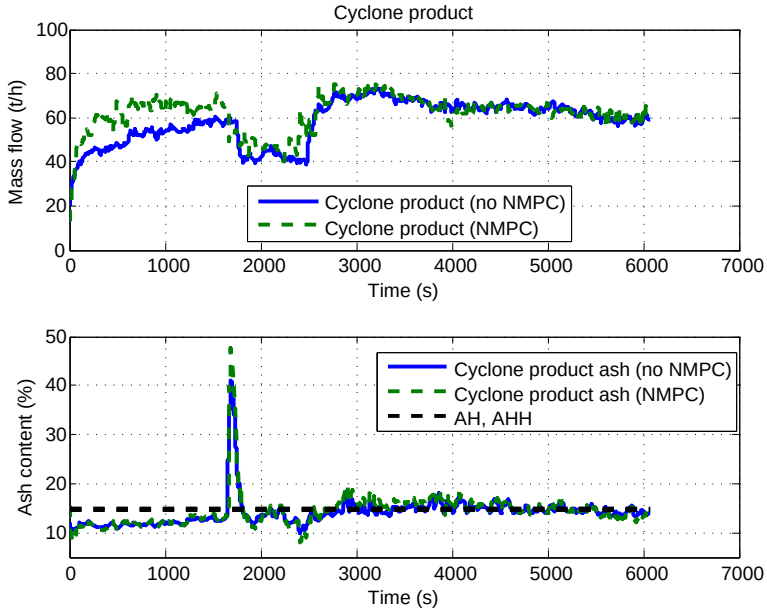


**Figure 4.59:** DMC NMPC overflow comparison (Cyclone product = WIT012; Cyclone product ash = $x_{c,o,ash}$).

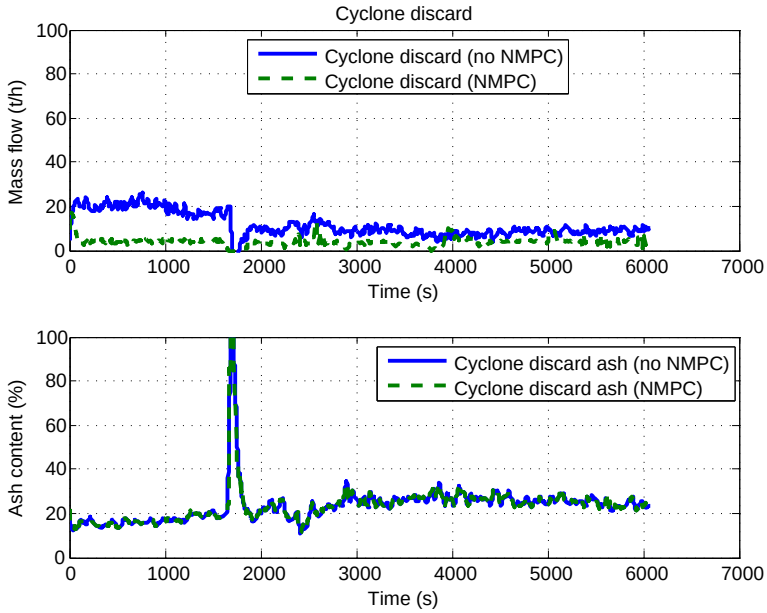


**Figure 4.60:** DMC NMPC underflow comparison (Cyclone discard = C14 - WIT012; Cyclone discard ash = $x_{c,u,ash}$).

**Table 4.36:** DMC manual control versus NMPC performance evaluation (Gains are represented as positive numbers while losses are represented as negative numbers).

| Measure | Manual control | NMPC | Gain/loss |
|---|---|---|---|
| Yield (%) | 83.3 | 88.4 | 5.1 |
| Ash content (%) | 14.8 | 14.4 | 0.4 |

numbers.

### 4.3.3 Unscented Kalman filter simulation

This subsection describes how the UKF algorithm is applied to the separation circuit. Each separator (i.e. the drum and cyclone) are simulated separately with the UKF. The UKF algorithm was applied to the nonlinear DMD and DMC model from the separation circuit derived in this thesis. Each separation area consists of dynamic models containing seven states [one mixing box state derived from Meyer and Craig (2010); six DMD states that can be obtained from Equations 3.21, 3.22 and 3.23; or six DMC states obtained from Equations 3.27, 3.28, 3.29 and 3.30] and four outputs.

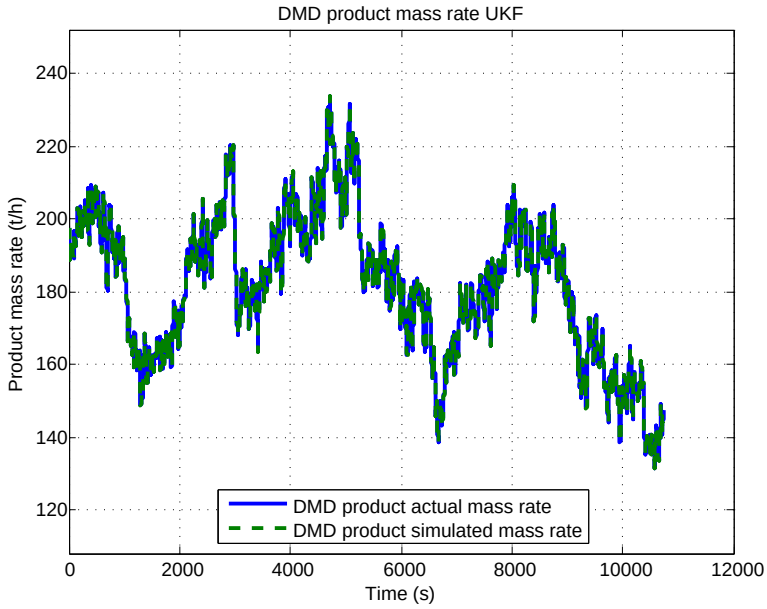


**Figure 4.61:** Drum separator floats product UKF (DMD product = C12).

For the DMD, the outputs are the product float (C12) and sink (C11 - C12) mass flow rate and product float and sink ash content ($x_{d,f,ash}$ and $x_{d,s,ash}$). For the DMC, the outputs are the product overflow (WIT012) and underflow (C14 - WIT012) mass flow rate and product float and sink ash content ($x_{c,o,ash}$ and $x_{c,u,ash}$).

#### 4.3.3.1 DMD area

The initial covariance of the original state ($\mathbf{P}_{d,0}$) was chosen as the identity matrix $\mathbf{I}_7$. The standard deviation $\mathbf{Q_d}$ of the process was chosen to be fairly large based on the measurement data,

$$\mathbf{Q_d} = \text{diag}([\ 5 \quad 5 \quad 5 \quad 0.01 \quad 0.01 \quad 0.02 \quad 0.02\ ]), \tag{4.33}$$

where the initial covariance for the process noise is determined as $\mathbf{P}_{d,v} = \mathbf{Q_d}^2$.

The standard deviation of all measurement noise was chosen to be a very small value of 1% ($r_d = 0.01$). This implies that the initial covariance for the measurement noise can be determined as $\mathbf{P}_{d,n} = r_d^2\mathbf{I}_4$.

Figures 4.61, 4.62, 4.63 and 4.65 illustrate the UKF simulation versus the measured process outputs. Figures 4.64 and 4.66 illustrate a detailed view of the float and sink ash content.

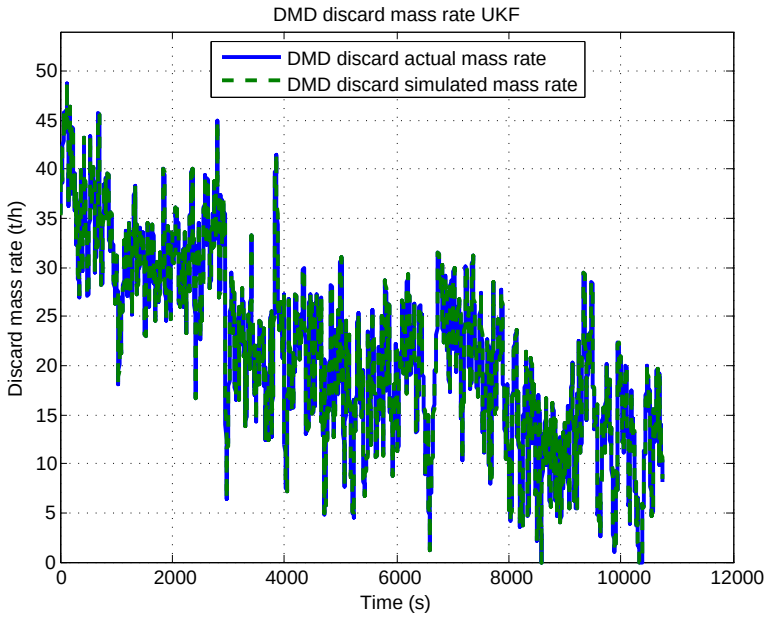


**Figure 4.62:** Drum separator sinks discard UKF (DMD discard = C11 - C12).

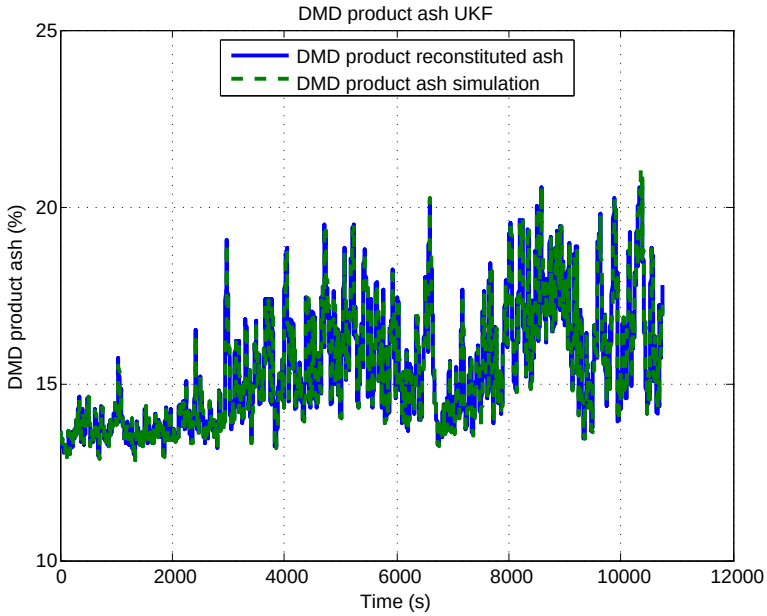


**Figure 4.63:** Drum separator floats product ash percentage UKF simulation (DMD product ash = $x_{d,f,ash}$).

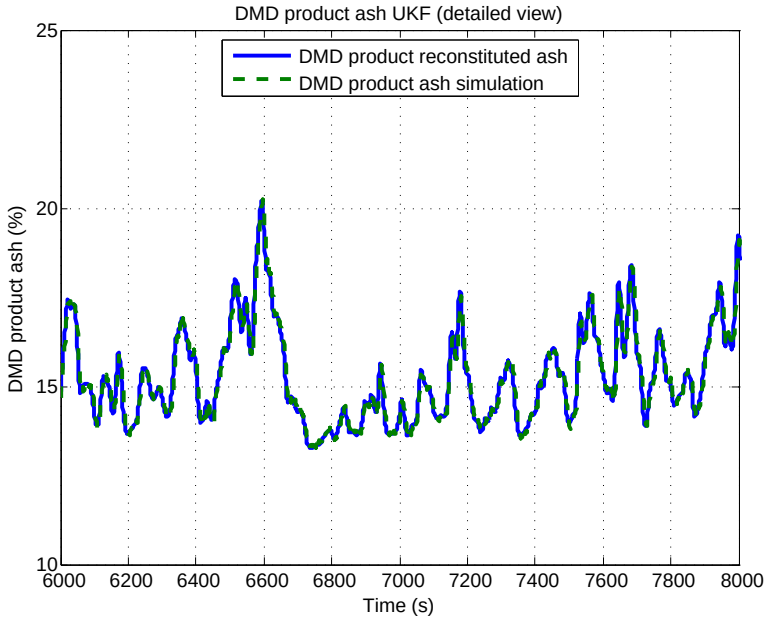


**Figure 4.64:** Drum separator floats product ash percentage UKF simulation (detailed view, DMD product ash = $x_{d,f,ash}$).

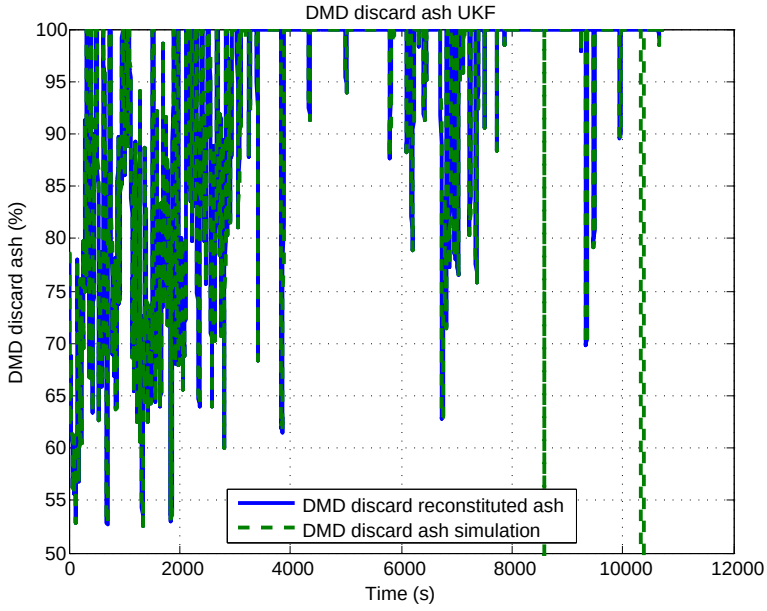


**Figure 4.65:** Drum separator sinks discard ash percentage UKF simulation (DMD discard ash = $x_{d,s,ash}$).

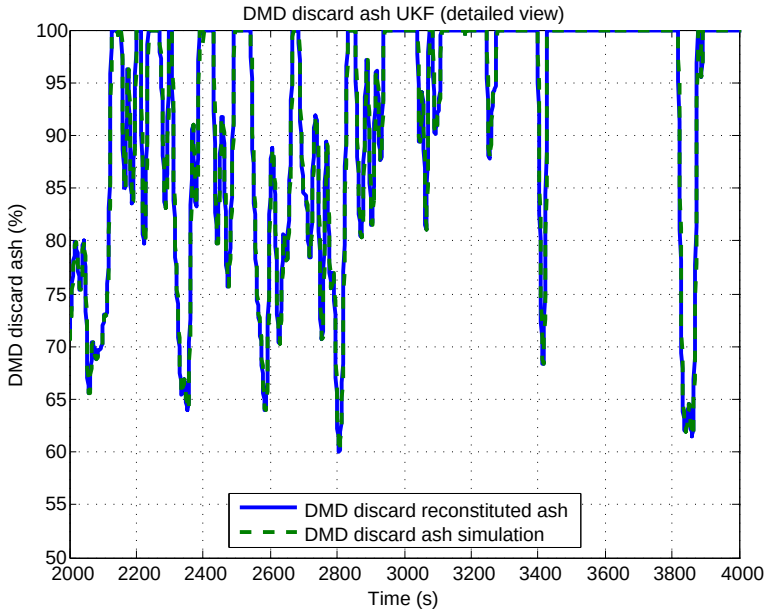


**Figure 4.66:** Drum separator sinks discard ash percentage simulation (detailed view, DMD discard ash = $x_{d,s,ash}$).

**Table 4.37:** DMD UKF performance results summary.

| Output | Fit (%) | Correlation |
|---|---|---|
| Product throughput | 97.7 | 1.00 |
| Discard throughput | 96.1 | 1.00 |
| Product grade (ash) | 86.0 | 0.99 |
| Discard grade (ash) | 40.3 | 0.85 |

Table 4.37 shows a summary of the model fit and correlation for the UKF simulation.

#### 4.3.3.2 DMC area

The initial covariance of the original state ($\mathbf{P}_{c,0}$) was chosen as the identity matrix $\mathbf{I}_7$. The standard deviation $\mathbf{Q_c}$ of the process was chosen to be fairly large based on the measurement data,

$$\mathbf{Q_c} = \text{diag}([\ 0.5 \quad 0.5 \quad 0.5 \quad 0.001 \quad 0.001 \quad 0.02 \quad 0.002\ ]), \tag{4.34}$$

where the initial covariance for the process noise is determined as $\mathbf{P}_{c,v} = \mathbf{Q_c}^2$.

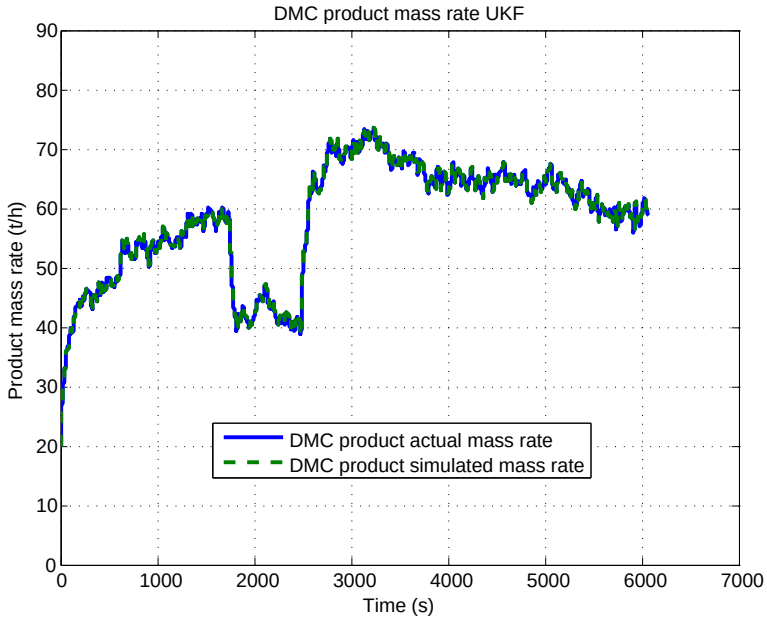


**Figure 4.67:** Cyclone separator product UKF (DMC product = WIT012).

**Table 4.38:** DMC UKF performance results summary.

| Output | Fit (%) | Correlation |
|---|---|---|
| Product throughput | 98.4 | 1.00 |
| Discard throughput | 91.4 | 1.00 |
| Product grade (ash) | 81.5 | 0.99 |
| Discard grade (ash) | 62.2 | 0.93 |

The standard deviation of all measurement noise was chosen to be a very small value of 1% ($r_c = 0.01$). This implies that the initial covariance for the measurement noise can be determined as $\mathbf{P}_{c,n} = r_c^2 \mathbf{I}_4$.

Figures 4.67, 4.68, 4.69 and 4.71 illustrate the UKF simulation versus the measured process outputs. Figures 4.70 and 4.72 illustrate a detailed view of the overflow and underflow ash content.

Table 4.38 shows a summary of the model fit and correlation for the UKF simulation.

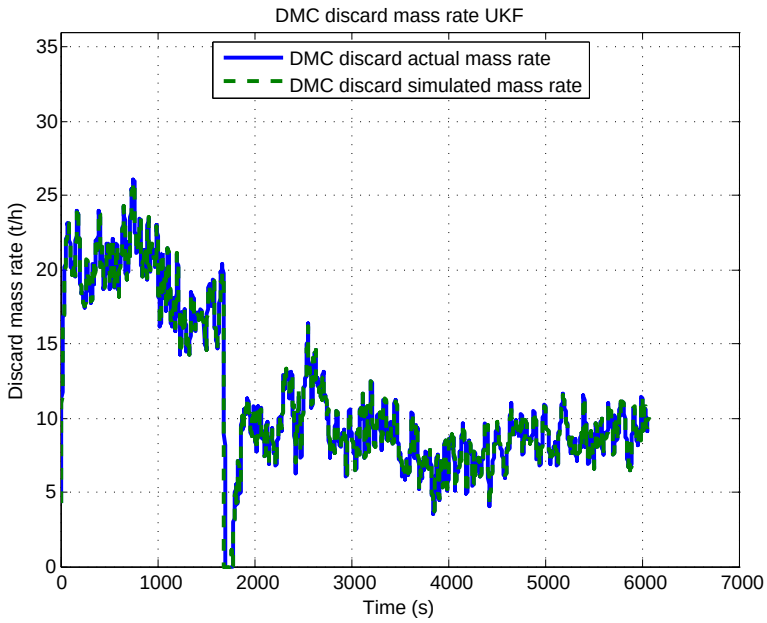


**Figure 4.68:** Cyclone separator discard UKF (DMC discard = C14 - WIT012).

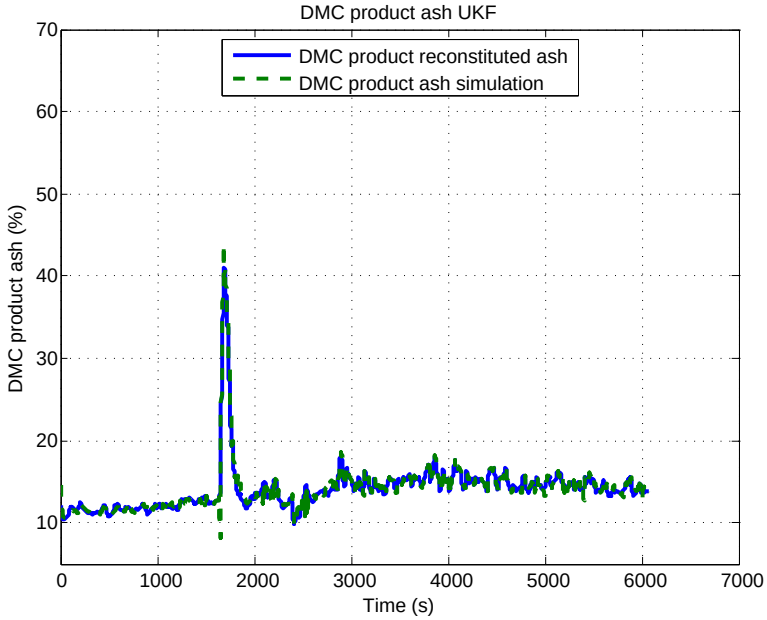


**Figure 4.69:** Cyclone separator product ash percentage UKF simulation (DMC product ash = $x_{c,o,ash}$).

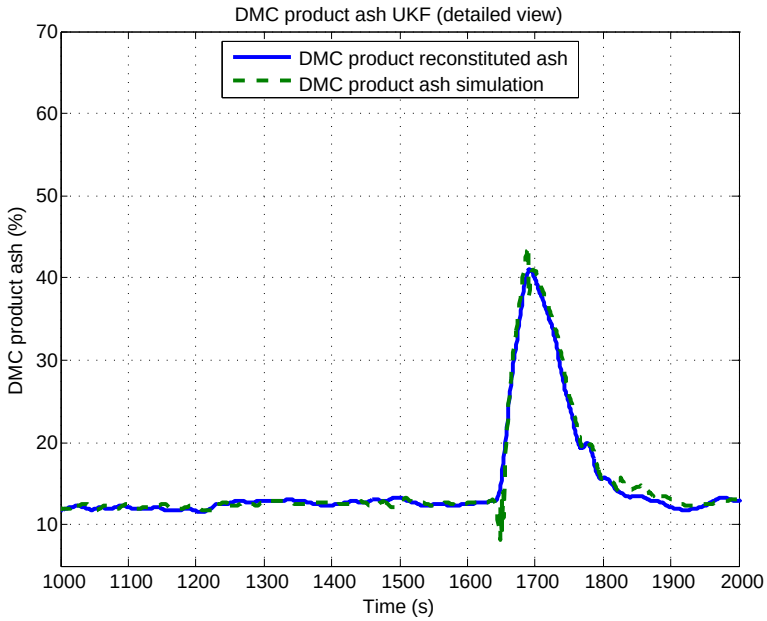


**Figure 4.70:** Cyclone separator product ash percentage UKF simulation (detailed view, DMC product ash = $x_{c,o,ash}$).

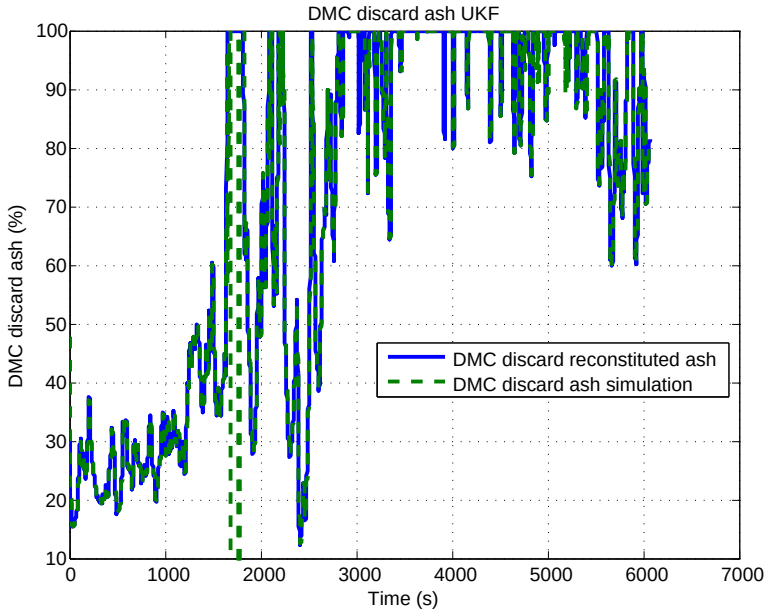


**Figure 4.71:** Cyclone separator discard ash percentage UKF simulation (DMC discard ash = $x_{c,u,ash}$).

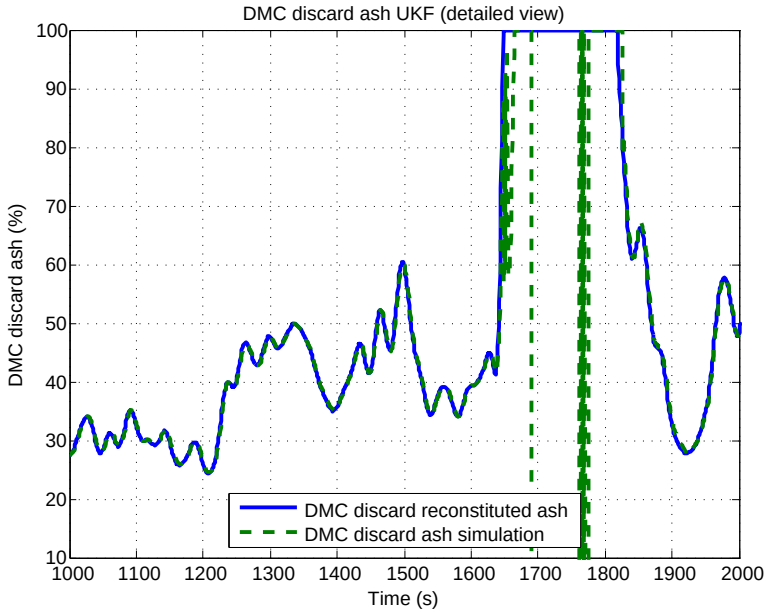


**Figure 4.72:** Cyclone separator discard ash percentage simulation (detailed view, DMC discard ash = $x_{c,u,ash}$).

### 4.3.4 Results overview

The coal separation area was broken down into two unit processes, namely, the DMD area and the DMC area. Each unit process area was modelled dynamically using the various equipment models from Chapter 3. These models were identified using actual plant data as detailed in Meyer and Craig (2010, 2014, 2015). The model fits and correlations are sufficient for control purposes as detailed in the various MPC simulations.

In order to show the control of the separation area, the control objectives of the DMD and DMC are applied using NMPC. The control simulations illustrate what possible yield and grade improvements can be expected from NMPC.

The UKF algorithm was applied to the DMD and DMC areas to illustrate that it is possible to estimate the model states and that the dynamic equipment models can be used for pure simulations.

A detailed discussion of all the coal separation simulation results are given in Chapter 5.

# CHAPTER 5 DISCUSSION

## 5.1 CHAPTER OVERVIEW

In this chapter, the results from Chapter 4 are discussed in more detail. Both the coal comminution and separation areas' results are explored. The system identification model fits and associated method are analysed. MPC objectives and results are described in terms of applicability for an actual controller implementation. Finally, the UKF results are investigated further for possible future work.

## 5.2 COAL COMMINUTION AREA

The coal comminution area detailed in Figure 4.1 in the previous chapter is an important unit process, also for other mineral processing circuits. Coal ROM is stockpiled and classified based on size through a screen and crush system in closed circuit. Sized coal is stored in a bin which is used as a buffer between the screen and crush plant and also provides feed to the downstream separation plants.

The dynamic models developed for the comminution area are applicable to three production areas:

- Stockpiling area
- Screen, crush and bin area
- DMS feed screen area

The three production areas are modelled using the dynamic equipment models detailed in Chapter 3. These models are identified with real industrial production data. The system identification results are discussed in more detail below. Thereafter, MPC was applied to the stockpiling area as well as the remaining downstream process. A complete simulation of the entire comminution circuit controlled from startup to shutdown with a process disturbance is discussed. The UKF results applied to the screen, crush and bin area serves to illustrate how state estimation could be implemented if model-based control were to be rolled out for the comminution area.

### 5.2.1 System identification results

The stockpiling area of the comminution circuit was identified using four sets of industrial experimental data. It was necessary to find production data which had enough perturbations in the seven bunker draw points. The parameters solved for the seven feeder models are sufficient to validate the stockpile mass flow rate output as given in the four experiments (Figures 4.2, 4.3, 4.4 and 4.5). The model experiment fits and correlations are very good as the first three experiments have model fits above 70% while the fourth experiment has a model fit almost 50%.

It is interesting to note experiment four has a lower fit than the other three experiments as experiment four has the same feeders used in experiment three. The reason for the lower model fit could be that the feeder model parameters change slightly over time. The physical coal stockpile within the bunker is very dynamic. The coal stockpile in the bunker supplies coal to the seven bunker draw points where the feeders remove coal. The coal stockpile feed mass flow rate and volume is not measured. The process to ensure that the stockpile is full of coal is manual and requires visual inspection. If one or more bunker draw points run empty, the feeder model does not have sufficient information to show that it cannot remove any more material (i.e. there is no stockpile mass state incorporated into the model).

A possible way to overcome this limitation on the stockpile model would be to include appropriate volume measurement of the stockpile bunker draw points and incorporate this volume into the dynamic model. Lichti *et al.* (2002) describes various ground-based laser scanners that can be used for real-time stockpile measurement. The feed rate into the bunker draw point or stockpile also needs to be measured which should be possible through the use of a belt scale. An alternative to measuring stockpile volume

could be to make use of a smart sensor or soft sensor (Pan, 2015, 2012). Another popular approach is to make use of gain scheduling for uncertain linear parameter-varying systems (Rugh and Shamma, 2000; Apkarian and Adams, 1998). Gain scheduling can be applicable to the dynamic bin model (Equations 3.12, 3.13 and 3.14) if the proportionality constants were assumed constant (i.e. if the relationship between total feed versus bin level as indicated in Figure 3.10 was not known). An observer such as the UKF to perform online parameter identification instead of state estimation could also be used (Van Der Merwe *et al.*, 2001).

The screen, crush and bin area dynamic model was identified with three sets of industrial experimental data. The three sets of experimental data were chosen to ensure that sufficient information in the bin level is available for the three phases or conditions shown in Figure 3.10. The thirty-nine parameters solved for the model fit describe the entire system sufficiently. The model fit for the screen and crush recycle mass flow rate, two bin module mass flow rates and bin level are very good for all three experiments. Unfortunately, the model was not able to describe the motor currents in experiment one and three very well as the fit results were all negative with very low correlations (correlations ranging from -0.03 to 0.82). The negative fit means that a portion of the dynamic model does not predict future values well. The weak correlation in motor current means that the model describing motor current does not have sufficient information to fit actual measured data.

The bin level validation for the three experiments in Figures 4.7, 4.10 and 4.13 show sufficient representation of bin level dynamics. The bias in the second experiment of the bin level validation (second half of Figure 4.10) is due to the deviation between the simulated and measured bin mass flow rates (second half of Figure 4.11). The lower simulated bin mass flow rate, specifically in module 1, results in less mass being removed from the bin and this leads to the bin level being higher than what it actually should be.

The good bin level validation results imply that the nonlinear bin level state (Equation 3.17 from Chapter 3) describes the bin level well given its stockpile geometric shape. The two module bin mass flow rates in Figures 4.8, 4.11 and 4.14 also describe the dynamics of the feeders very well. This result confirms the nonlinear description of the proportionality constants in Equations 3.15 and 3.16 for the feeders given the three phases in bin level.

The screen and crush recycle mass flow rate validation for the three experiments in Figures 4.6, 4.9 and

4.12 fits relatively well. There are time-periods when the model deviates from the measured output. The reason for this is probably due to the crusher motor current response not fitting the measured data well.

In the development of the dynamic crusher model, it was assumed that the mechanical system motor speed acceleration was zero. The reason for making this zero was because there was no available measurement data of the angular acceleration. If the angular acceleration state was incorporated into the system, it might improve the motor current fit results which in turn would improve the crusher recycle fit. When trying to fit the model with the angular acceleration state included (with no angular acceleration measurement) in the dynamic model, additional parameters are required to be solved. These additional parameters are difficult to solve if only the motor current measurement is available. The parameter identifiability technique applied in Meyer and Craig (2010) could be used to further analyse such a system.

The results of the DMS screen feed area model fit are very good for the purposes of the simulated feed to the downstream separation processes. The module one and two screen validation responses in Figures 4.15 and 4.16 illustrate the material size separation well. There is nothing complex about the size separation and the simplified screen model with one state representing the mass of material on the deck of the screen is sufficient. The oversize to the DMS plant one is also validated in Figure 4.17. Screen model fit and correlation results are also relatively high.

Further residual analysis on the models could be done such as the whiteness and independence tests described by Ljung (1987). The independence analysis tries to determine whether the model contains all the information available in the data. The whiteness analysis is used to ensure that the residuals are uncorrelated. Meyer (2010) illustrates how these residual tests have been applied to the dynamic models of the separation stage in coal processing. For the purposes of this thesis, these tests have been omitted as the primary objective is to obtain dynamic models of the entire coal beneficiation process for model-based control studies.

### 5.2.2 Model predictive control simulation results

The MPC simulation results from Chapter 4 for the coal comminution area illustrate how model-based control can be applied to coal minerals processing. Initially MPC is applied to the stockpile area with various conditions applied at specific time intervals to see how the system responds. Another MPC simulation is performed on the feed bin specifically, assuming that the stockpile area is under manual control. This allows for the comparison of the MPC performance to the manually operated process. A final MPC simulation is performed over the entire comminution circuit to illustrate how the plant can be automatically controlled from startup to shutdown.

The stockpile area was simulated with MPC to illustrate how the stockpile mass flow rate can be set from 500t/h to 50t/h and then back to 500t/h again. The MPC is able to actuate the seven feeder motor speeds (Figure 4.19) sufficiently to ensure the relevant reference trajectory is achieved over time. An additional simulated response is given to test what would happen if three feeders were deactivated. The MPC is able to manipulate the remaining four feeders to ensure the desired mass flow rate reference trajectory is maintained. The purpose of deactivating the three feeders is to test a scenario where the stockpile in the bunker begins to run empty and no coal is available for the feeder. As mentioned in the previous subsection, the dynamic model of the stockpile area does not have enough information to be able to determine if the stockpile itself is empty for any given draw point. The disabling of the feeder would have to be signalled from another system such as a stockpile laser measurement or smart sensor as discussed in the previous subsection.

An additional criteria incorporated into the MPC objective of the stockpile area control was to ensure that all feeders were utilised. This is to prevent the possibility of the optimiser choosing only specific feeders to perform the mass flow rate control and therefore not using other available feeders at all. The feeder utilisations are averaged every minute and also updated in the MPC objective function every minute. This is why there is a small deviation every minute in the stockpile MPC simulated response in Figure 4.20. The average utilisation of all the feeders during the simulation was 78%. Figure 4.20 also illustrates how the stockpile mass flow rate reaches the desired reference trajectories.

The MPC simulation of the stockpile area illustrates that the stockpile area can be controlled very well if it is separated or decoupled from the downstream screen, crush and bin processes. In practice,

the utilisation objective should be activated at much longer durations such as every hour, but for the purposes of the simulation, one minute is sufficient to illustrate the concept.

Another MPC simulation was performed specifically on the feed bin. The screen, crush, bin and DMS plant feed models were used for the simulation. This downstream process was decoupled from the stockpile area and it was assumed that the stockpile area was manually controlled. As a result, the input to the model was the measured disturbance stockpile mass flow rate.

The bin level control objective (Figure 4.21) is to ensure the bin level does not run empty or overflow. However, when the bin level is within safe limits, the objective is to maximise throughput by controlling the DMS plant feed mass flow rates to desired reference trajectories. In addition, the mass flow rates to the two DMC modules have to remain in balance.

Figure 4.22 illustrates the measured disturbance from the stockpile area and the associated bin level response based on the NMPC control moves. The benefit of having the input as a measured disturbance in this simulation is that it is possible to compare the NMPC performance to that of the current manually operated plant. The controller keeps the bin level within the specified level limits for maximum throughput.

Figure 4.24 illustrates how the NMPC was able to ensure the feed to the two DMC modules was kept in balance while maintaining a reference trajectory of 100t/h. Similarly, Figure 4.25 shows how the feed to the DMS plant one tries to maintain a rate of 300t/h. The simulation also incorporates another measured disturbance which is the bin bypass mass flow rate. This bypass is manually actuated by a flap gate. It can be seen that during the time intervals the bypass was opened (Figure 4.22), around 2000 seconds and 4000 seconds, the feed to DMS plant one increased significantly. This is because the bypass essentially goes toward the DMS plant one in the case when the bin modules one and two mass flow rates are starved. The upper constraint of 350t/h in the DMS plant feed mass flow rate causes the NMPC to react by switching off the bin feeder module two as shown in Figure 4.23.

When comparing the NMPC performance to the manual operation, there was an overall improvement in throughput of 3.6%. Another important benefit is that the bin level was controlled within safe limits whereas the manually operated plant was dangerously close to having the bin overflow. If the NMPC

were to be implemented, the need for the bypass stream from the bin should become unnecessary as the NMPC should ensure that the mass flow rates to the DMS plants are maintained.

The last MPC simulation demonstrates that it is possible to automatically control the entire comminution circuit from startup to shutdown. Similar stockpile and feed bin objectives were used as in the previous two MPC simulations. The feed bin level limits were adjusted to allow the bin to operate at higher bin levels. This is probably the more ideal scenario given the knowledge of how the bin feeders operate at higher bin levels. The higher the bin level, the more effective the bin feeders are able to perform (refer to Figure 3.10 describing the relationship between bin throughput and bin level).

Figure 4.26 illustrates the NMPC control moves for the stockpile feeder motor frequencies. A disturbance was introduced at 2500 seconds and removed at 3000 seconds where material was fed into the stockpile conveyor at 100t/h (shown in Figure 4.27). This is to simulate the possibility of a feeder failing and material being pushed into the bunker manually by a front end loader or material being thrown onto the stockpile conveyor belt. Is it assumed that the additional material is measured on the belt scale for the stockpile area such that the NMPC is able to react further downstream. After 3500 seconds, the plant is simulated to shutdown by reducing the stockpile mass flow rate to zero and emptying the bin.

Figure 4.28 shows the NMPC response for the bin level. The bin level limits were increased to higher levels. It can be seen that initially the bin level rises to the first lower limit from the zero initial condition. Once the bin level reached the second low level limit, it is pushed back down as the objective has changed to maximise throughput. The bin level objective will operate somewhere between the two lower bin level limits but not run lower than the lowest limit of 60% if the NMPC were to be implemented. After the shutdown signal at 3500 seconds, the bin level shows that the bin is emptied.

Figure 4.29 illustrates the mass flow rates for the DMS plant feed. During the plant startup (below 1000 seconds) it can be seen that module one DMC feed is available. However, module two DMC feed is not available until after about 1000 seconds. The reason for this is because the bin level is still within the lower level limits and the objective function is primary focussed on increasing the bin level. This means that the NMPC will reduce the mass flow from the bin itself to increase the bin level. Since the objective is to also ensure that the DMC mass flow rates of module one and two are in balance,

it conflicts with the objective of operating the mass flow rate of the DMS plant one at 300t/h. The result is that during the startup period the mass flow rates to the DMS plant feed are not at full capacity. Once the bin level is within safe limits, the throughput to the DMS plants is achieved.

Figure 4.26 also shows that the disturbance to the stockpile mass flow rate is handled by the NMPC to quickly ensure that the stockpile mass flow rate of 500t/h is maintained. This disturbance does not influence the bin level and DMS plant feed significantly.

### 5.2.3 Unscented Kalman filter results

The UKF was applied to the crush, screen and bin system to illustrate the concept of applying a state estimator for the possibility of actually implementing the NMPC on these systems. The results of the UKF show that the system states can quickly be adjusted given immediate past output data. This one-step-ahead prediction would be beneficial for an actual controller implementation to ensure that the model is always aligned to the immediate operational conditions. In practice, however, the UKF could only be applied every hour since the dynamic models fit the process well and are sufficient for the model prediction calculations.

Given the excellent model fit results of the UKF applied to the bin model as shown in Figures 4.30, 4.31 and 4.32, it is recommended that a UKF is used for a control system implementation. If the noise in the process and measurements increase significantly, but not such that the dynamics of the process are obscured, the UKF should still be able to return a good estimate of the correct model states. The good model fit for the UKF means that the UKF works well for pure simulations.

It is noted that the screen and crush recycle UKF simulation in Figure 4.30 deviates slightly while the all other outputs are tracked extremely well. As mentioned in the system identification discussion earlier, the dynamic model for the crushers could be improved. The UKF is able to ensure that the crusher model motor current fits well. This must have an impact on the throughput relationship for the crusher, given the insufficient information between motor current and throughput due the the angular acceleration not being measured and the assumption that the angular acceleration is zero.

## 5.3 COAL SEPARATION AREA

The coal separation area detailed in Figure 4.33 in the previous chapter is a critical part of the coal beneficiation process as it selectively upgrades ROM coal to required customer grade specifications. The separation stage can also significantly determine the yield of a coal operation as well. ROM is received from the comminution circuit described previously and classified based on size for the relevant separation unit process. Larger sized coal particles are separated from gangue using a drum separator, while smaller sized coal particles are separated from gangue through DMCs.

Plant model identification of unit processes for a coal separation area has been shown in various other publications (Meyer and Craig, 2010, 2014, 2015). For the purposes of this thesis, the actual downstream DMS plant from the comminution circuit was used. The DMD model from Meyer and Craig (2014) is the same, but the DMC model is new and differs from the previous DMC publications (Meyer and Craig, 2010, 2014). The model identification therefore includes the following DMS areas:

- DMD area
- DMC area

The two separation areas are modelled using the dynamic equipment models detailed in Chapter 3. These models are identified with real industrial production data. The system identification results are discussed in more detail below. Thereafter, the application of MPC to the DMD and DMC is discussed in more detail. The UKF results applied to the DMD and DMC models are then analysed, and this serves as an example of how state estimation could be implemented if model-based control were to be rolled out for the separation area.

### 5.3.1 System identification results

In the identification of both the DMD and DMC, the model parameters associated with the throughput outputs are firstly solved for. Thereafter the model parameters associated with grade are solved for through the use of a partition curve.

Production data from an industrial coal separation process was used to perform the system identification for both the DMD and DMC models. Figures 4.34 and 4.43 illustrate the inputs associated for the DMD and DMC. The mass flow rates into the unit processes are not controlled as they are determined by the comminution circuit upstream. Industrial production data were chosen in such a way that plant operations made a step change to the medium densities. The change in medium density allows for sufficient perturbations to model the DMD and DMC system responses.

The throughput and discard model fits for the DMD are sufficient for control purposes. Figures 4.35 and 4.36 illustrate how the DMD model is able to follow the measured outputs in terms of throughput. This is also true for the DMC as seen in Figures 4.44 and 4.45. No pressure measurement was available for the DMC and therefore could not be used as an additional input to the model. The mathematics describing the DMD and DMC models are very similar and explain the similarity in the quality of the model fit. However, the parameter values solved for the DMD are very different to the DMC given the larger residence time within the separator vessel.

In order to fit the DMS models to grade (ash content), and since no real-time measurements in ash were available, the ash content was reconstituted based on the actual coal washability and simulated equipment partition curves. The method of calculating the ash contents in this way is described in Chapter 4. It was assumed that the average float and sink ore densities are used and not the individual density fractions for the partitioning of the material. Another assumption was that the partition curve was normalised and applied at the initial value at which the medium density was set to. Ideally, an actual partition curve for the relative density fraction should be made available. However, this information was not available for the particular coal plant used in this thesis. The above-mentioned method might require further validation by using real-time online ash measurements.

Various technologies are available for measuring online ash content of coal. Galetakis *et al.* (2009) discuss the usage of a dual energy transmission analyser for quality control in coal mining. Borsaru and Jecny (2001) and Belbot *et al.* (1999) describe the use of the prompt gamma neutron activation analysis (PGNAA) technique for measurement of bulk coal samples. The PGNAA technique seems to be the most recent and accurate technology developed for online coal analysis (Nezamzadeh *et al.*, 1999). Cierpisz and Heyduk (2001) has shown how a radiometric online ash monitor can be used with fuzzy logic to control the time of measurement according to variations of an input signal for better measurement results.

**Table 5.1:** DMD and DMC partition curve efficiency parameters.

| Separation unit | Efficiency parameter | Value (SG) |
|---|---|---|
| DMD | $\rho_{50}$ | 1.470 |
| | EPM | 0.021 |
| DMC | $\rho_{50}$ | 1.692 |
| | EPM | 0.003 |

The partition curves for the DMD and DMC are simulated through steady-state simulations as detailed in Chapter 3. Table 5.1 shows a summary of the typical partition curve efficiency parameters.

The product and discard ash model responses for the DMD and DMC fit the reconstituted data well. Figure 4.39 illustrates that the DMD dynamic model follows the product ash responses very well. Figure 4.41 for the DMD discard ash could require improvement in model fit. The discard ash response was not used in the control simulations of the DMD, which is in accordance with current operational practices. However, the low model fit of the DMD discard ash output could imply that the model should either be improved, or the measured ash data needs to be verified with actual online analysis data. Figures 4.48 and 4.50 show good model fits for the DMC ash responses.

For this particular separation plant, the DMC receives approximately 25% of the total feed material. This small amount of material feed means that there are possible cases where yield can easily reach 100% depending on the grade of coal and medium density used. Since this particular plant is processing metallurgical coal, the grade is usually very high, hence the high separation efficiency (small EPM). In Figure 4.45 it can be seen that near 1700s the discard mass flow rate is zero (i.e. the yield is 100%). This high yield impacts the reconstituted ash contents as shown by the spike near 1700s in Figure 4.39. The DMC model does not fit this specific scenario well. In order to model the dynamics of these specific conditions, the dynamic model might need to be enhanced to include population balances at the different relative densities. However, data for such a model would be very difficult to obtain from an industrial coal plant facility and considerable pilot plant studies would be required before the model could be further investigated.

The DMD and DMC model performances are considered adequate for process control purposes as responses are in general qualitatively accurate.

### 5.3.2 Model predictive control simulation results

NMPC was applied to both the DMD and DMC with an objective function described by Figure 4.52. The control objective is based on the product ash content. If the ash is below a certain threshold, the objective of the NMPC is to maximise yield. If the ash content becomes too high, the objective changes to minimise ash. This competing objective between yield and ash is shown in Figure 2.9 where there is an inverse relationship between grade and throughput. The intention with NMPC is to increase both yield and grade by applying control to the DMD and DMC system.

For both the DMD and DMC NMPC simulations, the results are compared to that of the manually operated plants. Figure 4.54 illustrates the comparison between the DMD medium density actuated manually versus the NMPC control moves. It is clear that the NMPC makes use of a much wider range in RD versus the manually controlled process. The feasibility of allowing the medium to be actuated over such wide RD ranges over time needs to be investigated. The medium density control objective from Zhang *et al.* (2015) could be incorporated into the NMPC as well to try and minimise energy and inventory costs by reducing the amount of medium used in the circulating medium circuit. The medium recycle circuit is a secondary process and involved process water recovery. This secondary process could in future be further analysed, modelled and incorporated into the DMS dynamic models developed. Figure 4.54 shows that the NMPC operated the DMD at a much higher RD than the manually controlled plant. A higher RD is generally better as this will reduce the amount of process water addition in the density control, thereby reducing the amount of medium to be added to the medium make-up stage.

The NMPC simulated response for the floats versus the manual operation (Figure 4.55) shows very clearly how the NMPC has increased the yield. The result showing the ash response in Figure 4.55 is also very good in that it is clear that the NMPC was able to ensure that the ash content is primarily maintained below the desired threshold of 15% ash. This in-time control of product ash is ultimately the objective of a coal washing plant. In this simulation, the NMPC was able to optimise on the product

yield and grade by manipulating the medium density to its advantage. A yield improvement of 7.5% was achieved with an ash improvement (i.e. lower ash content) of 1.5%.

In the NMPC simulation of the DMC, Figure 4.58 illustrates how the medium density was manipulated automatically versus the manually operated plant. When comparing the amount of medium density movement in the DMD NMPC to the DMC, the DMD is much more volatile. This could be due to the fact that the DMD has a larger residence time and therefore more opportunity to gain from the medium density changes to control ash. The DMC NMPC ash response in Figure 4.59 visually shows very little improvement. However, a small improvement in ash of 0.4% (i.e. reduction in ash contents) was still possible. The NMPC was also able to improve yield by 5.1% for the DMC. The improvement in yield can be seen in Figure 4.59 in the first 2000 seconds where there was an opportunity for the NMPC to maximise throughput with little change in product ash contents.

### 5.3.3 Unscented Kalman filter results

The UKF was applied to the DMD and DMC dynamic models to illustrate the concept of applying a state estimator for the possibility of actually implementing the NMPC for the DMS circuit. The results of the UKF show that the system states can quickly be adjusted given immediate past output data. This one-step-ahead prediction would be beneficial for an actual controller implementation to ensure that the model is always aligned to the immediate operational conditions. In practice, for the DMD and DMC, the UKF should be applied every five minutes given the fast dynamics of the separation process.

Given the excellent model fit results of the UKF applied to the DMD model as shown in Figures 4.61, 4.62, 4.63 and 4.65, the UKF can be used for a control system implementation. Similarily, the UKF applied to the DMC shows similar results in Figures 4.67, 4.68, 4.69 and 4.71.

If the noise in the process and measurements increase significantly, but not such that the dynamics of the process are obscured, the UKF should still be able to return a good estimate of the correct model states. Further work can be done where the dynamic model parameters could be estimated online using the UKF algorithm.

**Table 5.2:** Comminution area model and UKF fit results summary (blank results in UKF fit indicate that no simulation was performed on the specific output).

| Comminution area | Output | Average model fit (%) | UKF fit (%) |
|---|---|---|---|
| Stockpile | Stockpile mass flow rate (WIT001) | 72.1 | |
| Screen, crush and bin | Screen and crush recycle (WIT002) | 75.9 | 43.4 |
| | 40mm crusher motor current (IIT001) | -41.1 | 92.9 |
| | 80mm crusher motor current (IIT002) | -45.7 | 92.3 |
| | Bin module one feeder (WIT005) | 67.1 | 98.9 |
| | Bin module two feeder (WIT004) | 61.7 | 98.4 |
| | Bin level (LIT001) | 58.4 | 99.8 |
| DMS screen feed | Module one undersize (C06) | 78.9 | |
| | Module two undersize (C08) | 61.1 | |
| | DMS plant one feed (WIT006) | 57.7 | |

The improvement in UKF fit for the DMD float ash and DMC overflow ash to the model output is an additional benefit for control purposes. As discussed earlier, the measurement of ash content is usually difficult to obtain using online ash monitors. These online measurements are sometimes not be reliable and the use of a UKF and dynamic model will significantly improve the overall control of coal product ash content. Further research could also be done to investigate the possibility of not only updating the dynamic model ash content states with the reconstituted ash calculation, but also to include an online ash monitor reading. Laboratory samples taken at much longer sampling times could also be used to adjust any bias in the online ash measurement readings.

## 5.4 CHAPTER SUMMARY

In order to summarise the discussion of the results of this thesis, the dynamic model and UKF fits are averaged and tabulated in Table 5.2 for the comminution area. The separation area model and UKF fit results are tabulated in Table 5.3.

**Table 5.3:** Separation area model and UKF fit results summary.

| Separation area | Output | Model fit (%) | UKF fit (%) |
|---|---|---|---|
| DMD | Product throughput (C12) | 69.0 | 97.7 |
| | Discard throughput (C11-C12) | 43.5 | 96.1 |
| | Product grade (ash) ($x_{d,f,ash}$) | 66.4 | 86.0 |
| | Discard grade (ash) ($x_{d,s,ash}$) | 56.3 | 40.3 |
| DMC | Product throughput (WIT012) | 61.2 | 98.4 |
| | Discard throughput (C14-WIT012) | 56.2 | 91.4 |
| | Product grade (ash) ($x_{c,o,ash}$) | 29.3 | 81.5 |
| | Discard grade (ash) ($x_{c,u,ash}$) | 46.6 | 62.2 |

**Table 5.4:** Area model MPC improvement results summary.

| Area | Performance measure | Improvement (%) |
|---|---|---|
| Screen, crush and bin | Total throughput | 3.6 |
| DMD | Yield | 7.5 |
| | Ash content | 1.5 |
| DMC | Yield | 5.1 |
| | Ash content | 0.4 |

The quantitative MPC improvements made to the screen, crush, bin and separation processes are tabulated in Table 5.4.

Some qualitative improvements that have also been made to the comminution circuit from the NMPC are summarised as follows:

- The stockpile mass flow rate is able to track a throughput reference trajectory automatically.
- The automatic control of the stockpile area is capable of overcoming disturbances provided the stockpile level is known.

- The stockpile feeders can be utilised equally over time to ensure that no bias is introduced.

- The feed bin level can be controlled automatically to ensure no material overflows or that the bin does not run empty.

- The bin bypass disturbance is rejected by the automatic control and will probably not be required once an automatic controller is installed.

- It was shown that the overall comminution process can automatically be started up and shut down.

- An automatic controller is capable of addressing disturbances such as additional feed material in the stockpile area that is currently unaccounted for.

# CHAPTER 6 CONCLUSION

This chapter provides a brief summary of the simulation results given in Chapter 5. Possible improvement that can be made is motivated using the simulation results and recent coal financial market indicators. Additional research topics that can be investigated are also suggested. Finally the conclusion investigates the overall control hierarchy and proposes a possible future topic for coal mine optimisation using MPC.

## 6.1 CONCLUDING REMARKS

Thwaites (2007) indicates that the overall objective of process control in metallurgical plants is to stabilise the process and then optimise it. The work developed in this thesis provides a means to stabilise and control a coal plant through the use of model-based control. Given that the available literature on dynamic models for coal plants is relatively limited, additional models were developed for the specific comminution circuit studied.

The results in Chapter 4 illustrate how the dynamic models for an actual industrial coal processing facility were developed in Chapter 3 and identified using industrial experimental data sets. Two fundamental areas of coal processing were investigated, namely the comminution circuit and separation circuit.

Once the comminution circuit and separation circuit had dynamic models which were fitted to the available industrial plant data, they were used in various MPC simulation studies. The discussion of the results of the MPC simulation studies from Chapter 5 highlights production improvement that is possible by applying certain process objectives and constraints to the comminution and separation areas.

It was also shown through simulation that the MPC is capable of removing certain process disturbances. Complete automatic control of the process from startup to shutdown is also possible.

Given the simulated process improvements in throughput, yield and grade for the specific coal plant used for this thesis (Table 5.4), it is possible to calculate the overall improvement that could be made to the entire coal processing value chain. Given that the ROM fed to the separation process is increased by 3.6% and that the average yield of the entire separation circuit is approximately 88%, the separation circuit yield could be increased through advanced control by up to 3.2%.

The improvement on the DMD and DMC with MPC can be combined to determine the overall separation improvement possible. If the DMC uses approximately 25% of the feed ROM, the overall yield improvement made to the entire separation from the MPC simulations is 6.9%.

This means that with the 3.2% increase in yield from the optimally controlled comminution circuit and the 6.9% increase in yield by controlling the separation circuit, a total increase in yield of 10.1% could potentially be possible. Although these simulations were performed over very short production periods, the potential increase in yield through the MPC simulations illustrate a great opportunity for improving a coal beneficiation plant in general.

Given metallurgical coal prices at approximately 90 USD/t for mid 2014 (International Energy Agency, 2014a), a 10% increase in yield for a metallurgical coal plant means a possible increase in revenue of 9 USD/t. A plant producing 1.5Mtpa of metallurgical coal could potentially increase its revenue by 13.5 million USD per annum. At a South African exchange rate of R13/USD, such an improvement for a South African-based coal plant could increase its revenue by R175.5 million per annum.

This potential increase in revenue is detailed in Table 6.1.

In addition to an increase in yield, the implementation of MPC would also ensure that the final product meets its required customer grade specification. This would also prevent paying penalties for coal product delivered to customers that is out of specification. Using automatic control to replace a manually operated coal plant will not replace the role of production operations personnel. The involvement from operational personnel will require more input that is specific to decision-making in the coal business such as deciding at what levels to set the controller objectives to enhance performance.

**Table 6.1:** Potential increase in revenue based on MPC simulation improvements made.

| Assumptions | Value |
|---|---|
| MPC ROM feed increase (%) | 3.6 |
| Average separation circuit yield (%) | 88 |
| Separation yield improvement due to ROM increase (%) | 3.2 |
| MPC DMC yield increase (%) | 7.5 |
| MPC DMD yield increase (%) | 5.1 |
| DMD:DMC mass split | 3:1 |
| Separation yield improvement due to DMD and DMC MPC (%) | 6.9 |
| Total increase in yield (%) | 10.1 |
| Metallurgical coal price (USD/t) | 90 |
| Total annual production (Mtpa) | 1.5 |
| South African exchange rate (R/USD) | 13 |
| Annual increase in revenue (R million per annum) | 175.5 |

This type of input required from operations adds more value instead of utilising plant operators to manually change medium densities and to start and stop feeders.

## 6.2 FURTHER RESEARCH POSSIBILITIES

Based on the discussion in Chapter 5, a number of possible future research topics could stem from this thesis. From the discussion regarding the simulations of the comminution circuit, the following points can be made:

- A study could be conducted on a stockpile with volumetric measurements that are incorporated into the stockpile feeder model developed.
- The double-roll crusher model could be improved by incorporating measurements of motor angular acceleration.

- Crusher motor currents could be used in the MPC objective function to optimise power consumption.

The simulations of the separation circuit could benefit from the following future research topics:

- The method of reconstituting the ash content from the coal washability and separator partition curves should be verified using online ash measurements and more comprehensive metallurgical data.

- The separator dynamic models can be tested in operating regions where a plant produces very high yields.

- Secondary processes for a coal facility such as medium recovery could also be modelled and incorporated into the controller objective to reduce medium consumption and prevent wastage of process water.

- The use of the UKF for the separator ash state estimation can be enhanced by including online ash monitor readings with the reconstituted ash based on the coal washability. The less frequent laboratory analyses can also be used to remove bias in online ash readings.

In general, the MPC simulation for the coal plant could be simulated over longer time periods to further validate the potential improvement in yield and ash content. A plant-wide MPC simulation could also be performed where the comminution and separation areas are combined. Further work can be done where the dynamic model parameters could be estimated online using the UKF algorithm. Other observer algorithms could also be evaluated with the bin model for further research. Theoretical observability and controllability analysis on the models could also be performed.

## 6.3 FUTURE POTENTIAL IN COAL OPTIMISATION

Qin and Badgwell (2003) show an interesting schematic relating MPC to the various hierarchies of control system functions. Figure 6.1 shows a modified version of the control system hierarchy for $N$ unit processes. Each unit process is controlled using basic dynamic control. MPC is used to perform

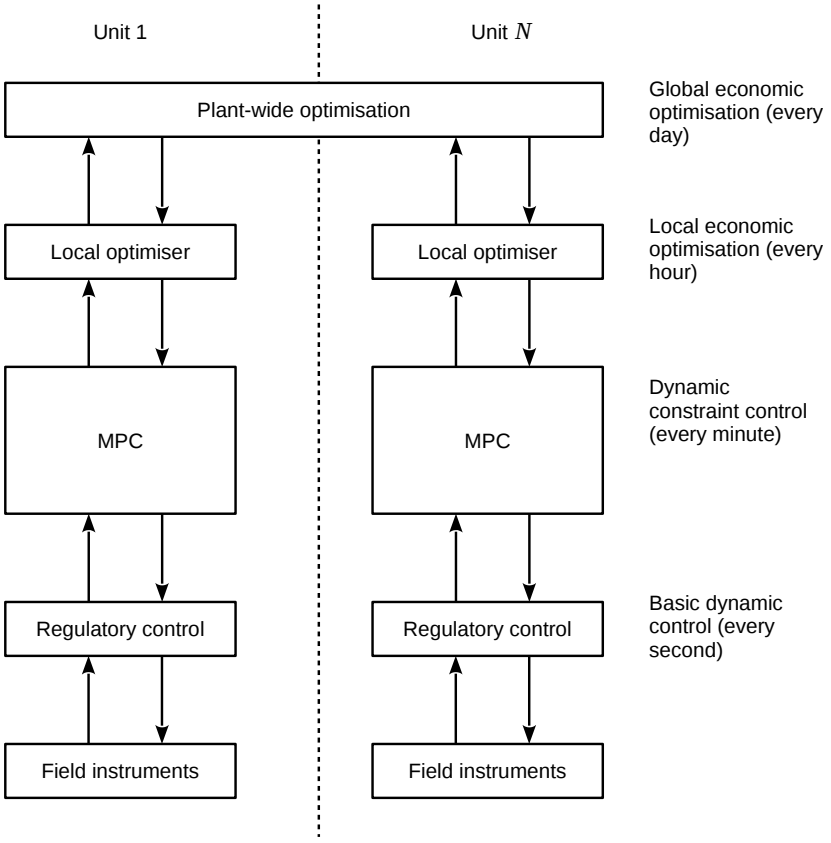


**Figure 6.1:** Hierarchy of control system functions in a typical processing plant [adapted from Qin and Badgwell (2003)].

dynamic constraint control every minute. A local optimiser is used to determine local economic optimisation every hour to determine required reference trajectories for the MPC. A global plant-wide optimiser is used to update each unit process local optimiser daily. The scope of this thesis focusses on simulating MPC for two coal unit processes (comminution and separation). The possibility of applying local or global economic optimisation for a coal business could provide even further benefits.

Munoz and Cipriano (1999) describe how a grinding-flotation plant was optimised by applying economic objectives. If MPC becomes standard practice for unit-level control in coal plants (i.e. comminution and separation areas), economic objectives could also be incorporated in the controllers. Enterprise- or mine-wide optimisation could be implemented to provide the necessary reference trajectories and objectives for each unit process MPC. Current coal business information such as mine planned tonnages, mined actual tonnages, coal geology, coal market prices, sales order requirements and energy costs can be incorporated into a mine-wide optimiser. Figure 6.2 illustrates an example of a proposed mine-wide control system architecture where the mine-wide optimisation results are fed

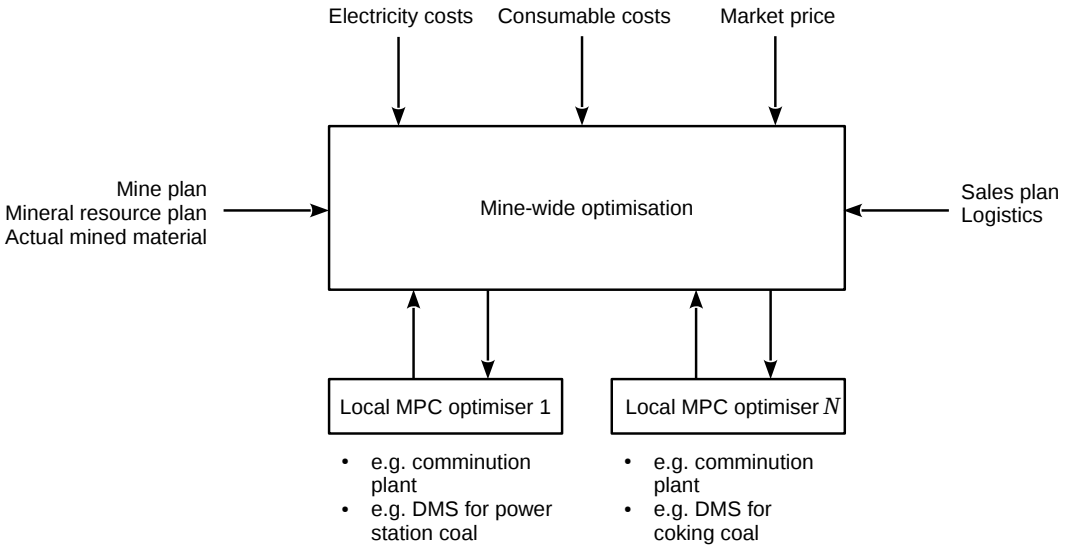


**Figure 6.2:** Mine-wide control architecture.

into the unit process MPCs. This concept is adapted from Qin and Badgwell (2003) as illustrated in Figure 6.1, but applied to a coal business operation.

# REFERENCES

Apkarian, P. and Adams, R. J. (1998). Advanced gain-scheduling techniques for uncertain systems, *Control Systems Technology, IEEE Transactions on* **6**(1): 21–32.

Arnold, B., Klima, M. and Bethell, P. (2007). *Designing the coal preparation plant of the future*, Society of Mining, Metallurgy, and Exploration, Inc. (SME), Colorado.

Asbjörnsson, G., Hulthén, E. and Evertsson, M. (2013). Modelling and simulation of dynamic crushing plant behavior with MATLAB/Simulink, *Minerals Engineering* **43**: 112–120.

Badwe, A. S., Gudi, R. D., Patwardhan, R. S., Shah, S. L. and Patwardhan, S. C. (2009). Detection of model-plant mismatch in MPC applications, *Journal of Process Control* **19**(8): 1305–1313.

Baguley, P. J. and Napier-Munn, T. J. (1996). Mathematical model of the dense medium drum, *Trans. Inst. Min. Met. (Section C)* **105**: C1–C8.

Barrientos, M. and Soria, C. (2015). Coal, South Africa export price, `http://www.indexmundi.com/commodities/?commodity=coal-south-african&months=120`. viewed 19 May 2015.

Bauer, M. and Craig, I. K. (2008). Economic assessment of advanced process control - a survey and framework, *Journal of Process Control* **18**: 2–18.

Belbot, M. D., Vourvopoulos, G., Womble, P. C. and Paschal, J. (1999). Elemental online coal analysis using pulsed neutrons, *SPIE's International Symposium on Optical Science, Engineering,*

*and Instrumentation*, International Society for Optics and Photonics, pp. 168–177.

Bengtsson, M., Svedensten, P. and Evertsson, C. M. (2009). Improving yield and shape in a crushing plant, *Minerals Engineering* **22**(7): 618–624.

Borsaru, M. and Jecny, Z. (2001). Application of PGNAA for bulk coal samples in a $4\pi$ geometry, *Applied Radiation and Isotopes* **54**(3): 519–526.

Bowen, R. M. and Jowett, A. (1986). Coal cleaning calculations based on alternatives to standard washability curves, *Fuel* **65**(1): 28–33.

Brennan, M. S. (2003). Multiphase CFD simulations of dense medium and classifying hydrocyclones, *Proceedings of the Third international Conference on CFD in the Minerals and Process Industries CSIRO, 10–12 December, 2003, Melbourne, Australia*, pp. 59–64.

Camacho, E. and Bordons, C. (2004). *Model predictive control*, Advanced Textbooks in Control and Signal Processing, 2 edn, Springer-Verlag, London.

Chen, J. F., Rotter, J. M., Ooi, J. Y. and Zhong, Z. (2005). Flow pattern measurement in a full scale silo containing iron ore, *Chemical Engineering Science* **60**: 3029–3041.

Chen, W., Zydek, N. and Parma, F. (2000). Evaluation of hydrocyclone models for practical applications, *Chemical Engineering Journal* **80**: 295–303.

Cierpisz, S. and Heyduk, A. (2001). Radiometric online ash monitor for coal industry using fuzzy logic, *Instrumentation and Measurement, IEEE Transactions on* **50**(5): 1176–1180.

Clarke, R., Waddington, J. and Wallace, J. (1989). The application of Kalman filtering to the load/pressure control of coal-fired boilers, *Kalman Filters: Introduction, Applications and Future Developments, IEE Colloquium on*, IET, pp. 2–1.

Clarkson, C. J. (1983). A model of dense medium cyclones, *Proceedings of the Dense Medium Operators Conference, 1983, Brisbane, Australia*, pp. 235–245.

Cleary, P. W. and Sinnott, M. D. (2014). Simulation of particle flows and breakage in crushers using DEM: Part 1–Compression crushers, *Minerals Engineering*.

Coetzee, L. C., Craig, I. K. and Kerrigan, E. C. (2010). Robust nonlinear model predictive control of a run-of-mine ore milling circuit, *Control Systems Technology, IEEE Transactions on* **18**(1): 222–229.

Concha, F. and Almendra, E. (1979). Settling velocities of particulate systems, 1. Settling velocities of individual spherical particles, *International Journal of Mineral Processing* **5**(4): 349–367.

Cortés, C. and Gil, A. (2007). Modelling the gas and particle flow inside cyclone separators, *Progress in Energy and Combustion Science* **33**: 409–452.

Cortinovis, A., Mercangoez, M., Mathur, T., Poland, J. and Blaumann, M. (2013). Nonlinear coal mill modeling and its application to model predictive control, *Control Engineering Practice* **21**(3): 308–320.

Cotabarren, I., Schulz, P. G., Bucalá, V. and Piña, J. (2008). Modeling of an industrial double-roll crusher of a urea granulation circuit, *Powder Technology* **183**(2): 224–230.

Craig, I. K. and Henning, R. G. D. (2000). Evaluation of advanced industrial control projects: a framework for determining economic benefits, *Control Engineering Practice* **8**: 769–780.

Daum, F. (2005). Nonlinear filters: beyond the Kalman filter, *Aerospace and Electronic Systems Magazine, IEEE* **20**(8): 57–69.

De Korte, J. G. (2003a). Comments on the use of tracers to test dense-medium plant efficiency, *International Journal of Coal Preparation and Utilization* **23**(5): 251–266.

De Korte, J. G. (2003b). Index of South African coal preparation plants, `http://www.sacoalprep.co.za/information.html`. viewed 20 September 2015.

De Korte, J. G. (2008). The influence of near-dense material on the separation efficiency of dense-medium processes, *International Journal of Coal Preparation and Utilization* **28**(2): 69–93.

Eberhard, A. (2011). The future of South African coal: market, investment, and policy challenges, `http://iis-db.stanford.edu/pubs/23082/WP_100_Eberhard_Future_of_South_African_Coal.pdf`. viewed 26 May 2015.

England, T., Hand, P. E., Michael, D. C., Falcon, L. M. and Yell, A. D. (2002). *Coal preparation in South Africa*, 4 edn, Natal Witness Commercial Printers, Pietermaritzburg, South Africa.

Erasmus, T. C. (1973). The fitting of a smooth curve to the experimentally determined coordinates of a tromp curve, *Technical Report 4*, Fuel Research Institute of South Africa.

Faure, K., Willis, J. P. and Claris Dreyer, J. (1996). The Grootegeluk formation in the Waterberg coalfield, South Africa: Facies, palaeoenvironment and thermal history-evidence from organic and clastic matter, *International Journal of Coal Geology* **29**(1): 147–186.

Firth, B. A. (2009). Dense medium cyclone control - a reconsideration, *International Journal of Coal Preparation and Utilization* **29**(3): 112–129.

Firth, B. A., Grice, C., Jenssen, E. and Weale, W. (1983). Computer simulation of coal preparation and its application at the Saxonvale mine, *Proceedings of the Second Australian Coal Preparation Conference, 10–14 October, 1983, Rockhampton, Australia*, Vol. 2, Australian Coal Preparation Society, pp. 421–443.

Galetakis, M., Alevizos, G., Pavloudakis, F., Roumpos, C. and Kavouridis, C. (2009). Prediction of the performance of on-line ash analyzers used in the quality control process of a coal mining system, *Energy Sources, Part A* **31**(13): 1115–1130.

González-Montellano, C., Gallego, E., Ramírez-Gómez, A. and Ayuga, F. (2012). Three dimensional discrete element models for simulating the filling and emptying of silos: Analysis of numerical results, *Computers and Chemical Engineering* **40**: 22–32.

González-Montellano, C., Ramírez, A. and Ayuga, E. G. F. (2011). Validation and experimental calibration of 3D discrete element models for the simulation of the discharge flow in silos, *Chemical Engineering Science* **66**: 5116–5126.

Gottfried, B. S. (1973). Computer simulation of coal preparation plants, *Technical Report Grant No. G0-155030*, United States Bureau of Mines.

Grüne, L. and Pannek, J. (2011). *Nonlinear model predictive control: Theory and algorithms*, Springer, London.

Gupta, A. and Yan, D. (2006). *Mineral processing design and operations: An introduction*, 1 edn, Elsevier, Amsterdam.

Halliday, D., Resnick, R. and Walker, J. (2001). *Fundamentals of physics*, 6 edn, John Wiley & Sons, Inc., United States of America.

Hatamura, Y. and Takeuchi, T. (1991). A proposal for an intelligent silo based on measured phenomena, *Advanced Powder Technology* **2**(4): 285–294.

Hayes, P. (2003). *Process principles in minerals and materials production*, 3 edn, Hayes Publishers, Brisbane.

He, Y. B. and Laskowski, J. S. (1994). Effect of dense medium properties on the separation performance of a dense medium cyclone, *Minerals Engineering* **7**(2): 209–221.

Herbst, J. A., Pate, W. T. and Oblad, A. E. (1992). Model-based control of mineral processing operations, *Powder Technology* **69**: 21–32.

Hodouin, D. (2011). Methods for automatic control, observation, and optimization in mineral processing plants, *Journal of Process Control* **21**(2): 211–225.

Honaker, R. Q. and Patwardhan, A. (2006). In-plant evaluation of dense medium process performances, *International Journal of Coal Preparation and Utilization* **26**(3): 149–164.

International Energy Agency (2014a). Average cost of metallurgical coal priced at coke plants and export docks, 2011Q2-2014Q2, `http://www.eia.gov/coal/news_markets/coal_price.cfm`. viewed 16 August 2015.

International Energy Agency (2014b). Medium-term coal market report 2014, http://www.iea.org/bookshop/495-Medium-Term_Coal_Market_Report_2014. viewed 17 May 2015.

Julier, S. J. and Uhlmann, J. K. (1997). A new extension of the Kalman filter to nonlinear systems, *Int. symp. aerospace/defense sensing, simul. and controls*, Vol. 3, Orlando, FL, pp. 3–2.

King, R. P. (2001). *Modeling and simulation of mineral processing systems*, Elsevier, Oxford.

King, R. P. and Juckes, A. H. (1984). Cleaning of fine coals by dense-medium hydrocyclones, *Powder Technology* **40**(1): 147–160.

King, R. P. and Juckes, A. H. (1988). Performance of dense-medium cyclone when beneficiating fine coal, *Coal Preparation* **5**: 185–210.

Klima, M., Arnold, B. and Bethell, P. (2012). *Challenges in fine coal processing, dewatering, and disposal*, Society of Mining, Metallurgy, and Exploration, Inc. (SME), Colorado.

Le Roux, J. D., Padhi, R. and Craig, I. K. (2014). Optimal control of grinding mill circuit using model predictive static programming: A new nonlinear MPC paradigm, *Journal of Process Control* **24**(12): 29–40.

Leite, M. M. (1990). Kinetic models for the simulation of crushing circuits, *Minerals Engineering* **3**(1): 165–180.

Lichti, D., Gordon, S. and Stewart, M. (2002). Ground-based laser scanners: operation, systems and applications, *Geomatica* **56**(1): 21–33.

Lim, G. (1997). On the conveying velocity of a vibratory feeder, *Computers & Structures* **62**(1): 197–203.

Lipták, B. G. (1995). *Instrument engineers' handbook: Process control*, 3 edn, Butterworth-Heinemann Ltd, UK, Europe.

Ljung, L. (1987). *System identification: Theory for the user*, 1 edn, Prentice-Hall, Inc, Englewood Cliffs, NJ.

Ljung, L. (2005). *System identification toolbox user's guide*, 7 edn, The MathWorks, Inc, Natick, MA.

Ljung, L. (2010). Perspectives on system identification, *Annual Reviews in Control* **34**: 1–12.

Luo, J., Huang, W. and Zhang, S. (2014). Energy cost optimal operation of belt conveyors using model predictive control methodology, *Journal of Cleaner Production* pp. 1–10.

Lyman, G. J., Askew, H., Wood, C. J. and Davis, J. J. (1982). Dynamic modelling of dense medium cyclone washing circuits, *Proceedings of the Mill Operations Conference, NW Queensland, Australia*, AusIMM, AusIMM, pp. 369–381.

Lyman, G. J., Denney, B., Wood, C. J., Askew, H. and Brenchley, R. (1983). Automatic control of product coal ash content using on-line coal ash gauge, *in* R. L. Whitmore (ed.), *Proceedings of the Second Australian Coal Preparation Conference, 1983, Rockhampton, Australia*, Vol. 2 of *Instrumentation and Control*, Australian Coal Preparation Society, Australian Coal Preparation Society, pp. 291–309.

Lynch, A. J. (1977). *Mineral crushing and grinding circuits: Their simulation, optimisation, design and control*, Elsevier Scientific Pub. Co., Amsterdam.

Mahfouz, A. A., Mohammed, M. and Salem, F. A. (2013). Modeling, simulation and dynamics analysis issues of electric motor, for mechatronics applications, using different approaches and verification by MATLAB/Simulink, *International Journal of Intelligent Systems and Applications (IJISA)* **5**(5): 39.

Majumder, A. K., Barnwal, J. P. and Ramakrishnan, N. (2004). A new approach to evaluate the performance of gravity-based coal washing equipment, *International Journal of Coal Preparation and Utilization* **24**(5): 277–284.

Maul, G. P. and Thomas, M. B. (1997). A systems model and simulation of the vibratory bowl feeder, *Journal of Manufacturing Systems* **16**(5): 309–314.

Mayer, F. (1950). Die mittelwertkurve, eine neue verwachsungskurve, *Glückauf* pp. 498–509.

Metals Consulting International (2015). Steelmaking commodity prices: World steel raw material & energy costs, `http://www.steelonthenet.com/commodity-prices.html`. viewed 17 May 2015.

Meyer, E. and Craig, I. (2015). Dynamic model for a dense medium drum separator in coal beneficiation, *Minerals Engineering* **77**: 78–85.

Meyer, E. J. (2010). *The development of dynamic models for a dense medium separation circuit in coal beneficiation*, Master's thesis, University of Pretoria.

Meyer, E. J. and Craig, I. K. (2010). The development of dynamic models for a dense medium separation circuit in coal beneficiation, *Minerals Engineering* **23**(10): 791–805.

Meyer, E. J. and Craig, I. K. (2011). Development of a steady-state partition curve from a dense medium cyclone dynamic model in coal beneficiation, *Proceedings of the 18th IFAC World Congress, Milan, Italy*, Vol. 18, IFAC, IFAC, pp. 10523–10528.

Meyer, E. J. and Craig, I. K. (2014). Coal dense medium separation dynamic and steady-state modelling for process control, *Minerals Engineering* **65**(15): 98–108.

Meyer, E. J., Craig, I. K. and Alvarado, V. (2015). Unscented Kalman filter for a coal run-of-mine bin, *Proceedings of the 4th Workshop on Mining, Mineral and Metal Processing, Oulu, Finland*, IFAC, IFAC.

Mukherjee, A. K., Sripriya, R., Rao, P. V. T. and Das, P. (2003). Effect of increase in feed inlet pressure on feed rate of dense medium cyclone, *International Journal of Mineral Processing* **69**: 259–274.

Munoz, C. and Cipriano, A. (1999). An integrated system for supervision and economic optimal control of mineral processing plants, *Minerals Engineering* **12**(6): 627–643.

Napier-Munn, T. J. (1991). Modelling and simulating dense medium separation processes - a progress report, *Minerals Engineering* **4**(3): 329–346.

Nezamzadeh, M., Alavi, S., Lamehi-Rachti, M., Rahimian, N. and Ghiassi-Nejad, M. (1999). Comparison between (n–$\gamma$),($\gamma$–$\gamma$) and natural $\gamma$-ray activity techniques for ash measurement of coal samples, *Applied Radiation and Isotopes* **50**(4): 685–691.

Numbi, B., Zhang, J. and Xia, X. (2014). Optimal energy management for a jaw crushing process in deep mines, *Energy* **68**: 337–348.

Olivier, L. E., Craig, I. K. and Chen, Y. (2012a). Fractional order and BICO disturbance observers for a run-of-mine ore milling circuit, *Journal of Process Control* **22**(1): 3–10.

Olivier, L. E., Huang, B. and Craig, I. K. (2012b). Dual particle filters for state and parameter estimation with application to a run-of-mine ore mill, *Journal of Process Control* **22**(4): 710–717.

Ooi, J. Y., Chen, J. F., Lohnes, R. A. and Rotter, J. M. (1996). Prediction of static wall pressures in coal silos, *Construction and Building Materials* **10**(2): 109–116.

Pan, X. (2012). Development of stockpile soft sensor, *AGH Journal of Mining and Geoengineering* **36**: 109–121.

Pan, X. (2015). Online smart sensor to measure stockpiles used in mineral processing, *International Conference on Mining, Minerals and Metallurgical Engineering (ICMMME'15) July 14-15, 2015 Harare (Zimbabwe)*.

Pindyck, R. S. (1999). The long-run evolution of energy prices, *The Energy Journal* pp. 1–27.

Plitt, L. R. (1971). The analysis of solid-solid separations in classifiers, *The Can. Minerals Metalurgy, Bul.*, pp. 1–6.

Pooe, D. and Mathu, K. (2011). The South African coal mining industry: A need for a more efficient and collaborative supply chain, *Journal of Transport and Supply Chain Management* **5**(1): 316–336.

Qin, S. J. and Badgwell, T. A. (2003). A survey of industrial model predictive control technology, *Control Engineering Practice* **11**(7): 733–764.

Rajamani, R. K. and Herbst, J. A. (1991). Optimal control of a ball mill grinding circuit-I. grinding circuit modeling and dynamic simulation, *Chemical Engineering Science* **46**(3): 861–870.

Rao, B. V. (2004). Weibull partition surface representation for gravity concentrators, *Minerals Engineering* **17**: 953–956.

Rao, B. V., Kapur, P. C. and Konnur, R. (2003). Modelling the size-density partition surface of dense-medium separators, *International Journal of Mineral Processing* **72**: 443–453.

Rathaba, L. P. (2004). *Model fitting for electric arc furnace refining*, Master's thesis, University of Pretoria.

Reinhardt, K. (1911). Characteristik der Feinkohlen und ihre aufbeteitung mit Rucksicht auf das grösste Ausbringen, *Glückauf* **47**(6): 221–228.

Roberts, A. W. and Wensrich, C. M. (2002). Flow dynamics or 'quaking' in gravity discharge from silos, *Chemical Engineering Science* **57**: 295–305.

Rugh, W. J. and Shamma, J. S. (2000). Research on gain scheduling, *Automatica* **36**(10): 1401–1425.

Scott, I. A. and Lyman, G. J. (1987). Metallurgical evaluation of iron ore drum separators using density tracers, *Proceeding of the Australian Institute of Mining and Metallurgy, February, 1987*, Vol. 1, pp. 49–56.

Scott, I. A. and Napier-Munn, T. J. (1992). Dense-medium cyclone model based on the pivot phenomenon, *Trans. Inst. Min. Metall. (Section C: Min. Proc. Extr. Metall.)* **101**: C61–C76.

Seborg, D. E., Edgar, T. F. and Mellichamp, D. A. (1995). *Process dynamics and control*, 2 edn, John Wiley and Sons, Inc, USA.

Sielamowicz, I., Czech, A. and Kowalewski, T. A. (2014). Comparative analysis of empirical descriptions of eccentric flow in silo model by the linear and nonlinear regressions, *Powder Technology*.

South African National Energy Development Institute (2015). Overview of the South African coal value chain, `http://www.sanedi.org.za/archived/wp-content/uploads/2013/08/sacrm%20value%20chain%20overview.pdf`. viewed 26 May 2015.

Stephanopoulos, G. (1984). *Chemical process control: an introduction to theory and practice*, 1 edn, Prentice-Hall, Inc., Englewood Cliffs, NJ.

Steyn, H. (2014a). Comminution and separation plant objectives, private communication.

Steyn, H. (2014b). Wemco drum and cyclone partition curve verification, private communication.

Suasnabar, D. J. and Fletcher, A. J. (1999). A CFD model for dense medium cyclones, *Proceedings of the Second international Conference on CFD in the Minerals and Process Industries CSIRO, 6–8 December, 1999, Melbourne, Australia*, pp. 199–204.

Terra, A. (1938). Theory of washing coal, *Revue Industrie Minerale* **425**: 383.

Thayalan, V. and Landers, R. G. (2006). Regulation of powder mass flow rate in gravity-fed powder feeder systems, *Journal of Manufacturing Processes* **8**(2): 121–132.

Thwaites, P. (2007). Process control in metallurgical plants - from an Xstrata perspective, *Annual Reviews in Control* **31**(2): 221–239.

Tsakalakis, K. (2000). Use of a simplified method to calculate closed crushing circuits, *Minerals Engineering* **13**(12): 1289–1299.

Tüzün, U. and Nedderman, R. M. (1985). Gravity flow of granular materials round obstacles - investigation of the effects of inserts on flow patterns inside a silo, *Chemical Engineering Science* **40**(3): 325–336.

Van Der Merwe, R., Wan, E. *et al.* (2001). The square-root unscented Kalman filter for state and parameter-estimation, *Acoustics, Speech, and Signal Processing, 2001. Proceedings.(ICASSP'01). 2001 IEEE International Conference on*, Vol. 6, IEEE, pp. 3461–3464.

Wan, E. A. and Van der Merwe, R. (2000). The unscented Kalman filter for nonlinear estimation, *Adaptive Systems for Signal Processing, Communications, and Control Symposium 2000. AS-SPCC. The IEEE 2000*, IEEE, pp. 153–158.

Wilkes, K. D. (2006). The practical application of the Wemco HMS drum separator in the mining and metals recycling industries, *Proceedings of the SAIMM Present Status and Future for DMS Gravity Concentration in the South African Mining Industry Conference, 18–20 July, 2006*, SAIMM, pp. 179–190.

Wills, B. A. and Napier-Munn, T. (2006). *Wills' mineral processing technology: An introduction to the practical aspects of ore treatment and mineral recovery*, 7 edn, Elsevier.

Wilson, D., Agarwal, M. and Rippin, D. (1998). Experiences implementing the extended Kalman filter on an industrial batch reactor, *Computers & Chemical Engineering* **22**(11): 1653–1672.

Yildiz, A. B. (2012). Electrical equivalent circuit based modeling and analysis of direct current motors, *International Journal of Electrical Power & Energy Systems* **43**(1): 1043–1047.

Zhang, L. and Xia, X. (2014). A model predictive control for coal beneficiation dense medium cyclones, *IFAC World Congress, Cape Town, South Africa*, Vol. 19, IFAC, IFAC, pp. 9810–9815.

Zhang, L., Xia, X. and Zhang, J. (2015). Medium density control for coal washing dense medium cyclone circuits, *Control Systems Technology, IEEE Transactions on* **23**(3): 1117–1122.

Zhang, S. and Xia, X. (2010). Optimal control of operation efficiency of belt conveyor systems, *Applied Energy* **87**(6): 1929–1937.

Zhang, S. and Xia, X. (2011). Modeling and energy efficiency optimization of belt conveyors, *Applied Energy* **88**(9): 3061–3071.

Zhao, L.-L., Wang, Z.-B. and Feng, Z. (2008). Multi-object optimization design for differential and grading toothed roll crusher using a genetic algorithm, *Journal of China University of Mining and Technology* **18**(2): 316–320.